

© 2018 Yajie Wang

DESIGN AND ENGINEERING OF MULTI-STEP (BIO)CATALYTIC SYSTEMS

BY

YAJIE WANG

DISSERTATION

Submitted in partial fulfillment of the requirements  
for the degree of Doctor of Philosophy in Chemical Engineering  
in the Graduate College of the  
University of Illinois at Urbana-Champaign, 2018

Urbana, Illinois

Doctoral Committee:

Professor Huimin Zhao, Chair  
Professor Hong Yang  
Professor Christopher V. Rao  
Professor Yi Lu

## Abstract

Nature has been a perpetual source of inspiration for biochemists. It is not only the vast diversity of compounds that living beings can create, but also the extraordinary strategies of synthesis deployed. Evidently, the catalysts used by living beings -enzymes- are key to nature's synthesis strategies. Biocatalysis is undoubtedly one of the most invaluable gifts given by nature to flourish the development of green chemical and pharmaceutical industries. With the development of protein and metabolic engineering tools and strategies, more and more enzymes have been used in the industries to improve the chemical processing; and microbes such as *Escherichia coli* and *Saccharomyces cerevisiae* have been engineered to produce a wide variety of value-added and bulk chemicals to replace traditional chemical synthesis. However, researchers have just explored the tip of the iceberg in the biocatalysis area. Proteins with new catalytic functionality should be discovered or engineered to broaden current biotransformation boundaries. New in vitro enzymatic or chemoenzymatic cascade reactions need to be designed and optimized to realize stronger synthetic power and more stable systems. Metabolic networks of traditional or new microorganisms should be largely rewired to meet the manufacturing standards.

In this work, I aimed at designing and engineering multi-step (bio) catalytic systems for selective synthesis of value-added chemicals. Microorganisms synthesize complex molecules from simple substrates by a series of enzymes working cooperatively. Inspired by how aromatic polyketides are synthesized by the teamwork between enzymes, I sought to couple biocatalysis with organometallic catalysis, two distinct catalytic disciplines, in one pot to realize synthetic power that cannot be achieved by either of them. I first developed a modular, one-pot, sequential chemoenzymatic system for the formal enantioselective construction of C-C bond in 2-aryl 1,4-

dicarbonyl compounds. This sequence comprises a rhodium-catalyzed diazocoupling that provides >9:1 selectivity for heterocoupling of two diazoesters and a reduction mediated by an ene-reductase (ER), which occurs in up to 99% enantiomeric excess (*ee*). The high yield and enantioselectivity of this system were resulted from the preferential generation of an (*E*)-alkene from the diazo coupling reaction and selective reduction of the (*E*)-alkene in a mixture of (*E*) and (*Z*) isomers by the ER. This work demonstrates the benefit of combining organometallic and enzymatic catalysis to create unusual overall transformations that do not require the isolation and purification of intermediates.

To make the system works better on a broader range of substrates, I later developed a new class of cooperative chemoenzymatic reactions that combine photocatalysts that isomerize alkenes with ene-reductases that reduce carbon-carbon double bonds to generate valuable enantioenriched products. I demonstrated that this method enables the stereoconvergent reduction of *E/Z* mixtures of alkenes or reduction of the unreactive stereoisomer of an alkene in yields and *ee*'s that match those obtained from the reduction of the pure, more reactive isomer. This new cooperative system overcomes the limitations of both individual catalysts and affords a range of synthetically valuable and biologically active enantioenriched compounds. More generally, these results illustrate the value of driving a chemical reaction with light to ensure compatibility between the chemical and enzymatic catalysts.

*In vitro* biocatalytic reaction normally has poor tolerance to harsh conditions such as low pH or high substrate concentrations. Cells membrane is natural compartmentalization and protects the enzymes from extracellular inhibitors. In addition, cell factories-based production provides an attractive alternative to chemical synthesis of value-added chemicals. I also worked on engineering a *S. cerevisiae* strain as a whole-cell catalyst for L-lactic acid overproduction in industrially



preferred low pH environment (pH 3) by metabolic engineering and genome-wide engineering methods. In addition, to establish an automated cellular engineering platform, I developed a growth-based L-lactic acid biosensor and an automated quantification assay by BioProfile Analyzer.

*To my Heavenly Father*  
*To my husband*  
*To my parents*  
*To my family and my friends.*

## Acknowledgements

First and foremost, I thank my advisor, Prof. Huimin Zhao, for granting me the opportunity to perform graduate research in his lab. His patience and trust in my judgment enabled me to pursue my goals to the best of my ability. Further, I am grateful for the guidance and opportunities he gave to me to nourish my interests and desires of being a scientist, which I think is the best accomplishment during Ph.D. study. I also thank my co-advisor, Prof. John Hartwig for his knowledgeable suggestions on my tandem reaction projects. My committee members Prof. Hong Yang, Prof. Christopher V. Rao and Prof. Yi Lu also have my grateful thankfulness for their valuable feedback. For technical assistance, I am grateful to Dr. Lucas Li and Dr. Alex Ulanov of the Roy J. Carver Metabolomics Center; Dr. Furong Sun of the SCS Mass Spectrometry Facility; and Dr. Xudong Guan of the IGB Core Facilities. For financial support, I am grateful for Dow Chemical Fellowship, 3M Fellowship, Chia-chen Chu Fellowship and Glenn E. and Barbara R. Ulliyot Graduate Fellowship.

I was so lucky to work with many wonderful people. I especially give my thankfulness to Dr. Carl A. Denard, Dr. Ryan E. Cobb and Dr. Mark J. Bartlett for their thoughtful and patient training. I also want to thank Dr. Zachary Litman and Dr. Mingzi Zhang for their hard work on the collaborative projects. I am forever thankful to a long list of people for their support and active discussion on my projects: Hengqian Ren, Xiong Xiong, Dr. Bin Wang, Dr. Fang Guo, Dr. Si Tong, Dr. Mingfeng Cao, Dr. Shangwen Luo, Dr. Teresa Martin, Vinh Tran and Lam Vo.

Last but not least, I want to thank my husband Yiming Pan for his unconditionally support and compromise. I want to thank my sisters and brothers at Vineyard Church, especially Huei-huei Chang, Dr. Wayne Chang, Xi Zhang, Xue Han, Dr. Daniel Chen, Dr. Chen-Yu Huang, Jie Yu,

Kailu Guan, Xi Teng, Ada Kao, Dr. Enchuan Huang, Stephen Skeirik, Ssu Yu Chen, Prof. Chia-Fon Lee and his wife Pastor Yu-yu for their lovely support, caring and prays.

# Table of Contents

|  |    |
|--|----|
| CHAPTER 1. Introduction.....   | 1  |
| 1.1 Biocatalysis .....   | 1  |
| 1.2 Natural Product Synthesis: How Nature Make Complex Molecules.....  | 4  |
| 1.3 <i>In vitro</i> Tandem Catalytic Reactions for Biochemical Productions.....  | 7  |
| 1.3.1. Enzymatic Tandem Reactions.....   | 8  |
| 1.3.2. Chemoenzymatic Tandem Reactions.....  | 12 |
| 1.3.2.1. One-pot Chemo-enzymatic Reactions in Organic Solvent.....   | 13 |
| 1.3.2.2. One-pot Chemo-enzymatic Reactions in Aqueous Solutions .....  | 14 |
| 1.3.2.3. Novel Strategies to Combine Transition Metals and Enzymes in One-pot Tandem<br>Reactions.....   | 18 |
| 1.4 Whole Cell Biocatalysis.....   | 24 |
| 1.5 Project Overview.....  | 26 |
| 1.6 References.....  | 28 |
| CHAPTER 2. Activation and Characterization of Biosynthetic Gene Clusters (BGCs) in <i>Streptomyces<br/>viridochromogenes</i> Using CRISPR-Cas System ..... | 35 |
| 2.1 Introduction.....  | 35 |
| 2.2 Results and Discussion .....   | 37 |
| 2.2.1. CRISPR-Cas9 Strategy for Promoter Knock-in in <i>Streptomyces Species</i> .....   | 37 |
| 2.2.2. Activation Silent Biosynthetic Gene Clusters (BGCs) in <i>Streptomyces viridochromogenes</i> .....  | 39 |
| 2.2.3. Identification and Characterization of Novel Type II PKS Compound C22-1 .....   | 42 |
| 2.2.4. Investigation the Biosynthetic Mechanism of C22-1 .....   | 44 |
| 2.3 Conclusion .....   | 47 |
| 2.4 Experimental Procedures .....  | 48 |
| 2.4.1. Reagents and Media.....   | 48 |
| 2.4.2. Strains and Growth Conditions .....   | 48 |
| 2.4.3. Construction of Genome Editing Plasmids.....  | 49 |
| 2.4.4. Interspecies Conjugation.....   | 53 |
| 2.4.5. Validation of Promoter Knock-in and Genome Editing .....  | 53 |
| 2.4.6. Metabolites Analysis.....   | 54 |
| 2.4.7. Isolation and Nuclear Magnetic Resonance Spectroscopy Analysis of C22-1 .....   | 55 |
| 2.4 References.....  | 63 |

|  |     |
|--|-----|
| CHAPTER 3. Combining Rh-catalyzed Diazocoupling and Enzymatic Reduction to Efficiently Synthesize Enantioenriched 2-substituted Succinate Derivatives..... | 65  |
| 3.1 Introduction.....  | 65  |
| 3.2 Results and Discussion .....   | 68  |
| 3.2.1. Selective Synthesis of Unsymmetrical ( <i>E</i> )-2-Aryl-substituted Alkenes .....  | 68  |
| 3.2.2. Enantioselective Enzymatic Reduction of C-C Double Bond .....   | 69  |
| 3.2.3. Two-step Sequential Reaction to Synthesize Enantioenriched 2-Aryl-Substituted Succinate Derivatives .....   | 73  |
| 3.2.4. Docking Experiments.....  | 74  |
| 3.3 Conclusions and Outlook.....   | 76  |
| 3.4 Experimental Procedures .....  | 76  |
| 3.4.1. Materials .....   | 76  |
| 3.4.2. Cloning, Expression and Purification of Enzymes .....   | 77  |
| 3.4.3. General Procedure for Alkene Synthesis via Rh-catalyzed Diazocoupling .....   | 81  |
| 3.4.4. General Procedure for Enzymatic Alkene Reduction and Quantification .....   | 84  |
| 3.4.5. General Procedure for One-Pot Sequential Diazocoupling–Enzymatic Alkene Reduction.....  | 87  |
| 3.4.6. Synthesis of Racemic Products: Representative Procedure for Alkene Hydrogenation .....  | 88  |
| 3.4.7. GC/MS Method.....   | 89  |
| 3.5 Representative Traces .....  | 90  |
| 3.5.1. Representative NMR Traces .....   | 90  |
| 3.5.2. Representative HPLC and SFC Traces .....  | 107 |
| 3.6 References.....  | 116 |
| CHAPTER 4. Cooperative Asymmetric Reactions Combining Photocatalysis and Enzyme Catalysis ...  | 120 |
| 4.1 Introduction.....  | 120 |
| 4.2 Results and Discussion .....   | 124 |
| 4.2.1. Development of Conditions for Cooperative Reaction.....   | 124 |
| 4.2.2. Substrates Scope .....  | 130 |
| 4.2.3. Cooperative Concurrent Reaction Versus Sequential Reaction.....   | 136 |
| 4.2.4. Derivatization of Synthesized Enantioenriched Products .....  | 137 |
| 4.3 Conclusion .....   | 140 |
| 4.4 Experimental procedures .....  | 140 |
| 4.4.1. General Materials.....  | 140 |
| 4.4.2. Photocatalyst Abbreviations, CAS Numbers, and Structures .....  | 143 |
| 4.4.3. Experimental Apparatus.....   | 144 |

|   |     |
|---|-----|
| 4.4.4. Cloning, Expression and Purification of Enzymes .....  | 144 |
| 4.4.5. GC/MS Methods and Calibration Curve.....   | 149 |
| 4.4.6. Photocatalyzed Isomerization of Alkenes and Control Experiments.....   | 157 |
| 4.4.7. General Synthetic Procedures for the Cooperative and Non-Cooperative Enzymatic Reduction of Alkenes .....                              | 159 |
| 4.4.8. Procedure for Sequential Isomerization and Reduction of Alkenes .....  | 162 |
| 4.4.9. Preparative Scale Cooperative Reactions.....   | 163 |
| 4.4.10. Investigating the Plausibility of Direct Photoreduction of (Z)-1a and the Photoracemization of (R)-2a.....                            | 167 |
| 4.5 HPLC Traces for the Cooperative Enzymatic Reduction of Alkenes and Control Experiments.....   | 170 |
| 4.6 References.....   | 203 |
| CHAPTER 5. Automated Cellular Engineering of <i>Saccharomyces cerevisiae</i> Strains With High Resistance and Production of Lactic Acid ..... | 206 |
| 5.1 Introduction.....   | 206 |
| 5.2 Results and Discussion .....  | 207 |
| 5.2.1. Creation of L-LA Producing Mutants with RNAi and CRISPR-AID Machinery .....  | 207 |
| 5.2.2. Establishing Screening Methods for L-LA Overproduction .....   | 213 |
| 5.2.2.1. Bromocresol Green Assay .....  | 213 |
| 5.2.2.2. Lactate Oxidase Assay .....  | 214 |
| 5.2.2.3. L-Lactic Acid Biosensor .....  | 216 |
| 5.2.3. Establishing Screening Methods for Low pH Tolerance .....  | 221 |
| 5.2.4. CADnm-RNAi RAGE 2.0 Library .....  | 223 |
| 5.2.5. PK2M3nm-RNAi RAGE 2.0 Library .....  | 227 |
| 5.2.6. PK2M3nm-PAID6 CRISPR-AID Library .....   | 230 |
| 5.2.7. Fermentation .....   | 233 |
| 5.3 Conclusion .....  | 233 |
| 5.4 Future Work.....  | 234 |
| 5.5 Experimental Procedures .....   | 235 |
| 5.5.1. Strains and Media and Culture Conditions .....   | 235 |
| 5.5.2. Plasmid Construction.....  | 237 |
| 5.5.3. Construction of Genetically Manipulated Strains .....  | 238 |
| 5.5.4. Analytical Methods.....  | 239 |
| 5.5.5. Bromocresol Green Assay .....  | 239 |
| 5.5.6. LOD Assay.....   | 239 |

|   |     |
|---|-----|
| 5.5.7. Sensor Activity Assays .....             | 240 |
| 5.5.8. Library Construction and Screening ..... | 241 |
| 5.6 References.....                             | 242 |



# CHAPTER 1. Introduction

## 1.1 Biocatalysis

Biocatalysis is defined as the use of enzymes in their purified form, as part of cell lysates, or whole cells to convert a molecular substrate into a product of interest.<sup>1</sup> In 1858, biologist Louis Pasteur provided the first example of modern biocatalysis by realizing the resolution of racemic tartaric acid through fermentation with microorganisms, such as the common mold *Penicillium glaucum*. He also laid the foundation of stereochemistry in those experiments where (-)-tartaric acid was accumulated while (+)-tartaric acid was consumed. At the end of the 19<sup>th</sup> century, the specific action of an enzyme with a specific substrate was explained using a “Lock and Key” analogy and it was firstly postulated by Emil Fischer.<sup>2</sup> Meanwhile, Eduard Buchner discovered the cell-free fermentation for biocatalytic processes.<sup>3</sup>

Those milestones led to discovery and development of numerous biocatalytic processes in the 20<sup>th</sup> century. Especially the unique characteristics and benefits of biocatalysis have kept on drawing biochemists’ strong interests in pushing the boundaries of natural-occurring biotransformations and bringing biocatalysis to industrial applications. Enzymes can be considered as green catalysts. Unlike transition metal-based chemical catalysts that rely on mining and harsh, energy intensive process conditions, biocatalysts are biodegradable and easily replaced through inexpensive and environmentally friendly fermentation processes. Transition metal catalysts normally have high turnover numbers (TONs), but the economic burden posed by enzymes can potentially be further minimized by engineering more active variants than that being found in nature, optimizing the expression efficiencies and fermentation yields, improving the enzymatic

stabilities, and immobilizing the enzymes for recycling. More importantly, the high regio-, stereo- and enantioselectivity of biocatalysis make it an invaluable alternative in pharmaceutical industries.

One famous example on how enzymes can improve industrial chemical processing is acrylamide synthesis. As an alternative to Cu or Mg based chemical catalysis method, the use of nitrile hydratases has now converted acrylonitrile to acrylamide, the monomer used to prepare polyacrylamide, on tens of thousands of metric tons per year.<sup>4</sup> The replacement largely reduced the catalyst waste generated per kilogram of the products. Another powerful example of biocatalytic applications exploiting the chiral nature of these catalysts is the use of ene-reductases to prepare a chiral precursor of pregabalin, the active agent in Lyrica<sup>®</sup> for treatment of epilepsy, neuropathic pain, fibromyalgia and generalized anxiety disorder.<sup>5</sup> The manufacturing process of pregabalin involving old yellow enzymes (OYEs) has been patented by Pfizer Manufacturing Ireland.

One of the major reasons prohibiting the broad application of biocatalysis in manufacturing of chemicals is that limited unnatural reactions could be catalyzed by biocatalysts. Beginning in the late 1970s with pioneering work of Michael Smith and later amplified by contributions from Pim Stemmer and Frances Arnold, microbiologists began developing techniques that enabled directed evolution of enzymes.<sup>6-8</sup> This approach has been successfully used to engineer or customize the enzymes that react with unnatural substrates or under unnatural reaction conditions that are different from those found in natural systems. For example, carbonic anhydrase has been engineered to sustain catalytic activity at 107 °C at pH > 3;<sup>9</sup> and proteins have been engineered to deliver chemical reactions such as enantioselective cyclopropanations,<sup>10</sup> silylations,<sup>11</sup> and borylation<sup>12</sup> reactions which are unprecedented in nature.

There are also several applications of engineered biocatalysts in the pharmaceutical industry. Early examples include the development of a ketoreductase (CDX-026) capable of reducing the large, hydrophobic ketone substrate **1** to yield alcohol **2**. **2** serves as a precursor to montelukast, widely used to treat asthma and seasonal rhinitis (Figure 1A).<sup>13</sup> A Baeyer-Villiger monooxygenase (BVMO) has also been engineered to enantioselectively oxidize sulfide **3** to provide esomeprazole **4**, used to treat acid reflux (Figure 1B). An engineered transaminase successfully converted the sitagliptin ketone **5** to sitagliptin **6**, a DPP4 inhibitor used for the treatment of type II diabetes (Figure 1C).<sup>1</sup>

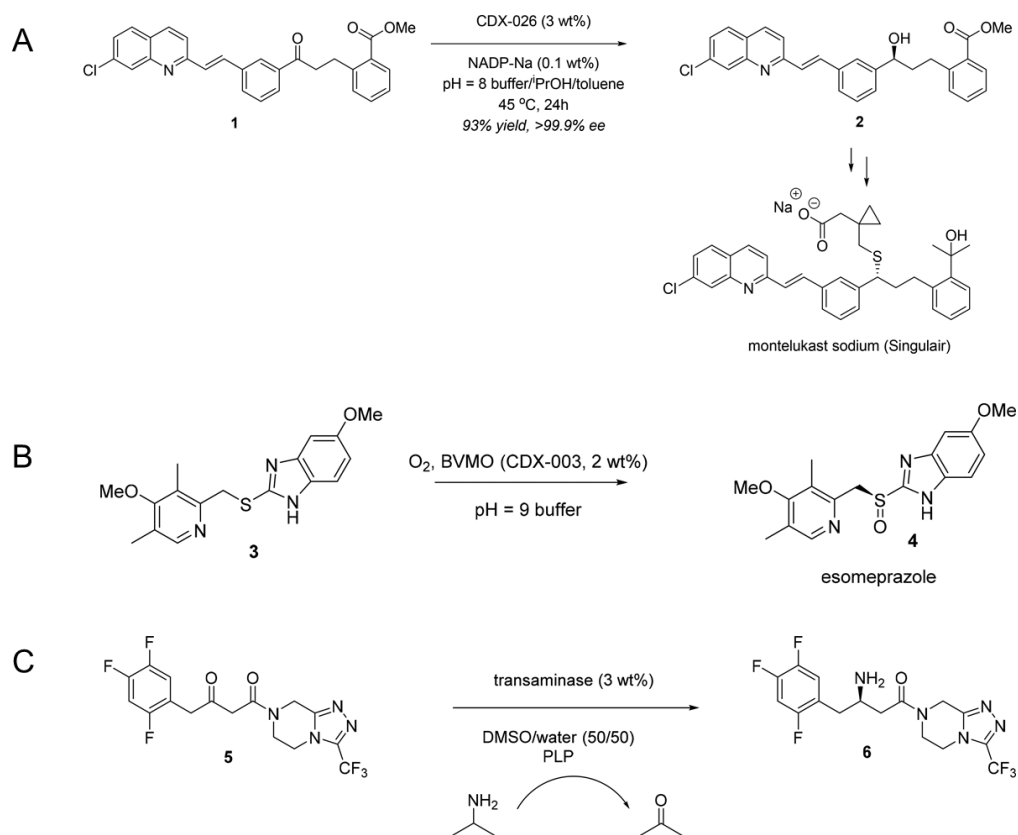


**Figure 1.1.** A) Biocatalytic approach to montelukast; B) BVMO catalyzed sulfide oxidation to produce esomeprazole; C) Preparation of sitagliptin using an engineered transaminase.

In addition to directed evolution, several new strategies in biocatalysis also have been developed and applied to further broaden the substrate scope, reaction type and reaction condition

of current biocatalysis applications. Those strategies include but are not limited to development of artificial metalloenzymes, enzyme catalyzed protein conjugations, biocatalytic cascades, chemoenzymatic tandem reactions, computational and library design strategies for enzyme engineering, and metabolic pathways for chemical biosynthesis. In my study, I focused on studying naturally-occurring biocatalytic cascade reactions, developing in vitro chemoenzymatic transformations and engineering metabolic pathways for chemical overproduction.

## 1.2 Natural Product Synthesis: How Nature Make Complex Molecules

In living organisms, an individual enzyme catalyzes limited simple reactions, but the cooperative action of a series of enzymes build up complex molecules from simple molecules to support the biological functions such as generation or storage of energy, and environmental sensing and communication. The cascade or concurrent reactions catalyzed by multiple enzymes demonstrate the strongest synthetic power in nature, which makes an irreversible process reversible, eliminates inhibition problems caused by excess product, or circumvents the lack of substrate scattered in bulk solution.

Natural products are chemical compounds synthesized by a series of enzymes working cooperatively in organisms. Natural products have played key roles over the past century in the development of medicine. More than two-thirds of clinically used antibiotics are natural products or their semisynthetic derivatives.<sup>14</sup> Studying the biosynthetic mechanisms of natural products also enables us to gain deeper insights into enzymatic teamwork, thus enlightening us design artificial enzymatic cascades for selective synthesis of valuable compounds.

Type II polyketide synthase is one of the best examples to demonstrate production of aromatic polyketides by teamwork between enzymes. Type II polyketides comprise a large class

of structurally and functionally diverse bacterial natural products. This class is rich in pharmacologically relevant compounds, especially anticancer agents. In analogy to type II bacterial and plant fatty acid synthases, type II polyketides are comprised of several individual enzymes encoded by the genes clustered in the same region in the genomic DNA. Although different type II polyketides have very diverse structure, they all share a minimal set of iteratively used enzymes, each expressed from a distinct gene. In general, this so-called ‘minimal PKS’ consists of two ketosynthase units ( $KS_{\alpha}$  and  $KS_{\beta}$ ) and an acyl carrier protein (ACP), which serves as an anchor for the growing polyketide chain. With a few exceptions, genes encoding these three proteins are grouped together, and show a typical  $KS_{\alpha}/KS_{\beta}/ACP$  architecture. Additional PKS subunits, including ketoreductases, cyclases and aromatases define the folding pattern of the nascent poly- $\beta$ -ketone intermediates. Finally, the polyphenols are tailored by oxygenases, glycosyl and methyl transferases to different compounds with diverse structures (Figure 1.2).

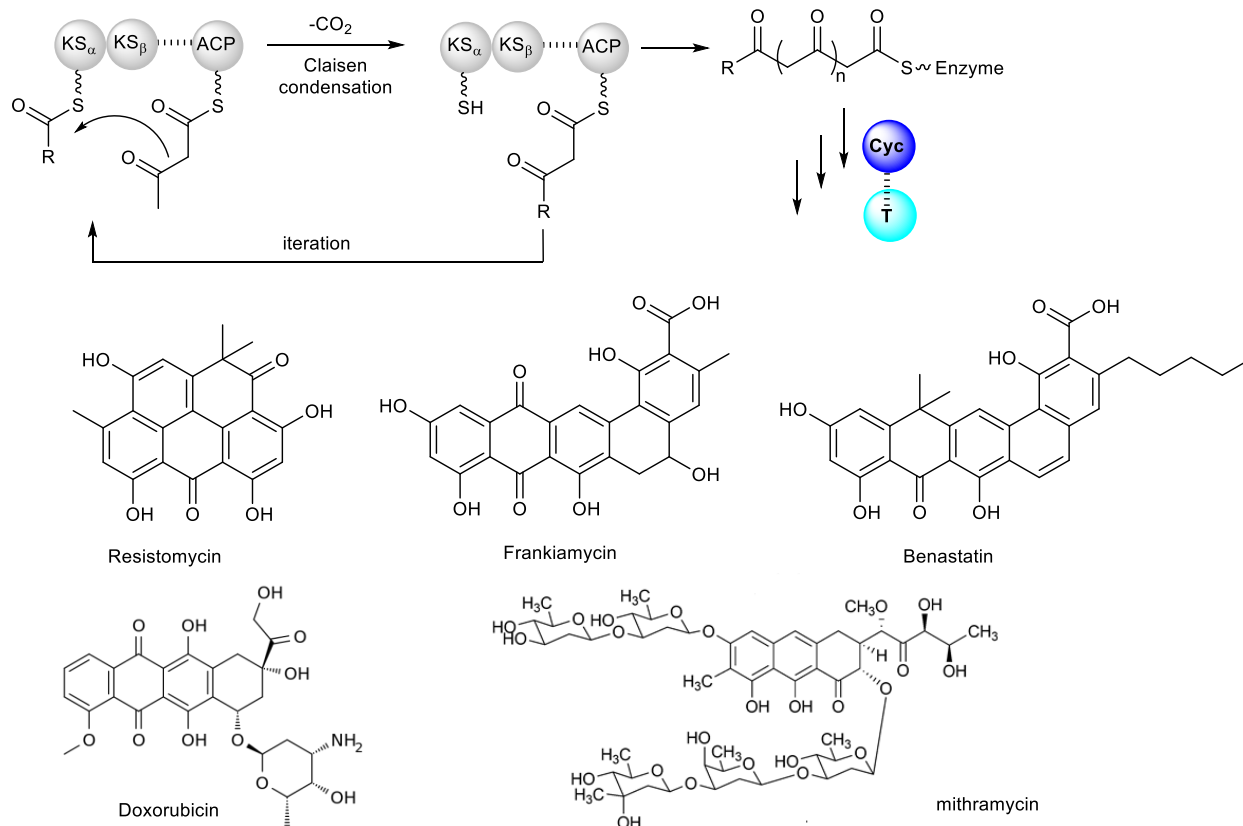


**Figure 1.2.** Schematic of type II polyketide synthase. Type II PKS gene clusters encode dissociable polyketide synthase assemblies. The minimal polyketide synthase (min-PKS) consists of three proteins: KS $\alpha$ , KS $\beta$ , and ACP. The nascent polyketide chains, ranging from 16 to 30 carbons, are constructed by iterative condensation of malonyl-CoA catalyzed by min-PKS. The reactive beta-keto chains are converted into structurally diverse molecules by the action of tailoring enzymes (T) including cyclases (Cyc) and reductases, giving rise to final branching, oxidation state, and cyclization pattern.

Although natural products have been and continue to be the source and inspiration for a substantial fraction of human therapeutics and knowledge of biology, the discoveries of natural products with new structure and unique synthesis mechanism have been greatly hindered within recent decades. With the advent of fast and inexpensive next generation sequencing technologies, additional numerous silent biosynthetic gene clusters (BGCs) coding uncharacterized secondary metabolites have been identified and they are the rich sources for the discovery of new compounds and enzymes. Because natural products encoded by silent BGCs are hard to be detected using

current analytical methods due to minimal or zero BGCs expression under laboratory conditions, strategies to activate BGC expression and trigger metabolite production are critical to realize the full potential of nature's chemical repertoire. While heterologous expression bypasses native regulation networks and can be engineered rationally, the entire biosynthetic pathways, often spanning large areas of genomes, will have to be cloned and refactored.<sup>15</sup> Importantly, some natural products cannot be produced in heterologous hosts due to lack of regulatory, enzymatic, or metabolic requirements for product biosynthesis. Technologies that improve the genetic manipulation of native hosts will expedite discovery and study of the BGCs in their native contexts. In the first part of the thesis, an efficient CRISPR-Cas9 knock-in strategy has been developed to activate silent BGCs in *Streptomyces viridochromogenes*. A new type II polyketide has been characterized and its corresponding synthetic enzymes has been identified.

### 1.3 *In vitro* Tandem Catalytic Reactions for Biochemical Productions

The synergistic effect of natural synthetic networks inspires chemists to develop artificial multi-step tandem reactions for selective synthesis of complex molecules.<sup>16</sup> To date, tandem reactions by using whole microorganisms (*in vivo*) have been extensively studied in the synthetic biology and metabolic engineering fields.<sup>17</sup> There are growing interests to build cooperative tandem reactions by coupling multiple enzymes or organometallic catalysts with biocatalysts *in vitro* since the resulting catalytic systems are simpler for optimization, generate less side products and waste, and allow for easy product purification.<sup>18</sup>

To date, *in vitro* tandem enzymatic reactions have been well developed for the preparation of alcohols, acids and their derivatives, amino acids, amines, nucleosides/nucleotides, nucleosides/nucleotides derivatives, oligosaccharides and glycoconjugates.<sup>19</sup> The field of tandem

chemo-enzymatic reaction is still in its infancy.<sup>20</sup> Recently lipase has been successfully coupled with various transition metal complexes for readily deracemizing secondary alcohols and primary amines.<sup>21</sup> This accomplishment clearly shows the advantages of multistep one-pot processes, so-called tandem reactions. Compared with step-wise synthesis, one-pot tandem reactions improve overall synthetic efficiency and reduce waste generation by avoiding intermediate purification steps. Additionally, tandem reactions improve the overall asymmetric synthesis efficiency by converting achiral substrates to single enantiopure product containing a single enantiomer. Last but not least, the cooperative effect among different catalytic steps enhances the selectivity and activity by an equilibrium process.

However, combining multiple enzymes or enzymes with chemical catalysts in a tandem process is not simply replicating the catalytic behavior of each catalyst. For multi-enzymatic reactions, several strategies have been developed to balance the reaction rate of each step and maintain enzymatic activity under reaction conditions, including cell free metabolic engineering (CFME) and modeling.<sup>22</sup> Protein engineering methods have been applied, such as protein immobilization and fusion protein construction, to improve the overall efficiency of multi-enzymatic reactions.<sup>23,24</sup> Specifically, it is more challenging to find conditions to enable catalytic activity of organometallic catalysts and biocatalysts in one-pot due to incompatibility and mutual inactivation. To overcome those difficulties, several novel strategies have been developed, including supramolecular assembly and compartmentalization.

### 1.3.1. Enzymatic Tandem Reactions

From aerobic respiration to photosynthesis, millions of compounds are synthesized through enzymatic reactions during the lifespan of all living organisms. These compounds, even those with very complex structures, are converted from simple chemical resources such as glucose, through



the metabolic network in the cell. Tandem enzymatic reactions, or pathways in other words, can be considered as subunits of the whole metabolic network. Although enzymatic reactions have long been used for chemical synthesis due to many of their excellent features, particularly the high selectivity and specificity, multiple tandem enzymatic reaction systems developed by chemists recently are not simple combinations of enzymatic reactions catalyzed by individual enzymes. Besides all the advantageous properties of enzymatic reactions, tandem enzymatic reactions can be much more cost-effective by using inexpensive substrates, potentially making them economically feasible. Moreover, one-pot tandem enzymatic reactions simply avoid the purification of the intermediates, which makes the process more efficient than step-wise enzymatic reactions.

While such tandem enzymatic reactions can be accomplished *in vivo*, as widely used in today's fermentation industry, there are many advantages to use *in vitro* systems. First, as no competing pathways exist in the *in vitro* system and no metabolic burden or toxicity issues need to be considered, the yield can be much closer to the theoretical yield than the *in vivo* system. Second, due to its simplicity, it would be more practical and effective to optimize the system through modeling and adjusting the enzymes' concentrations. Moreover, artificial tandem enzymatic reactions which can produce non-natural compounds are readily set up without potential toxicity issues brought by the product. In the past decade, many tandem enzymatic reaction systems have been developed to produce tremendous chemicals.<sup>25</sup>

Although *in vitro* tandem enzymatic reactions have a number of advantages over *in vivo* tandem enzymatic reactions, their weaknesses are also obvious, with the main weakness being the decreased flexibility. For example, most of the tandem reactions only include two or three enzymes. For example, through computational design, researchers have engineered the promiscuous aldolase

RA95.5-8 to catalyze asymmetric Michael additions and Knoevenagel reactions via Schiff base intermediates. Recently Hilvert's group discovered novel activities of those aldolase variants. The variant RA95.5-8F can catalyze the synthesis of (*R*)-methodol from acetone and 6-methoxy-2-naphthaldehyde, while the variant T53L/K210H RA95.5-8 can catalyze the dehydrated (*R*)-methodol to  $\gamma$ -nitroketones<sup>26,27</sup>. By combination of those two aldolase variants, they achieved similar yield and stereoselectivity in one-pot as the reaction using the purified intermediate (Figure 1).

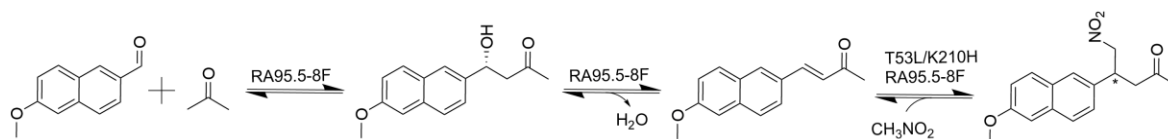


**Figure 1.3.** Synthesis of  $\gamma$ -nitroketones by aldolase variants.<sup>27</sup>

In principle, an ideal *in vitro* tandem reaction system should be sufficiently flexible to generate a broader product scope while using the low-cost substrates. Therefore, *in vitro* tandem reaction systems with higher complexity for synthesizing chemicals, such as carbohydrates, fuels, and fine chemicals are desired.<sup>28-32</sup> In recent years, great efforts were spent in the emerging CFME field to address such a challenge.<sup>22</sup> A CFME system usually involves four or more enzymes and uses inexpensive substrates if possible, as the cost-effectiveness is a required design criteria.<sup>33,34</sup> Ideally, it should combine catabolic pathways and anabolic pathways, so that both the building blocks and the energy for synthesizing the target molecules can be generated from simple resources, such as glucose. However, the design and test of such a system would be very challenging as tens of enzymes might be involved.<sup>35</sup> Recently, Bowie and coworkers successfully combined the Embden-Meyerhof-Parnas glycolytic pathway and the mevalonate pathway to produce monoterpenes.<sup>36</sup> A super-complex system with 27 enzymes was reconstituted in one-pot which enabled the system to synthesize monoterpenes by using glucose as the only substrate. While

specific designs, such as the enzymatic purge valve nodes, helped the catabolic pathway and the anabolic pathway work harmonically in the system.<sup>37</sup> By switching the monoterpene synthases in the system, different types of monoterpenes such as limonene, pinene and sabinene can be produced. This system can produce monoterpenes with titers an order of magnitude higher than the cellular toxicity limit (15 g/L) with an almost theoretical yield (>95%), which demonstrates the great advantage of using enzymatic tandem reaction *in vitro*.

In addition to transferring the existing pathways from *in vivo* to *in vitro*, scientists are also able to design *de novo* complex pathways, which can accomplish difficult biosynthetic tasks. In 2017, the crotonyl-coenzyme A (CoA)/ethylmalonyl-CoA/hydroxybutyryl-CoA (CETCH) cycle was constructed by Erb and coworkers, which provides a seventh CO<sub>2</sub> fixation pathway besides the six naturally evolved ones (Figure 1.4).<sup>38</sup> Instead of being restricted to known enzymes, the researchers sought for all reactions that are biochemically feasible. Multiple cycles were designed from scratch and their thermodynamic feasibility was evaluated. Then, enzymes that can catalyze the reactions in the CETCH cycle were identified from bioinformatics databases and characterized individually *in vitro*. After combining the auxiliary proofreading and cofactor regeneration processes, the CETCH cycle involves 17 enzymes in total which came from nine different organisms from all three domains of life. Through enzyme engineering and metabolic proofreading, the CETCH cycle can convert CO<sub>2</sub> into organic molecules at a rate of 5 nanomoles of CO<sub>2</sub> per minute per milligram of protein.

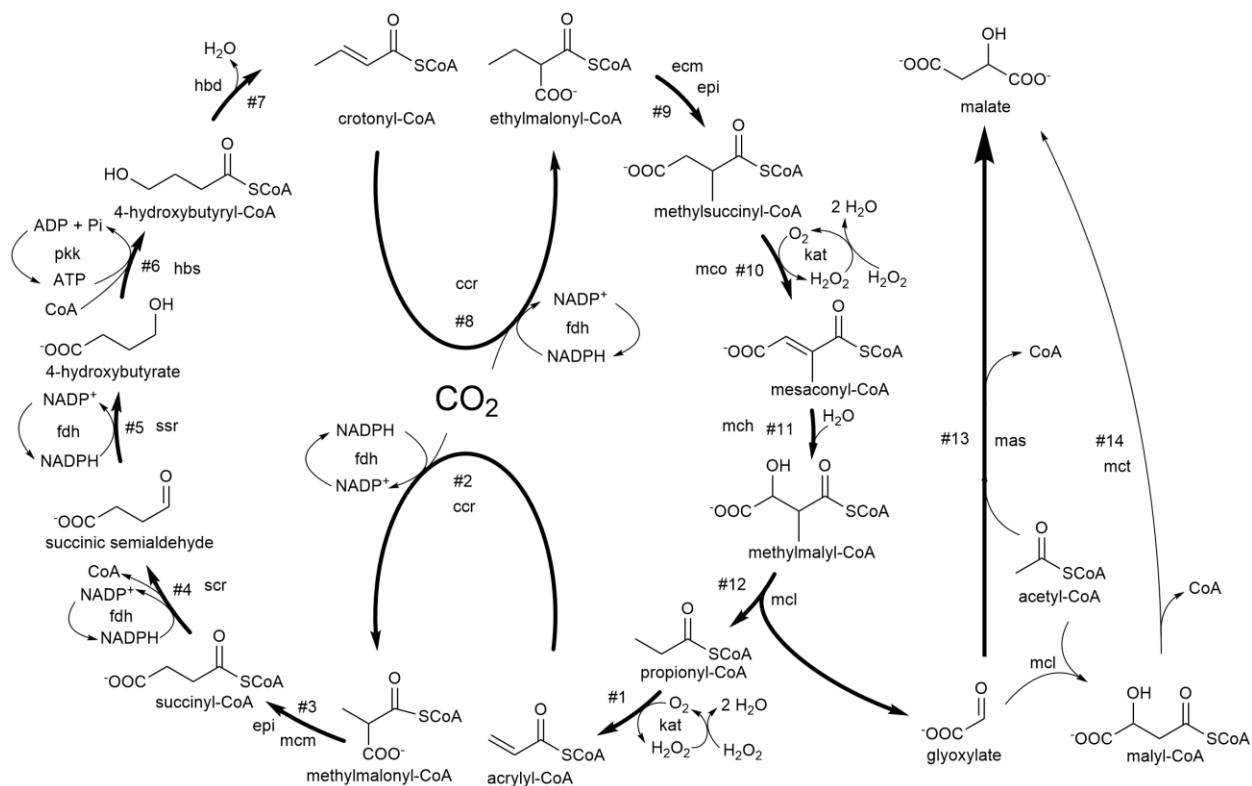


**Figure 1.4.** The CETCH cycle contains 17 enzymes from 9 different organisms, which can convert  $\text{CO}_2$  into organic molecules at a rate of 5 nanomoles of  $\text{CO}_2$  per minute per milligram of protein<sup>38</sup>. Ccr: crotonyl-CoA carboxylase/reductase; Ecm: ethylmalonyl-CoA mutase; Epi: ethylmalonyl-CoA/methylmalonyl-CoA epimerase; Fdh: formate dehydrogenase; Hbd: 4-hydroxybutyryl-CoA dehydratase; Hbs: 4-hydroxybutyryl-CoA synthetase; Kat: katalase; Mas: malate synthase; Mch: mesaconyl-CoA hydratase; Mcl:  $\beta$ -methylmalyl-CoA lyase; Mcm: methylmalonyl-CoA mutase; Mco: methylsuccinyl-CoA oxidase; Mct: malyl-CoA thioesterase; Pco: propionyl-CoA oxidase; Pkk: polyphosphate kinase; Scr: succinyl-CoA reductase; Ssr: succinic semialdehyde reductase.

### 1.3.2. Chemoenzymatic Tandem Reactions

Organometallic catalysis and biocatalysis are two different disciplines in terms of reaction categories, catalytic conditions, substrates scopes and selectivities. Organometallic catalysts have wide substrate scopes and high productivity and are still the key for bulk chemical manufacturing. Biocatalysis is becoming more widely used in the pharmaceutical industry due to its high regio-, stereo- and enantioselectivity, and growing advances in enzyme discovery and engineering. To access the advantages of both catalytic disciplines, there is a growing interest to combine

organometallic catalysts in tandem with enzymes to realize synthetic power that cannot be achieved by either of them alone.<sup>20,39</sup>

Unlike developing tandem enzymatic reactions, it is more challenging to combine organometallic catalysts and biocatalysts due to incompatibility and mutual inactivation of metal complexes and enzymes. Up to date, only lipases and serine proteases could maintain high catalytic activity in organic solvents and at high temperature. Similarly, most transition-metal complexes are inhibited in aqueous solution with or without cellular components. In this section, we will summarize the major tandem chemo-enzymatic reactions developed in organic solvent and aqueous buffer solutions, and discuss the novel strategies used to combine organometallic catalysts with biocatalysts in one-pot.

#### 1.3.2.1. One-pot Chemo-enzymatic Reactions in Organic Solvent

Dynamic kinetic resolution (DKR) of alcohols and amines based on transition metal-catalyzed racemization and lipase-catalyzed resolution in pure organic solvent has been developed towards a mature technology for preparation of enantiopure secondary alcohols and primary amines (Figure 1.5). Lipase deracemizes a mixture of enantiomers by selectively acylating desired enantiomer. The drawback of such enzymatic kinetic resolution is that a maximum yield of only 50% can be obtained. However, it can be resolved by using a racemization catalyst to replenish the consumed enantiomer and drive the resolution up to 100% yield of desired enantiomer. Since the pioneering demonstration of the DKR concept by the group of Williams,<sup>40</sup> Bäckvall<sup>41</sup> and Kim,<sup>42</sup> intense studies were conducted to develop efficient racemization catalysts, improve enzyme stability and expand substrate scope.<sup>20,21</sup> To date, immobilized *Candida antarctica* lipase B (CALB) and *C. antarctica* lipase A (CALA) are the best enzymes of choice due to their robustness and activities in pure organic solvent at elevated temperature up to 100 °C.<sup>43</sup>

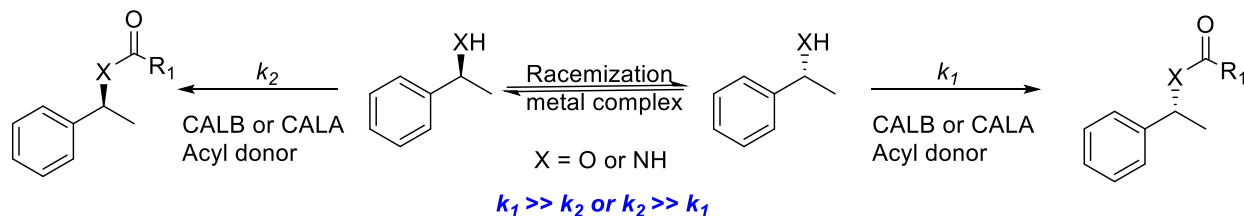


**Figure 1.5.** Dynamic kinetic resolution of amines or alcohols by coupling CALB or CALA in tandem with racemization catalysts.

Ruthenium, iridium, alumina and vanadium complexes are the most well-developed catalysts for alcohol racemization. They were used in tandem with various lipases to deracemize a wide range of functionalized secondary alcohols, including aliphatic, allylic alcohols, chlorohydrins, diols, homoallylic alcohols, and *N*-heterocyclic 1,2-amino alcohols,  $\alpha$ -hydroxyl ketones with excellent yields and enantiomeric excess (*ee*).<sup>21</sup> Besides the above-mentioned homogeneous catalysts, heterogeneous acids, zeolites<sup>44,45</sup> and vanadium based mesoporous silica<sup>46</sup> were also reported as racemization catalysts of secondary alcohols. The DKR of amines is more challenging due to a lack of efficient racemization catalysts. To date, coupling ruthenium complexes, analogues of Shvo catalyst, with CALB is the most practical approach for DKR of aliphatic or benzylic primary amines at 90 °C.<sup>21</sup> In recent years, Pd nanoparticles-based heterogeneous catalysts were employed for racemization of benzylic primary amines under mild conditions. However, they did not work well for aliphatic amines.<sup>47</sup>

### 1.3.2.2. One-pot Chemo-enzymatic Reactions in Aqueous Solutions

Except for lipases and serine proteases, most biocatalysts have poor stability in organic solvents and at elevated temperature. In the past 20 years, there has been a growing interest to develop tandem reactions in aqueous solutions to combine unique transformations catalyzed by organometallic catalysts and biocatalysts.<sup>20</sup> The major motivation to associate biocatalysts with

organometal catalyst in one pot is to utilize the synthetic power from each discipline for specific transformations that could not be realized by either of them alone. In nature, enzymes have specific substrate binding site for highly regio- stereo- and enantioselective synthesis. Accordingly, organometallic catalysts could access some reactions that enzymatic processes do not exist or work only on limited substrate scope, for example, hydrogenation, cross-coupling reaction, Wacker-oxidation, olefin metathesis, etc.

Unlike the DKR system in organic solvents, the development of tandem chemo-enzymatic reactions in aqueous solution is still in its infancy. The number of transformations amenable to these processes are small portion of catalytic reactions reported in organometallic chemistry or synthetic biology. Table 1.1 summarizes the representative work of one-pot chemo-enzymatic reactions that can occur in aqueous-based solution. They are metal-catalyzed hydrogenation in tandem with isomerase or hydrolase catalyzed reactions; organometallic-catalyzed racemization in tandem with enantioselective hydrolysis; Pd/Cu catalyzed Wacker oxidation in tandem with enzymatic catalyzed asymmetric reduction or reductive amination; metal-catalyzed metathesis in tandem with enzymatic decarboxylation, ester hydrolysis or P450-catalyzed epoxidation; metal-catalyzed cross coupling in tandem with enzymatic reduction, oxidation and hydrolysis; Au catalyzed isomerization in tandem with enzymatic hydrolysis.

Those reactions were either performed in one-pot sequential manner by avoiding the purification of intermediates when different reaction conditions are required for organometallic and enzymatic step, or in concurrent manner when two catalytic steps are compatible with each other. Enlighteningly, a few cooperative concurrent reactions were reported to reveal the significance of tandem reactions compared with the sequential transformations. For example, Zhao and Hartwig groups jointly reported an example of Ru-catalyzed olefin metathesis coupled with a

P450-monoxygenase that selectively oxidized one of the cross-metathesis products against others.

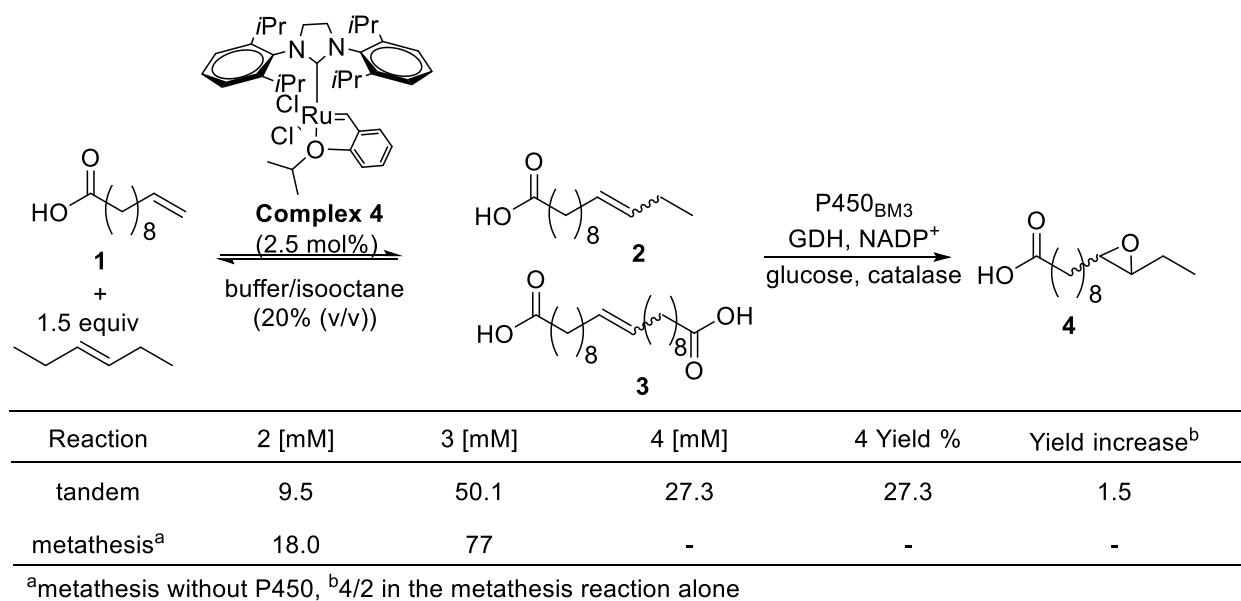
The overall yield of concurrent reactions is 1.5 times higher than the sequential one (Figure 1.6).<sup>48</sup>

Table 1.1. Typical one-pot tandem chemo-enzymatic reactions in aqueous solution

| Organometal Catalysts                               | Comments      | Enzymatic Reaction                                  | Reaction Type              | Product  | Citation |
|---|---------------|---|----------------------------|--|----------|
| Pt (hydrogenation)                                  | HE/Whole cell | D-glucose isomerase/<br>monoamine oxidase           | concurrent/<br>cooperative | D-mannitol/ Chiral<br>quinoline                        | 49-51    |
| Rh (hydrogenation)                                  | HE            | hydrolase   | sequential                 | L-alanine  | 52       |
| Pt (racemization)                                   | HO            | hydrolase   | DKR                        | Enantiopure allyl<br>alcohol                           | 40       |
| Pyridoxal 5-phosphate<br>(racemization)             | HO            | hydrolase   | DKR                        | L-amino acid   | 53       |
| Fe (Hydrogenation-<br>racemization)                 | HO            | lipase (acylation)                                  | cooperative                | Enantiopure secondary<br>alcohol                       | 54       |
| Pd/Cu (Wacker oxidation)                            | HO/Compat.    | (R) - ADH (ketone<br>reduction)                     | sequential/<br>concurrent  | Chiral alcohols  | 55,56    |
| Pd/Cu (Wacker oxidation)                            | HO/Compat.    | transaminase<br>(asymmetric reductive<br>amination) | concurrent                 | Chiral amines  | 57       |
| Ru (metathesis)                                     | HO/Compat.    | decarboxylase<br>(Decarboxylation)                  | concurrent                 | Antioxidant 4,4'-<br>dihydroxylstilbene<br>derivatives | 58       |
| Ru (metathesis)                                     | HO            | esterase (Hydrolysis)                               | sequential                 | Cyclic malonic acid<br>monoesters                      | 59       |
| Ru (metathesis)                                     | HO/biphasic   | P450 (epoxidation)                                  | cooperative<br>/sequential | Epoxide  | 48,60    |
| Ru (metathesis)                                     | HC            | MAO-N (Aromatizing)                                 | concurrent                 | Pyrrolines   | 61       |
| Pd (Suzuki-coupling)                                | HO            | ADH (Ketone reduction)                              | concurrent<br>/sequential  | Chiral biaryl alcohol                                  | 62,63    |
| Ir (Barbier-type coupling)                          | HO            | galactose (alcohol<br>oxidation)                    | sequential                 | Homoallylic sec-<br>alcohols                           | 64       |
| Pd (Heck coupling)                                  | HE            | (R)-ADH (Ketone<br>reduction)                       | sequential                 | 4-(4-Methoxyphenyl)-<br>butan-2-one                    | 65       |
| Rh (diazo-coupling)                                 | HO            | ene-reductase<br>(reduction)                        | sequential                 | Chiral 2-aryl-substitued<br>succinate derivatives      | 66       |
| Au (cycloisomerization)                             | HO            | lipase (hydrolysis)                                 | concurrent                 | 2,5-dihydrofurans                                      | 67       |
| Au (hydroalkoxylation)<br>Ru (olefin isomerization) | Supramol.     | esterase/lipase/ADH                                 | concurrent                 | Substituted<br>tetrahydrofuran<br>/propanal            | 68       |
| Organocatalytic aldol<br>reaction                   | HO            | ADH   | Concurrent                 | 1,3-Diols  | 69       |
| Potassium phosphate<br>(cyclization)                | HO            | carbolygase/transaminase                            | Sequential                 | Trisubstitued<br>tetrahydroisoquinolines               | 70       |

Abbreviation: HO: homogeneous catalysts, HE: heterogeneous catalysts, Compat.: compartmentalization, Supramol. Supramolecular encapsulation, HC: whole cell.





**Figure 1.6.** Concurrent olefin cross-metathesis/epoxidation of 10-undecenoic acid with *trans*-3-hexene.

Chemocatalysts have also been extensively used to support the catalytic function of enzyme. The practical applications of one of the largest classes of enzymes, oxidoreductases, contributing to producing critical chemicals and pharmaceuticals, are limited by the dependence on high cost and instable cofactors that have to be regenerated. So far, NADP(H) regeneration by enzymes has been well-developed and applied practically at industrial scale. However, large quantity of water-soluble byproducts generated causes enzyme deactivation and requires costly downstream purification. As a result, more cofactor generation methods have been researched and developed to target the goals of sustainability and productivity, including chemical, homogeneous catalytic, electrochemical, photocatalytic and heterogeneous catalytic approaches.<sup>71,72</sup> Importantly, visible-light photoredox catalysis has entered the realm of biocatalysis to form a synergistic framework to circumvent the application of cofactors.<sup>73-75</sup> Recently, Park and co-workers employed eosin Y as a photosensitizer directly transferring photoinduced electrons to P450 heme domain under illumination.<sup>76</sup> Instead of coupling with oxidation enzyme, Park and co-workers realized the direct

activation of ene-reductases by transferring photoexcited electrons from xanthene dyes to prosthetic flavin moiety, for the asymmetric reduction of C=C bonds.<sup>76</sup> Although this technology is still in its infancy, it is the first case to realize direct electron transfer from water to enzyme with O<sub>2</sub> as the sole by product.

### 1.3.2.3. Novel Strategies to Combine Transition Metals and Enzymes in One-pot Tandem Reactions

Incompatibility of the individual reaction steps with one another is the major challenge to combining transition metal catalysts with biocatalysts in one-pot. Besides immobilized lipases and serine proteases, the majority of biocatalysts have poor stability in organic solvents. Most of the transition metal catalysts are not active in aqueous solution. Mutual inactivation also occurs frequently due to the coordination of the transition metal complex to the protein catalysts. In this section, we will discuss some novel strategies developed so-far to combine transition metals and enzymes in one-pot, including supramolecular assemblies, artificial metalloenzymes, compartmentalization, whole cells, and co-immobilization (Table 1.2).

**Table 1.2.** The novel strategies to couple transition metals (or chemical catalysts) with enzymes in one-pot tandem reactions.

| Strategy  | Advantages   | Tandem Reactions   |
|---|--|--|
| Supramolecular Assembly (Artificial metalloenzyme ) | <ul style="list-style-type: none"> <li>realize catalytic activity of metal catalysts in aqueous solution</li> <li>stabilize metal complexes and improve turn over number (TON)</li> <li>prevent interaction of metal complexes with enzymes</li> <li>provide extra selectivity of metal catalysts</li> </ul> | <ul style="list-style-type: none"> <li>Au or Ru in tandem with esterase, lipase, ADH;</li> <li>Ir in tandem with oxidoreductases</li> </ul>  |
| Compartmentalization                                | <ul style="list-style-type: none"> <li>protect enzyme from organic solvent</li> <li>protect metal catalysts from aqueous solution</li> <li>prevent mutual inactivation</li> </ul>  | <ul style="list-style-type: none"> <li>Ru in tandem with decarboxylase;</li> <li>proline in tandem with ADH;</li> <li>Wacker oxidation in tandem with enzymatic reduction or hydroamination</li> </ul> |

Table 1.2. cont.

|                   |  |  |
|-------------------|--|--|
| Whole-cell        | <ul style="list-style-type: none"> <li>• protect biocatalysts from metal catalysts</li> <li>• prevent interaction of metal with cellular components</li> <li>• avoid protein purification</li> </ul> | <ul style="list-style-type: none"> <li>• Pd(0)-catalyzed reduction in tandem with monoamine oxidation</li> </ul>                         |
| Co-immobilization | <ul style="list-style-type: none"> <li>• stabilize metal catalysts</li> <li>• improved synergic effect</li> <li>• catalyst regeneration</li> </ul>   | <ul style="list-style-type: none"> <li>• CALB and Pd nanoparticles co-immobilized into the mesoporous silica for DKR of amine</li> </ul> |

Incorporation of transition metal complexes within supramolecular hosts is a valuable way to solve those problems. A long-term goal of supramolecular chemistry is construction of assemblies that mimic the desirable qualities of protein catalysts.<sup>77</sup> It has been found that supramolecular assemblies could stabilize reactive metal complexes and increase their turn over numbers.<sup>78</sup> Additionally, supramolecular complexes enable the catalytic activity of several transition metal catalysts in water by providing a bio-inspired hydrophobic cavity.<sup>79-81</sup> Importantly, supramolecular cage prevents the direct interaction of transition metal with enzymes, thereby averting their mutual inactivation.<sup>68,82</sup> Lastly, supramolecular assemblies provide extra stereo-, regio- and enantio-selectivity by providing a well-defined cavity for the reaction compared with the reaction performed in bulk solvent.<sup>83,84</sup> Using a supramolecular approach, Toste and coworkers created various tandem reactions employing esterases, lipases or alcohol dehydrogenase with gold (I) or ruthenium (II) complexes encapsulated in a Ga<sub>4</sub>L<sub>6</sub> tetrahedral supramolecular cluster without mutual inactivation (Figure 1.7).<sup>68</sup> Their findings suggested that supramolecular assemblies may provide a general strategy for carrying out classic organic reactions in tandem with enzymatic reactions in aqueous solution.

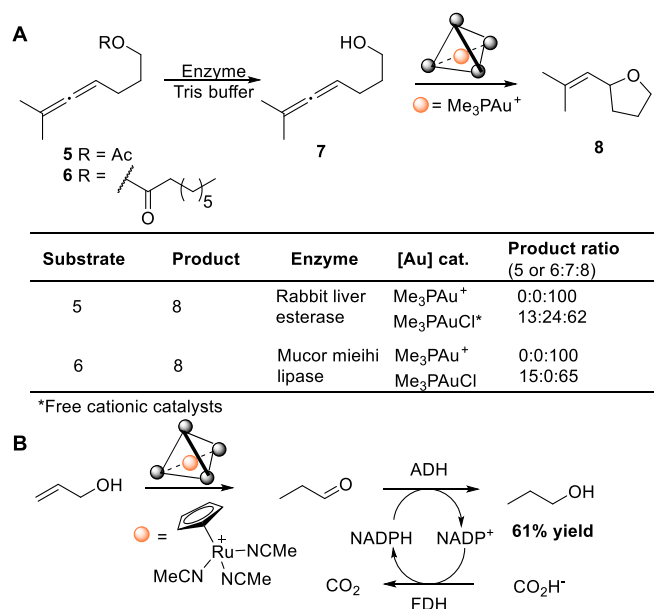


**Figure 1.7.** A, Esterase- or lipase-mediated acetate hydrolysis followed by Au (I)-catalyzed hydroalkoxylation. B, Ru(II)-mediated olefin isomerization followed by ADH-catalyzed reduction.<sup>68</sup>

Artificial metalloenzyme resulting from encapsulation of transition metal catalyst within a protein scaffold is a special form of supramolecular host-assemblies. Ward and coworkers developed an artificial (*R*)-selective transfer-hydrogenase (ATHase) by incorporation of a biotinylated [Cp\*Ir(Biot-*p*-L)Cl] complex within streptavidin (Sav). Sav worked as a neutral shield for the Ir complex to keep it from interacting with other biocatalysts. In that way, they successfully combined ATHase with various NADH-, FAD- and haem-dependent enzymes resulting in orthogonal redox cascades that could not be achieved when the free Ir-complex was used,<sup>82</sup> including a double stereoselective amine deracemization, production of L-pipecolic acid from L-lysine (Figure 1.8).

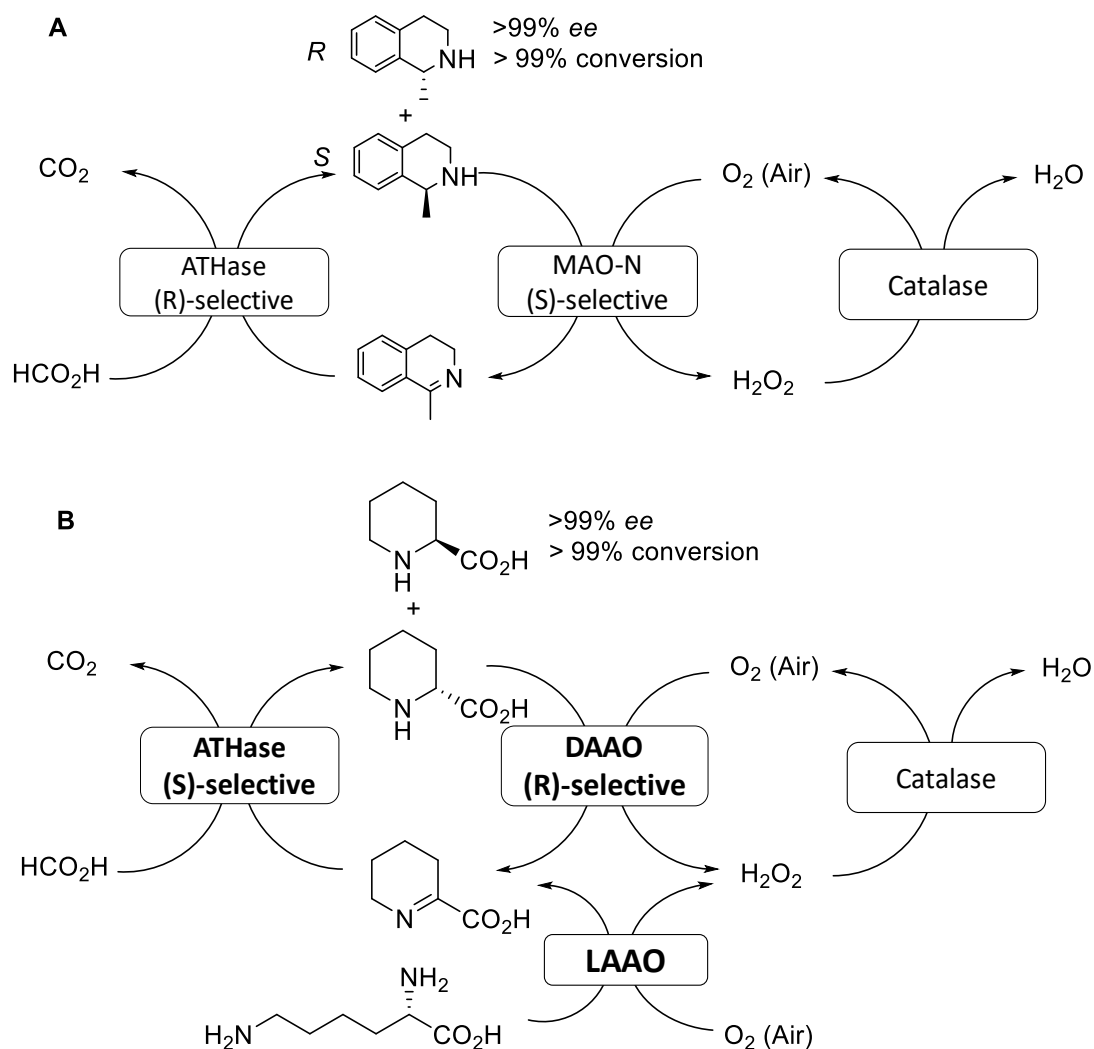


**Figure 1.8.** A, (*S*)-selective monoamine oxidase (MAO-N) was coupled with (*R*)-selective ATHase for double stereoselective deracemization of amines. B, Production of L-pipecolic acid from L-lysine by combining (*S*)-selective ATHase with an L-amino acid oxidase (LAO) and a D-selective amino acid oxidase (DAAO). Catalase was used to decompose H<sub>2</sub>O<sub>2</sub> generated in both cases.<sup>82</sup>

Compartmentalization is another strategy to couple chemical catalysts with biocatalysts in one-pot by protecting the enzymes from the organic solvent or metal catalysts from cellular components; as well as shielding catalytic centers from one another to avoid mutual inactivation. Besides the traditional biphasic system,<sup>85</sup> more novel methods have been developed for compartmentalization purpose including hydrogel immobilization, membrane filtration and whole-cell isolation. Gröger and coworkers realized enzymatic decarboxylation<sup>58</sup> and alcohol

dehydrogenation<sup>86</sup> in organic solvent by encapsulating the enzymes in poly(vinyl alcohol)/poly(ethylene glycol) cryogels or acrylate-based superabsorbent polymer respectively. They coupled these two enzymes with ruthenium-catalyzed metathesis and a proline-derivative-catalyzed aldol reaction for efficient preparation of antioxidants 4,4'-dihydroxystilbene and 1,3-diols separately. In another study, they combined Wacker oxidation with enzymatic reduction or hydroamination in a one-pot process in aqueous media by withholding the detrimental effect of *Cu* ions from biotransformation in the interior of a polydimethylsiloxane thimble (PDMS) that only enabled the free exchange of organic chemical (Figure 1.9).<sup>55,57</sup>

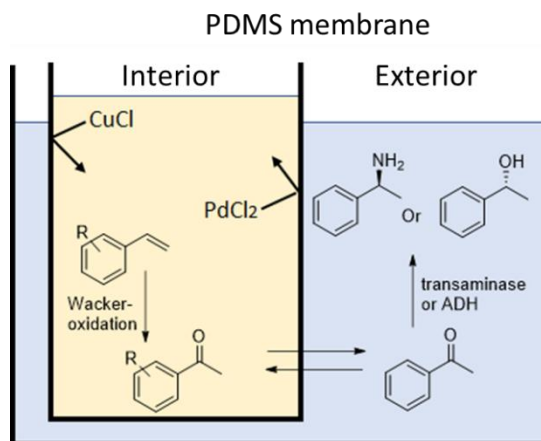


**Figure 1.9.** Site-isolation of catalysts using a PDMS thimble for the combination of a Wacker oxidation and an enzymatic reduction catalyzed by ADH or transamination catalyzed by transaminase.<sup>55</sup>

Although supramolecular strategies have enabled the catalytic activity of several transition metal catalysts in aqueous environment, many metal cofactors are still inhibited by the cellular components and therefore require purified protein for tandem reactions in most cases. Using cellular membrane as a barrier to protect metal catalysts from cellular inhibitors is an attractive strategy. Recently, Ward and coworkers created an *E. coli* strain for periplasmic expression of Sav with a biotinylated Hoveyda-Grubbs catalyst for olefin metathesis *in vivo*.<sup>87</sup> The periplasm provided an environment with low concentrations of inhibitors for metathesis and thus enabled the

high-throughput directed evolution of artificial metalloenzymes *in vivo*. Additionally, the use of whole cell provides a natural protection for biocatalysts. Lloyd and coworkers prepared (*R*)-1-methyltetrahydroisoquinoline (MTQ) with 96% *ee* by a cooperative tandem reaction consisting of enantioselective monoamine oxidation catalyzed by an engineered *E. coli* strain and nonselective reduction catalyzed by nanoscale Pd (0) coated on the cell surface (Figure 1.10).<sup>51</sup>

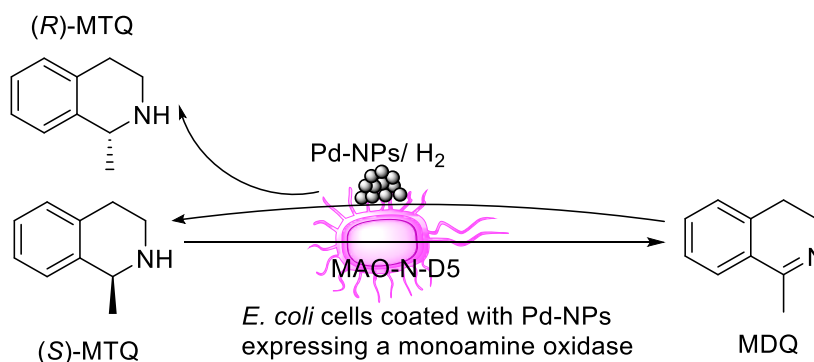


**Figure 1.10.** The cyclic deracemization of MTO through MDQ using palladized biocatalysts with the monoamine oxidase-N insert.<sup>51</sup>

Another interesting strategy to enable chemo-enzymatic reactions in one pot is to create hybrid enzyme-metal nanoparticles that bear orthogonal but cooperative catalytic centers. This design straddles the disciplines of supramolecular and compartmentalization. The peptide is a robust biomaterial and can stabilize the performance of inorganic catalysts.<sup>88</sup> The resulting enzyme-metal complex could work as a metalloenzyme with the catalytic activity originated from the introduced metal. Significantly, the surrounding proteins not only serve as protecting cage but also work as catalysts for distinct bioactivity.<sup>88-90</sup> In one example, Bäckvall and coworkers created a hybrid catalyst consisting of CALB and Pd nanoparticles co-immobilized into the compartments of mesoporous silica for DKR of 1-phenylethylamine.<sup>90</sup> The co-immobilization resulted in a more efficient cooperation between two catalysts and recyclability of both Pd nanoparticles and CALB at the same time (Figure 1.11).

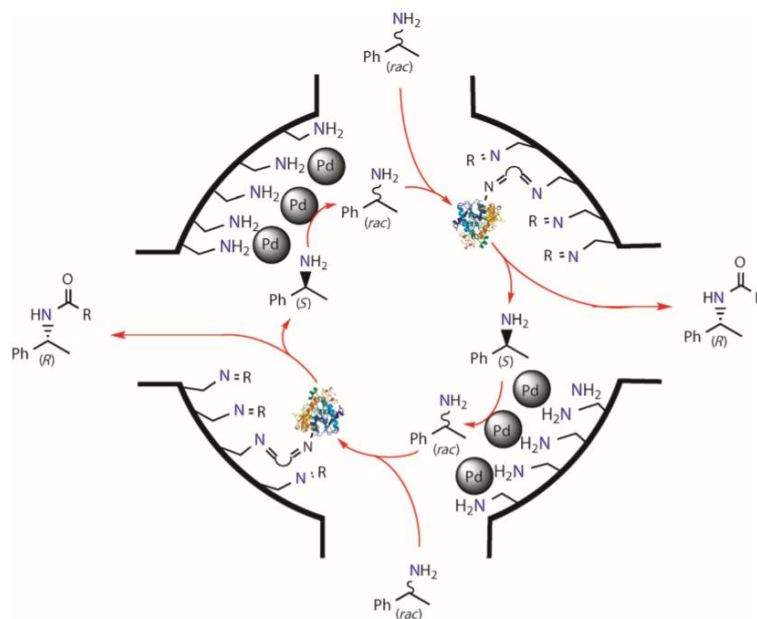


**Figure 1.11.** DKR of amine with a bifunctional catalyst in which Pd nanoparticles and CALB are co-immobilized in the same pore of siliceous mesocellular foams.<sup>90</sup>

## 1.4 Whole Cell Biocatalysis

Chemical synthesis is a well-established route for bulk manufacturing of nutraceuticals, pharmaceuticals and other bulk chemicals. It lays the foundations for our daily life to provide necessities such as food, medicines and fuels. However, some drawbacks also exist in the process of chemical synthesis, such as unstable intermediates, multistep reactions, complex process control, etc., which result in high energy input, low production efficiency and tremendous waste generation. Those drawbacks are motivating the development of green and sustainable processes for chemical manufacturing. Cell factories-based production provides an attractive alternative to these challenges.

Whole cell biocatalysis has several advantages. Microorganisms can convert renewable resources into fuels and value-added chemicals under mild fermentation condition that is environmentally friendly. Like proteins, whole-cell biocatalysis have relatively high selectivity over substrates and the products. High regio-, chemo-, diastereo- and enantioselectivity is very



desirable in chemical synthesis. Some chiral compounds or sophisticated chemicals that are challenges for chemical synthesis could be easily generated by biotransformation. The high specificity of biotransformation generally results in high catalytic efficiency, minimized side reactions and simplified downstream process. In addition, whole-cell biocatalysis has stronger tolerance against harsh reaction conditions compared with the naked enzymes. For example, the toxicity effect of concentrated substrates on enzyme could be largely alleviated by using microorganisms as a reaction unit. A few microorganisms have or can be engineered to have strong tolerance to elevated temperature or low pH.<sup>91,92</sup> Last but not least, whole-cell biocatalysts allow for the facile implementation of enzymatic cascades that span multiple reactions, with an integrated supply of the myriad cofactors that are expensive but essential for complex biotransformation.<sup>93</sup> This internal supply greatly simplifies cofactors regeneration and makes the addition of expensive external cofactors unnecessary.<sup>92</sup>

*Saccharomyces cerevisiae* has been widely used in the industry for bioproduction of value-added compounds or bulk chemicals such as ethanol, lipids,<sup>94</sup> fatty acids,<sup>95</sup> lactic acid,<sup>96</sup> xylitol,<sup>97</sup> etc. Its “generally regarded as safe (GRAS)” status is suitable for large-scale operation. Unlike prokaryotes, *S. cerevisiae* has multiple organelles to compartmentalize different reactions. Furthermore, *S. cerevisiae* exhibits high tolerance against harsh industrial conditions, such as low pH and high glucose concentrations.<sup>98</sup> Because microorganisms are evolved to maintain metabolic homeostasis under different conditions, their metabolisms must be intensively rewired to achieve high titer, rate, and yield for commercial production.

As a model eukaryotic system, molecular and cell biology of *S. cerevisiae* has been studied in-depth with ample genetic engineering tools available. In addition, tremendous metabolic engineering strategies have also been developed on *S. cerevisiae* at the biological parts level, at

the pathway level, at the organelle level and at the systems levels.<sup>98</sup> Those synthetic biology tools and metabolic engineering strategies play key roles in the science of rewiring cellular metabolism and has broad applications in cell factory development, including extended substrate scopes; increased production of the desired products; enabled production of novel compounds and improved cellular properties, such as tolerance to harsh industrial conditions. Among those strategies, there is growing interest to develop genome-wide engineering strategies for multiplex and precise genome editing of *S. cerevisiae*. Our lab has developed several genome-wide engineering tools such as, RNAi-Assisted Genome Evolution (RAGE),<sup>99</sup> tri-functional CRISPR system for gene activation, interference and deletion (CRISPR-AID)<sup>100</sup> and a CRISPR-CAS9 and homology-directed-repair-assisted-genome-scale engineering method (CHANGE).<sup>101</sup> Coupling those strategies with an automated cellular engineering platform, iBioFAB, we aim at engineering whole-cell biocatalysts with different properties in a high throughput manner.

## 1.5 Project Overview

My research was focused on designing and engineering of multi-step (bio) catalytic systems for selective synthesis of chiral building blocks of bioactive compounds or biodegradable polymers. In Chapter 2, my colleagues and I demonstrated that CRISPR-Cas9 can be used to efficiently and precisely introduce heterologous promoters into *Streptomyces* genomes for BGCs activation. I further applied this CRISPR-Cas9 promoter knock-in strategy in *S. viridochromogenes* to activate a few silent BGCs by precisely inserting strong constitutive promoters in front of target BGCs and successfully identified a new type II polyketide compound C22-1.<sup>102</sup> This CRISPR-Cas9 mediated gene knock-out strategy was further used to narrow down the essential genes used for C22-1 biosynthesis and a biosynthetic mechanism was proposed.

Inspired by the cooperated action of multiple enzymes for efficient synthesis, I started to combine transition metal catalysts with enzymes in one-pot to realize the synthetic power that cannot be achieved by using either of them. In Chapter 3, I described the development of a modular, one-pot, sequential chemoenzymatic system for the formal enantioselective construction of the C-C bond in 2-aryl 1,4-dicarbonyl compounds. This sequence comprises a rhodium-catalyzed diazocoupling that provides >9:1 selectivity for heterocoupling of two diazoesters and a reduction mediated by an ene-reductase (ER), which occurs in up to 99% enantiomeric excess (*ee*). The high yield and enantioselectivity of this system result from the preferential generation of an (*E*)-alkene from the diazo coupling reaction and selective reduction of the (*E*)-alkene in a mixture of (*E*) and (*Z*) isomers by the ER. Screening of a panel of ERs revealed that OPR1 from *Lycopersicum esculentum* catalyzes the reduction of bulky tert-butyl or benzyl esters to afford chiral diesters that are poised for orthogonal reactions at the two distinct ester units of the product. Overall, this work demonstrates the benefit of combining organometallic and enzymatic catalysis to create unusual overall transformations that do not require the isolation and purification of intermediates.<sup>66</sup>

The system developed in Chapter 2 has a few disadvantages. First, diazocoupling reaction is hard to scale up due to its strict reaction condition and exploratory raw materials. However, if we prepare alkenes by the most convenient or scale-up friendly ways like Wittig-type reactions or olefin metathesis, we would obtain racemates with diastereomer unflavored by the ERs. In such case, our old system will result in low yield. This challenge inspired us to develop a new class of cooperative chemoenzymatic reactions that combine photocatalysts that isomerize alkenes with ene-reductases that reduce carbon-carbon double bonds to generate valuable enantioenriched products. In Chapter 4, we demonstrated that this method enables the stereoconvergent reduction of *E/Z* mixtures of alkenes or reduction of the unreactive stereoisomer of an alkene in yields and

*ee*'s that match those obtained from the reduction of the pure, more reactive isomer. This new cooperative system overcomes the limitations of both individual catalysts and affords a range of synthetically valuable and biologically active enantioenriched compounds. More generally, these results illustrate the value of driving a chemical reaction with light to ensure compatibility between the chemical and enzymatic catalysts.<sup>103</sup>

Microbial lactic acid (LA) production under acidic fermentation conditions is highly desirable to reduce the production cost. However, overcoming the acid toxicity remains a major challenge. To develop whole-cell biocatalysis with higher tolerance to an industrially preferred low pH environment, in Chapter 5, I applied RAGE and CRISPR-AID guided genome-wide engineering methods to engineer *S. cerevisiae* and identify a few mutant strains with up to 3-fold improved acid tolerance and 1.5-fold higher LA production compared with the parent strain. The best mutant strain could produce 52 g/L LA in fed-batch fermentation with minimum medium at pH 3. In addition, to establish an Automated Cellular Engineering (ACE) platform, I developed a growth-based LA biosensor and an automated quantification assay by BioProfile Analyzer.

## 1.6 References

- 1 Hughes, G. & Lewis, J. C. Introduction: Biocatalysis in Industry. *Chem. Rev.* **118**, 1-3, (2018).
- 2 Fischer, E. Einfluss der Configuration auf die Wirkung der Enzyme. *Berichte der deutschen chemischen Gesellschaft* **27**, 2985-2993, (1894).
- 3 Kohler, R. The background to Eduard Buchner's discovery of cell-free fermentation. *J. Hist. Biol.* **4**, 35-61, (1971).
- 4 Hann, E. C. *et al.* 5-Cyanovaleramide production using immobilized pseudomonas chlororaphis B23. *Bioorg. Med. Chem.* **7**, 2239-2245, (1999).
- 5 Winkler, C. K. *et al.* Chemoenzymatic Asymmetric Synthesis of Pregabalin Precursors via Asymmetric Bioreduction of  $\beta$ -Cyanoacrylate Esters Using Ene-Reductases. *The Journal of Organic Chemistry* **78**, 1525-1533, (2013).
- 6 Packer, M. S. & Liu, D. R. Methods for the directed evolution of proteins. *Nat Rev Genet* **16**, 379-394, (2015).

- 7 Turner, N. J. Directed evolution drives the next generation of biocatalysts. *Nat. Chem. Biol.* **5**, 567-573, (2009).
- 8 Romero, P. A. & Arnold, F. H. Exploring protein fitness landscapes by directed evolution. *Nat. Rev. Mol. Cell Biol.* **10**, 866-876, (2009).
- 9 Alvizo, O. *et al.* Directed evolution of an ultrastable carbonic anhydrase for highly efficient carbon capture from flue gas. *Proc. Natl. Acad. Sci. U. S. A.* **111**, 16436-16441, (2014).
- 10 Coelho, P. S., Brustad, E. M., Kannan, A. & Arnold, F. H. Olefin cyclopropanation via carbene transfer catalyzed by engineered cytochrome P450 enzymes. *Science* **339**, 307-310, (2013).
- 11 Kan, S. B., Lewis, R. D., Chen, K. & Arnold, F. H. Directed evolution of cytochrome c for carbon-silicon bond formation: Bringing silicon to life. *Science* **354**, 1048-1051, (2016).
- 12 Kan, S. B. J., Huang, X., Gumulya, Y., Chen, K. & Arnold, F. H. Genetically programmed chiral organoborane synthesis. *Nature* **552**, 132, (2017).
- 13 Liang, J. *et al.* Development of a Biocatalytic Process as an Alternative to the (-)-DIP-Cl-Mediated Asymmetric Reduction of a Key Intermediate of Montelukast. *Org Process Res Dev* **14**, 193-198, (2010).
- 14 Fischbach, M. A. & Walsh, C. T. Antibiotics for emerging pathogens. *Science* **325**, 1089-1093, (2009).
- 15 Zhang, M. M., Wang, Y., Ang, E. L. & Zhao, H. Engineering microbial hosts for production of bacterial natural products. *Nat. Prod. Rep.* **33**, 963-987, (2016).
- 16 Clomburg, J. M., Crumbley, A. M. & Gonzalez, R. Industrial biomanufacturing: The future of chemical production. *Science* **355**, (2017).
- 17 Nielsen, J. & Keasling, Jay D. Engineering Cellular Metabolism. *Cell* **164**, 1185-1197, (2016).
- 18 Kohler, V. & Turner, N. J. Artificial concurrent catalytic processes involving enzymes. *Chem. Commun. (Camb.)* **51**, 450-464, (2015).
- 19 Bornscheuer, U. T. *et al.* Engineering the third wave of biocatalysis. *Nature* **485**, 185-194, (2012).
- 20 Wang, Y. & Zhao, H. Tandem Reactions Combining Biocatalysts and Chemical Catalysts for Asymmetric Synthesis. *Catalysts* **6**, 194, (2016).
- 21 Verho, O. & Bäckvall, J.-E. Chemoenzymatic Dynamic Kinetic Resolution: A Powerful Tool for the Preparation of Enantiomerically Pure Alcohols and Amines. *J. Am. Chem. Soc.* **137**, 3996-4009, (2015).
- 22 Dudley, Q. M., Karim, A. S. & Jewett, M. C. Cell-free metabolic engineering: Biomanufacturing beyond the cell. *Biotechnol. J* **10**, 69-82, (2015).
- 23 Ji, Q. Z., Wang, B. C., Tan, J., Zhu, L. C. & Li, L. Y. Immobilized multienzymatic systems for catalysis of cascade reactions. *Process Biochem.* **51**, 1193-1203, (2016).
- 24 Jia, F., Narasimhan, B. & Mallapragada, S. Materials-Based Strategies for Multi-Enzyme Immobilization and Co-Localization: A Review. *Biotechnol. Bioeng* **111**, 209-222, (2014).
- 25 Oroz-Guinea, I. & Garcia-Junceda, E. Enzyme catalysed tandem reactions (vol 17, pg 236, 2013). *Curr. Opin. Chem. Biol.* **17**, 1039-1039, (2013).
- 26 Obexer, R. *et al.* Emergence of a catalytic tetrad during evolution of a highly active artificial aldolase. *Nat. Chem.* **9**, 50-56, (2017).
- 27 Garrabou, X., Verez, R. & Hilvert, D. Enantiocomplementary Synthesis of  $\gamma$ -Nitroketones Using Designed and Evolved Carboligases. *J. Am. Chem. Soc.* **139**, 103-106, (2017).

- 28 Schoevaart, R., van Rantwijk, F. & Sheldon, R. A. A Four-Step Enzymatic Cascade for the One-Pot Synthesis of Non-natural Carbohydrates from Glycerol. *JOC* **65**, 6940-6943, (2000).
- 29 Guterl, J.-K. *et al.* Cell-Free Metabolic Engineering: Production of Chemicals by Minimized Reaction Cascades. *Chemsuschem* **5**, 2165-2172, (2012).
- 30 Fessner, W.-D. Systems Biocatalysis: Development and engineering of cell-free “artificial metabolisms” for preparative multi-enzymatic synthesis. *N. Biotechnol* **32**, 658-664, (2015).
- 31 Khattak, W. A. *et al.* Yeast cell-free enzyme system for bio-ethanol production at elevated temperatures. *Process Biochem.* **49**, 357-364, (2014).
- 32 Wagner, N., Bosshart, A., Failmezger, J., Bechtold, M. & Panke, S. A Separation-Integrated Cascade Reaction to Overcome Thermodynamic Limitations in Rare-Sugar Synthesis. *Angew. Chem. Int. Ed.* **54**, 4182-4186, (2015).
- 33 Caschera, F. & Noireaux, V. A cost-effective polyphosphate-based metabolism fuels an all *E. coli* cell-free expression system. *Metab. Eng* **27**, 29-37, (2015).
- 34 Zhang, Y. H. Production of biofuels and biochemicals by in vitro synthetic biosystems: Opportunities and challenges. *Biotechnol. Adv.* **33**, 1467-1483, (2015).
- 35 Karzbrun, E., Shin, J., Bar-Ziv, R. H. & Noireaux, V. Coarse-Grained Dynamics of Protein Synthesis in a Cell-Free System. *Phys. Rev. Lett.* **106**, 048104, (2011).
- 36 Korman, T. P., Opgenorth, P. H. & Bowie, J. U. A synthetic biochemistry platform for cell free production of monoterpenes from glucose. *Nature Commun.* **8**, 15526, (2017).
- 37 Opgenorth, P. H., Korman, T. P. & Bowie, J. U. A synthetic biochemistry molecular purge valve module that maintains redox balance. *Nature Commun.* **5**, 4113, (2014).
- 38 Schwander, T., Schada von Borzyskowski, L., Burgener, S., Cortina, N. S. & Erb, T. J. A synthetic pathway for the fixation of carbon dioxide in vitro. *Science* **354**, 900-904, (2016).
- 39 Denard, C. A., Hartwig, J. F. & Zhao, H. Multistep One-Pot Reactions Combining Biocatalysts and Chemical Catalysts for Asymmetric Synthesis. *ACS Catal.* **3**, 2856-2864, (2013).
- 40 Allen, J. V. & Williams, J. M. J. Dynamic kinetic resolution with enzyme and palladium combinations. *Tetrahedron Lett* **37**, 1859-1862, (1996).
- 41 Pamies, O. & Backvall, J. E. Combination of enzymes and metal catalysts. A powerful approach in asymmetric catalysis. *Chem. Rev.* **103**, 3247-3262, (2003).
- 42 Kim, M. J. *et al.* (S)-selective dynamic kinetic resolution of secondary alcohols by the combination of subtilisin and an aminocyclopentadienylruthenium complex as the catalysts. *J. Am. Chem. Soc.* **125**, 11494-11495, (2003).
- 43 Martin-Matute, B. & Backvall, J. E. Dynamic kinetic resolution catalyzed by enzymes and metals. *Curr. Opin. Chem. Biol.* **11**, 226-232, (2007).
- 44 Xu, Y. *et al.* Dynamic kinetic resolution of aromatic sec-alcohols by using a heterogeneous palladium racemization catalyst and lipase. *Catal. Sci. Technol.*, (2017).
- 45 Magadum, D. B. & Yadav, G. D. One-pot synthesis of (R)-1-(pyridin-4-yl)ethyl acetate using tandem catalyst prepared by co-immobilization of palladium and lipase on mesoporous foam: Optimization and kinetic modeling. *Chirality* **29**, 811-823, (2017).
- 46 Sugiyama, K. *et al.* Spatial effects of oxovanadium-immobilized mesoporous silica on racemization of alcohols and application in lipase-catalyzed dynamic kinetic resolution. *Catal. Sci. Technol.* **6**, 5023-5030, (2016).

- 47 Zhang, X. *et al.* Positional immobilization of Pd nanoparticles and enzymes in hierarchical yolk-shell@shell nanoreactors for tandem catalysis. *Chem Commun* **53**, 7780-7783, (2017).
- 48 Denard, C. A. *et al.* Cooperative Tandem Catalysis by an Organometallic Complex and a Metalloenzyme. *Angew. Chem. Int. Ed.* **53**, 465-469, (2014).
- 49 Makkee, M., Kieboom, A. P. G., Van Bekkum, H. & Roels, J. A. Combined action of enzyme and metal catalyst, applied to the preparation of D-mannitol. *J.C.S. Chem. Comm.*, 930-931, (1980).
- 50 Makkee, M., Kieboom, A. P. G. & van Bekkum, H. Combined action of an enzyme and a metal catalyst on the conversion of d-glucose/d-fructose mixtures into d-mannitol. *Carbohydr. Res.* **138**, 237-245, (1985).
- 51 Foulkes, J. M., Malone, K. J., Coker, V. S., Turner, N. J. & Lloyd, J. R. Engineering a Biometallic Whole Cell Catalyst for Enantioselective Deracemization Reactions. *ACS Catal.* **1**, 1589-1594, (2011).
- 52 Simons, C., Hanefeld, U., Arends, I. W. C. E., Maschmeyer, T. & Sheldon, R. A. Towards catalytic cascade reactions: asymmetric synthesis using combined chemo-enzymatic catalysts. *Topics in Catalysis* **40**, 35-44, (2007).
- 53 Chen, S.-T., Huang, W.-H. & Wang, K.-T. Resolution of Amino Acids in a Mixture of 2-Methyl-2-propanol/water (19:1) Catalyzed by Alcalase via in Situ Racemization of One Antipode Mediated by Pyridoxal 5-Phosphate. *JOC* **59**, 7580-7581, (1994).
- 54 El-Sepelgy, O., Brzozowska, A. & Rueping, M. Asymmetric Chemoenzymatic Reductive Acylation of Ketones by a Combined Iron-Catalyzed Hydrogenation-Racemization and Enzymatic Resolution Cascade. *Chemsuschem* **10**, 1664-1668, (2017).
- 55 Sato, H., Hummel, W. & Gröger, H. Cooperative Catalysis of Noncompatible Catalysts through Compartmentalization: Wacker Oxidation and Enzymatic Reduction in a One-Pot Process in Aqueous Media. *Angew. Chem. Int. Ed.* **54**, 4488-4492, (2015).
- 56 Schnapperelle, I., Hummel, W. & Groger, H. Formal asymmetric hydration of non-activated alkenes in aqueous medium through a "chemoenzymatic catalytic system". *Chemistry (Easton)* **18**, 1073-1076, (2012).
- 57 Uthoff, F., Sato, H. & Gröger, H. Formal Enantioselective Hydroamination of Non-Activated Alkenes: Transformation of Styrenes into Enantiomerically Pure 1-Phenylethylamines in Chemoenzymatic One-Pot Synthesis. *Chemcatchem* **9**, 555-558, (2017).
- 58 Gómez Baraibar, Á. *et al.* A One-Pot Cascade Reaction Combining an Encapsulated Decarboxylase with a Metathesis Catalyst for the Synthesis of Bio-Based Antioxidants. *Angew. Chem. Int. Ed.* **55**, 14823-14827, (2016).
- 59 Tenbrink, K., Seßler, M., Schatz, J. & Gröger, H. Combination of Olefin Metathesis and Enzymatic Ester Hydrolysis in Aqueous Media in a One-Pot Synthesis. *Adv. Synth. Catal.* **353**, 2363-2367, (2011).
- 60 Denard, C. A. *et al.* Development of a One-Pot Tandem Reaction Combining Ruthenium-Catalyzed Alkene Metathesis and Enantioselective Enzymatic Oxidation To Produce Aryl Epoxides. *ACS Catalysis* **5**, 3817-3822, (2015).
- 61 Scalacci, N. *et al.* Unveiling the Biocatalytic Aromatizing Activity of Monoamine Oxidases MAO-N and 6-HDNO: Development of Chemoenzymatic Cascades for the Synthesis of Pyrroles. *ACS Catalysis* **7**, 1295-1300, (2017).

- 62 Burda, E., Hummel, W. & Gröger, H. Modular Chemoenzymatic One-Pot Syntheses in Aqueous Media: Combination of a Palladium-Catalyzed Cross-Coupling with an Asymmetric Biotransformation. *Angew. Chem. Int. Ed.* **47**, 9551-9554, (2008).
- 63 Gauchot, V., Kroutil, W. & Schmitzer, A. R. Highly recyclable chemo-/biocatalyzed cascade reactions with ionic liquids: one-pot synthesis of chiral biaryl alcohols. *Chemistry (Easton)* **16**, 6748-6751, (2010).
- 64 Fuchs, M. *et al.* Homoallylic Alcohols via a Chemo-Enzymatic One-Pot Oxidation–Allylation Cascade. *Adv. Synth. Catal.* **353**, 2354-2358, (2011).
- 65 Boffi, A. *et al.* The Heck Reaction of Allylic Alcohols Catalyzed by Palladium Nanoparticles in Water: Chemoenzymatic Synthesis of (R)-(-)-Rhododendrol. *Chemcatchem* **3**, 347-353, (2011).
- 66 Wang, Y., Bartlett, M. J., Denard, C. A., Hartwig, J. F. & Zhao, H. Combining Rh-Catalyzed Diazocoupling and Enzymatic Reduction To Efficiently Synthesize Enantioenriched 2-Substituted Succinate Derivatives. *ACS Catalysis*, 2548-2552, (2017).
- 67 Asikainen, M. & Krause, N. Tandem Enzyme/Gold-Catalysis: From Racemic  $\alpha$ -Allenic Acetates to Enantiomerically Enriched 2,5-Dihydrofurans in One Pot. *Adv. Synth. Catal.* **351**, 2305-2309, (2009).
- 68 Wang, Z. J., Clary, K. N., Bergman, R. G., Raymond, K. N. & Toste, F. D. in *Nat. Chem.* Vol. 5 100-103 (2013).
- 69 Rulli, G., Duangdee, N., Hummel, W., Berkessel, A. & Gröger, H. First Tandem-Type One-Pot Process Combining Asymmetric Organo- and Biocatalytic Reactions in Aqueous Media Exemplified for the Enantioselective and Diastereoselective Synthesis of 1,3-Diols. *European J. Org. Chem.* **2017**, 812-817, (2017).
- 70 Erdmann, V. *et al.* Enzymatic and Chemoenzymatic Three-Step Cascades for the Synthesis of Stereochemically Complementary Trisubstituted Tetrahydroisoquinolines. *Angew. Chem. Int. Ed.* **56**, 12503-12507, (2017).
- 71 Wang, X. *et al.* Cofactor NAD(P)H Regeneration Inspired by Heterogeneous Pathways. *Chem* **2**, 621-654, (2017).
- 72 Lang, X., Zhao, J. & Chen, X. Cooperative photoredox catalysis. *Chem. Soc. Rev.* **45**, 3026-3038, (2016).
- 73 Tran, N. H. *et al.* An efficient light-driven P450 BM3 biocatalyst. *J. Am. Chem. Soc.* **135**, 14484-14487, (2013).
- 74 Peers, M. K. *et al.* Light-driven biocatalytic reduction of  $\alpha,\beta$ -unsaturated compounds by ene reductases employing transition metal complexes as photosensitizers. *Catal Sci Technol* **6**, 169-177, (2016).
- 75 Mifsud, M. *et al.* Photobiocatalytic chemistry of oxidoreductases using water as the electron donor. *Nat Commun* **5**, 3145, (2014).
- 76 Lee, S. H. *et al.* Cofactor-Free, Direct Photoactivation of Enoate Reductases for the Asymmetric Reduction of C=C Bonds. *Angewandte Chemie International Edition*, (2017).
- 77 Wiester, M. J., Ulmann, P. A. & Mirkin, C. A. Enzyme Mimics Based Upon Supramolecular Coordination Chemistry. *Angew. Chem. Int. Ed.* **50**, 114-137, (2011).
- 78 Brown, C. J., Miller, G. M., Johnson, M. W., Bergman, R. G. & Raymond, K. N. High-Turnover Supramolecular Catalysis by a Protected Ruthenium(II) Complex in Aqueous Solution. *J. Am. Chem. Soc.* **133**, 11964-11966, (2011).
- 79 Bistri, O. & Reinaud, O. Supramolecular control of transition metal complexes in water by a hydrophobic cavity: a bio-inspired strategy. *Org. Biomol. Chem.* **13**, 2849-2865, (2015).



- 80 Pluth, M. D., Bergman, R. G. & Raymond, K. N. Acid Catalysis in Basic Solution: A  
Supramolecular Host Promotes Orthoformate Hydrolysis. *Science* **316**, 85-88, (2007).
- 81 Kaphan, D. M., Levin, M. D., Bergman, R. G., Raymond, K. N. & Toste, F. D. A  
supramolecular microenvironment strategy for transition metal catalysis. *Science* **350**,  
1235-1238, (2015).
- 82 Kohler, V. *et al.* Synthetic cascades are enabled by combining biocatalysts with artificial  
metalloenzymes. *Nat. Chem.* **5**, 93-99, (2013).
- 83 Brown, C. J., Bergman, R. G. & Raymond, K. N. Enantioselective Catalysis of the Aza-  
Cope Rearrangement by a Chiral Supramolecular Assembly. *J. Am. Chem. Soc.* **131**,  
17530-17531, (2009).
- 84 Yoshizawa, M., Tamura M Fau - Fujita, M. & Fujita, M. Diels-alder in aqueous molecular  
hosts: unusual regioselectivity and efficient catalysis. *Science* **312**, 251-254, (2006).
- 85 Marr, A. C. & Liu, S. Combining bio- and chemo-catalysis: from enzymes to cells, from  
petroleum to biomass. *Trends Biotechnol* **29**, 199-204, (2011).
- 86 Heidlindemann, M., Rulli, G., Berkessel, A., Hummel, W. & Gröger, H. Combination of  
Asymmetric Organo- and Biocatalytic Reactions in Organic Media Using Immobilized  
Catalysts in Different Compartments. *ACS Catal.* **4**, 1099-1103, (2014).
- 87 Jeschek, M. *et al.* Directed evolution of artificial metalloenzymes for in vivo metathesis.  
*Nature* **537**, 661-665, (2016).
- 88 San, B. H. *et al.* Platinum Nanoparticles Encapsulated by Aminopeptidase: A  
Multifunctional Bioinorganic Nanohybrid Catalyst. *Angew. Chem. Int. Ed.* **50**, 11924-  
11929, (2011).
- 89 Filice, M., Marciello, M., Morales, M. d. P. & Palomo, J. M. Synthesis of heterogeneous  
enzyme–metal nanoparticle biohybrids in aqueous media and their applications in C–C  
bond formation and tandem catalysis. *Chem Commun* **49**, 6876, (2013).
- 90 Engström, K. *et al.* Co-immobilization of an Enzyme and a Metal into the Compartments  
of Mesoporous Silica for Cooperative Tandem Catalysis: An Artificial Metalloenzyme.  
*Angew. Chem. Int. Ed.* **52**, 14006-14010, (2013).
- 91 Lin, B.-X., Zhang, Z.-J., Liu, W.-F., Dong, Z.-Y. & Tao, Y. Enhanced production of N-  
acetyl-d-neuraminic acid by multi-approach whole-cell biocatalyst. *Appl. Microbiol.*  
*Biotechnol.* **97**, 4775-4784, (2013).
- 92 McAuliffe, J. C. in *Handbook of Industrial Chemistry and Biotechnology* (ed James A.  
Kent) 1183-1227 (Springer US, 2012).
- 93 Ladkau, N., Schmid, A. & Bühler, B. The microbial cell—functional unit for energy  
dependent multistep biocatalysis. *Curr. Opin. Biotechnol.* **30**, 178-189, (2014).
- 94 Veen, M. & Lang, C. Production of lipid compounds in the yeast *Saccharomyces cerevisiae*.  
*Appl. Microbiol. Biotechnol.* **63**, 635-646, (2004).
- 95 Yu, T. *et al.* Metabolic engineering of *Saccharomyces cerevisiae* for production of very  
long chain fatty acid-derived chemicals. *Nature Communications* **8**, 15587, (2017).
- 96 Baek, S. H. *et al.* Improvement of d-Lactic Acid Production in *Saccharomyces cerevisiae*  
Under Acidic Conditions by Evolutionary and Rational Metabolic Engineering. *Biotechnol*  
*J* **12**, (2017).
- 97 Hallborn, J. *et al.* Xylitol production by recombinant *Saccharomyces cerevisiae*.  
*Biotechnology. (N. Y.)* **9**, 1090-1095, (1991).

- 98 Lian, J., Mishra, S. & Zhao, H. Recent advances in metabolic engineering of *Saccharomyces cerevisiae*: New tools and their applications. *Metabolic Engineering*, (2018).
- 99 Si, T. *et al.* Automated multiplex genome-scale engineering in yeast. *Nature Communications* **8**, 15187, (2017).
- 100 Lian, J., Hamedirad, M., Hu, S. & Zhao, H. Combinatorial metabolic engineering using an orthogonal tri-functional CRISPR system. *Nature Communications* **8**, 1688, (2017).
- 101 Bao, Z. *et al.* Genome-scale engineering of *Saccharomyces cerevisiae* with single-nucleotide precision. *Nat. Biotechnol.* **36**, 505, (2018).
- 102 Zhang, M. M. *et al.* CRISPR-Cas9 strategy for activation of silent *Streptomyces* biosynthetic gene clusters. *Nat. Chem. Biol.*, (2017).
- 103 Litman, Z. C., Wang, Y., Zhao, H. & Hartwig, J. F. Cooperative asymmetric reactions combining photocatalysis and enzymatic catalysis. *Nature* **560**, 355-359, (2018).

# CHAPTER 2. Activation and Characterization of Biosynthetic Gene Clusters (BGCs) in *Streptomyces viridochromogenes* Using CRISPR-Cas System

## 2.1 Introduction

*Streptomyces* are among the most prolific and well-studied producers of diverse secondary metabolites that are rich sources of drugs and biologically active compounds.<sup>1</sup> Genome sequencing efforts have identified a tremendous number of silent gene clusters encoding unknown secondary metabolites that have never been detected under laboratory conditions. Importantly, they have revealed a much larger capacity for biosynthesis of specialized natural products than previously thought. Study of these pathways also enables us to discover new enzymes with uncharacterized functionality and also to elucidate new biosynthetic mechanism, which greatly facilitates rational design of multi-step catalysis for selective synthesis of valuable compounds.

Silent biosynthetic gene clusters (BGCs) can be activated by either: (i) manipulating of the native organisms or (ii) heterologously expressing silent BGCs in suitable hosts such as *S. coelicolor*, *S. lividans*, and *S. albus*.<sup>2</sup> With the advent of recombinant DNA and synthetic biology technologies that enable efficient capture and refactoring of BGCs, heterologous hosts are increasingly employed for microbial natural product production. Those hosts have been well studied and plenty of genetic manipulation tools are available. However, the main drawback of a heterologous production system is the lack of critical biosynthetic precursors of enzyme function, which differ for different classes of BGCs. On the other hand, native hosts have all essential elements required by BGCs expression, but they lack well-developed tools for genetic manipulation.

To expand the tools for genome editing of *Streptomyces*, we reconstituted Type II CRISPR (clustered regularly interspaced palindromic repeats) system in *S. albus*, *S. lividans*, and *S. viridochromogenes* to delete genes and BGCs or introduce point mutations with high efficiency (60-100%).<sup>3</sup> Type II CRISPR-Cas9 technology has revolutionized genome engineering, enabling the genetic manipulation of a number of genetically recalcitrant organisms. Compared to other site-specific genome engineering technologies, the Cas9 nuclease can be directed to nearly any site on the genome simply by transcribing a synthetic guide RNA (sgRNA), requiring only a protospacer adjacent motif (PAM) sequence at the target site. *Streptococcus pyrogens* Cas9 PAMs (NGG) are especially abundant in the GC-rich *Streptomyces* genomes, greatly increasing the number of potential target sites and coverage of CRISPR-Cas9 genome editing in these prolific natural product producers.

In this study, my colleagues and I demonstrated that CRISPR-Cas9 can be used to efficiently and precisely introduce heterologous promoters into *Streptomyces* genomes for BGC activation. We performed proof of concept experiments in model *Streptomyces* species: *Streptomyces albus* and *Streptomyces lividans*. I further applied this CRISPR-Cas9 promoter knock-in strategy in *S. viridochromogenes* to activate a few silent BGCs by precisely inserting strong constitutive promoters in front of BGCs and successfully identified a new Type II PKS compound. My colleagues simultaneously applied this strategy to *S. roseosporus* and *S. venezuelae* to activate silent BGCs encoding characterized or uncharacterized natural products.<sup>4</sup>

## 2.2 Results and Discussion

### 2.2.1. CRISPR-Cas9 Strategy for Promoter Knock-in in *Streptomyces Species*

To demonstrate that CRISPR-Cas9 can be used to precisely insert strong constitutive promoters into *Streptomyces* genomes for BGC activation, we selected the indigoidine (BLUE) cluster in *S. albus* as well as the actinorhodin (ACT) and undecylprodigiosin (RED) clusters in *S. lividans*. These transcriptionally silent BGCs have been characterized and their pigmented products make them excellent model clusters for testing our strategy for cluster activation.<sup>5</sup> Using CRISPR–Cas9-mediated knock-in, we replaced the upstream promoter regions of the main biosynthetic operons with a strong constitutive promoter *kasO*\**p* that worked in multiple *Streptomyces* species (Figure 2.1A) and successfully activated ACT and RED gene clusters (Figure 2.2B).<sup>4</sup>

In *S. albus*, CRISPR-Cas9 mediated double-stranded breaks upstream of the indigoidine synthetase gene significantly enhanced the knock-in efficiency of the constitutive *kasO*\**p* promoter (Figure 2.1B). The higher knock-in efficiency observed with editing templates containing 2 kb compared to 1 kb homologous arms was consistent with homology-directed repair mechanism of the double-stranded breaks. Co-introduction of heterologous genes, such as ~1 kb thiostrepton-resistance cassette (*tsr*) together with *kasO*\**p*, was also achieved at lower efficiencies, but still more efficient than inserting *kasO*\**p* alone by simple homologous recombination.<sup>4</sup>

These results showed that CRISPR-Cas9 can be used to precisely introduce heterologous genetic elements into the genome of *Streptomyces* model strains at high efficiencies. Additionally, these relatively minor genetic manipulations can be enough to activate silent BGCs and trigger production of the encoded metabolites. Additionally, we also test the CRISPR-Cas9 guided promoter knock-in in other non-model *Streptomyces* species such as *S. viridochromogenese*, *S.*

*roseosporus* and *S. venezuelae*. The enhanced knock-in efficiencies observed in all cases would enable us to use donor DNA with shorter homology flanks as well as introduce larger genetic elements, both of which would have been challenging without the CRISPR-Cas9 system. Although homologous recombination occurs efficiently in some *Streptomyces* species like *S. albus* and *S. lividans*, the efficiency increase by CRISPR-Cas9 is essential in allowing genetic manipulation of otherwise challenging strains such as *S. roseosporus* (Figure 2.1B).

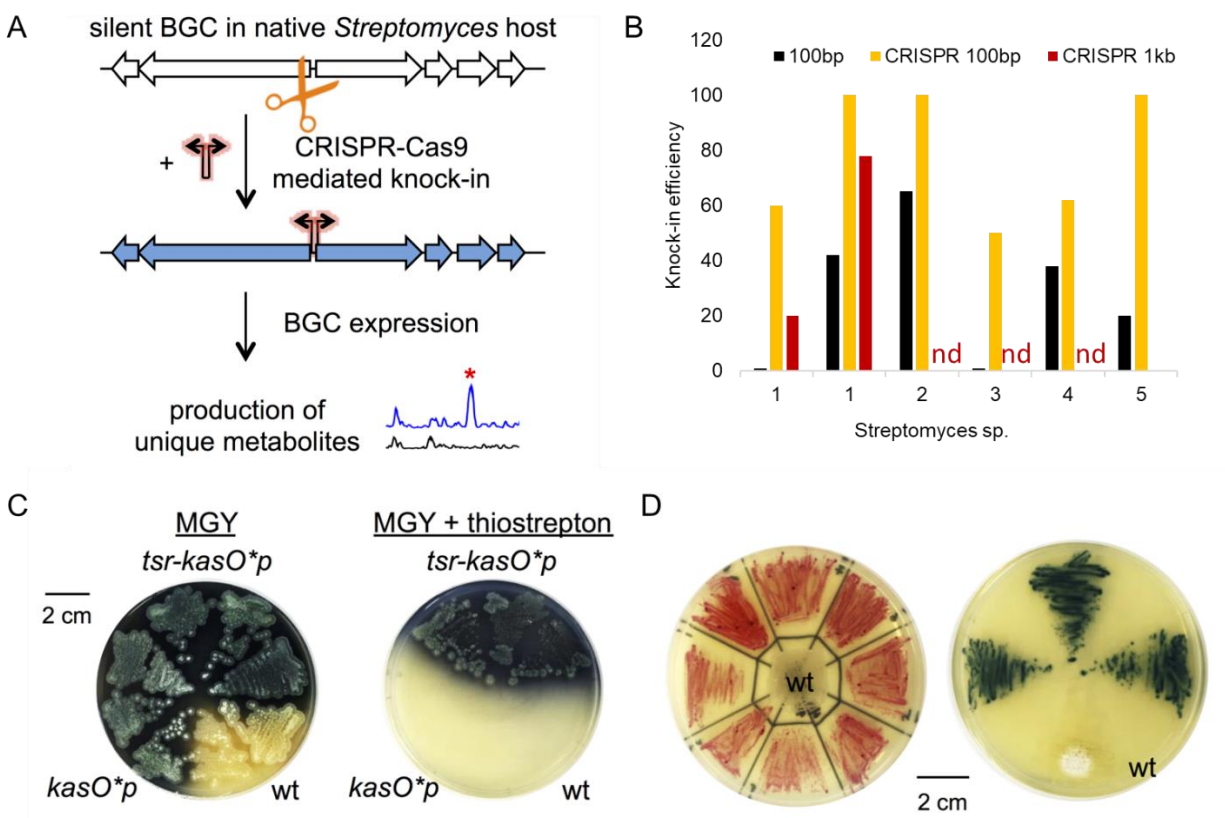


**Figure 2.1.** CRISPR-Cas9-based promoter knock-in strategy to activate silent biosynthetic gene clusters in streptomyces. (A) Using CRISPR-Cas9, efficient and precise introduction of promoter cassettes (red-shaded arrows) drives expression of biosynthetic genes (blue) and triggers the production of unique metabolites (\*) that are not detected in the parent strain. (B) Knock-in efficiencies with and without use of CRISPR-Cas9 in different *Streptomyces* species: (1) *S. albus*, (2) *S. lividans*, (3) *S. roseosporus*, and (4) *S. venezuelae*, (5) *S. viridochromogenes*. For *S. albus*, the knock-in efficiencies for different-sized inserts (100-bp versus 1-kb) using editing templates with different homology lengths (1-kb versus 2-kb) were examined. No knock-in was observed for *S. roseosporus* without CRISPR-Cas9. n.d., not determined. (C) Wild-type (wt) or indicated engineered *S. albus* strains on MGY or MGY + thiostrepton plates. (D) Wildtype and engineered

*S. lividans* strains with activated RED (left) or ACT (right) clusters on MGY plates. Ammonia fuming confirmed production of pH-sensitive actinorhodin-related pigments

### 2.2.2. Activation Silent Biosynthetic Gene Clusters (BGCs) in *Streptomyces viridochromogenes*

*S. viridochromogenes* is known to produce phosphinothricin, a well-known herbicide that irreversibly inhibits glutamine synthetase.<sup>6</sup> Besides, there are additional 32 uncharacterized BGCs of secondary metabolites based on antiSMASH analysis (Table 2.1).<sup>7</sup> Additionally, CRISPR-Cas9 system has highest editing efficiency in *S. viridochromogenes* based on a previous study.<sup>8</sup> It would be valuable and convenient to activate silent BGCs in this species. Target BGCs were chosen based on the following criteria: i) the BGCs must be uncharacterized, ii) the similarity between the selected BGCs and the characterized gene clusters in other species should be less than 70%; iii) most of the biosynthetic genes should be in the same operon. 7 BGCs were selected for activation, including Type II PKS: C22; Type I PKS: C32, C6 and C24; Lantipeptide: C7 and C20.

**Table 2.1.** AntiSMASH analyses of *S. viridochromogenes* DSM 40736 (NCBI Reference Sequence: NZ\_ACEZ 00000000.1).

| Cluster    | Type                         | From    | To      | Compound                 | Study                            |
|------------|------------------------------|---------|---------|--------------------------|----------------------------------|
| Cluster 1  | Terpene-nrps-t1pks           | 147228  | 209213  |                          |                                  |
| Cluster 2  | Melanin-terpene              | 350984  | 374124  |                          |                                  |
| Cluster 3  | Nrps                         | 614938  | 667909  | Coelichelin <sup>a</sup> |                                  |
| Cluster 4  | T1pks-<br>butyrolactone      | 925309  | 1004775 |                          |                                  |
| Cluster 5  | Lasso peptide                | 996947  | 1020529 |                          |                                  |
| Cluster 6  | T1pks                        | 1023099 | 1074657 | <i>m/z</i> 439           | This study                       |
| Cluster 7  | T1pks                        | 1068135 | 1123254 | No New peak              | This study                       |
| Cluster 8  | Nrps-t1pks                   | 1124345 | 1179652 |                          |                                  |
| Cluster 9  | Nrps-phosphonate             | 1172570 | 1240729 | Phosphonothricin         | Metcalf et al, 2005 <sup>9</sup> |
| Cluster 10 | Ectoine                      | 1986466 | 1997781 | Ectoine <sup>b</sup>     |                                  |
| Cluster 11 | NRPS-t1PKS                   | 2482772 | 2542826 |                          |                                  |
| Cluster 12 | Terpene                      | 2721388 | 2743906 |                          |                                  |
| Cluster 13 | Lasso peptide                | 3108492 | 3120837 |                          |                                  |
| Cluster 14 | Melanin                      | 3108492 | 3120837 |                          |                                  |
| Cluster 15 | Siderophore                  | 4468051 | 3223680 |                          |                                  |
| Cluster 16 | Butyrolactone                | 5785193 | 4479215 |                          |                                  |
| Cluster 17 | Lantipeptide                 | 4691917 | 4720311 |                          |                                  |
| Cluster 18 | T1pks                        | 4852429 | 4915920 |                          |                                  |
| Cluster 19 | Linaridin                    | 4917000 | 4938204 |                          |                                  |
| Cluster 20 | Lantipeptide-nrps            | 5099822 | 5150004 | No new peak              | This study                       |
| Cluster 21 | Terpene                      | 5973704 | 5895857 |                          |                                  |
| Cluster 22 | T2pks                        | 6046899 | 6089394 | C22-1                    | This study                       |
| Cluster 23 | Siderophore                  | 6516102 | 6529476 |                          |                                  |
| Cluster 24 | T1pks                        | 6568627 | 6618163 | No New peak              | This study                       |
| Cluster 25 | Ectoine                      | 6692399 | 6703527 |                          |                                  |
| Cluster 26 | Bacteriocin                  | 6914884 | 6926688 |                          |                                  |
| Cluster 27 | Terpene                      | 6959775 | 6982425 |                          |                                  |
| Cluster 28 | Siderophore                  | 7169194 | 7182469 |                          |                                  |
| Cluster 29 | Terpene                      | 7611221 | 7638254 |                          |                                  |
| Cluster 30 | Terpene                      | 8121206 | 8142742 |                          |                                  |
| Cluster 31 | Bacteriocin-<br>lantipeptide | 8164951 | 8193467 |                          |                                  |
| Cluster 32 | T1pks                        | 8282728 | 8326427 | <i>m/z</i> 524           | This study                       |
| Cluster 33 | Other                        | 8476453 | 8521258 |                          |                                  |

<sup>a</sup>100% of genes show similarity with coelichelin BGC of *S. coelicolor* A3(2)<sup>10,11</sup>

<sup>b</sup>100% of genes show similarity with ectoine BGCs of *S. chrysomallus*.<sup>12</sup>



For pathway-specific activation, we targeted single (*kasO\***p*) or bi-directional (*kasO\***p*-*rcfp*) promoter cassettes to the start of the first ORF(s) of the main biosynthetic operon(s) predicted based on gene directionality alone (Figure 2.2A, B). The overall knock-in efficiency varied from 80% to 100%. Introduction of bidirectional promoter cassettes into additional clusters of *S. viridochromogenes* led to overproduction of a compound that was poorly produced in the parent strain. For example, cluster C32 was predicted to encode a nucleoside type I polyketide synthase (PKS). It may be an iterative type I PKS where core catalytic domains occur on a single module that is used repetitively to generate the entire polyketide backbone. The core catalytic domains including ketosynthase (KS), acyltransferase (AT), and acyl carrier protein (ACP). The insertion of bidirectional promoter *kasO\***p* and *rcfp* between the main gene module encoding a loading domain, PKS core catalytic domain, and an important decoration domain, aldo/keto reductase, triggered the overproduction of a major metabolite with *m/z* 524 by more than 10 thousand folds (Figure 2.2C).

Introduction of a single promoter cassette upstream of the main synthetic containing-operons activated the cryptic pathway and led to production of unique compounds that were not observed in the parent strains (Figure 2.2D and Figure 2.3). For example, a distinct compound with *m/z* 440 observed for another engineered *S. viridochromogenes* strain in which *kas\***Op* was introduced upstream of a major operon including a few polyketide synthase modules encoding a type I polyketide (Figure 2.2D).

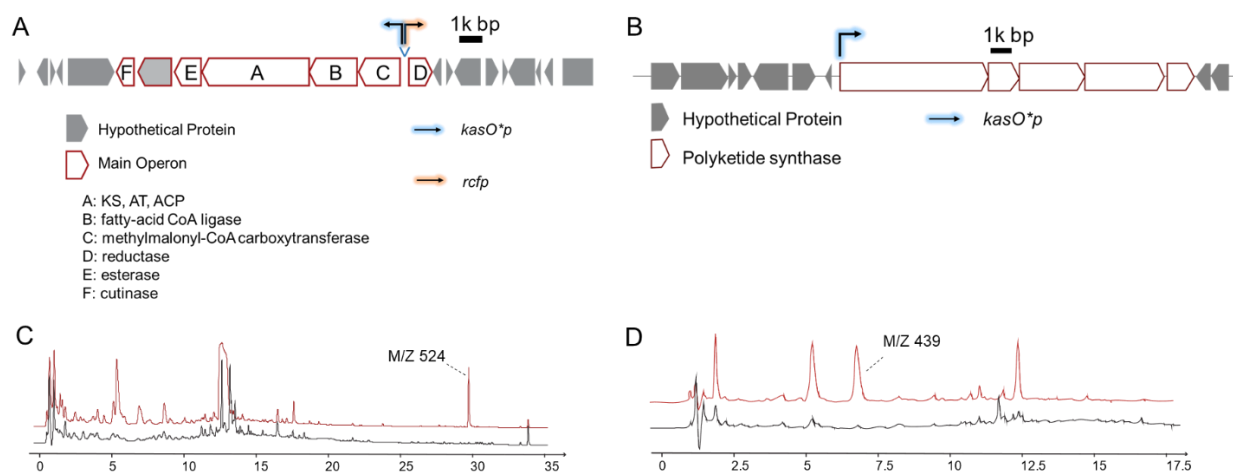


**Figure 2.2.** Activation of biosynthetic gene clusters (A) C32 and (B) C6 in *S. viridochromogenese*. C) HPLC analysis of ethyl acetate extracts from wild-type *S. viridochromogenese* (black) and an engineered strain (red) in which *kasO*\**p* and *rcpf* bidirectional promoter was introduced in cluster 32. The UV wavelength of detection is at 280 nm. Major metabolites uniquely produced by the engineered strains are not observed in wild-type strains are highlighted with indicated *m/z* value at 524. D) HPLC analysis of ethyl acetate extracts from wild-type *S. viridochromogenese* (black) and an engineered strain (red) in which *kasO*\**p* promoter was introduced in cluster 6. The UV wavelength of the detection is at 210 nm. Major metabolites uniquely produced by the engineered strains are not observed in wild-type strains are highlighted with indicated *m/z* value at 439.

### 2.2.3. Identification and Characterization of Novel Type II PKS Compound C22-1

C22 (NZ\_GG657757) was predicted to be a silent, uncharacterized type II PKS gene cluster. Based on protein-protein BLAST analysis, this operon contains evolutionarily conserved genes of type II PKS, including a ketosynthase  $KS_{\alpha}$  (SSQG\_RS26900), chain-length factor  $KS_{\beta}$  (SSQG\_RS26905), acyl carrier protein ACP (SSQG\_RS26910), and three polyketide cyclases: TcmJ (SSQG\_RS26895), TcmN (SSQG\_RS26915) and TcmI (SSQG\_RS26920). This core part has the same gene arrangement as the spore-pigment BGC in *S. avermitilis* (AB070937.1) with protein sequence homologies ranging from 64%-84%. Additionally, there are three extra tailoring enzymes: amidohydrolase (SSQG\_RS26925), FAD-hydroxylase (SSQG\_RS26930), and cytochrome P450 (SSQG\_RS26935).

Compared to the wild type *S. viridochromogenes*, the engineered strain *S. viridochromogenes*-895 in which *kas\*Op* was inserted in front of the main biosynthetic operon, SSQG\_RS26895-RS26920 secreted an obvious brown pigment in both liquid and solid MYG medium before sporulation with a major unique metabolite C22-1 observed by HPLC (Figure 2.3). HRMS of the C22-1 predicted a molecular formula  $C_{23}H_{16}O$  (Figure 2.5).  $^1H$  NMR,  $^{13}C$  NMR, COSY/TOCSY, HSQC and HMBC analyses revealed a novel polyketide with a dihydrobenzo [ $\alpha$ ] naphthacenequinone core that is shared by a family of polyketides including frankiamycin, benastatin, and pradimicin<sup>13</sup> (Figure 2.3C). The cyclohexanone (ring E) in C22-1 is atypical and has not been observed for pentangular aromatic polyketides.<sup>14</sup>

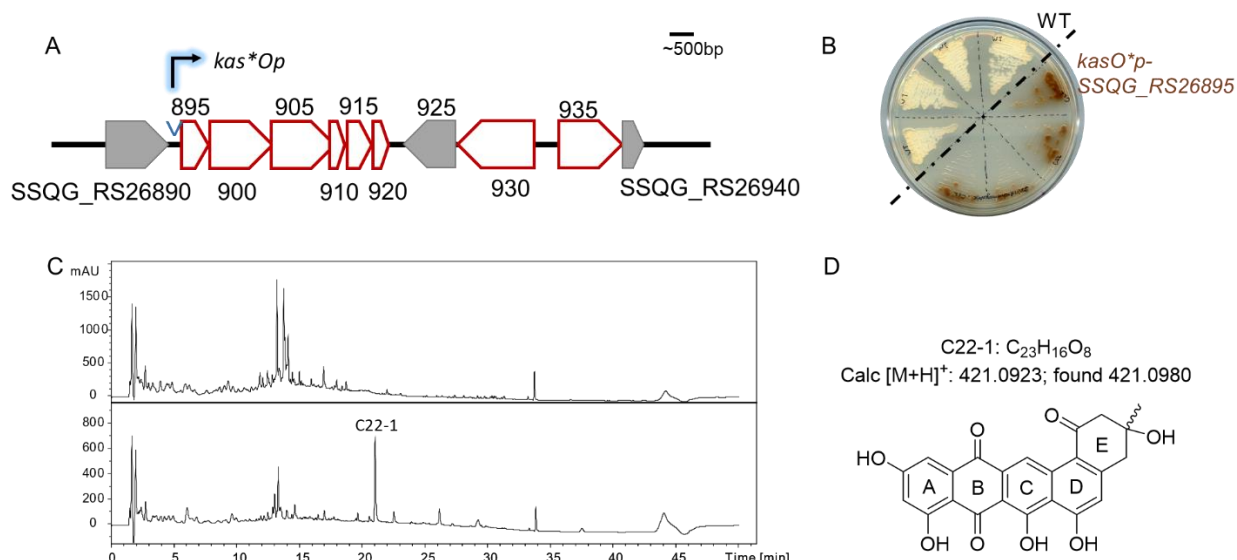


**Figure 2.3.** Activation of type II PKS biosynthetic gene cluster in *S. viridochromogenes* resulted in a mutant *S. viridochromogenes*-895 yielding a novel pigmented compound. **(A)** Partial schematic of NZ\_GG657757 containing majority of biosynthetic genes (orange) and the position of promoter knock-in. **(B)** Production of brown pigment by the engineered strain and not wild type (wt) *S. viridochromogenes* on MGY medium. **(C)** HPLC analysis of extracts from an engineered *S. viridochromogenes* strain harbouring a *kasO\*p* knock-in before SSQG\_RS26895 (bottom) compared to that from the parent strain (top). Indicated is the major metabolite C22-1 that is uniquely produced by the engineered strain. **(D)** Chemical structure of compound C22-1. The five rings are labelled A-E.

## 2.2.4. Investigation the Biosynthetic Mechanism of C22-1

Based on the study of evolutionary chemical diversity by coordinated gene swaps in type II polyketide gene clusters,<sup>14</sup> C22, similar to other BGCs annotated as spore pigments, belongs to ancestor 3 that is the antecedent of other aromatic polyketides with carbon ranging from 20-24, including most of identified bioactive compounds: Frankiamycin, Pradimicin, Benastatin, Medermycin, etc. Ancestor 3 is a big category and around 50% aromatic polyketides gene clusters belong to this family. More analyses have been done to locate the position of C22 in this big family. The whole gene cluster was blasted against a library of 480 *Streptomyces* species. 232 out of 480 contain conserved synthetic genes (I-VII) arranged in the order as shown in Figure 2.4. Those clusters annotated as spore pigment should produce aromatic polyketides with similar core structures. Interestingly, when taking other tailoring enzymes into consideration, C22 belongs to a very special group (Figure 2.4), 15 out of 232, which have the most tailoring enzymes, including cytochrome P450 and amidohydrolase that cannot be found in other groups.

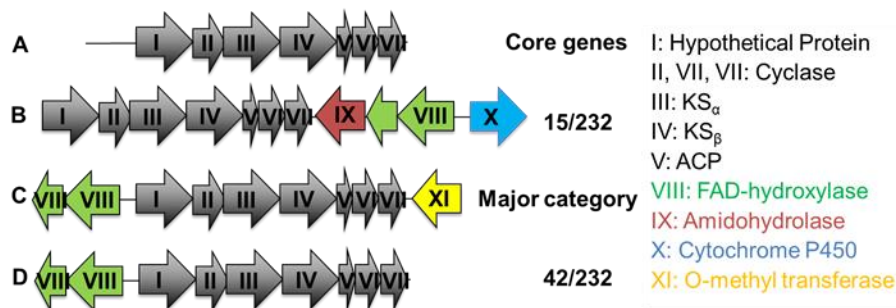


**Figure 2.4.** Schematic of major genes in different categories of Type II PKS gene clusters annotated as spore pigments. *whiE*-, *sch*- and *cur*- are all from category C.

Real time qPCR was performed to elucidate the expression level of SSQG\_RS26925, SSQG\_RS26930 and SSQG\_RS26935 in both wild type and mutant *S. viridochromogenes*-895. Gene KS<sub>α</sub> was only transcribed in the mutant *S. viridochromogenes*-895, which further proved that the silent gene cluster C22 was activated by introducing *kasO*\**p* in front of the core operon. Minor

expression of amidohydrolase (925), FAD-hydroxylase (930) and P450 (935) was detected in *S. viridochromogenes*-895. Interestingly, P450 was also detected in wildtype and it may not belong to the cluster C22 (Figure 2.5A).

To investigate whether SSQG\_RS26925, SSQG\_RS26930, and SSQG\_RS26935 were involved in the biosynthesis of C22-1 or any other additional new compounds, we created *S. viridochromogenes*-895-OE where SSQG\_RS26925, SSQG\_RS26930, and SSQG\_RS26935 were cloned in an operon and overexpressed by the constitutive strong promoter *psf* in an integration plasmid pET616. The kanamycin resistance gene was used as a reporter to confirm the translation of the whole operon (Figure 2.5C). We also created *S. viridochromogenes*-895-KO with SSQG\_RS26925, SSQG\_RS26930, and SSQG\_RS26935 being knocked out. Since the hypothetical protein SSQG\_RS26890 is also a conserved gene in BGCs for spore pigment synthesis, *S. viridochromogenes\_kasO\*p-890* was created by locating *kasO\*p* in front of SSQG\_RS26890. It is interesting to find that all mutants shared the same metabolic profile (Figure 2.5B). Including the characterized C22-1, there are 8 major new peaks with retention time at 21.1, 21.8, 22.5, 24.8, 25.1, 25.4, 26.2, and 26.4 min respectively compared with the wild type. C22-1 (21.1 min) was the major product if the fermentation took more than 10 days. Compound C22-3 (22.7 min), C22-4 (26.3 min) and C22-5 (26.5 min) were the major product if the fermentation were extracted within 5 days. They have *m/z* at 450, 546.5 and 547.5, respectively. Those data proved that SSQG\_RS26925, SSQG\_RS26930, and SSQG\_RS26935 did not participate in the biosynthesis of C22-1 and additional new compounds.

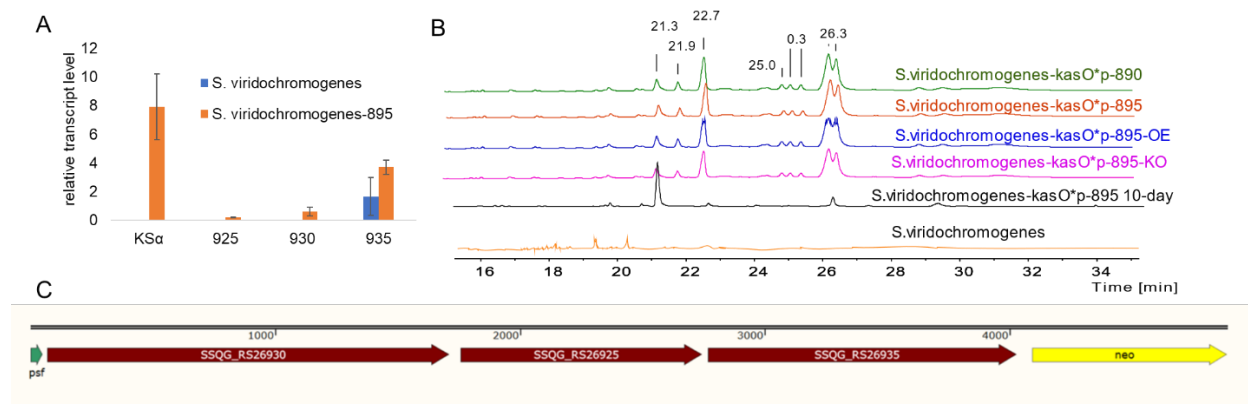


**Figure 2.5.** A) RT-qPCR analysis of *S. viridochromogenes-kas\*Op-895*, cluster 22. Relative gene expression of each indicated gene after normalization to the sigma factor for both wild type (blue) and engineered (red) strains. Error bars represent the standard deviation of biologically triplicates. (B) HPLC analysis of extracts from several engineered *S. viridochromogenes* strains compared to that from the wild type. Without specification, the fermentation took 5 days. (C) Part of scheme of pET616-pcf-SSQG-RS26930-925-935-neo for overexpression of SSQG-RS26930, 925 and 935 in a single operon.

Based on the experimental data, the hypothetical biosynthetic mechanism of C22-1 was proposed as in Figure 2.6. The minimal polyketide synthase (min-PKS) consists of three proteins: KS $\alpha$ , KS $\beta$  and ACP. The nascent polyketide chains consisting of 24 carbons, are constructed by iterative condensation of malonyl-CoA catalyzed by min-PKS. The reactive beta-keto chains are converted into hypothetical intermediate **1** by the action of tailoring enzymes TcmN, TcmI and TcmJ. It is not very clear how **1** was converted to C22-1. The reduction may occur spontaneously or catalyzed by another FAD-hydroxylase. Another major product C22-3 was also isolated and high-resolution electrospray ionization mass spectrometry in negative mode showed an  $m/z$  of 449.1490 (calculated: 450.1490). However, we failed to characterize its structure since C22-3 was not stable in any tested NMR solvents. C22-1 was the only stable compound derived from gene cluster C22.

Up to now, three BGCs have been experimentally related to spore pigments production. They are *cur-* from *Streptomyces curacoi*,<sup>15</sup> *sch-* from *Streptomyces halstedii*,<sup>16</sup> and *whiE-* spore

pigment cluster from *Streptomyces coelicolor*.<sup>17</sup> However, none of them has been structurally elucidated. Although ectopic expression of the *whiE*-, *sch*- and *cur*- spore pigment gene clusters led to the isolation of polycyclic aromatic polyketides, those partially cyclized compounds were more likely to be fragments instead of the fully cyclized products. Thus, C22-1 was the only characterized structure of spore-pigment up to date.

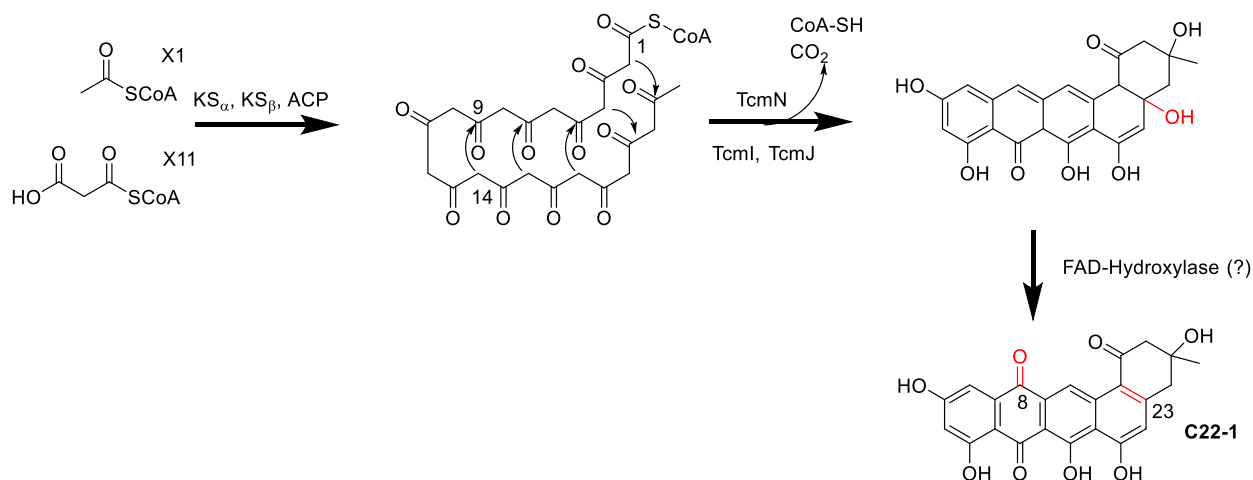


**Figure 2.6.** Proposed mechanism of C22-1 biosynthesis.

## 2.3 Conclusion

In this study, we showed that relatively small genome perturbations in the form of promoters being strategically introduced by CRISRP-Cas9 strategy are sufficient to activate the silent BGCs of different classes in multiple *Streptomyces* species with high to excellent efficiency, including type I (this study), type II (this study), and type III (our collaborator's work), non-ribosomal peptide synthetase (NRPS, our collaborator's work), hybrid PKS-NRPS (our collaborator's work) and non-ribosomal peptide synthetase (NRPS, our collaborator's work). With this strategy, one out of seven BGCs were overexpressed and 2 out of seven BGCs were activated. A novel type II PKS

compound C22-1 was characterized and it was the first fully characterized compound with completed cyclization corresponding to the spore pigment.

## 2.4 Experimental Procedures

### 2.4.1. Reagents and Media

Unless otherwise indicated, all reagents are obtained from Sigma. 1 L of MGY medium contains 10 g malt extract broth, 4 g Bacto yeast extract (BD Biosciences), 4 g glucose (1st Base, Axil Scientific) and for MGY agar plates, an additional 20 g of Bacto agar (BD Biosciences). Conjugation experiments involving WM6026 and WM3780 *E. coli* strains were performed on R2 agar without sucrose: 0.25 g K<sub>2</sub>SO<sub>4</sub>, 10.12 g MgCl<sub>2</sub>·6H<sub>2</sub>O, 10 g glucose, 0.1 g Bacto casamino acids (BD Biosciences), 5.73 g TES, 20 g agar in 1 L water, autoclaved, after which 1 mL filter-sterilized 50 mg/mL KH<sub>2</sub>PO<sub>4</sub> solution and filter-sterilized 2.94 g CaCl<sub>2</sub>·2H<sub>2</sub>O and 3 g L-proline in 5 mL 1 N NaOH were added to the medium.

### 2.4.2. Strains and Growth Conditions

Strains and plasmids used in this study are listed in Table 2.2. Unless otherwise indicated, strains are propagated in MGY medium at 30 °C. Spore preparations and conjugation protocols were similar to those described by Keiser and Bibb.<sup>18</sup> For spore preparations, 1:1000 of a spore preparation or 1:100 dilution of a saturated seed culture is plated on MGY plates and incubated at 30 °C until thick spores are observed. Spores were removed from the plate using 5-mm glass beads (Sigma) and resuspended in sterile TX buffer (50 mM Tris, pH 7.4, 0.001% (v/v) Triton X) by vigorous vortexing for 30 s. The eluant containing free spores was pelleted by spinning at maximum speed in an Eppendorf 5810R centrifuge for 10 min, resuspended in 1 mL sterile water



and re-pelleted. The spores were then resuspended in water and stored at -80 °C. A typical spore prep contains  $\sim 10^7$ – $10^9$  spores per milliliter as determined by serial dilution plating.

**Table 2.2.** Bacterial strains and plasmids used in this study.

| Strains and plasmids                            | Description  | Source   |
|---|--|--|
| pCRISPomyces-2 (pCm2)                           | <i>AprR</i> , <i>oriT</i> , <i>rep<sup>pSG5(ts)</sup></i> , <i>ori<sup>ColE1</sup></i> , <i>sSpcas9</i> , sgRNA, cassette  | Cobb et al. <sup>8</sup>                               |
| pCm2-adapter1- <i>kasO</i> *p adapter2          | pCM2 with adapters to facilitate assembly of editin flanks upstream and downstream of <i>kasO</i> *p   | This work  |
| pCm2-adapter1- <i>rcfp-kasO</i> *p adapter2     | pCM2 with adapters to facilitate assembly of editing flanks upstream and downstream of bidirectional <i>rcfp-kasO</i> *p   | This work  |
| pET616- <i>pcf</i> -SSQG-RS26930-925-935-neo    | pET616 with SSQG-RS26930, SSQG-RS26925, SSQG-RS26935 and neo being expressed by <i>pcf</i> in a single operon  | This work  |
| <i>Escherichia coli</i> DH5 $\alpha$            | <i>F</i> - $\Phi$ 80 <i>lacZ</i> $\Delta$ M15 $\Delta$ ( <i>lacZYA-argF</i> ) U169 <i>recA1 endA1 hsdR17 (rK-, mK+)</i> <i>phoA supE44</i> $\lambda$ - <i>thi-1 gyrA96 relA1</i> | Zhao laboratory stock                                  |
| <i>Escherichia coli</i> WM6026                  | diaminopimelic acid auxotroph  | William Metcalf laboratory                             |
| <i>Escherichia coli</i> WM3780                  | <i>dam</i> <sup>-</sup> <i>dcm</i> <sup>-</sup>  | William Metcalf laboratory                             |
| <i>Streptomyces albus</i> J1074                 | wild type  | Prof. Wenjun Zhang, University of California, Berkeley |
| <i>Streptomyces lividans</i> 66                 | wild type  | Zhao laboratory stock                                  |
| <i>Streptomyces viridochromogenes</i> DSM 40736 | wild type  | Zhao laboratory stock                                  |

### 2.4.3. Construction of Genome Editing Plasmids

All DNA manipulations were carried out in *Escherichia coli* DH5 $\alpha$  or NEB5 $\alpha$  (New England Biolabs). Primers used in this study are listed in Table 2.3. Restriction enzymes were obtained from New England Biolabs. Helper pCRISPomyces-2 plasmids for making promoter knock-in

constructs were made by ligating adaptor sequences, containing restriction sites flanking the promoter of choice (Figure 2.7) to facilitate insertion of homology arms at the *XbaI* site of pCRISPomyces-2.<sup>8</sup> The protospacer of a target cluster was first inserted via *BbsI*-mediated Golden Gate Assembly as previously described<sup>8</sup>. The helper plasmid (pCRISPomyces-2-*kasO*\**p*, pCRISPomyces-2-*rcfp-kasO*\**p*) was linearized using *SpeI* and assembled with the downstream homology arm (2-kb unless otherwise indicated) by Gibson assembly (New England Biolabs). The second upstream homology arm (2-kb unless otherwise indicated) was subsequently inserted by Gibson assembly using *HindIII* or *NheI* linearized construct containing the first homology arm. See Figure 2.8 for workflow to construct genome editing plasmids.

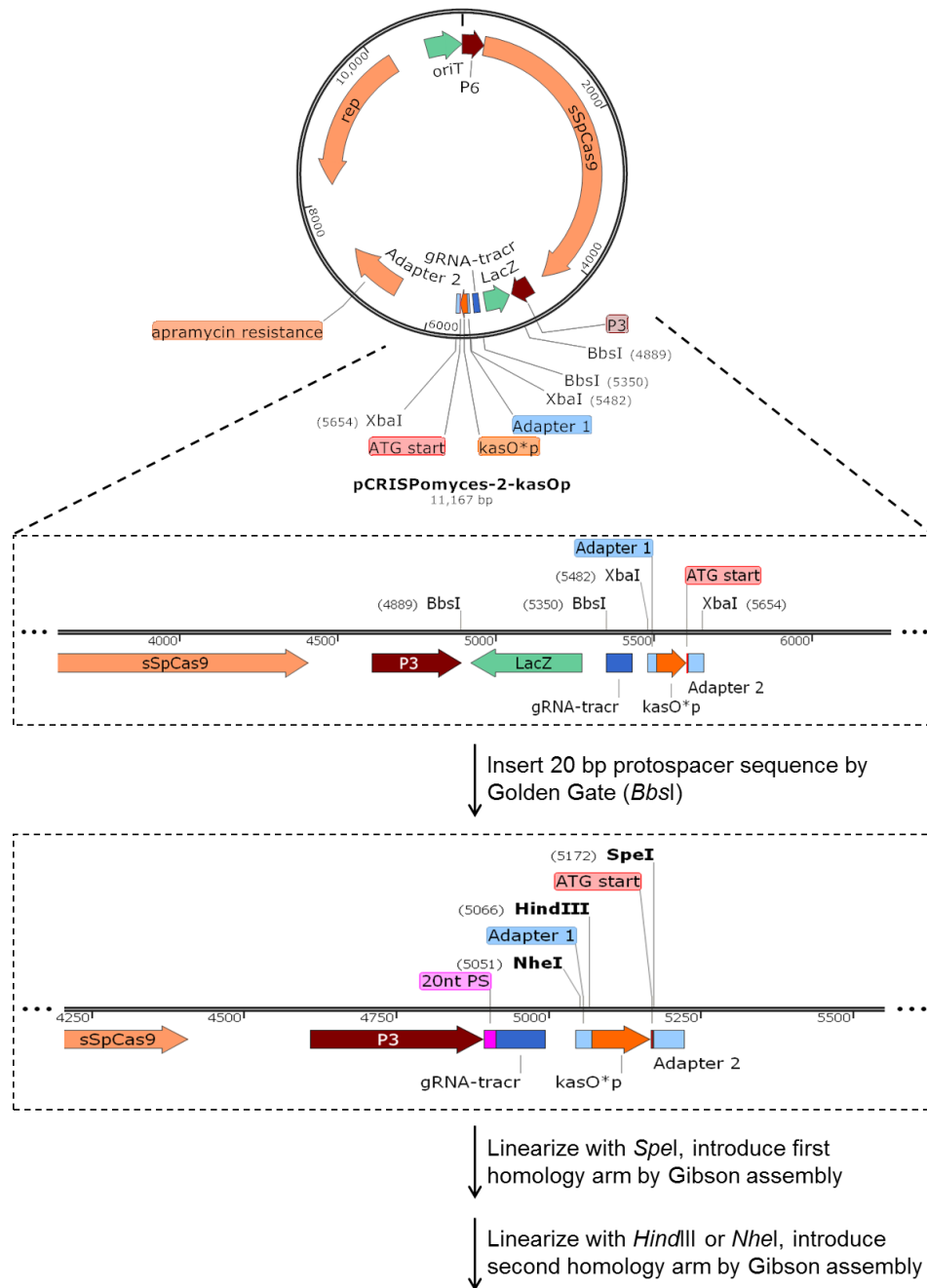
**Table 2.3.** Oligonucleotides used in this study

| Primers  | Sequence                  | Comments  |
|--|---------------------------|---|
| <i>Complementary oligonucleotides for BsaI Golden Gate assembly of protospacers. 20 bp protospacer sequences are represented in lowercase letters.</i> |                           |   |
| pCm2-C22-for   | ACGCccatgggtccgtctccaaggt | Cluster 22 protospacer in <i>S. viridochromogenes</i> |
| pCm2-C22-rev   | AAACaccttgagacggaccatgg   |   |
| pCm2-C24-for   | ACGCccccgtgtagctgcacaggg  | Cluster 24 protospacer in <i>S. viridochromogenes</i> |
| pCm2-C24-rev   | AAACccctgtgcagctacacgggg  |   |
| pCm2-C32-for   | ACGCctcaactccccacacagaa   | Cluster 32 protospacer in <i>S. viridochromogenes</i> |
| pCm2-C32-rev   | AAACttctgtgtgggggagttgag  |   |
| pCm2-C17-1-for-v2  | ACGCccgcatcagaattcgctg    | Cluster 17 protospacer in <i>S. viridochromogenes</i> |
| pCm2-C17-1-rev-v2  | AAAC ccgcatcagaattcgctg   |   |
| pCm2-C20-2-for   | ACGCgccaactcctctgagtaaat  | Cluster 20 protospacer in <i>S. viridochromogenes</i> |
| pCm2-C20-2-rev   | AAACatttactcagaggagttggc  |   |
| pCm2-C16-for   | ACGCgggggatggcggttctcga   | Cluster 16 protospacer in <i>S. viridochromogenes</i> |
| pCm2-C16-rev   | AAACtcgagaacgcgcatacccc   |   |
| pCm2-C6-1-for  | ACGCctcgatgagatcgccgatgg  | Cluster 6 protospacer in <i>S. viridochromogenes</i>  |
| pCm2-C6-1-rev  | AAACccatcggcgatctcatcgag  |   |

| Promoter      | Sequence  |
|---------------|---|
| <i>kas*Op</i> | AACTCCCCAGTCCTGCACGCTGTCGTATTCTCTGGCCACGACTTTACAACACCGCACAGCATG<br>TTGTCAAAGCAGAGACCGTTCGAATGTGAACA   |
| <i>rcfp</i>   | CCGCCCGCGGGACGTGACGAGCGGCACGACTCGACGACTCCGGGCTCCTTTGACGCTGTCCGT<br>CGCGCCGGGTAGCGTAGGACACCGTGCCCGCGCCGTCGGGCCCTCGCGCTGCACTCGGTGCG<br>ACCGTCCCTGCCGGAGTGGGTGCGGGTGACGGGGTGGCTCCCCACCTCTCTCGGATCGGT<br>CCTCGGGACTGCCGCCGTGCGGAGGACCGGGGGCGACACGCCCGGGCGCGGGGGTTCGGTGC<br>GGGACTCCAGACCTCCGGGGTAGTCTGTCGACGGGGCGACGATCCGGGCCGAGCCGGCCGTCC<br>TGGGTGACGGGTGCCGGTACAGACCAGAGAACACCGACAGACGGAGACGTA |



**Figure 2.7.** Constitutive promoters used for cluster activation. (A) sequences of constitutive promoters used in this study; (B, C) scheme and sequences of adapters introduced into pCRISPomyces at the *XbaI* site for making (B) monodirectional and (C) bidirectional promoter knock-in constructs. Restriction sites of selected enzymes are indicated in the sequence maps.



**Genome editing plasmid for conjugation/transformation into streptomycetes**

**Figure 2.8.** Workflow for constructing genome editing plasmid for promoter knock-in. Helper pCRISPomyces-2 plasmid (e.g. pCRISPomyces-2-*kasO\*p*) for making promoter knock-in constructs were made by ligating adapter sequences, containing restriction sites flanking the promoter of choice to facilitate insertion of homology arms into pCRISPomyces-2. The protospacer of a target cluster was first inserted via *BbsI*-mediated Golden Gate Assembly. The final editing plasmid was achieved by sequential insertion of the first and second homology arms by Gibson assembly.

#### 2.4.4. Interspecies Conjugation

Promoter knock-in constructs were used to transform conjugating *E. coli* strains and colonies with the appropriate antibiotic resistance (for example, 50 mg/L apramycin) were picked into LB with antibiotics. WM6026 requires diaminopimelic acid in LB for growth, which was added to LB for subsequent wash and resuspension steps. Overnight cultures were diluted 1:100 into fresh LB with antibiotics and grown to an OD<sub>600</sub> of 0.4–0.6. 400 µL of the culture was pelleted, washed twice and resuspended in LB without antibiotics. The washed *E. coli* cells were then mixed with spores at 1:5 volume ratio and spotted on R2 without sucrose plates. After incubation for 16–20 h at 30 °C, the plates were flooded with nalidixic acid and apramycin and incubated until exconjugants appear. Exconjugants were streaked onto MGY plates containing apramycin at 30 °C followed by restreaking to MGY plates at 37 °C to cure the CRISPR–Cas9 plasmid containing a temperature-sensitive origin of replication. Apramycin-sensitive clones growing at 37 °C were then subjected to validation of promoter knock-in and genome editing as described in Section 4.4.5.

#### 2.4.5. Validation of Promoter Knock-in and Genome Editing

Genomic DNA from wild type and exconjugants from the indicated strains were isolated from liquid cultures using the Blood and Tissue DNeasy kit (Qiagen) after pretreating the cells with 20 mg/mL lysozyme for 0.5–1 h at 30 °C. PCR was performed using control primers beyond the homology regions or knock-in specific primers (Table 2.3) with KODXtreme Taq polymerase (Millipore). Where indicated, PCR products were subjected to digestion with specific restriction enzymes to differentiate between PCR products of wild type genomic sequences and successful genome editing by knock-ins. Positive samples were purified using Qiaquick PCR purification kit (Qiagen) and validated by Sanger sequencing.

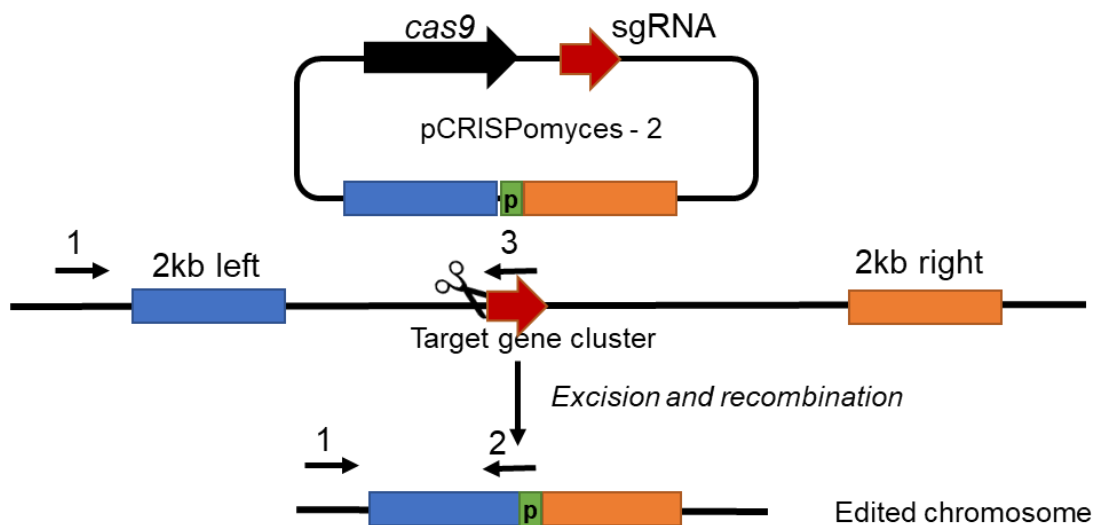


**Figure 2.9.** Diagnostic PCR verification of CRISPR-Cas9 mediated promoter knock-in for activation of silent BCGs. The positive candidates with correct promoter (P) cassette inserted should give 2kb band by using primer pairs 1 and 2. For the negative control, the PCR product should not show band with primer pairs 1 and 3.

#### 2.4.6. Metabolites Analysis

Liquid seed cultures (2 mL MGY) of wild type and engineered *S. viridochromogenes* strains were inoculated from a plate or spore stock in 14-mL culture tubes. Seed cultures were incubated at 30 °C with 250-rpm shaking until achieving turbidity or high particle density (typically 2–3 days). Seed cultures were diluted 1:100 into 50 mL of MGY broth in 250-mL baffled flasks containing ~30–40 5-mm glass beads and incubated at 30 °C with 250-rpm shaking for 5 days. The cultures were harvested by pelleting at maximum speed in an Eppendorf 5810R centrifuge for 10 min. The cell pellet was stored at -80 °C while the supernatants were split into two 50-mL Falcon tubes. Culture supernatants were extracted three times with equal volume ethyl acetate. For solid state cultures, the strains were grown on MGY plates at 30 °C for 10 days. The plates were chopped into small pieces and extracted twice with ethyl acetate. Extracts were dried and resuspended in methanol and analyzed by LC-MS using ESI source in positive ion mode (Bruker, Amazon SL Ion Trap) equipped with a Kinetex 2.6 μm XB-C18 100 Å (Phenomenex). HPLC parameters were as

follows: solvent A, 0.1% trifluoroacetic acid in water; solvent B, 0.1% trifluoroacetic acid in acetonitrile; gradient at a constant flow rate of 0.2 mL/min, 10% B for 5 min, 10% to 100% B in 35 min, maintain at 100% B for 10 min, return to 10% B in 1 min, and finally, maintain at 10% B for 10 min; detection by UV spectroscopy at 210, 254, 280, and 320 nm.

#### 2.4.7. Isolation and Nuclear Magnetic Resonance Spectroscopy Analysis of C22-1

Large-scale cultivation on solid plates (equivalent to 5L liquid culture) of the knock-in strain was carried out to obtain enough amount of the potential new compound. 10-day-growth, solid plates were soaked in equal volume ethyl acetate overnight. The extract was fractionated using C18 flash column chromatography and the fraction containing the target compound was further subjected to silica gel flash column chromatography. The column elution was monitored by TLC and the fractions containing the target compound were further confirmed by HPLC. High-resolution electrospray ionization mass spectrometry in positive mode showed an  $m/z$  of 421.0934 (calculated: 420.0934) and predicted molecular formula as  $C_{21}H_{16}O_8$  (Figure 2.10). Its chemical structure was elucidated by extensive one- and two-dimensional NMR spectroscopy ( $^1H$ ,  $^{13}C$ , Double-Quantum Filtered Correlation spectroscopy (COSY), Total correlation spectroscopy (TOCSY), Heteronuclear single-quantum correlation spectroscopy (HSQC), Heteronuclear multiple-bond correlation spectroscopy HMBC (Figure 2.11-2.17). NMR analysis was performed on an Agilent 600-MHz NMR spectrometer. The NMR peak assignment for C22-1 was summarized in Table 2.4.

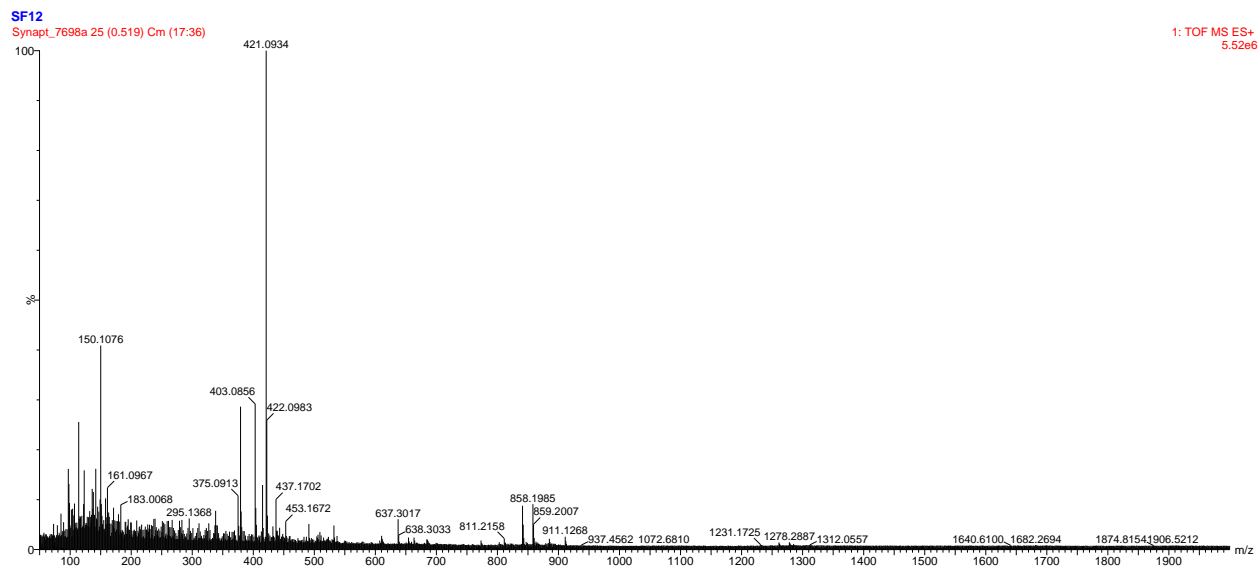
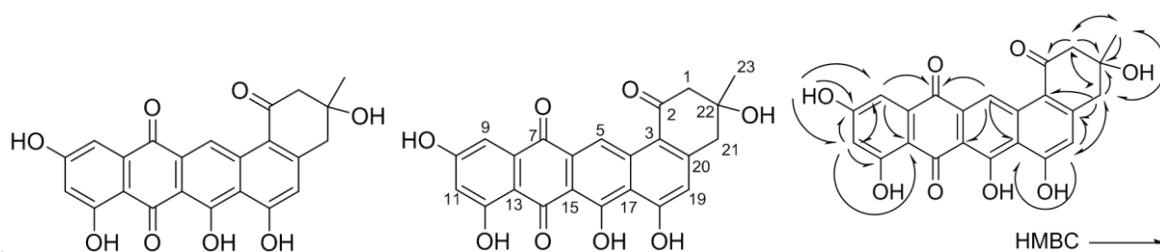


**Figure 2.10.** High-resolution electrospray ionization mass spectrometry in positive mode of compound C22-1.



**Table 2.4** NMR peak assignment of compound C22-1

| No.   | $\delta_C$ | viridomycin A (1)                |                |                         |
|-------|------------|----------------------------------|----------------|-------------------------|
|       |            | $\delta_H$ (J in Hz)             | COSY/<br>TOCSY | HMBC                    |
| 1     | 54.2       | 2.73, d (15.3)<br>2.61, d (15.3) |                | 2, 21, 22, 23           |
| 2     | 196.8      |                                  |                |                         |
| 3     | 150.7      |                                  |                |                         |
| 4     | 137.0      |                                  |                |                         |
| 5     | 115.2      | 9.30, s                          |                | 7, 15, 17               |
| 6     | 135.5      |                                  |                |                         |
| 7     | 183.5      |                                  |                |                         |
| 8     | 133.0      |                                  |                |                         |
| 9     | 105.8      | 7.07, s                          | 11             | 7, 11, 13               |
| 10    | 162.8      |                                  |                |                         |
| 11    | 108.1      | 6.52, s                          | 9              | 9, 10, 12, 13           |
| 12    | 164.4      |                                  |                |                         |
| 13    | 111.4      |                                  |                |                         |
| 14    | 184.1      |                                  |                |                         |
| 15    | 108.7      |                                  |                |                         |
| 16    | 169.2      |                                  |                |                         |
| 17    | 119.0      |                                  |                |                         |
| 18    | 175.2      |                                  |                |                         |
| 19    | 113.2      | 6.43, s                          | 21             | 17, 20, 21              |
| 20    | 117.1      |                                  |                |                         |
| 21    | 44.9       | 3.07, d (15.6)<br>2.95, d (15.6) | 19             | 1, 3, 19, 20, 22,<br>23 |
| 22    | 69.6       |                                  |                |                         |
| 23    | 28.9       | 1.26, s                          |                | 1, 21, 22               |
| 10-OH |            | 10.70, s                         |                | 9, 10, 11               |
| 12-OH |            | nd                               |                |                         |
| 16-OH |            | nd                               |                |                         |
| 18-OH |            | nd                               |                |                         |
| 22-OH |            | 4.77, s                          |                | 1, 21, 22, 23           |



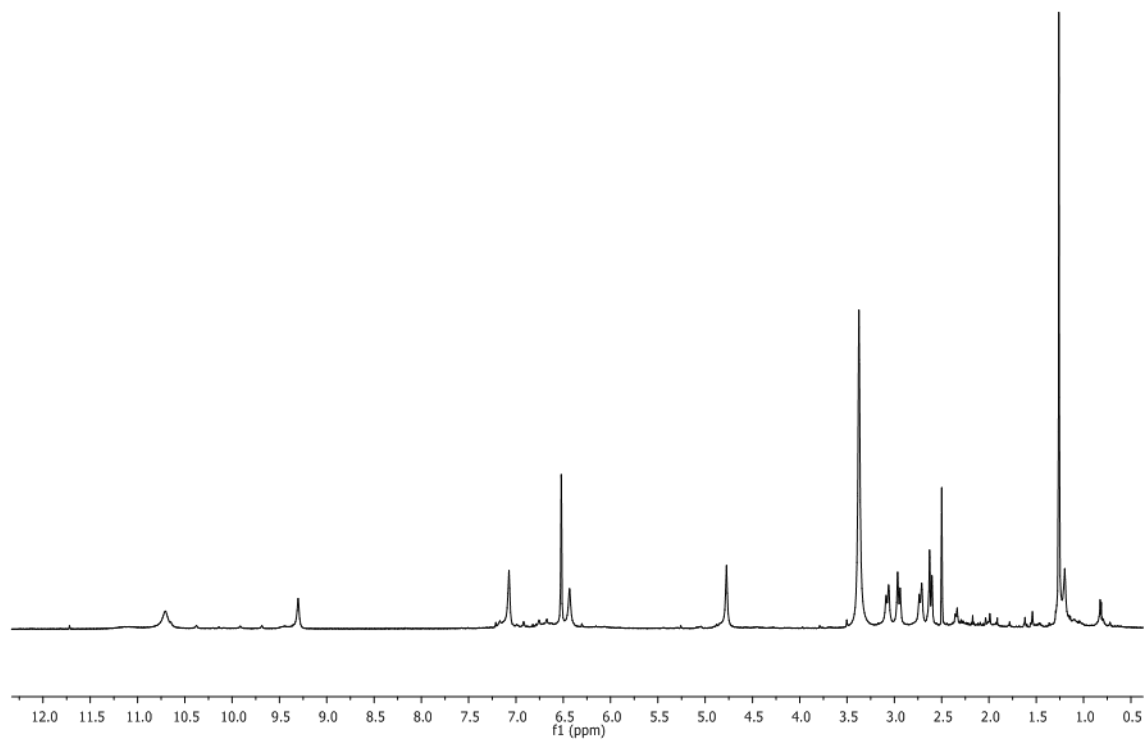


**Figure 2.11.**  $^1\text{H}$  NMR of C22-1 ( $\text{DMSO-}d_6$ )

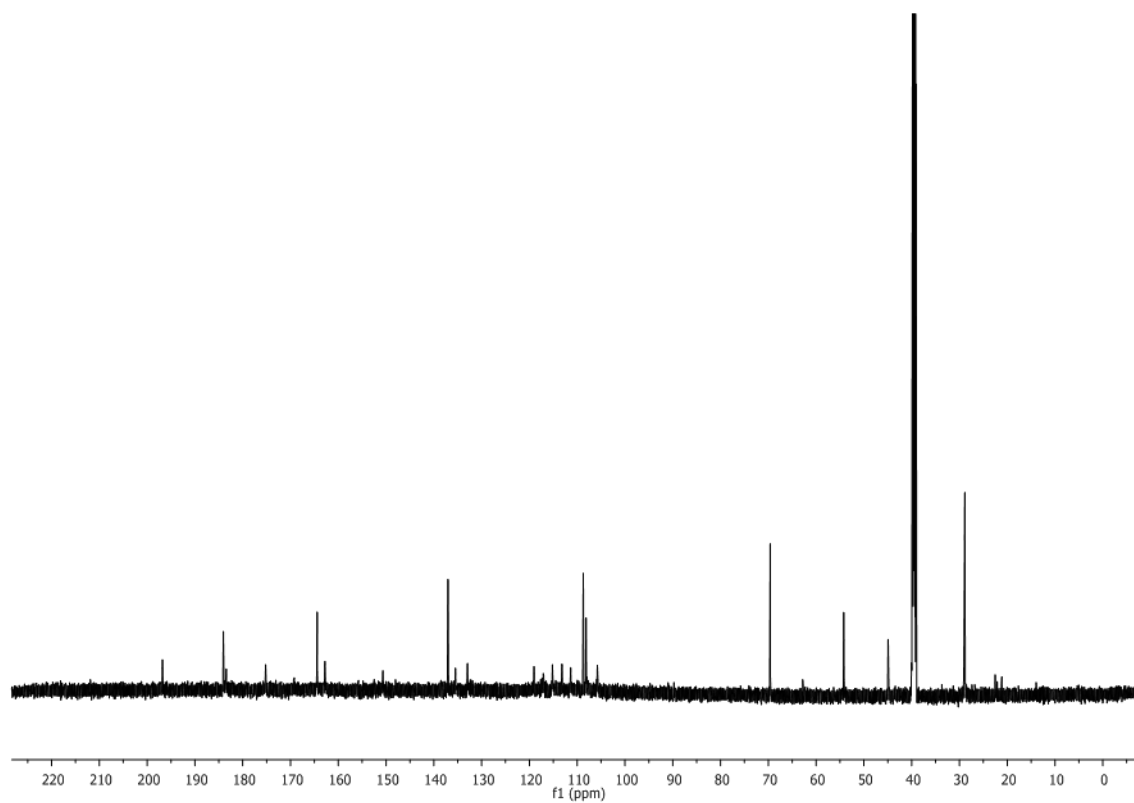


**Figure 2.12.**  $^{13}\text{C}$  of C22-1 (DMSO- $d_6$ )

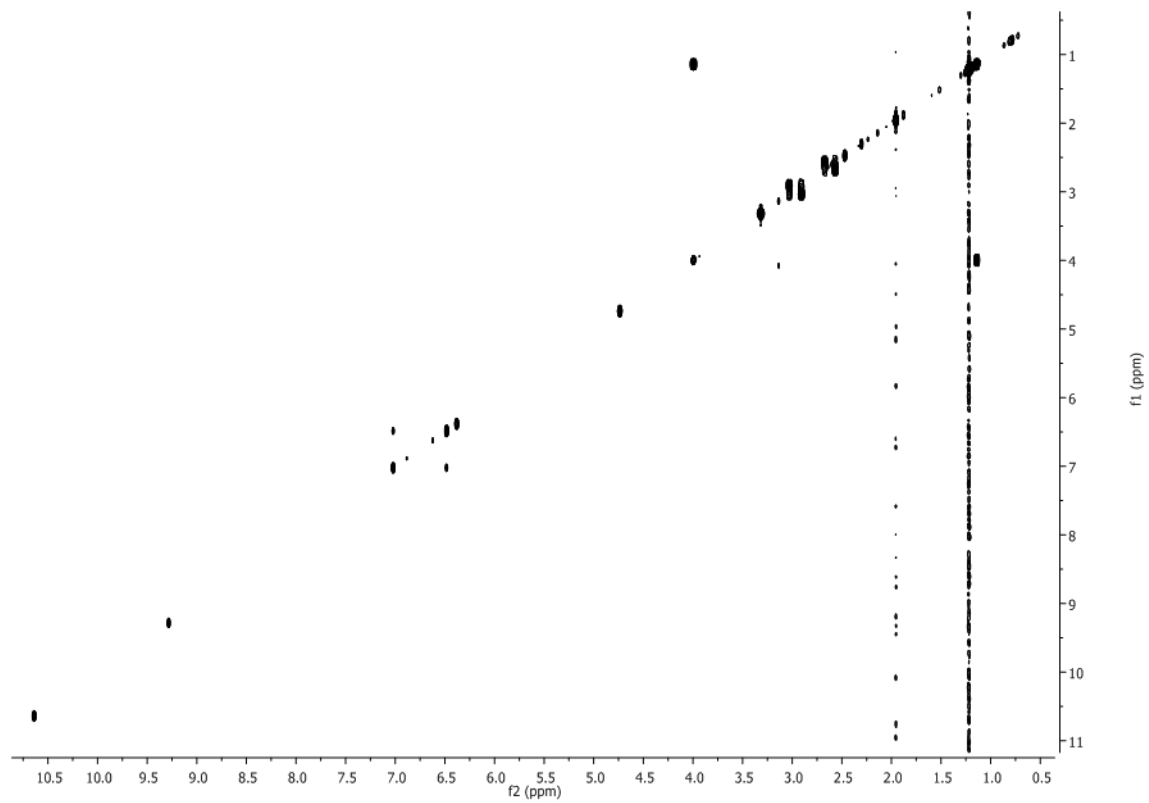


**Figure 2.13.** COSY of C22-1 (DMSO- $d_6$ )

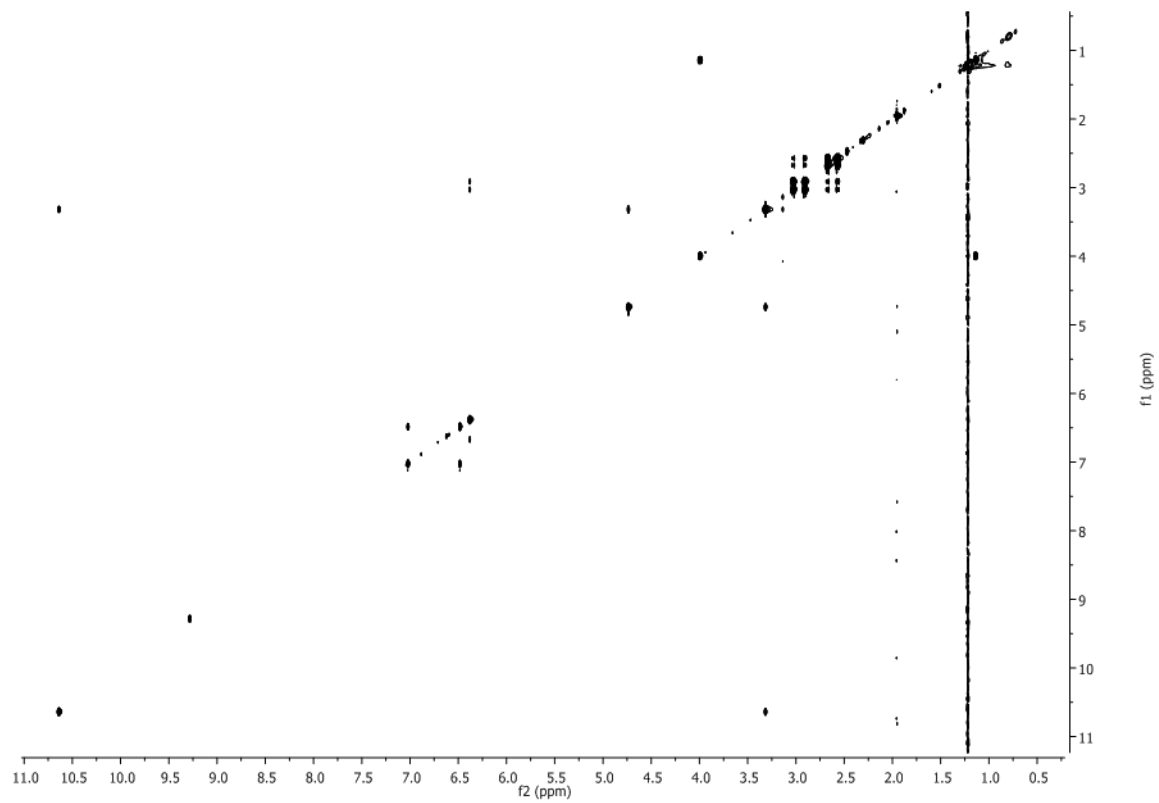


**Figure 2.14.** TOCSY of C22-1 (DMSO- $d_6$ )

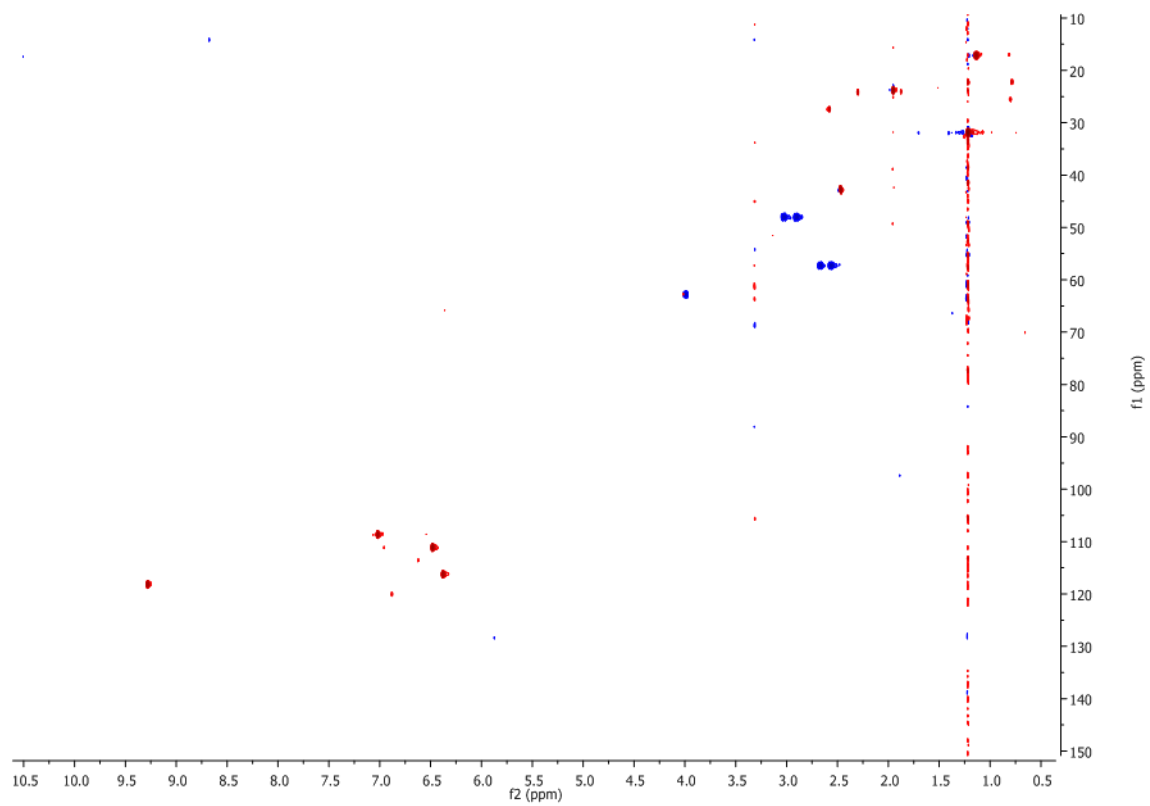


**Figure 2.15.** HSQC of C22-1 (DMSO- $d_6$ )

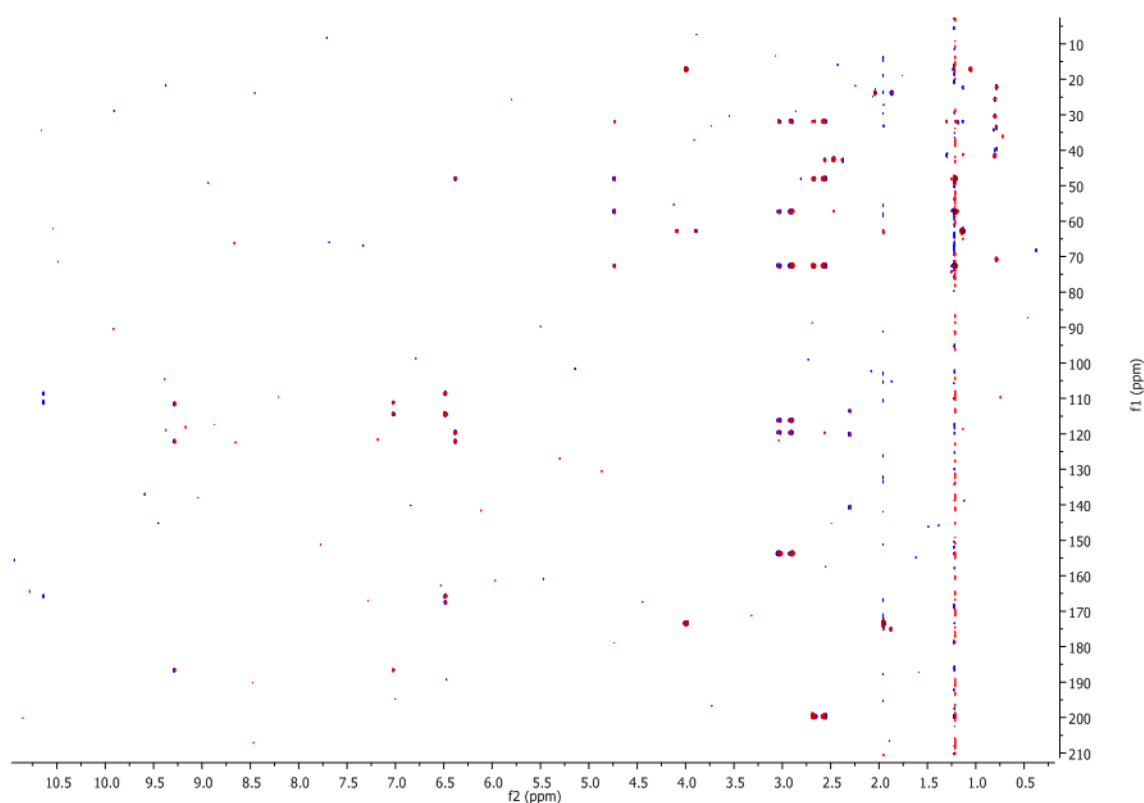


**Figure 2.16.** HMBC of C22-1 (DMSO- $d_6$ )

## 2.4 References

- 1 Baltz, R. H. Streptomyces and Saccharopolyspora hosts for heterologous expression of secondary metabolite gene clusters. *J. Ind. Microbiol. Biotechnol.* **37**, 759-772, (2010).
- 2 Zhang, M. M., Wang, Y., Ang, E. L. & Zhao, H. Engineering microbial hosts for production of bacterial natural products. *Nat. Prod. Rep.* **33**, 963-987, (2016).
- 3 Cobb, R. E., Wang, Y. & Zhao, H. High-efficiency multiplex genome editing of Streptomyces species using an engineered CRISPR/Cas system. *ACS synthetic biology* **4**, 723-728, (2015).
- 4 Zhang, M. M. *et al.* CRISPR-Cas9 strategy for activation of silent Streptomyces biosynthetic gene clusters. *Nat. Chem. Biol.*, (2017).
- 5 Olano, C. *et al.* Activation and identification of five clusters for secondary metabolites in Streptomyces albus J1074. *Microbial biotechnology* **7**, 242-256, (2014).
- 6 Bayer, E. *et al.* [Metabolic products of microorganisms. 98. Phosphinothricin and phosphinothricyl-alanyl-analine]. *Helv. Chim. Acta* **55**, 224-239, (1972).
- 7 Weber, T. *et al.* antiSMASH 3.0—a comprehensive resource for the genome mining of biosynthetic gene clusters. *Nucleic Acids Res.* **43**, W237-W243, (2015).
- 8 Cobb, R. E., Wang, Y. & Zhao, H. High-Efficiency Multiplex Genome Editing of Streptomyces Species Using an Engineered CRISPR/Cas System. *ACS synthetic biology*, (2014).

- 9 Blodgett, J. A., Zhang, J. K. & Metcalf, W. W. Molecular cloning, sequence analysis, and heterologous expression of the phosphinothricin tripeptide biosynthetic gene cluster from *Streptomyces viridochromogenes* DSM 40736. *Antimicrob. Agents Chemother.* **49**, 230-240, (2005).
- 10 Bentley, S. D. *et al.* Complete genome sequence of the model actinomycete *Streptomyces coelicolor* A3(2). *Nature* **417**, 141-147, (2002).
- 11 Redenbach, M. *et al.* A set of ordered cosmids and a detailed genetic and physical map for the 8 Mb *Streptomyces coelicolor* A3(2) chromosome. *Mol. Microbiol.* **21**, 77-96, (1996).
- 12 Prabhu, J., Schauwecker, F., Grammel, N., Keller, U. & Bernhard, M. Functional Expression of the Ectoine Hydroxylase Gene (*thpD*) from *Streptomyces chrysomallus* in *Halomonas elongata*. *Appl. Environ. Microbiol.* **70**, 3130-3132, (2004).
- 13 Kang, H. S. & Brady, S. F. Mining soil metagenomes to better understand the evolution of natural product structural diversity: pentangular polyphenols as a case study. *J. Am. Chem. Soc.* **136**, 18111-18119, (2014).
- 14 Hillenmeyer, M. E., Vandova, G. A., Berlew, E. E. & Charkoudian, L. K. Evolution of chemical diversity by coordinated gene swaps in type II polyketide gene clusters. *Proc. Natl. Acad. Sci. U. S. A.* **112**, 13952-13957, (2015).
- 15 Bergh, S. & Uhlen, M. Analysis of a polyketide synthesis-encoding gene cluster of *Streptomyces curacoi*. *Gene* **117**, 131-136, (1992).
- 16 Blanco, G. *et al.* A hydroxylase-like gene product contributes to synthesis of a polyketide spore pigment in *Streptomyces halstedii*. *J. Bacteriol.* **175**, 8043-8048, (1993).
- 17 Davis, N. K. & Chater, K. F. Spore colour in *Streptomyces coelicolor* A3(2) involves the developmentally regulated synthesis of a compound biosynthetically related to polyketide antibiotics. *Mol. Microbiol.* **4**, 1679-1691, (1990).
- 18 Kieser, T. *et al.* *Practical Streptomyces Genetics*. (John Innes Foundation, 2000).



# CHAPTER 3. Combining Rh-catalyzed Diazocoupling and Enzymatic Reduction to Efficiently Synthesize Enantioenriched 2-substituted Succinate Derivatives

## 3.1 Introduction

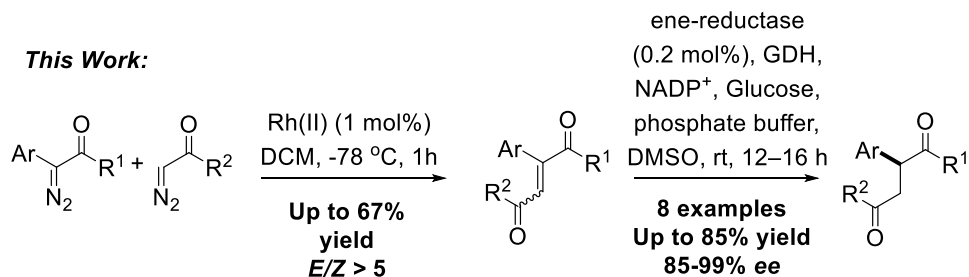
The increasing demand for chiral building blocks, particularly those used for the preparation of biologically active compounds, has motivated the development of novel strategies for enantioselective synthesis. To this end, systems that catalyze enantioselective carbon-carbon bond formation have been studied intensively.<sup>1-3</sup> Biocatalysts are increasingly employed to provide levels of chemo-, regio- and stereoselectivity that are challenging to achieve with a small-molecule catalyst, but applications of biocatalysts for carbon-carbon bond formation are limited.<sup>4-6</sup> The combination of chemical and biological catalysts in one-pot could enable transformations that cannot be achieved by either of the two catalysts alone,<sup>4,7</sup> and we considered that formal, enantioselective C-C bond formation could be achieved by combining a chemical catalyst that forms a C-C bond and an enzyme that can set a stereogenic center at one of the carbons of the new bond.

Asymmetric 2-substituted succinic acid derivatives are versatile building blocks for the preparation of biologically active compounds,<sup>8-11</sup> particularly natural products containing the  $\gamma$ -butyrolactone-unit.<sup>12-16</sup> Rhodium-catalyzed asymmetric hydrogenation of itaconic acid derivatives (Figure 3.1a) has been widely used to prepare enantiomerically enriched 2-substituted succinic acid derivatives, but these methods are not applicable to the synthesis of 2-aryl substituted succinic acid derivatives.<sup>17-20</sup> Meanwhile, the synthesis of 2-aryl succinic acid derivatives via organocatalytic and transition metal-catalyzed asymmetric hydrogenation of prochiral aryl-substituted fumaric (E)

and maleic (*Z*) acid derivatives remains challenging.<sup>21-36</sup> Only recently did Pfaltz and coworkers report an enantioselective Ir-catalyzed hydrogenation of 2-aryl-substituted fumarates and maleates (Figure 3.1b).<sup>21</sup> However, the hydrogenation reactions were limited to symmetric diesters and required high catalyst loadings and hydrogen pressure.

Alternative methods to prepare enantioenriched 2-aryl succinic derivatives include Rh-catalyzed 1,4-additions of arylboronic acids to fumarate derivatives (Figure 3.1c),<sup>37</sup> Cinchona alkaloid-catalyzed parallel kinetic resolution of monosubstituted succinic anhydrides (Figure 3.1d),<sup>38</sup> or enantioselective N-heterocyclic carbene (NHC)-catalyzed  $\beta$ -protonation through the orchestration of three distinct organocatalysts: triazolium salt, thiourea (HDB), and DMAP (Figure 3.1e).<sup>39</sup> However, each reaction has its limitations, such as requiring di-*tert*-butyl fumarates for high enantioselectivity, forming inseparable mixtures of constitutional isomers from fumarates bearing two different ester functional groups, having a maximum yield of 50%, and forming product with lower *ee* at higher conversion.

Enzymatic C=C bond reduction was once coupled with olefin synthesis to prepare non-chiral products.<sup>40</sup> Here we report a two-step, one-pot sequential chemoenzymatic transformation to prepare enantioenriched 2-aryl 1,4-dicarbonyl compounds with good yield and excellent enantioselectivity. This transformation combines a Rh(II)-catalyzed diazo coupling reaction with an enzymatic reduction into one-pot catalytic sequence that occurs in greater efficiency than the two individual steps, while avoiding purification of the alkene intermediates (Figure 3.1). This process constitutes a novel chemoenzymatic carbon-carbon bond formation with control of the absolute configuration of the new stereogenic center at one of the two carbons, while addressing limitations of the prior syntheses of 2-aryl succinic acid derivatives.



R<sup>1</sup> = OMe, Me  
R<sup>2</sup> = OEt, *Ot*Bu, OBn, 4-F-Ph

**Previous Work:**

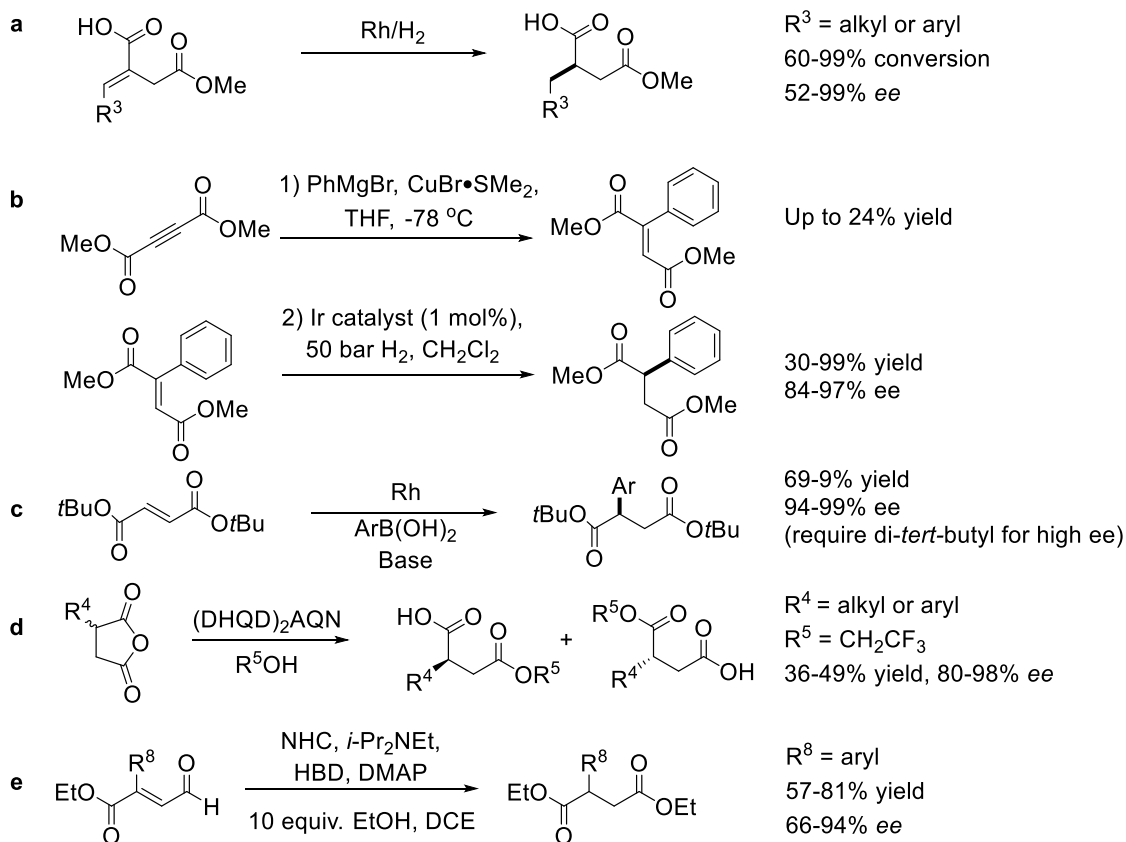


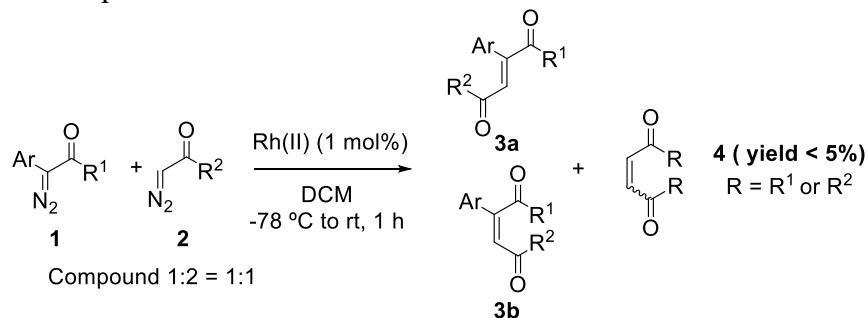
**Figure 3.1.** Synthesis of 2-aryl succinate derivatives using sequential rhodium- and enzyme catalysis (GDH: Glucose dehydrogenase, rt: room temperature).

## 3.2 Results and Discussion

### 3.2.1. Selective Synthesis of Unsymmetrical (*E*)-2-Aryl-substituted Alkenes

To create a modular, enantioselective route to 2-aryl-fumarate derivatives, we first investigated the synthesis of unsymmetrical 2-aryl-substituted, alkenes containing carbonyl groups at the 1 and 4 positions of the alkene. Davies and co-workers reported the  $[\text{Rh}_2(\text{OPiv})_4]$ -catalyzed cross-coupling of diazo compounds to form 2-aryl-fumarate derivatives with high chemo- and stereoselectivity,<sup>3</sup> and we tested reactions catalyzed by both  $[\text{Rh}_2(\text{OPiv})_4]$  and the commercially available rhodium(II) octanoate dimer  $[\text{Rh}_2(\text{Oct})_4]$ . As shown in Table 3.1, cross-coupling of aryldiazo compounds **1** with diazoacetate derivatives **2** affords predominantly the dicarbonyl compounds **3a** and **3b** with only trace amounts (<5%) of homodimerization product **4**. Importantly, the reaction catalyzed by  $[\text{Rh}_2(\text{OPiv})_4]$  occurs with high selectivity for formation of *E* alkenes (100% stereoselectivity favoring the (*E*)-diester, >10:1 stereoselectivity favoring (*E*)-ketone-ester, except entry 8). The reactions catalyzed by  $[\text{Rh}_2(\text{Oct})_4]$  occur with yields, chemoselectivity and stereoselectivity that are similar to those of reactions catalyzed by  $[\text{Rh}_2(\text{OPiv})_4]$ . With improved methods for preparation of diazo-compounds,<sup>41,42</sup> Rh(II)-catalyzed carbenoid-induced cross-coupling of diazo compounds serves as an attractive convergent method for the synthesis of unsymmetrical alkenes.

**Table 3.1.** Synthesis of asymmetric 2-aryl-substituted dicarbonyl alkenes by Rh-catalyzed cross-coupling of diazo compounds



| Entry | Ar                    | R <sup>1</sup> | R <sup>2</sup> | [Rh <sub>2</sub> (Oct) <sub>4</sub> ] |                        | [Rh <sub>2</sub> (OPiv) <sub>4</sub> ] |                        |
|-------|-----------------------|----------------|----------------|---------------------------------------|------------------------|--|------------------------|
|       |                       |                |                | <b>3a</b> <sup>a</sup>                | <b>3b</b> <sup>a</sup> | <b>3a</b> <sup>a</sup>                 | <b>3b</b> <sup>b</sup> |
| 1     | Ph                    | OMe            | OEt            | 44%                                   | -                      | 67%                                    | -                      |
| 2     | Ph                    | OMe            | OfBu           | 57%                                   | -                      | 74%                                    | -                      |
| 3     | Ph                    | OMe            | OBn            | 44%                                   | 6%                     | 67%                                    | -                      |
| 4     | Ph                    | OtBu           | OEt            | 39%                                   | -                      | N.A.                                   | N.A.                   |
| 5     | 4-F-Ph                | Me             | OEt            | 64%                                   | 7%                     | 57%                                    | 5%                     |
| 6     | 4-Cl-Ph               | Me             | OEt            | 68%                                   | 7%                     | 64%                                    | 4%                     |
| 7     | 3-CF <sub>3</sub> -Ph | Me             | OEt            | 47%                                   | 10%                    | 46%                                    | 3%                     |
| 8     | Ph                    | OMe            | 4-F-Ph         | 32%                                   | 4% <sup>c</sup>        | 20%                                    | 3%                     |

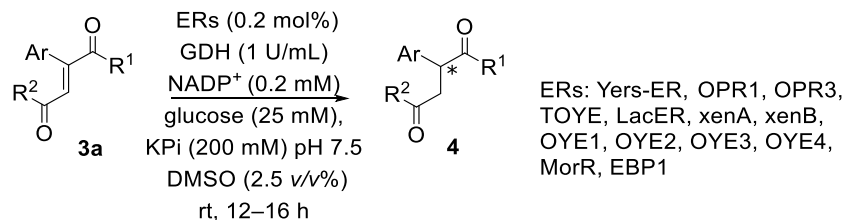
<sup>a</sup>Isolated yield. <sup>b</sup>Yield determined by GC analysis.

### 3.2.2. Enantioselective Enzymatic Reduction of C-C Double Bond

Ene-reductase (ER) containing flavin mononucleotides (FMN) require NADPH or NADH as co-factors to catalyze asymmetric reduction. In this study, glucose dehydrogenase (GDH) from *Bacillus megaterium* was used to recycle NADPH continuously by reduction of NADP<sup>+</sup> with concomitant conversion of glucose to gluconic acid. We tested the reduction of the 2-aryl fumaric and maleic acid derivatives with a series of ERs originating from different organisms, including Old Yellow Enzymes OYE1, OYE2 and OYE3 from *Saccharomyces cerevisiae*, OYE4 from *Achromobacter sp.*, 1, 2-oxophytodienoate reductases OPR1 and OPR3 from *Lycopersicon esculentum*, alkene reductase YersER from *Yersinia bercovieri*; thermophilic ‘ene’-reductase TOYE from *Thermoanaerobacter pseudethanolicus*, LacER from *Lactobacillus casei*, XenA and XenB from *Pseudomonas putida*, and NADPH dehydrogenase EBP1 from *Candida albicans*.

Most of the ERs catalyzed the reduction of the E isomers (**3a**) of 2-aryl-substituted, 1,4-dicarbonyl alkenes generated from the cross-coupling reactions of the diazo compounds, but some of them resulted in products with poor *ee* (Table 3.3). None of the ERs we tested reduced the trace amount of Z isomers **3b** (<5%), based on GC evaluation. Table 3.2 shows the asymmetric reduction of (*E*)-2-aryl-substituted, 1,4-dicarbonyl alkenes by the ERs that gave the product in 65%-85% yield. In general, ERs catalyzed the reduction of the alkenes containing two esters with excellent enantioselectivity (>99%) (Entries 1&2) and the reduction of alkenes containing one ketone and one ester with good to excellent enantioselectivity (85%-99%) (Entry 5-8). OPR1 is the only enzyme we tested that reduced the unsaturated 1,4-dicarbonyl compounds containing bulky ester groups at the carbon  $\beta$  to the aryl group (Entries 2&3) to form enantioenriched 2-aryl succinate derivatives bearing two distinct esters that allow orthogonal reactivity at each terminus.<sup>39</sup> None of the enzymes catalyzed the reduction of the substrate containing a bulky ester group and aryl group on the same alkene carbon (Entry 4).

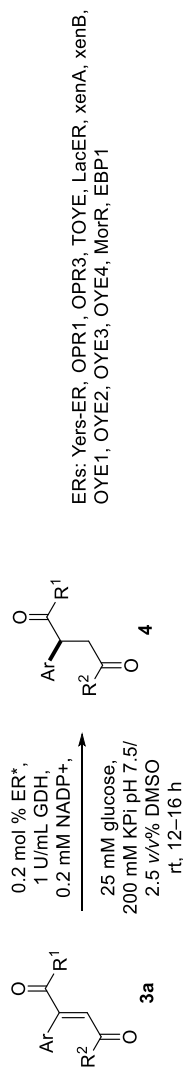
Compared to metal-catalyzed hydrogenation of dimethyl 2-phenylmaleates,<sup>21</sup> the enzymatic reduction offers several advantages. The turnover numbers for the enzymatic reduction were seventy times higher than those obtained with current catalysts, and the process occurred with excellent enantioselectivity (>99%) at room temperature, in phosphate buffer under atmospheric pressure. Furthermore, YersER tolerates both water miscible organic solvents, such as DMSO and ethylene glycol, and immiscible organic solvents such as hexane and toluene.<sup>43</sup> This tolerance toward organic solvents enhances the potential use of ERs for reactions of less water-soluble substrates.

**Table 3.2.** Enzymatic reduction of (E)-2-aryl-substituted, 1,4-dicarbonyl alkenes by ene-reductases

| Entry | Ar                    | R <sup>1</sup> | R <sup>2</sup> | Yield <sup>a</sup> <b>4</b> | % <i>ee</i>  | Most selective ER      | Large scale isolated yield <sup>b</sup> | TON <sup>e</sup>         |
|-------|-----------------------|----------------|----------------|-----------------------------|--|------------------------|---|--------------------------|
| 1     | Ph                    | OMe            | OEt            | 91%<br>71% <sup>f</sup>     | >99% <sup>c</sup>  | YersER                 | 84%                                     | 455<br>7071 <sup>f</sup> |
| 2     | Ph                    | OMe            | O <i>t</i> Bu  | 76%                         | >99% <sup>c</sup>  | OPR1                   | 65%                                     | 650                      |
| 3     | Ph                    | OMe            | OBn            | 86%                         | >99% <sup>c</sup>  | OPR1                   | 80%                                     | 430                      |
| 4     | Ph                    | O <i>t</i> Bu  | OEt            | -                           | -  | -                      | -                                       | -                        |
| 5     | 4-F-Ph                | Me             | OEt            | 80%                         | 87% <sup>c</sup>   | YersER                 | 75%                                     | 375                      |
| 6     | 4-Cl-Ph               | Me             | OEt            | 85%                         | 85% <sup>d</sup>   | YersER                 | 78%                                     | 423                      |
| 7     | 3-CF <sub>3</sub> -Ph | Me             | OEt            | 78%                         | 85% <sup>d</sup>   | YersER                 | 70%                                     | 322                      |
| 8     | Ph                    | OMe            | 4-F-Ph         | 87%<br>74%<br>93%           | >99% <sup>d</sup><br>>99% <sup>d</sup><br>93% <sup>d</sup> | OYE2<br>YersER<br>OPR1 | 80%<br>69%<br>85%                       | 460<br>370<br>465        |

<sup>a</sup>GC yield. <sup>b</sup>large-scale (0.2 mmol) reactions and isolated yield. <sup>c</sup>*ee* determined by chiral SFC. <sup>d</sup>*ee* determined by chiral HPLC. <sup>e</sup>Turn over number (TON) is defined as the number of moles of substrate that a mole of catalyst can convert before becoming inactivated. KPi: sodium phosphate buffer. <sup>f</sup>Reaction with 0.01 mol% enzyme loading

**Table 3.3.** Enzymatic reduction of 2-aryl substituted fumarate derivatives by various ERs.



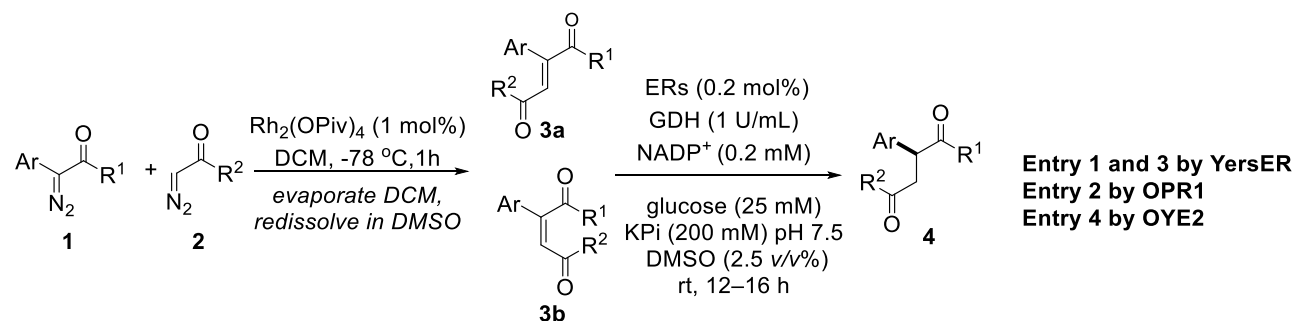
| Entry                                  | Yers-ER | OYE1                          | OYE2 | OYE3 | TOYE | OPR1                          | OPR3 | XenA | XenB | OYE4 | EBP1 |
|--|---------|-------------------------------|------|------|------|-------------------------------|------|------|------|------|------|
| R <sup>1</sup> = OMe                   | Yield   | 47%                           | 46%  | 49%  | 39%  | - <sup>a</sup>                | -    | -    | -    | -    | -    |
| R <sup>2</sup> = OEt                   | % ee    | >99% (α <sub>D</sub> : -128°) | >99% | >99% | >99% | -                             | -    | -    | -    | -    | -    |
| R <sup>3</sup> = Ph                    |         |                               |      |      |      |                               |      |      |      |      |      |
| R <sup>1</sup> = OMe                   | Yield   | 19%                           | 20%  | 13%  | 6%   | 76%                           | 1%   | 3%   | 15%  | 0%   | 0%   |
| R <sup>2</sup> = <i>i</i> Bu           | % ee    | -                             | -    | -    | -    | >99% (α <sub>D</sub> : -108°) | -    | -    | -    | -    | -    |
| R <sup>3</sup> = Ph                    |         |                               |      |      |      |                               |      |      |      |      |      |
| R <sup>1</sup> = OMe                   | Yield   | 7%                            | 13%  | 12%  | 3%   | 86%                           | 0%   | 1%   | 8%   | 0%   | 0%   |
| R <sup>2</sup> = OBn                   | % ee    | -                             | -    | -    | -    | >99% (α <sub>D</sub> : -56°)  | -    | -    | -    | -    | -    |
| R <sup>3</sup> = Ph                    |         |                               |      |      |      |                               |      |      |      |      |      |
| R <sup>1</sup> = Me                    | Yield   | 80%                           | 44%  | 48%  | 68%  | 58%                           | 76%  | 51%  | 69%  | 17%  | 93%  |
| R <sup>2</sup> = OEt                   | % ee    | 87% (α <sub>D</sub> : -253°)  | 81%  | 81%  | 82%  | 80%                           | 82%  | 82%  | 82%  | -    | 73%  |
| R <sup>3</sup> = 4-F-Ph                |         |                               |      |      |      |                               |      |      |      |      |      |
| R <sup>1</sup> = Me                    | Yield   | 75%                           | 66%  | 76%  | 63%  | 84%                           | 93%  | 59%  | 66%  | 63%  | 93%  |
| R <sup>2</sup> = OEt                   | % ee    | 85% (α <sub>D</sub> : -150°)  | 76%  | 80%  | 79%  | 82%                           | 81%  | 80%  | 81%  | 76%  | 70%  |
| R <sup>3</sup> = 4-Cl-Ph               |         |                               |      |      |      |                               |      |      |      |      |      |
| R <sup>1</sup> = Me                    | Yield   | 32%                           | 44%  | 41%  | -    | 33%                           | 40%  | 24%  | 39%  | 9%   | 22%  |
| R <sup>2</sup> = OEt                   | % ee    | 85% (α <sub>D</sub> : -239°)  | 51%  | 49%  | -    | 79%                           | 56%  | 79%  | 82%  | 5%   | 76%  |
| R <sup>3</sup> = 3-CF <sub>3</sub> -Ph |         |                               |      |      |      |                               |      |      |      |      |      |
| R <sup>1</sup> = OMe                   | Yield   | 87%                           | 87%  | -    | -    | 91%                           | -    | -    | -    | -    | -    |
| R <sup>2</sup> = 4-F-Ph                | % ee    | >99% (α <sub>D</sub> : -98°)  | >99% | -    | -    | 93%                           | -    | -    | -    | -    | -    |
| R <sup>3</sup> = Ph                    |         |                               |      |      |      |                               |      |      |      |      |      |



### 3.2.3. Two-step Sequential Reaction to Synthesize Enantioenriched 2-Aryl-Substituted Succinate Derivatives

Having identified an ER that reduces the substrates of the Rh-catalyzed coupling of diazocompounds, we sought to develop conditions to conduct the two reactions in one pot without purification of the intermediates. After conducting the diazo coupling reaction, we evaporated the DCM, added all reagents and the ER for the reduction step into the crude mixture. The one-pot process formed the enantioenriched succinate derivatives in >70% yield by completely converting the (E)-alkenes, the major product from cross-coupling reaction (Table 3.4) and leaving the (Z)-alkene unreacted. Similar yield and enantioselectivity were observed with purified samples of the alkene (Table 3.2), suggesting that the ERs are compatible with the Rhodium(II) catalyst and trace amounts of chemical impurities contained in the crude cross coupling reaction.

**Table 3.4.** Two-step sequential reaction to synthesize enantioenriched 2-aryl-substituted succinate derivatives



| Entry | Ar                    | R <sup>1</sup> | R <sup>2</sup> | Yield <sup>a</sup> |                 |                | %ee <sup>d</sup> | Isolated yield over two steps <sup>e</sup> | TON |
|-------|-----------------------|----------------|----------------|--------------------|-----------------|----------------|------------------|--|-----|
|       |                       |                |                | 3a <sup>b</sup>    | 3b <sup>b</sup> | 4 <sup>c</sup> |                  |  |     |
| 1     | Ph                    | OMe            | OEt            | 78%                | 0%              | 93%            | >99%             | 62%  | 465 |
| 2     | Ph                    | OMe            | OBn            | 72%                | 0%              | 88%            | >99%             | 54%  | 440 |
| 3     | Ph                    | OMe            | 4-F-Ph         | 38%                | 4%              | 90%            | >99%             | 26%  | 450 |
| 4     | 3-CF <sub>3</sub> -Ph | Me             | OEt            | 56%                | 4%              | 82%            | 89%              | 37%  | 410 |

<sup>a</sup>Determined by GC analysis. <sup>b</sup>Trace amount of reaction mixture was taken after the diazocoupling reaction and evaluated by GC analysis. <sup>c</sup>Calculated based on the starting materials for enzymatic reaction. <sup>d</sup>ee determined by chiral HPLC. <sup>e</sup>Calculated based on the starting materials of the cross-coupling reaction.

### 3.2.4. Docking Experiments

To provide possible explanations of the origin of the selectivity of ERs for (E)-alkenes over (Z)-alkenes, we conducted computational docking studies. Docking of 4-ethyl 1-methyl 2-phenylfumarate and 4-ethyl 1-methyl 2-phenylmaleate into the active site of OPR1 was conducted using the crystal structure of OPR1 (Figure 3.2) containing p-hydroxybenzoic acid (PHB) bound to the active site.

As shown in Figure 3.3A, the carbonyl oxygen of 4-ethyl 1-methyl 2-phenylfumarate is hydrogen bonded to His-187 N $\epsilon$ 2 and His-190 N $\delta$ 1 with distances of 3.2 Å and 2.8 Å respectively. The distance between the N(5) of FMNH2 (transferring a hydride) and the carbon of the alkene that is  $\beta$  to the aryl group ( $\beta$ -carbon) of the substrate is 4.0 Å, and the distance between the Tyr 192 (a proton donor) and  $\alpha$ -carbon of the substrate is 3.9 Å. The (Z)-alkene 4-ethyl 1-methyl 2-phenylmaleate binds to the same site of OPR1 (Figure 3.3B). However the distance between N(5) of FMNH2 and the  $\beta$  carbon is more than 5.0 Å. This distance would be too large for the reaction to occur. In addition, the more hindered 4-(tert-butyl) 1-methyl 2-phenylfumarate did not dock into most of the ERs (data are not shown), but it did dock into OPR1. As shown in Figure 3.3C, the distance between the N(5) of FMNH2 and the  $\beta$ -carbon of 4-(tert-butyl) 1-methyl 2-phenylfumarate, and the distance between Tyr 192 and  $\alpha$ -carbon of 4-(tert-butyl) 1-methyl 2-phenylfumarate are both 4.0 Å. These distances are comparable to those between the proton and hydride donors of OPR1 to 4-ethyl 1-methyl 2-phenylfumarate. A pocket formed by Tyr-78, Lys-79 and Tyr-358 at the entrance of active site accommodates the phenyl ring, while the relatively open active site entrance may tolerate the bulky tert-butyl group (Figure 3.3D).

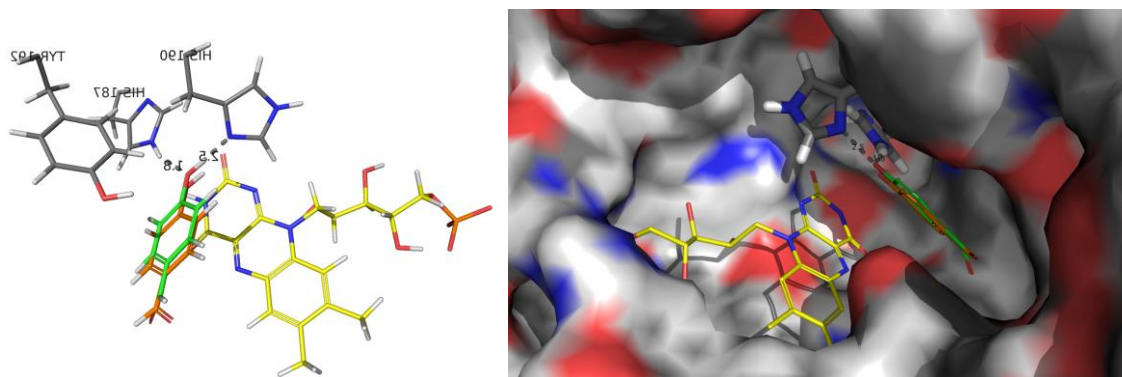


**Figure 3.2.** Docking of p-hydroxybenzoic acid (PHB) into the active site of OPR1 in the crystal structure. (Left) Overlay of docked PHB (green) with original PHB (orange) in the crystal structure. (Right) Surface representation of the active site view of OPR1 with PHB docked at the active site.

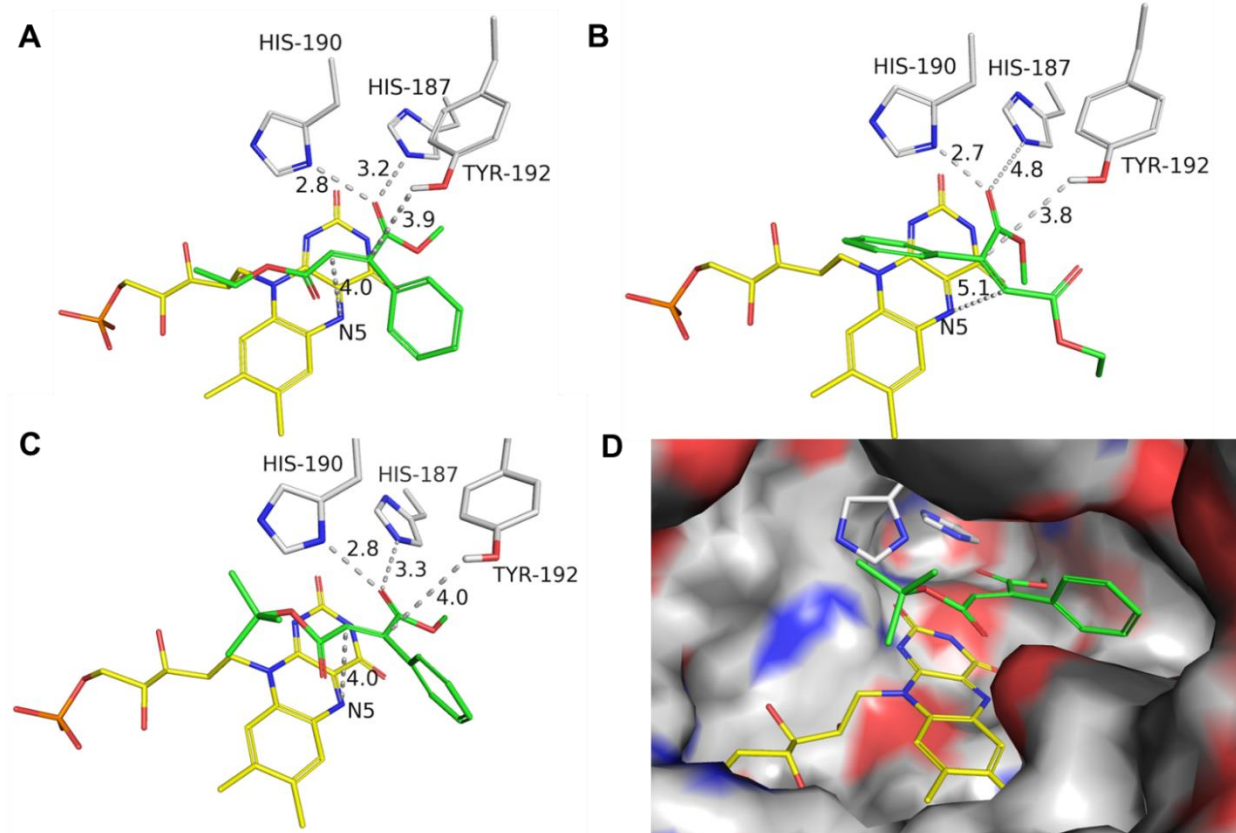


**Figure 3.3.** Docking of A) 4-ethyl 1-methyl 2- phenylfumarate, B) 4-ethyl 1-methyl 2-phenylmaleate, and C) 4-(*tert*-butyl) 1-methyl 2-phenylfumarate within the active site of OPR1. D) the surface representation of the active site view of OPR1 with 4-(*tert*-butyl) 1-methyl 2-phenylfumarate docked at active site. In the stick models, substrates shown in green, FMN shown in yellow, protein residues shown in grey.

### 3.3 Conclusions and Outlook

In summary, we have developed a one-pot, sequential catalytic system for the synthesis of 2-aryl-succinate derivatives by formal asymmetric C-C bond formation created by integrating a transition-metal catalyst with an enzyme, whereby a Rh-catalyzed cross-coupling of car-bene units is followed by an ER-catalyzed enantioselective reduction of (E)-2-aryl-substituted dicarbonyl alkenes among a mixture of the E and Z isomers. With this system, 2-aryl-substituted succinate derivatives are generated from two different diazoesters or ketones and reducing equivalents in high yield and excellent ee with-out purification of the alkene intermediates or separation of E and Z isomers. Evaluation of a panel of ERs as catalyst led to the identification of OPR1, which reacts with substrates containing bulky tert-butyl esters and produces enantioenriched, chiral unsymmetrical diesters that have great potential as synthetic intermediates.

### 3.4 Experimental Procedures

#### 3.4.1. Materials

Unless otherwise stated, all chemicals, reagents and catalysts were purchased from Sigma-Aldrich. *E. coli* DH5 $\alpha$  cells were purchased from the Cell Media Facility at the University of Illinois at Urbana-Champaign (Urbana, IL). *Escherichia coli* BL21 (DE3) and plasmid pET28a<sup>+</sup> were purchased from Novagen (Madison, WI). Oligonucleotides for cloning were purchased from Integrated DNA Technologies (IDT) (Coralville, IO). Restriction enzymes were purchased from New England Biolabs (Ipswich, MA). NADPH was purchased from Enzo Life Sciences (Farmingdale, NY). NADP<sup>+</sup> was purchased from Roche Diagnostics (Indianapolis, IN). Isopropyl- $\beta$ -D-thiogalactoside (IPTG) was purchased from GoldBio (St. Louis, MO). The strain *Bacillus megaterium* (B14308) was obtained from the NRRL culture collection (Peoria, IL).

### 3.4.2. Cloning, Expression and Purification of Enzymes

The YersER investigated in this research is from *Yersinia bercovieri*. The codon-optimized gene was synthesized by IDT and cloned in pET28a with N-terminal His-tag. For expression of YersER, a BL21 clone harboring pET28a-YersER was inoculated in 5 mL LB medium containing 100 µg/mL ampicillin and grown overnight at 37 °C. This overnight culture was used to inoculate 500 mL of TB medium containing 50 µg/mL kanamycin, which was grown at 37 °C until an OD of ~0.6 was reached, and subsequently induced with the addition of 0.3 mM IPTG. The induced culture was placed at 25 °C, 250rpm, for 16 h for protein production.

The OYE1/2/3 investigated in this research is from baker's yeast. The plasmid pET30a-OYE1/2/3 with N-terminal His-tag was a gift from Dr. Francesco G. Gatti. The plasmid was transformed into *E. coli* BL21. For expression of OYE1/2/3, a BL21 clone harboring pET30a-OYE1/2/3 respectively was inoculated in 5 mL LB medium containing 50 µg/mL kanamycin and grown overnight at 37 °C. This overnight culture was used to inoculate 500 mL of LB medium containing 50 µg/mL kanamycin, which was grown at 37 °C until an OD of ~0.6 was reached, and subsequently induced with the addition of 0.1 mM IPTG. The induced culture was placed at 25 °C, 250 rpm, for 16 h for protein production.

The OPR1 investigated in this research is from *Lycopersicon esculentum* (tomato). The plasmid pET21b-OPR1 with C-terminal His-tag was a gift from Dr. Kurt Faber. The plasmid was transformed into *E. coli* BL21. For expression of OPR1, a BL21 clone harboring pET21b-OPR1 was inoculated in 5 mL LB containing 100 µg/mL ampicillin and grown overnight at 37 °C. This overnight culture was used to inoculate 500 mL of TB medium containing 100 µg/mL ampicillin, which was grown at 37 °C until an OD of ~0.6 was reached, and subsequently induced with the

addition of 1 mM IPTG. The induced culture was placed at 25 °C, 250 rpm, for 16 h for protein production.

The OPR3 investigated in this research is from *Lycopersicon esculentum* (tomato). The plasmid pET21b-OPR3 with C-terminal His-tag was a gift from Dr. Kurt Faber. The plasmid was transformed into *E. coli* BL21. For expression of OPR3, a BL21 clone harboring pET21b-OPR3 was inoculated in 5 mL LB medium containing 100 µg/mL ampicillin and grown overnight at 37 °C. This overnight culture was used to inoculate 500 mL of TB medium containing 100 µg/mL ampicillin, which was grown at 37 °C until an OD of ~0.6 was reached, and subsequently induced with the addition of 1 mM IPTG. The induced culture was placed at 25 °C, 250 rpm, for 16 h for protein production.

KYE1 is from *Kluyveromyces lactis* NRRL Y-1140. The gene was synthesized by IDT and codon-optimized for *E. coli* expression. The gene was cloned into pET28a using restriction enzymes *NdeI* and *XhoI*. The plasmid pET28a-KYE1 was transformed into *E. coli* BL21 with N-terminal His-tag. For expression of KYE1, a BL21 clone harboring pET28a-KYE1 was inoculated in 5 mL LB medium containing 50 µg/mL kanamycin and grown overnight at 37 °C. This overnight culture was used to inoculate 500 mL of TB medium containing 50 µg/ml kanamycin, which was grown at 37 °C until an OD of ~0.5-0.6 was reached, and subsequently induced with the addition of 0.1 mM IPTG. The induced culture was placed at 25 °C for 16 h for protein production.

MorR is from *Pseudomonas putida*. The gene was synthesized by IDT and codon-optimized for *E. coli* expression. The gene was cloned into pET28a using restriction enzymes *NdeI* and *XhoI* with N-terminal His-tag. The plasmid pET28a-MorR was transformed into *E. coli* BL21. For expression of MorR, a BL21 clone harboring pET28a-MorR was inoculated in 5 mL LB medium containing 50 µg/mL kanamycin and grown overnight at 37 °C. This overnight culture

was used to inoculate 500 mL of TB medium containing 50 µg/ml kanamycin, which was grown at 37 °C until an OD of ~0.5-0.6 was reached, and subsequently induced with the addition of 1 mM IPTG. The induced culture was placed at 20 °C for 16 h for protein production.

SYE1 is from *Shewanella oneidensis* MR-1. The gene was synthesized by IDT and codon-optimized for *E. coli* expression. The gene was cloned into pET28a between restriction enzymes *Nde*I and *Xho*I with N-terminal His-tag. The plasmid pET28a-SYE1 was transformed into *E. coli* BL21. For expression of MorR, a BL21 clone harboring pET28a-SYE1 was inoculated in 5 mL LB medium containing 50 µg/mL kanamycin and grown overnight at 37 °C. This overnight culture was used to inoculate 500 mL of TB medium containing 50 µg/ml kanamycin, which was grown at 37 °C until an OD of ~0.5-0.6 was reached, and subsequently induced with the addition of 0.5 mM IPTG. The induced culture was placed at 28 °C for 15 h for protein production.

The XenA and XenB investigated in this research are from *Pseudomonas putida* ATCC 17453. The plasmid pGaston-xenA and pGaston-xenB with C-terminal His-tag was a gift from Dr. Uwe T. Bornscheuer. The plasmid was transformed into *E. coli* BL21. For expression of *xenA* or *xenB*, a BL21 clone harboring pGaston-xenA/xenB was inoculated in 5 mL LB medium containing 100 µg/mL ampicillin and grown overnight at 37 °C. This overnight culture was used to inoculate 500 mL of LB medium containing 100 µg/mL ampicillin, which was grown at 37 °C at 180 rpm until an OD of ~0.6-0.8 was reached, and subsequently induced with the addition of 0.2% (w/v) rhamnose. The induced culture was placed at 25 °C (XenB) or 30 °C (XenA) for 8 h.

The LacER investigated in this research is from *Lactobacillus casei*, The plasmid pET21a(+)-LacER with C-terminal His-tag was a gift from Dr. Dunming Zhu. The plasmid was transformed into *E. coli* BL21. For expression of LacER, a BL21 clone harboring pET21b-LacER was inoculated in 5 mL LB medium containing 100 µg/mL ampicillin and grown overnight at 37

°C. This overnight culture was used to inoculate 500 mL of LB medium containing 100 µg/mL ampicillin, which was grown at 37 °C until an OD of ~0.6-0.8 was reached, and subsequently induced with the addition of 1 mM IPTG. The induced culture was placed at 30 °C, 250 rpm, for 15 h for protein production

The TOYE investigated in this research is from *Thermoanaerobacter pseudotahnolicus* E39. The plasmid pET21b-TOYE with C-terminal His-tag was a gift from Dr. Uwe T. Bornscheuer. The plasmid was transformed into *E. coli* BL21. For expression of TOYE, a BL21 clone harboring pET21b-TOYE was inoculated in 5 mL LB medium containing 100 µg/mL ampicillin and grown overnight at 37 °C. This overnight culture was used to inoculate 500 mL of LB medium containing 100 µg/mL ampicillin, which was grown at 25 °C at 250 rpm until an OD of ~0.5 was reached, and subsequently induced with the addition of 0.4 mM IPTG. The induced culture was placed at 25 °C for 12 h.

The GDH used in this research is from *Bacillus megaterium* B14308. B14398 was inoculated in 5 mL TGY medium and grown at 30 °C for 18 h. Genomic DNA was isolated using the Wizard<sup>®</sup> Genomic DNA purification kit from Promega according to the manufacturer's protocol. The gene encoding the *gdh* was amplified from the genome of *B. megaterium* using primers *gdh*-NdeI-for and *gdh*-HindIII-rev. Restriction sites are underlined. The gene was ligated into pET28a<sup>+</sup> and transformed into *E. coli* DH5α. The plasmid pET28a-*gdh* was transformed into *E. coli* BL21. For expression of GDH, a BL21 clone harboring pET28a-*gdh* was inoculated in 5 mL LB medium containing 50 µg/mL kanamycin and grown overnight at 37 °C. This overnight culture was used to inoculate 500 mL of TB medium containing 50 µg/ml kanamycin, which was grown at 37 °C until an OD of ~0.7 was reached, and subsequently induced with the addition of 0.3 mM IPTG. The induced culture was placed at 25 °C for 16 h for protein production.



All proteins were purified in the same way. Following expression, BL21 cells were recovered by centrifugation (6000 x *g* for 15 min), lysed by sonication and clarified by centrifugation (18 000 x *g* for 30 min). The protein was subsequently purified by affinity chromatography using a HisTrap column fitted to an AKTA FPLC system (GE Health Life Sciences, Pittsburgh, PA). The purified protein was buffer exchanged against 100 mM phosphate buffer, pH 8.1 using an Amicon Ultra concentration tube (10 kDa cut-off) before being stored in 15% glycerol as 100  $\mu$ L aliquots at -80 °C.

### 3.4.3. General Procedure for Alkene Synthesis via Rh-catalyzed Diazocoupling

To a solution of rhodium carboxylate dimer, 1 mol % of either Dirhodium(II) tetrakis(pivaloate) [Rh<sub>2</sub>(OPiv)<sub>4</sub>] or rhodium(II) octanoate dimer [Rh<sub>2</sub>(Oct)<sub>4</sub>] in dichloromethane at -78 °C was added an equimolar solution of a donor-acceptor diazocompound and an  $\alpha$ -diazocarbonyl compound in dichloromethane (0.2 M final concentration) in 3 portions over 30 minutes. The reaction was stirred at -78 °C for 1 hour before slowly warming to room temperature. The solvent was removed *in vacuo* and the crude product purified by silica gel chromatography.

The yield of 4-Ethyl 1-Methyl 2-phenylfumarate is 44% by [Rh<sub>2</sub>(Oct)<sub>4</sub>] and 67% by [Rh<sub>2</sub>(OPiv)<sub>4</sub>]. <sup>1</sup>H NMR (600 MHz, Chloroform-*d*)  $\delta$  7.38–7.35 (m, 3H), 7.23 (m, 2H), 7.02 (s, 1H), 4.04 (q, *J* = 7.1 Hz, 2H), 3.81 (s, 3H), 1.06 (t, *J* = 7.1 Hz, 3H). Characterization data matches those previously reported.<sup>3</sup>

The yield of 4-(*tert*-Butyl) 1-Methyl 2-phenylfumarate is 57% by [Rh<sub>2</sub>(Oct)<sub>4</sub>] and 74% by [Rh<sub>2</sub>(OPiv)<sub>4</sub>]. <sup>1</sup>H NMR (600 MHz, Chloroform-*d*)  $\delta$  7.37–7.35 (m, 3H), 7.22 (m, 2H), 6.97 (s, 1H), 3.79 (s, 3H), 1.23 (s, 9H). Characterization data matches those previously reported.<sup>44</sup>

The yield of 4-Benzyl 1-Methyl 2-phenylfumarate is 49% (*E:Z* = 8:1) by [Rh<sub>2</sub>(Oct)<sub>4</sub>] and 67% by [Rh<sub>2</sub>(OPiv)<sub>4</sub>]. <sup>1</sup>H NMR (600 MHz, Chloroform-*d*) δ 7.40–7.31 (m, 3H), 7.30–7.28 (m, 3H), 7.23 (m, 2H), 7.10 (m, 2H), 7.07 (s, 1H), 5.03 (s, 2H), 3.80 (s, 3H). <sup>13</sup>C NMR (151 MHz, Chloroform-*d*) δ 166.7, 165.0, 144.0, 135.0, 133.8, 128.9, 128.8, 128.6, 128.4, 128.2, 128.2, 127.9, 126.7, 117.2, 66.7, 52.9. IR (film): 3034, 2953, 1715, 1633, 1497, 1435, 1380, 1352, 1249, 1023 cm<sup>-1</sup>. HRMS–ESI (*m/z*): [M+H]<sup>+</sup> calculated for C<sub>18</sub>H<sub>16</sub>O<sub>4</sub>H: 297.1127, found: 297.1126.

The yield of Methyl (*E*)-4-(4-Fluorophenyl)-4-oxo-2-phenylbut-2-enoate is 36% (*E:Z* = 8:1) by [Rh<sub>2</sub>(Oct)<sub>4</sub>] and 22.8% (*E:Z* = 7:1) by [Rh<sub>2</sub>(OPiv)<sub>4</sub>]. Alkene geometry was assigned based on comparison with the <sup>1</sup>H NMR data of similar alkenes reported by Davies and coworkers.<sup>Error! Bookmark not defined.</sup> <sup>1</sup>H NMR (600 MHz, Chloroform-*d*) δ 7.83 (m, 2H), 7.64 (s, 1H), 7.24–7.17 (m, 5H), 7.02 (t, *J* = 8.6 Hz, 2H), 3.87 (s, 3H). <sup>13</sup>C NMR (151 MHz, CDCl<sub>3</sub>) δ 192.24, 166.07 (d, *J* = 256.1 Hz), 165.22, 140.68, 136.12, 133.74, 132.78, 132.76, 131.79 (d, *J* = 9.6 Hz), 129.50, 128.86, 128.11, 115.90 (d, *J* = 22.1 Hz), 53.05. <sup>19</sup>F NMR (376 MHz, CDCl<sub>3</sub>) δ -105.94. IR (film): 3060, 2954, 1716, 1668, 1595, 1506, 1435, 1410, 1259, 1154, 1098, 1077 cm<sup>-1</sup>. HRMS–ESI (*m/z*): [M+Na]<sup>+</sup> calculated for C<sub>17</sub>H<sub>13</sub>FO<sub>3</sub>Na: 307.0741, found: 307.0742.

The yield of Ethyl (*E*)-4-oxo-3-(3-(trifluoromethyl)phenyl)pent-2-enoate is 47% by [Rh<sub>2</sub>(Oct)<sub>4</sub>] and 56.4% by [Rh<sub>2</sub>(OPiv)<sub>4</sub>]. Alkene geometry was assigned based on comparison with the <sup>1</sup>H NMR data of similar alkenes reported by Davies and coworkers.<sup>Error! Bookmark not defined.</sup> <sup>1</sup>H NMR (600 MHz, Chloroform-*d*) δ 7.64 (d, *J* = 8.9 Hz, 1H), 7.52 (t, *J* = 7.5 Hz 1H), 7.43 (s, 1H), 7.36 (d, *J* = 7.5 Hz, 1H), 6.84 (s, 1H), 4.04 (q, *J* = 7.4 Hz, 2H), 2.38 (s, 3H), 1.05 (t, *J* = 7.0 Hz, 3H). <sup>13</sup>C NMR (152 MHz, CDCl<sub>3</sub>) δ 197.98, 165.16, 149.37, 135.40, 132.23, 130.67 (d, *J* = 130 Hz), 128.81, 128.61, 125.7 (q, *J* = 4.05 Hz), 125.34 (q, *J* = 3.77), 163.66 (d, *J* = 273.6), 61.53, 27.72, 13.82. <sup>19</sup>F NMR (470 MHz, CDCl<sub>3</sub>) δ -63.04. IR (film): 3071, 2988, 2976, 2940, 2359,

1737, 1726, 1711, 1691, 1681, 1639, 1631, 1611, 1467 1486, 1441, 1433, 1368, 1351, 1324, 1162, 1096, 1074, 1036,  $\text{cm}^{-1}$ . HRMS–ESI ( $m/z$ ):  $[\text{M}+\text{H}]^+$  calculated for  $\text{C}_{14}\text{H}_{13}\text{F}_3\text{O}_3\text{H}$ : 287.0895, found: 287.0900.

The yield of Ethyl (Z)-4-oxo-3-(3-(trifluoromethyl)phenyl)pent-2-enoate is 10% by  $[\text{Rh}_2(\text{Oct})_4]$  and 1.3% by  $[\text{Rh}_2(\text{OPiv})_4]$ . Alkene geometry was assigned based on comparison with the  $^1\text{H}$  NMR data of similar alkenes reported by Davies and coworkers.<sup>Error! Bookmark not defined.</sup>  $^1\text{H}$  NMR (600 MHz, Chloroform-*d*)  $\delta$  7.70 (s, 1H), 7.69 (d,  $J = 8.18$  Hz, 1H), 7.605 (d,  $J = 7.78$  Hz, 1H), 7.54 (t,  $J = 8.0$  Hz, 1H), 6.19 (s, 1H), 4.25 (q,  $J = 5.3$  Hz, 2H), 2.44 (s, 3H), 1.32 (t,  $J = 7.3$  Hz, 3H).  $^{13}\text{C}$  NMR (152 MHz,  $\text{CDCl}_3$ )  $\delta$  203.71, 165.17, 156.66, 133.97, 130.12, 129.88, 127.155 (q,  $J = 3.57$  Hz), 123.68 (q,  $J = 3.90$  Hz), 117.62, 110.18, 102.57, 61.45, 30.53, 14.25.  $^{19}\text{F}$  NMR (470 MHz,  $\text{CDCl}_3$ )  $\delta$  -63.25. HRMS–ESI ( $m/z$ ):  $[\text{M}+\text{H}]^+$  calculated for  $\text{C}_{14}\text{H}_{13}\text{F}_3\text{O}_3\text{H}$ : 287.0895, found: 287.0890.

The yield of Ethyl (*E*)-3-(4-fluorophenyl)-4-oxopent-2-enoate is 64% by  $[\text{Rh}_2(\text{Oct})_4]$  and 156% by  $[\text{Rh}_2(\text{OPiv})_4]$ . Each alkene was isolated separately ( $[\text{Rh}_2(\text{Oct})_4]$ : 0.34 g, 64% yield;  $[\text{Rh}_2(\text{OPiv})_4]$ : 0.30g, 56.4% yield).  $^1\text{H}$  NMR (600 MHz, Chloroform-*d*)  $\delta$  7.14 (m, 2H), 7.08 (t,  $J = 8.0$  Hz, 2H), 6.77 (s, 1H), 4.06 (q,  $J = 7.2$  Hz, 2H), 2.34 (s, 3H), 1.10 (t,  $J = 7.1$  Hz, 3H).  $^{13}\text{C}$  NMR (151 MHz,  $\text{CDCl}_3$ )  $\delta$  198.77, 165.48, 163.79, 162.15, 150.00, 130.68 (d,  $J = 8.2$  Hz), 127.65, 115.32 (d,  $J = 21.6$  Hz), 61.14, 27.88, 13.99.  $^{19}\text{F}$  NMR (376 MHz,  $\text{CDCl}_3$ )  $\delta$  -115.16. IR (film): 2985, 2939, 1732, 1716, 1699, 1634, 1602, 1465, 1368, 1225, 1157, 1097, 1035  $\text{cm}^{-1}$ . HRMS–ESI ( $m/z$ ):  $[\text{M}+\text{Na}]^+$  calculated for  $\text{C}_{13}\text{H}_{13}\text{FO}_3\text{Na}$ : 259.0741, found: 259.0740.

The yield of Ethyl (Z)-3-(4-fluorophenyl)-4-oxopent-2-enoate is 7 % by  $[\text{Rh}_2(\text{Oct})_4]$  and 0.8% by  $[\text{Rh}_2(\text{OPiv})_4]$ . Each alkene was isolated separately ( $[\text{Rh}_2(\text{Oct})_4]$ : 0.038 g, 7% yield;  $[\text{Rh}_2(\text{OPiv})_4]$ : <0.005g, <1% yield).  $^1\text{H}$  NMR (500 MHz, Chloroform-*d*)  $\delta$  7.43 (m, 2H), 7.10 (m,

2H), 6.10 (s, 1H), 4.23 (q,  $J = 7.1$  Hz, 2H), 2.43 (s, 3H), 1.31 (t,  $J = 7.1$  Hz, 3H).  $^{13}\text{C}$  NMR (126 MHz, Chloroform-*d*)  $\delta$  204.48, 165.48, 165.23, 163.22, 157.10, 128.97 (d,  $J = 8.8$  Hz), 116.48 (d,  $J = 21.6$  Hz), 115.46, 61.23, 30.51, 14.26.  $^{19}\text{F}$  NMR (376 MHz,  $\text{CDCl}_3$ )  $\delta$  -111.61. IR (film): 3076, 2984, 2939, 1715, 1699, 1616, 1601, 1506, 1417, 1370, 1277, 1239, 1185, 1108, 1032  $\text{cm}^{-1}$ . HRMS–ESI ( $m/z$ ):  $[\text{M}+\text{Na}]^+$  calculated for  $\text{C}_{13}\text{H}_{13}\text{FO}_3\text{Na}$ : 259.0741, found: 259.0739.

The yield of Ethyl (E)-3-(4-chlorophenyl)-4-oxopent-2-enoate is 68% by  $[\text{Rh}_2(\text{Oct})_4]$  and 64% by  $[\text{Rh}_2(\text{OPiv})_4]$ .  $^1\text{H}$  NMR (600 MHz, Chloroform-*d*)  $\delta$  7.36 (m, 2H), 7.11 (m, 2H), 6.77 (s, 1H), 4.07 (q,  $J = 7.1$  Hz, 2H), 2.34 (s, 3H), 1.11 (t,  $J = 7.2$  Hz).  $^{13}\text{C}$  NMR (151 MHz, Chloroform-*d*)  $\delta$  198.47, 165.34, 149.91, 134.77, 132.99, 130.17, 128.49, 127.81, 61.22, 27.89, 13.99. HRMS–ESI ( $m/z$ ):  $[\text{M}+\text{Na}]^+$  calculated for  $\text{C}_{13}\text{H}_{13}\text{ClO}_3\text{Na}$ : 275.0451, found: 275.0463.

The yield of Ethyl (E)-3-(4-chlorophenyl)-4-oxopent-2-enoate is 7% by  $[\text{Rh}_2(\text{Oct})_4]$  and 3.3% by  $[\text{Rh}_2(\text{OPiv})_4]$ .  $^1\text{H}$  NMR (600 MHz, Chloroform-*d*)  $\delta$  7.38 (m, 4H), 6.13 (s, 1H), 4.23 (q,  $J = 7.1$  Hz, 2H), 2.42 (s, 3H), 1.31 (t,  $J = 7.2$  Hz, 1H).  $^{13}\text{C}$  NMR (151 MHz, Chloroform-*d*)  $\delta$  204.14, 165.38, 156.99, 136.96, 131.41, 129.99, 128.21, 116.10, 61.30, 30.52, 14.27. HRMS–ESI ( $m/z$ ):  $[\text{M}+\text{Na}]^+$  calculated for  $\text{C}_{13}\text{H}_{13}\text{ClO}_3\text{Na}$ : 275.0451, found: 275.0450.

#### 3.4.4. General Procedure for Enzymatic Alkene Reduction and Quantification

To a solution of  $\text{NADP}^+$  (80  $\mu\text{L}$  of 20 mM stock, 0.04 equiv), glucose (200  $\mu\text{L}$  of a 1 M stock, 5 equiv), GDH (1 U/mL) and enoate reductase (0.2 mol %) in 200 mM pH 7.5 phosphate buffer (6.08 mL) was added a solution of enoate (0.04 mmol, 1 equiv) in DMSO (200  $\mu\text{L}$ ) at room temperature. Final concentrations are as follows: 0.2 mM  $\text{NADP}^+$ , 25 mM glucose, 1 U/mL GDH, 10  $\mu\text{M}$  ene-reductase, 5 mM enoate substrate, 2.5  $v/v\%$  DMSO. The reaction was incubated overnight at 27  $^\circ\text{C}$  and 100 rpm before the addition of EtOAc (3 mL) and dodecane (200  $\mu\text{L}$  of 20  $\mu\text{L}/\text{mL}$  stock in EtOAc). An aliquot was removed from the organic layer for GC (ZB-5MS)

analysis. The reaction mixture was extracted twice with EtOAc and the combined organic layers were concentrated *in vacuo* and purified by preparative TLC. The partially purified product was analyzed by chiral SFC or Chiral HPLC as described below. In some cases, the alkene starting material co-elutes with one of the product enantiomers and complete consumption of the starting material was required for chiral SFC analysis.

Molar concentration of ene-reductase was obtained by dividing the mass concentration, obtained from Bradford Assay, by its molecular weight.

Isolated yields were obtained by performing 10 times scale-up reaction in conical flask and extracting the reaction mixture 3 times with EtOAc. The combined organic layers were dried over MgSO<sub>4</sub>, filtered and concentrated *in vacuo*. The crude product was purified by silica gel chromatography.

The isolated yield of 4-Ethyl 1-Methyl (*R*)-2-Phenylsuccinate is 84%. <sup>1</sup>H NMR (600 MHz, Chloroform-*d*) δ 7.33 (t, *J* = 7.5 Hz, 2H), 7.30–7.25 (m, 3H), 4.13 (q, *J* = 7.3 Hz, 2H), 4.09 (dd, *J* = 10.2, 5.3 Hz, 1H), 3.68 (s, 3H), 3.19 (dd, *J* = 16.9, 10.2 Hz, 1H), 2.66 (dd, *J* = 17.1, 5.4 Hz, 1H), 1.22 (t, *J* = 7.2 Hz, 3H). <sup>13</sup>C NMR (151 MHz, CDCl<sub>3</sub>) δ 173.6, 171.6, 137.9, 129.0, 127.9, 127.8, 60.9, 52.5, 47.3, 38.1, 14.3. Chiral SFC: AD-H column, 2.5% *i*PrOH, 2.5 mL/min, 220 nm; *t*<sub>R</sub>(major): 2.07 min, *t*<sub>R</sub>(minor): not observed, >95% *ee*. [α]<sub>D</sub><sup>25</sup>: –128° (*c* = 1.0, CHCl<sub>3</sub>). Characterization data matches those previously reported.<sup>44</sup>

The isolated yield of 4-(*tert*-Butyl) 1-Methyl (*R*)-2-Phenylsuccinate is 65%. <sup>1</sup>H NMR (600 MHz, Chloroform-*d*) δ 7.32 (m, 2H), 7.30–7.26 (m, 3H), 4.02 (dd, *J* = 10.0, 5.4 Hz, 1H), 3.67 (s, 3H), 3.11 (dd, *J* = 16.7, 10.1 Hz, 1H), 2.60 (dd, *J* = 16.6, 5.4 Hz, 1H), 1.40 (s, 9H). <sup>13</sup>C NMR (151 MHz, CDCl<sub>3</sub>) δ 173.66, 170.78, 137.98, 128.92, 127.97, 127.70, 81.11, 52.38, 47.54, 39.25, 28.15. IR (film): 2979, 1732, 1497, 1435, 1455, 1393, 1368, 1257, 1149, 1032, 1005, 953 cm<sup>-1</sup>. HRMS–

ESI ( $m/z$ ):  $[M+Na]^+$  calculated for  $C_{15}H_{20}O_4Na$ : 287.1254, found: 287.1250. Chiral SFC: AD-H column, 2.5% *i*PrOH, 2.5 mL/min, 220 nm;  $t_R$ (major): 1.53 min,  $t_R$ (minor): not observed (3.29 min), >99% *ee*.

The isolated yield of Ethyl 3-(4-Fluorophenyl)-4-oxopentanoate is 75%.  $^1H$  NMR (500 MHz, Chloroform-*d*)  $\delta$  7.18 (m, 2H), 7.03 (m, 2H), 4.17 (dd,  $J = 9.4, 5.3$  Hz, 1H), 4.09 (m, 2H), 3.16 (dd,  $J = 16.9, 9.6$  Hz, 1H), 2.50 (dd,  $J = 16.9, 5.3$  Hz, 1H), 2.11 (s, 3H), 1.21 (t,  $J = 7.1$  Hz, 3H).  $^{13}C$  NMR (126 MHz, Chloroform-*d*)  $\delta$   $^{13}C$  NMR (126 MHz,  $CDCl_3$ )  $\delta$  206.82, 172.04, 162.41 (d,  $J = 247.0$  Hz), 133.26 (d,  $J = 3.2$  Hz), 129.94 (d,  $J = 8.1$  Hz), 116.22 (d,  $J = 21.4$  Hz), 60.88, 54.08, 37.26, 29.05, 14.26. IR (film): 2984, 2934, 1733, 1716, 1601, 1507, 1418, 1374, 1354, 1293, 1190, 1161, 1099, 1029  $cm^{-1}$ . HRMS–ESI ( $m/z$ ):  $[M+Na]^+$  calculated for  $C_{13}H_{15}FO_3Na$ : 261.0897, found: 261.0896. Chiral SFC: AD-H column, 2.5% *i*PrOH, 2.5 mL/min, 220 nm;  $t_R$ (major): 1.79 min,  $t_R$ (minor): 3.06 min, 87% *ee*.  $[\alpha]_D^{25}$ :  $-253^\circ$  ( $c = 1.0$ ,  $CHCl_3$ ).

The isolated yield of Ethyl 3-(4-chlorophenyl)-4-oxopentanoate is 78%.  $^1H$  NMR (600 MHz, Chloroform-*d*)  $\delta$  7.31 (d,  $J = 8.5$  Hz, 2H), 7.16 (d,  $J = 8.5$  Hz, 2H), 4.15 (dd,  $J = 9.6, 5.4$  Hz, 1H), 4.09 (m, 2H), 3.16 (dd,  $J = 17.9, 10.1$  Hz, 1H), 2.50 (dd,  $J = 17.2, 5.4$  Hz, 1H), 2.11 (s, 3H), 1.21 (t,  $J = 7.1$  Hz, 3H).  $^{13}C$  NMR (126 MHz,  $CDCl_3$ )  $\delta$  206.43, 171.90, 136.04, 133.90, 129.72, 129.69, 60.90, 54.26, 37.13, 29.07, 14.26. HRMS–ESI ( $m/z$ ):  $[M+Na]^+$  calculated for  $C_{13}H_{15}ClO_3Na$ : 277.0607, found: 261.0609. Chiral HPLC: OJ-H column, 100% Hexane, 0.8 mL/min, 220 nm;  $t_R$ (major): 22.24 min,  $t_R$ (minor): 23.92 min, 85% *ee*.

The isolated yield of Ethyl 4-oxo-3-(3-(trifluoromethyl)phenyl)pentanoate is 70%.  $^1H$  NMR (600 MHz, Chloroform-*d*)  $\delta$  7.555 (d,  $J = 7.5$  Hz, 1H), 7.49 (s, 1H), 7.415 (d,  $J = 7.7$  Hz, 1H), 4.26 (dd,  $J = 9.8, 5.5$  Hz, 1H), 4.10 (m, 2H), 3.21 (dd,  $J = 17.2, 9.7$  Hz, 1H), 2.54 (dd,  $J = 17.9, 6.1$  Hz, 1H), 2.14 (s, 3H), 1.21 (t,  $J = 7.1$  Hz, 3H).  $^{13}C$  NMR (126 MHz, Chloroform-*d*)  $\delta$   $^{13}C$

NMR (126 MHz, CDCl<sub>3</sub>)  $\delta$  205.12, 170.73, 137.54, 130.66, 130.71 (q,  $J = 32.7$  Hz), 128.82, 124.21 (q,  $J = 3.4$  Hz), 123.85 (q,  $J = 3.7$  Hz), 122.04, 60.00, 53.61, 36.23, 28.28, 13.24. <sup>19</sup>F NMR (470 MHz, CDCl<sub>3</sub>)  $\delta$  -63.08. HRMS–ESI ( $m/z$ ): [M+Na]<sup>+</sup> calculated for C<sub>14</sub>H<sub>15</sub>F<sub>3</sub>O<sub>3</sub>Na: 311.0871, found: 311.0870. Chiral HPLC: OJ-H column, 5% *i*PrOH, 0.8 mL/min, 220 nm;  $t_R$ (major): 10.78 min,  $t_R$ (minor): 12.77 min, 85% *ee*.

The isolated yield of Methyl 4-(4-fluorophenyl)-4-oxo-2-phenylbutanoate is 69%~85%. %.

<sup>1</sup>H NMR (500 MHz, Chloroform-*d*)  $\delta$  8.00 (m, 2H), 7.35 (m, 4H), 7.30 (m, 1H), 7.12 (m, 2H), 4.29 (dd,  $J = 10.3, 4.1$  Hz, 1H), 3.92 (dd,  $J = 18.7, 10.3$  Hz, 1H), 3.70 (s, 3H), 3.23 (dd,  $J = 18.0, 4.0$  Hz, 1H). <sup>13</sup>C NMR (126 MHz, Chloroform-*d*)  $\delta$  <sup>13</sup>C NMR (126 MHz, CDCl<sub>3</sub>)  $\delta$  196.18, 171.97, 165.87 (d,  $J = 255$ Hz), 138.37, 133.00 (d,  $J = 3.8$  Hz), 130.92, 130.85, 129.10, 127.94, 127.76, 115.95, 115.81, 52.53, 46.49, 42.87. <sup>19</sup>F NMR (470 MHz, CDCl<sub>3</sub>)  $\delta$  -106.15. HRMS–ESI ( $m/z$ ): [M+Na]<sup>+</sup> calculated for C<sub>17</sub>H<sub>15</sub>FO<sub>3</sub>Na: 309.0903, found: 309.0900. Chiral HPLC: OJ-H column, 5% *i*PrOH, 0.8 mL/min, 220 nm;  $t_R$ (major): 29.40 min,  $t_R$ (minor): not observed (~25.875 min), >99% *ee*.

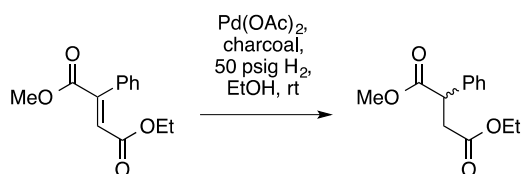
### 3.4.5. General Procedure for One-Pot Sequential Diazocoupling–Enzymatic Alkene Reduction

To a solution of rhodium carboxylate dimer, 1 mol % of either Dirhodium(II) tetrakis(pivaloate) [Rh<sub>2</sub>(OPiv)<sub>4</sub>] or in dichloromethane at –78 °C was added an equimolar solution of methyl 2-diazo-2-phenylacetate (0.25 g, 1.5 mmol) and ethyl 2-diazoacetate (0.16 mL, 0.17 g, 1.6 mmol) in dichloromethane (0.2 M final concentration) in 3 portions over 30 minutes. The reaction was stirred at –78 °C for 1 hour before slowly warming to room temperature. The solvent was removed *in vacuo* and the crude product was re-dissolved in 3.75 mL DMSO.

To a solution of NADP<sup>+</sup> (3 mL of 20 mM stock, 0.04 equiv), glucose (7.5 mL of a 1 M stock, 5 equiv), GDH (2 U/mL) and enoate reductase (0.2 mol %) in 200 mM pH 7.5 phosphate buffer (150 mL) was added a previously prepared solution of chemical in DMSO (3.75 mL) at room temperature. Final concentrations are as follows: 0.4 mM NADP<sup>+</sup>, 50 mM glucose, 2 U/mL GDH, 20 μM enoate reductase, 10 mM enoate substrate, 2.5 v/v% DMSO. The reaction was incubated overnight at 27 °C and 100 rpm. 1 mL reaction mixture was extracted by the addition of EtOAc (2 mL) and dodecane (20 μL of 20 mg/mL stock in EtOAc). An aliquot was removed from the organic layer for GC (ZB-5MS) analysis. The reaction mixture was later extracted twice with EtOAc (100 mL) and the combined organic layers were concentrated *in vacuo* and purified by silica gel chromatography (neutral pH silica). The purified product was dried *in vacuo* and further dried under high vacuum system. The purified product was verified by <sup>1</sup>H NMR and analyzed by chiral HPLC as described in section 2.4.4.

### 3.4.6. Synthesis of Racemic Products: Representative Procedure for Alkene Hydrogenation

Preparation of 4-Ethyl 1-Methyl (±)-2-Phenylsuccinate:



Procedure adapted from the literature.<sup>45</sup> A solution of 4-ethyl 1-methyl 2-phenylfumarate (25 mg, 0.11 mmol, 1 equiv) in ethanol (1.1 mL, 0.1 M) was added to a vial containing Pd(OAc)<sub>2</sub> (2.4 mg, 0.01 mmol, 10 mol %) and activated charcoal (22 mg). The resulting suspension was transferred to a hydrogenation bomb and charged with H<sub>2</sub> (50 psig). The reaction was stirred overnight at room temperature. The reaction mixture was filtered through Celite and solvent removed *in vacuo*.



The product was obtained in >90% purity (<sup>1</sup>H NMR) and could be purified further using preparative TLC (10% EtOAc/hexanes). Characterization data matches those obtained from enzyme catalyzed reduction. The same method was used to prepare other racemic products: 4-(tert-butyl) 1-methyl 2-phenylsuccinate, ethyl 3-(4-fluorophenyl)-4-oxopentanoate, ethyl 3-(4-chlorophenyl)-4-oxopentanoate, ethyl 4-oxo-3-(3-(trifluoromethyl)phenyl)pentanoate and methyl 4-(4-fluorophenyl)-4-oxo-2-phenylbutanoate.

To prepare 4-benzyl 1-methyl 2-phenylsuccinate, benzylation was performed after normal hydrogenation as described above. Procedure adapted from the patent.<sup>46</sup> Na<sub>2</sub>CO<sub>3</sub> (34.98 mg, 0.33 mmol, 3 equiv) and benzyl bromide (18.81 mg, 0.11 mmol, 1 equiv) were added to a solution of 4-methoxy-4-oxo-3-phenylbutanoic acid (22.88 mg, 0.11 mmol, 1 equiv) from hydrogenation of 4-benzyl 1-methyl 2-phenylfumarate, in DMA (3.154 mL). The mixture was stirred for 18 hours under nitrogen at room temperature. Water (6 mL) was added and then the mixture was extracted twice with toluene (3.5 mL). The combined organic layers were washed twice with (2 mL) water and the solvent was removed under reduced pressure. The product was purified by preparative TLC (15% EtOAc/hexanes). Characterization data matches those obtained from enzyme catalyzed reduction.

#### 3.4.7. GC/MS Method

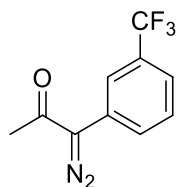
1 μL was injected in a split mode (20:1) into the GC-MS system consisted of an Agilent 6890 (Agilent Inc, Palo Alto, CA, USA) gas chromatograph, an Agilent 5973 mass selective detector and Agilent 7683B autosampler. Gas chromatography was performed on a 30 m Optima-5 column with 0.25 mm inner diameter (I.D.) and 0.5 μm film thickness (Macherey-Nagel, Germany) with an injection temperature of 250<sup>0</sup>C, MSD transfer line of 250<sup>0</sup>C, and the ion source adjusted to 230<sup>0</sup>C. The helium carrier gas was set at a constant flow rate of 1 ml min<sup>-1</sup>. The

temperature program was different for different samples . 2-min at 100<sup>0</sup>C, followed by an oven temperature ramp of 8<sup>0</sup>C min<sup>-1</sup> to 280<sup>0</sup>C for 1 min, then 15<sup>0</sup>C min<sup>-1</sup> to 310<sup>0</sup>C a final 5 min. The mass spectrometer was operated in positive electron impact mode (EI) at 69.9 eV ionization energy in m/z 30-500 scan range. The spectra of all chromatogram peaks were evaluated using the HP Chemstation (Agilent, Palo Alto, CA, USA).

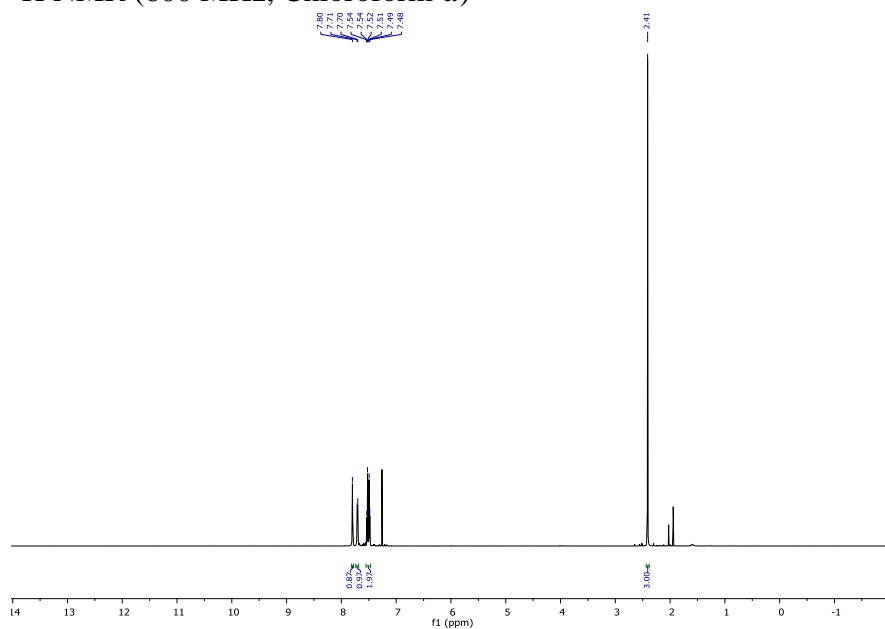
## 3.5 Representative Traces

### 3.5.1. Representative NMR Traces

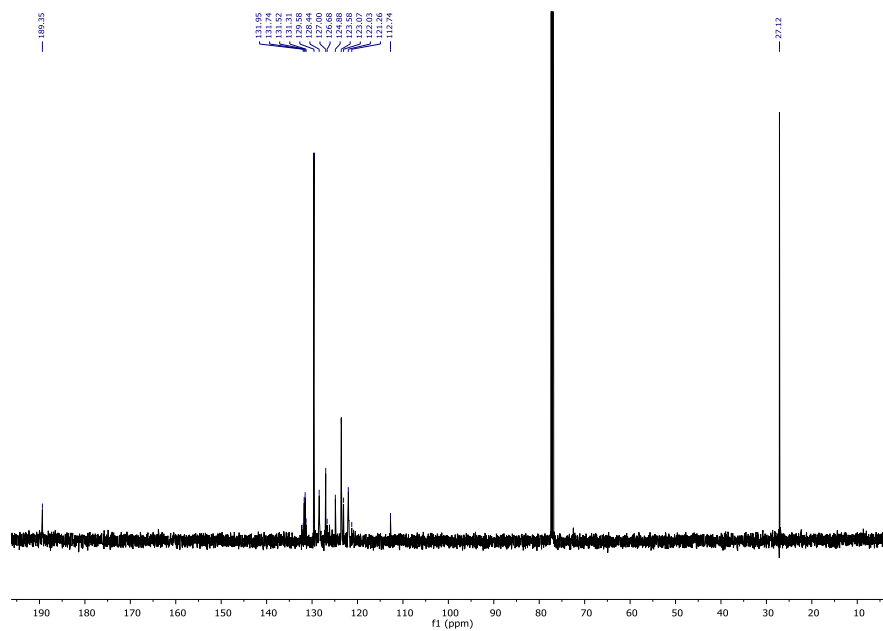
#### 1-diazo-1-(3-(trifluoromethyl)phenyl)propan-2-one



<sup>1</sup>H NMR (600 MHz, Chloroform-*d*)

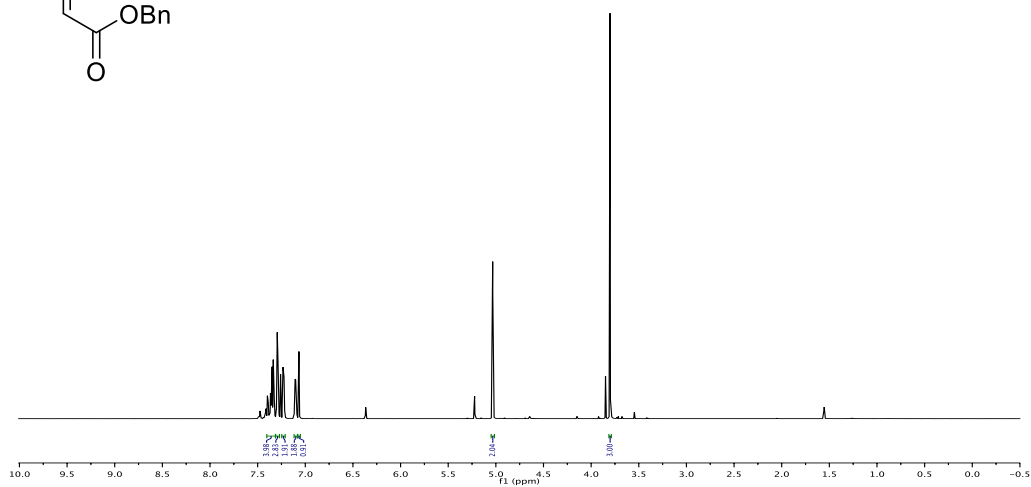
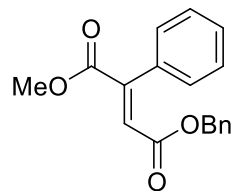


$^{13}\text{C}$  NMR (154 MHz, Chloroform-*d*)

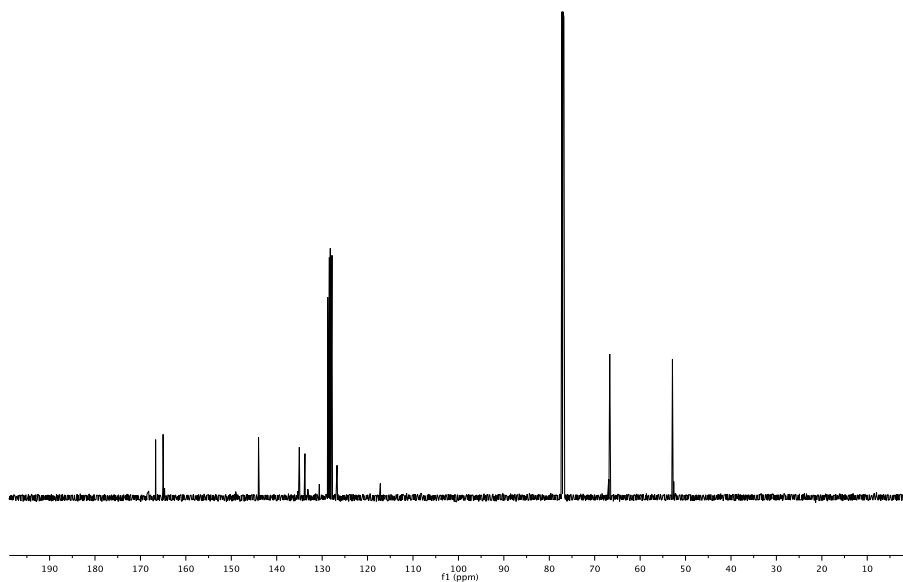


**4-Benzyl 1-Methyl 2-phenylfumarate (~8:1, *E:Z*)**

$^1\text{H}$  NMR (600 MHz, Chloroform-*d*)

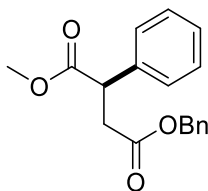


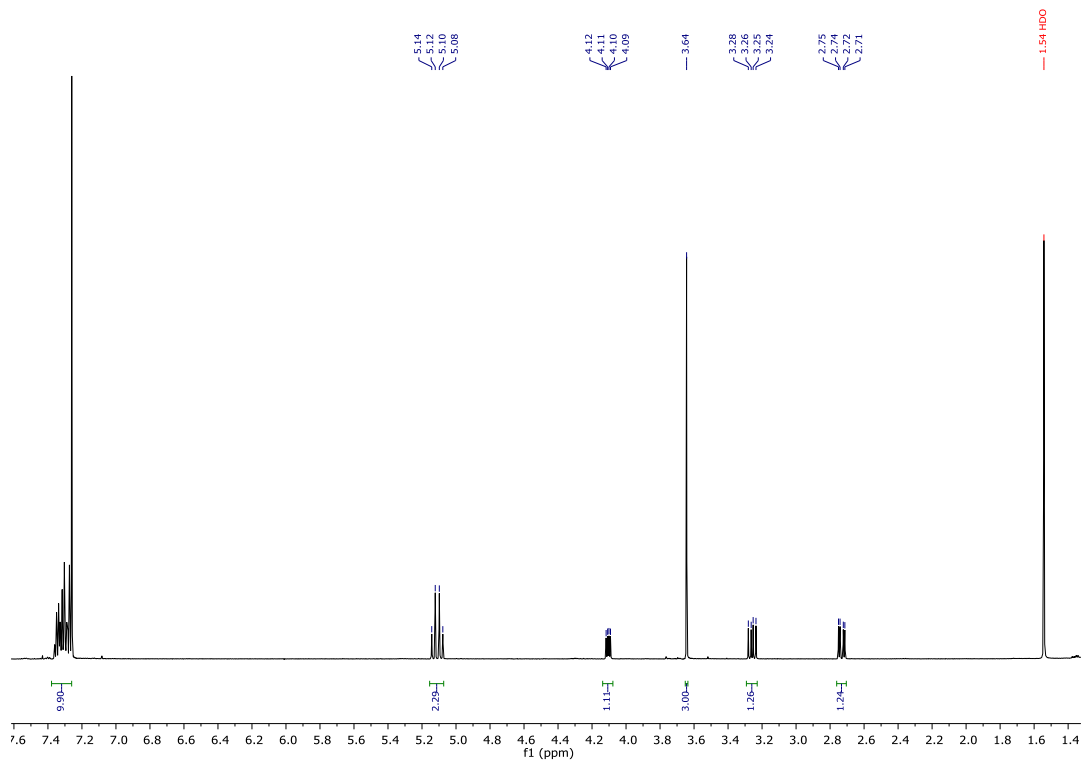
$^{13}\text{C}$  NMR (151 MHz, Chloroform-*d*)



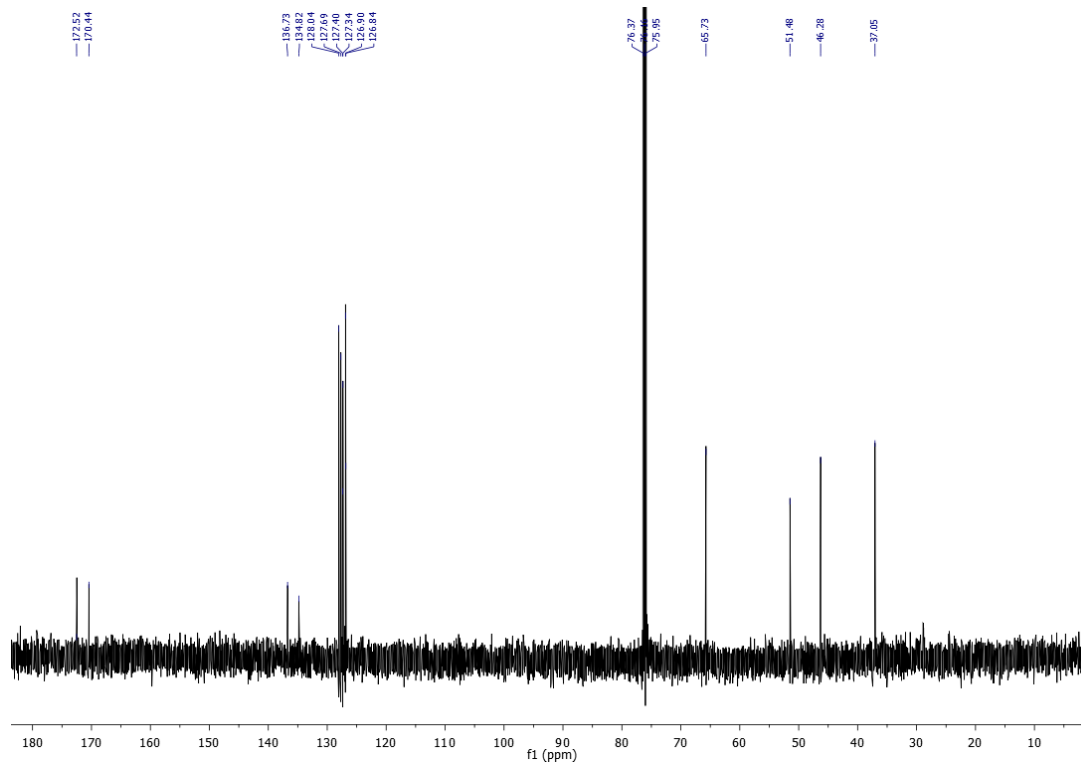
**4-benzyl 1-methyl (R)-2-phenylsuccinate**

$^1\text{H}$  NMR (600 MHz, Chloroform-*d*)



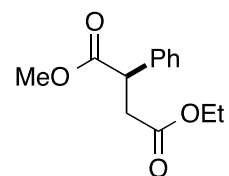


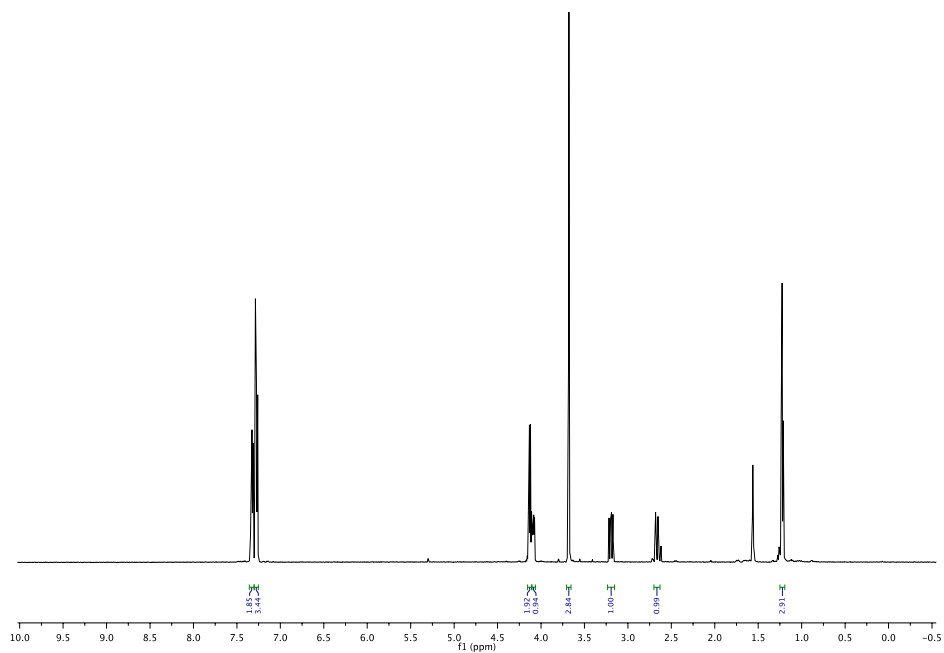
$^{13}\text{C}$  NMR (151 MHz, Chloroform-*d*)



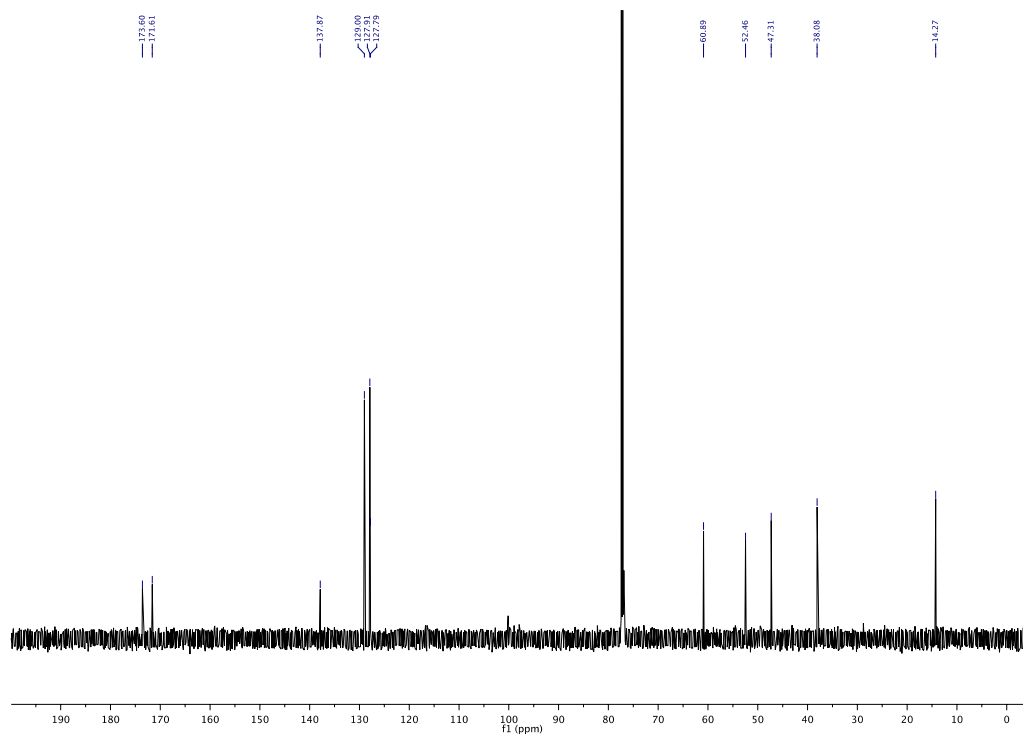
**4-Ethyl 1-Methyl-2-Phenylsuccinate**

$^1\text{H}$  NMR (600 MHz, Chloroform-*d*)



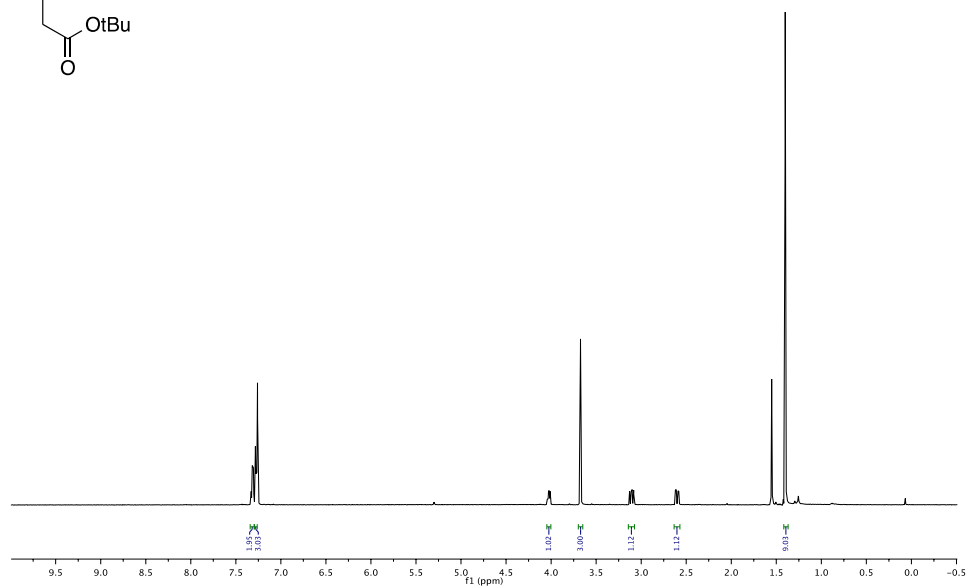
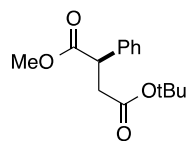


<sup>13</sup>C NMR (151 MHz, Chloroform-*d*)

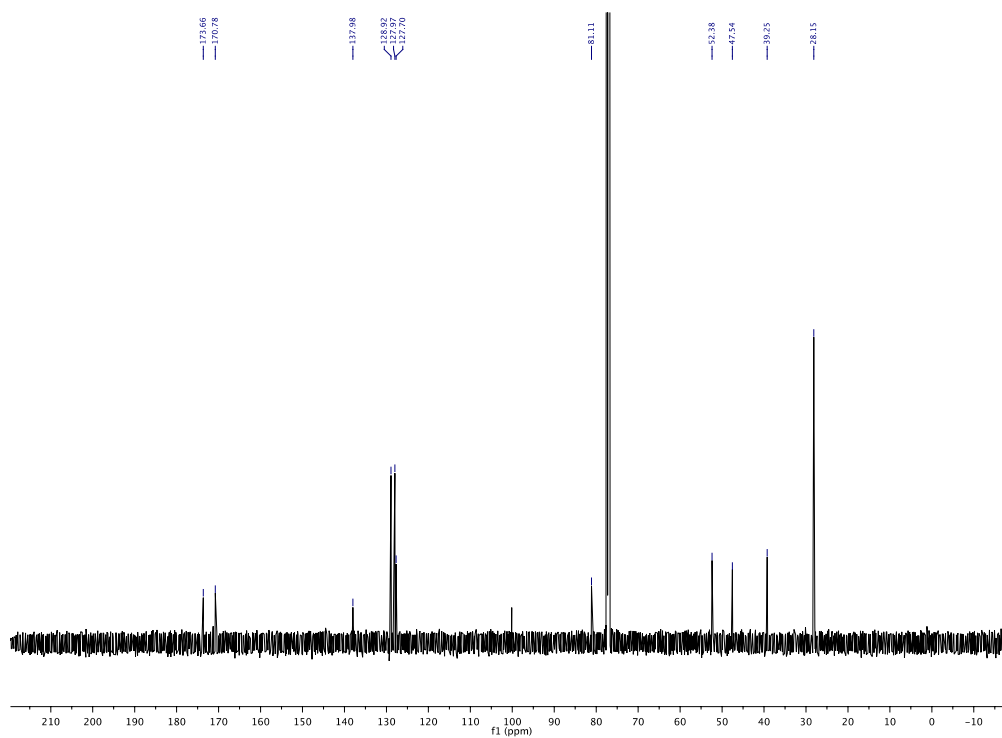


### 4-(*tert*-Butyl) 1-Methyl (*R*)-2-Phenylsuccinate

<sup>1</sup>H NMR (600 MHz, Chloroform-*d*)

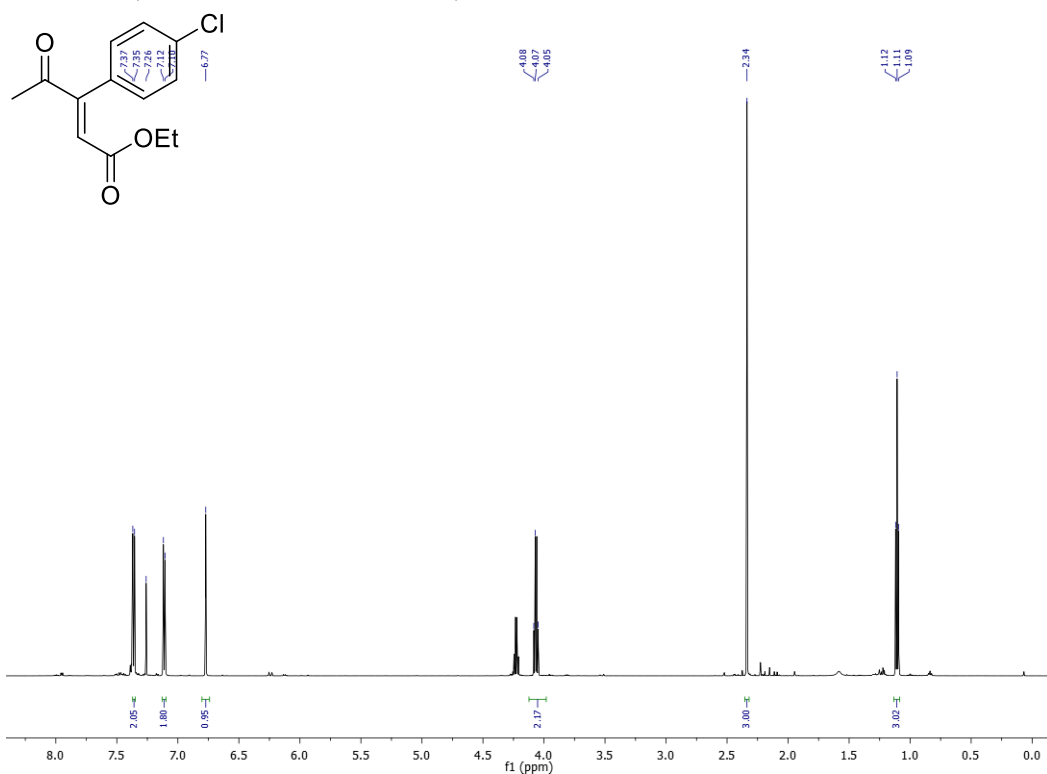


<sup>13</sup>C NMR (151 MHz, Chloroform-*d*)

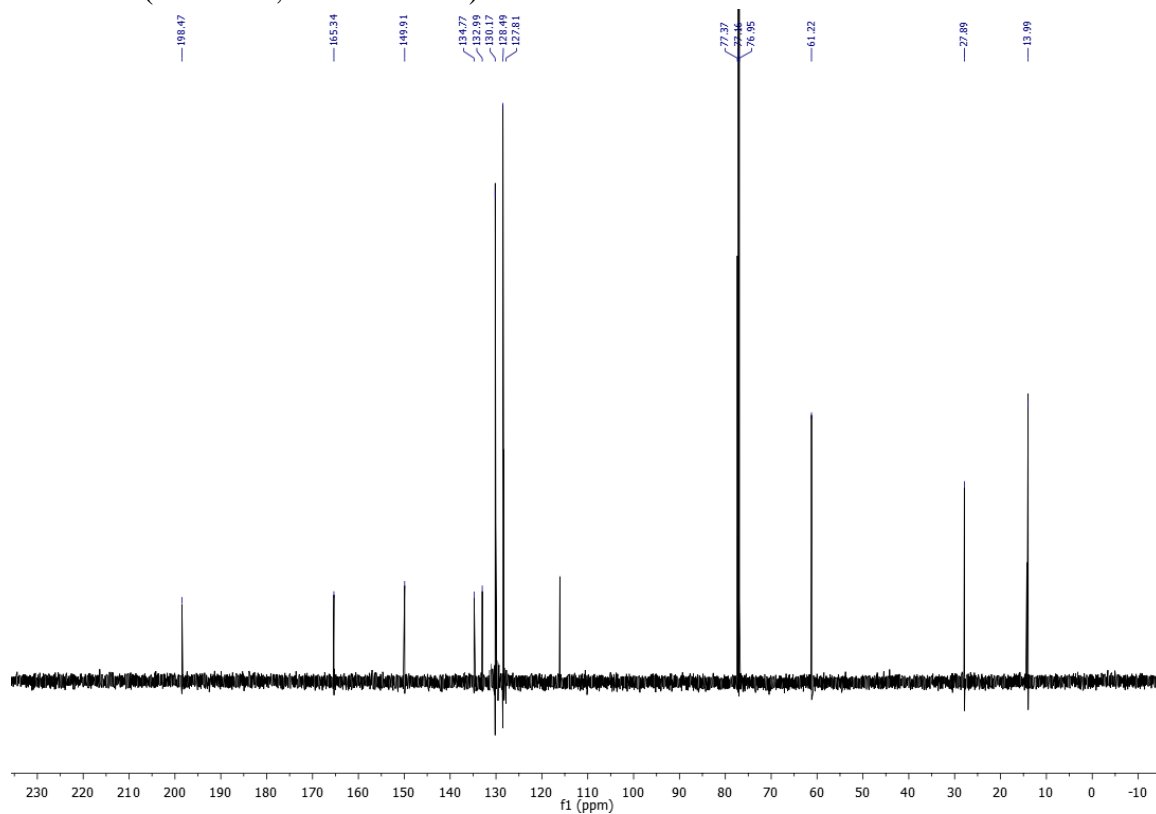


### Ethyl (*E*)-3-(4-chlorophenyl)-4-oxopent-2-enoate

$^1\text{H}$  NMR (600 MHz, Chloroform-*d*)



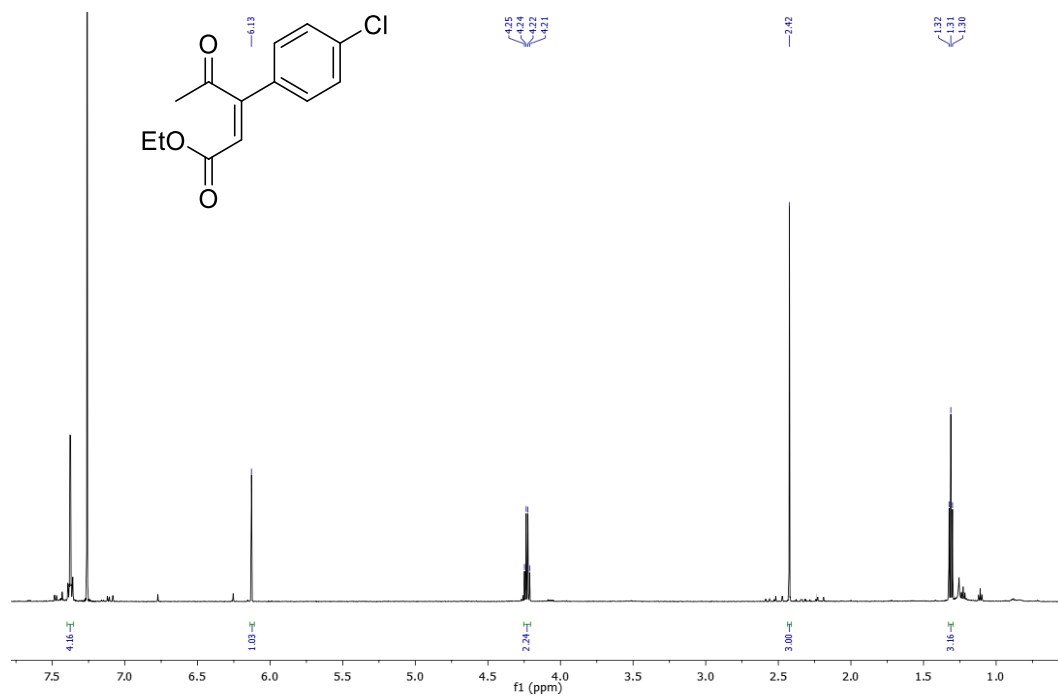
$^{13}\text{C}$  NMR (151 MHz, Chloroform-*d*)



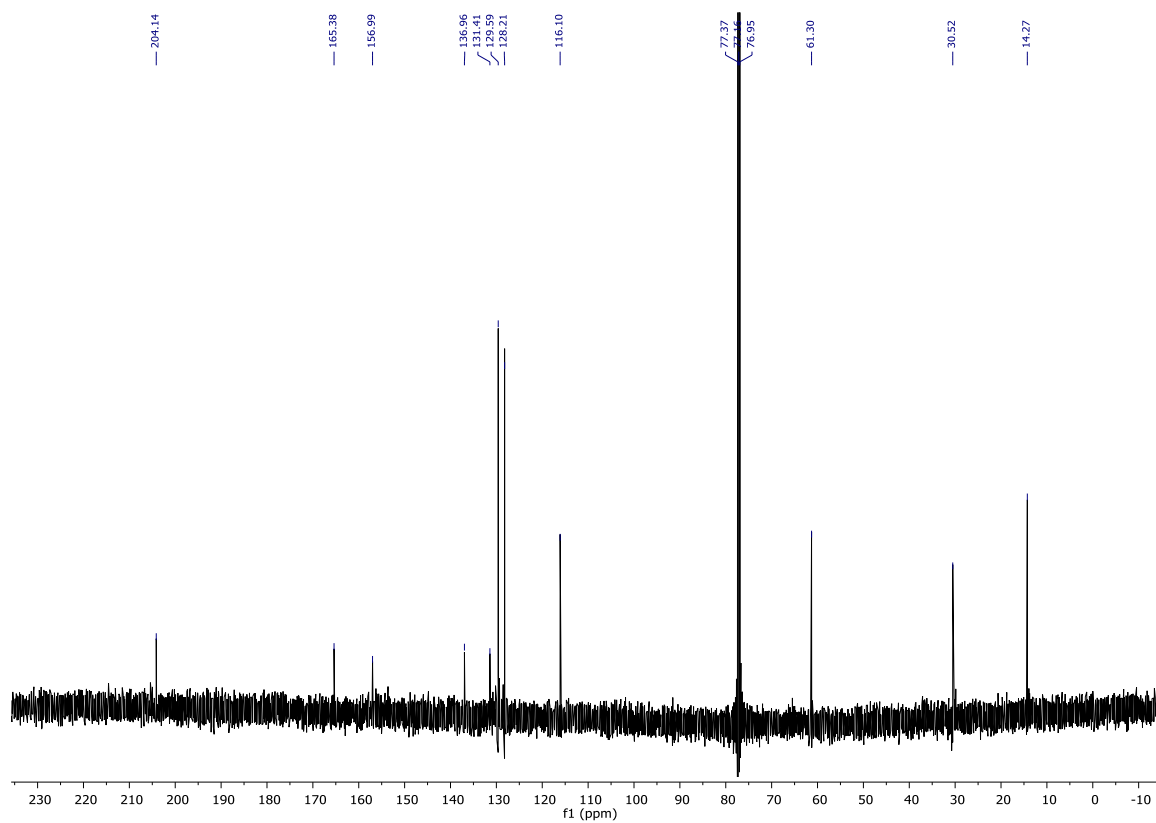
**Ethyl (Z)-3-(4-chlorophenyl)-4-oxopent-2-enoate**



$^1\text{H}$  NMR (600 MHz, Chloroform-*d*)

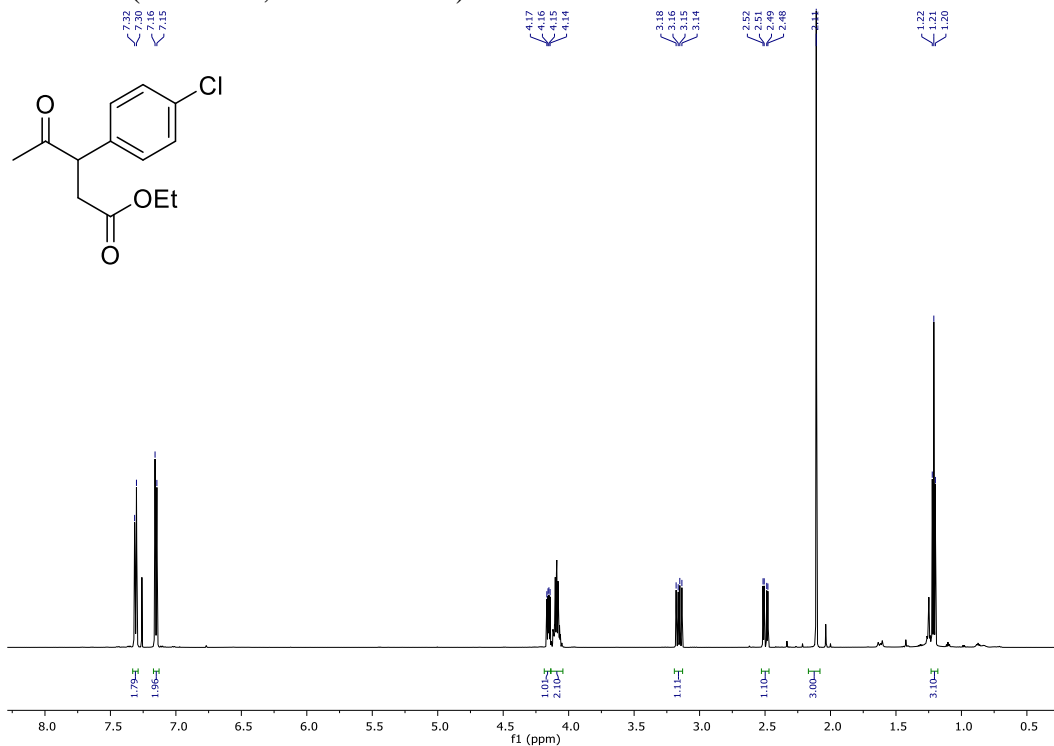


$^{13}\text{C}$  NMR (151 MHz, Chloroform-*d*)

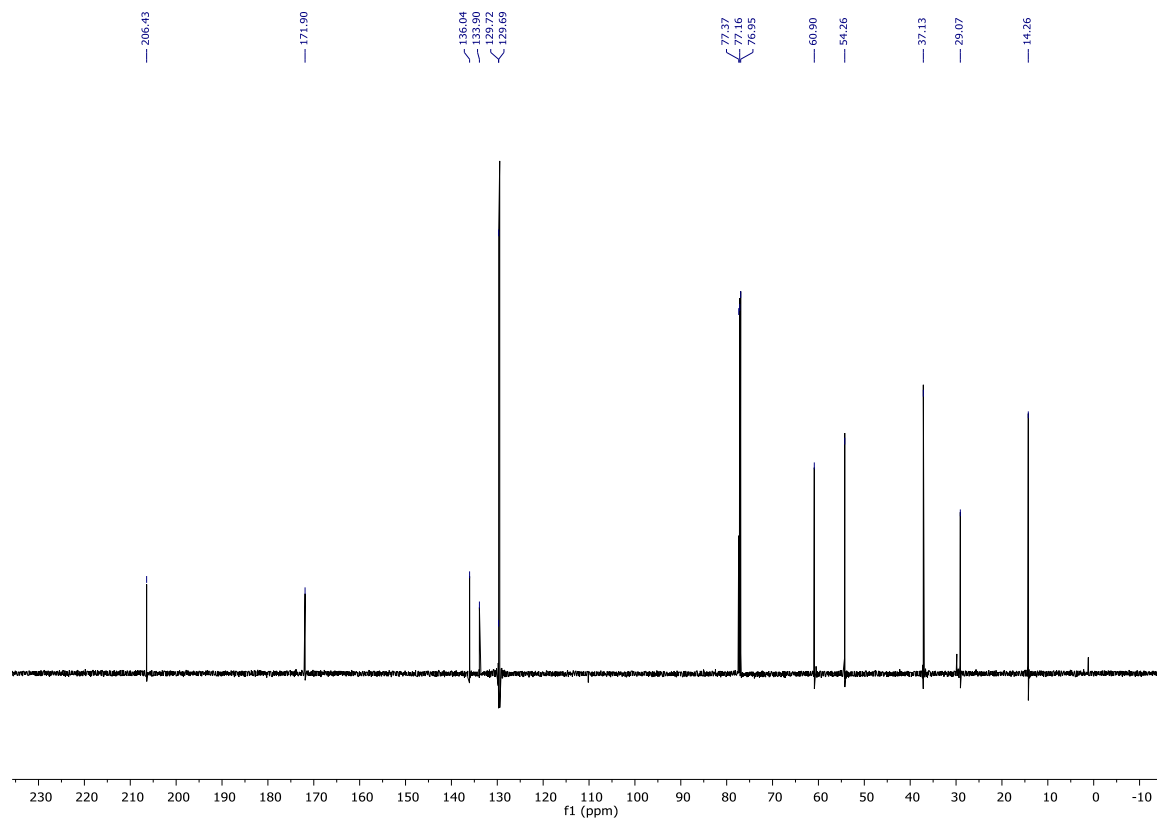


# Ethyl 3-(4-chlorophenyl)-4-oxopentanoate

$^1\text{H}$  NMR (600 MHz, Chloroform-*d*)

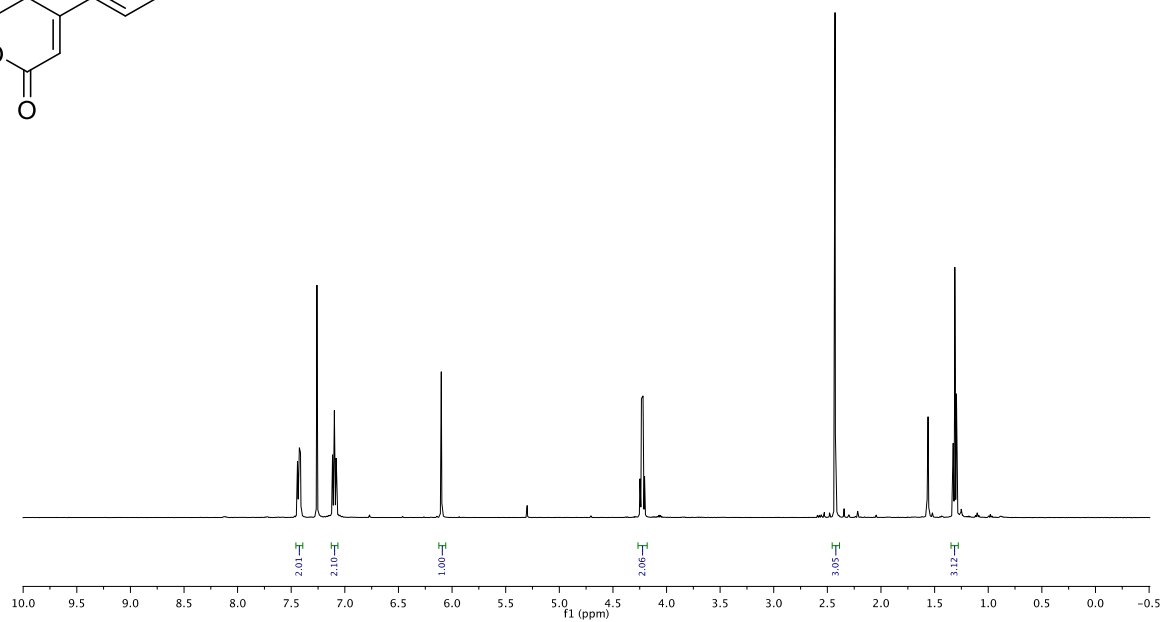
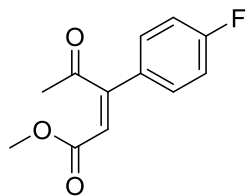


$^{13}\text{C}$  NMR (151 MHz, Chloroform-*d*)

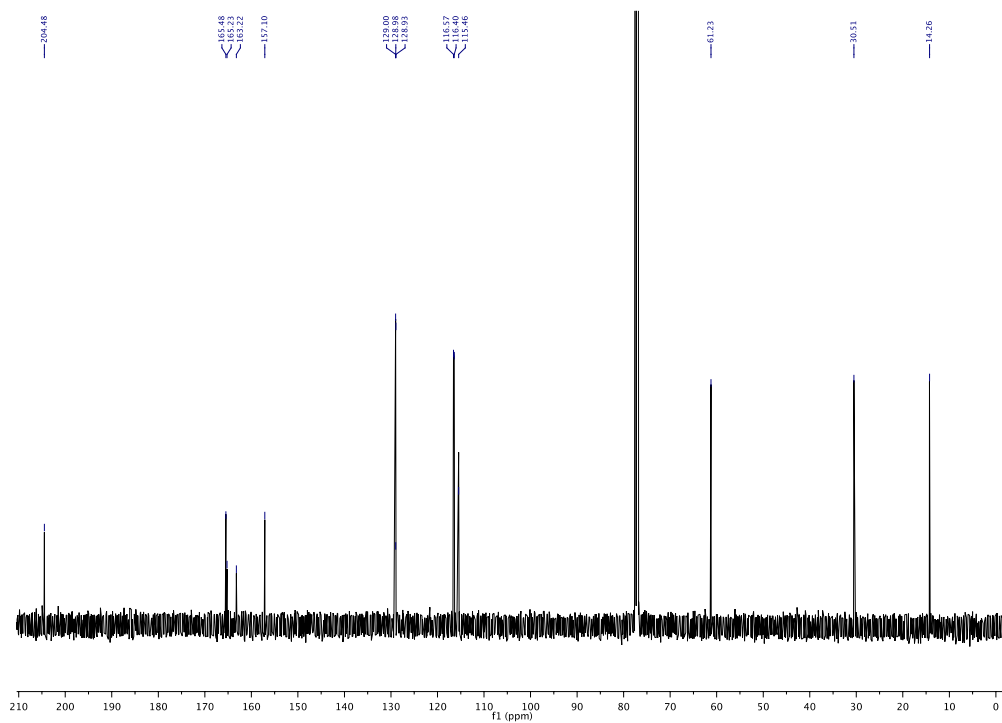


# Ethyl (Z)-3-(4-fluorophenyl)-4-oxopent-2-enoate

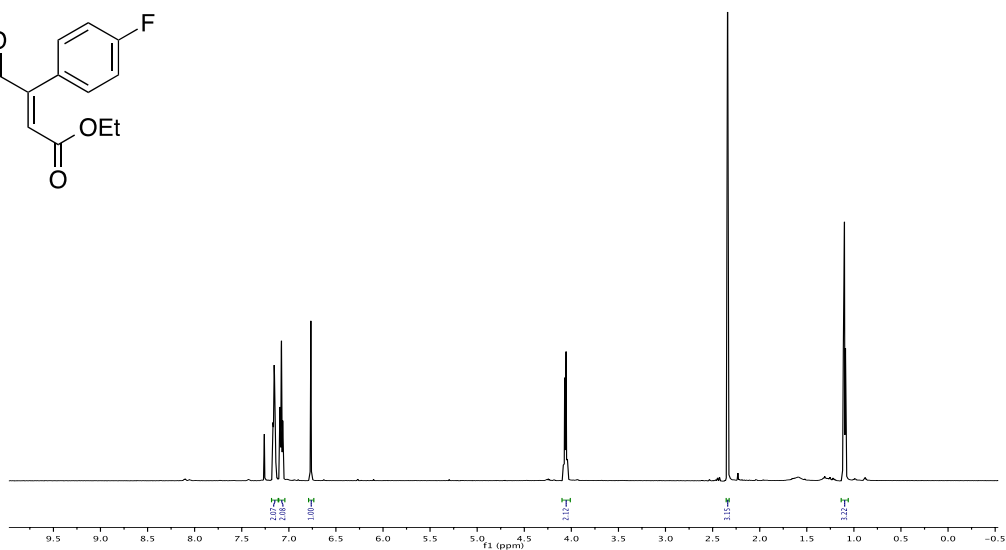
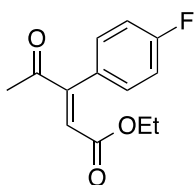
$^1\text{H}$  NMR (600 MHz, Chloroform-*d*)



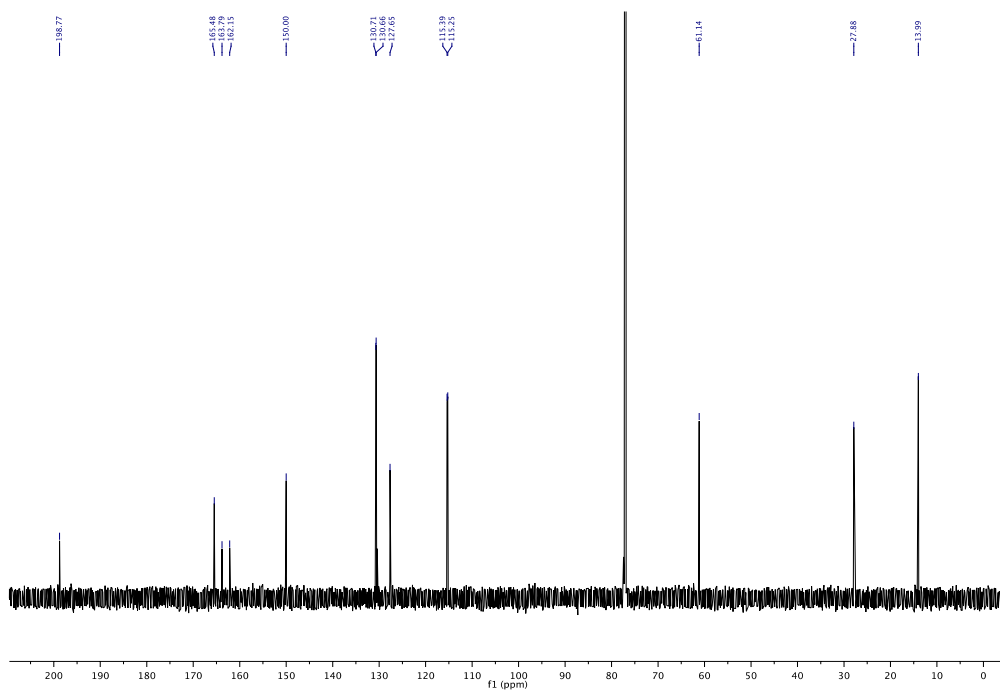
$^{13}\text{C}$  NMR (126 MHz, Chloroform-*d*)



**Ethyl (*E*)-3-(4-fluorophenyl)-4-oxopent-2-enoate**  
<sup>1</sup>H NMR (600 MHz, Chloroform-*d*)

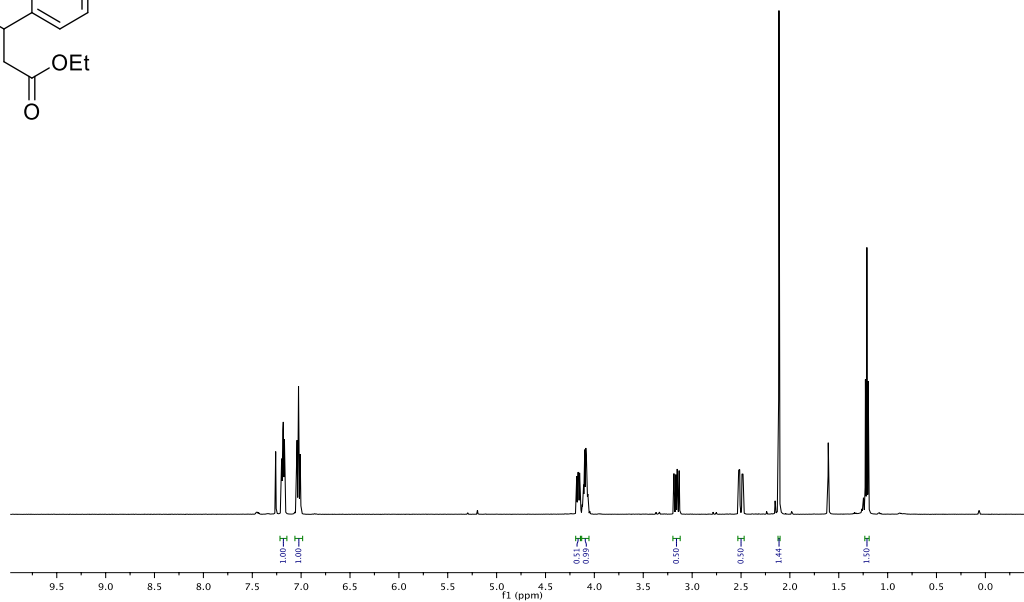
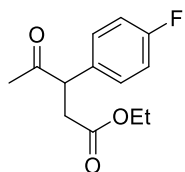


<sup>13</sup>C NMR (151 MHz, Chloroform-*d*)

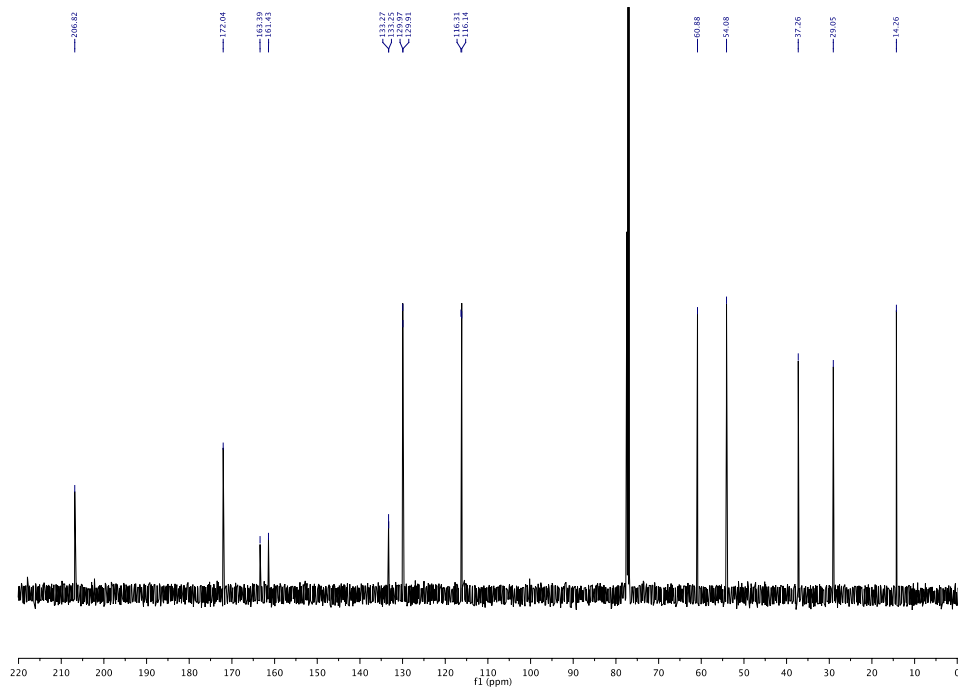


# Ethyl 3-(4-Fluorophenyl)-4-oxopentanoate

$^1\text{H}$  NMR (500 MHz, Chloroform-*d*)

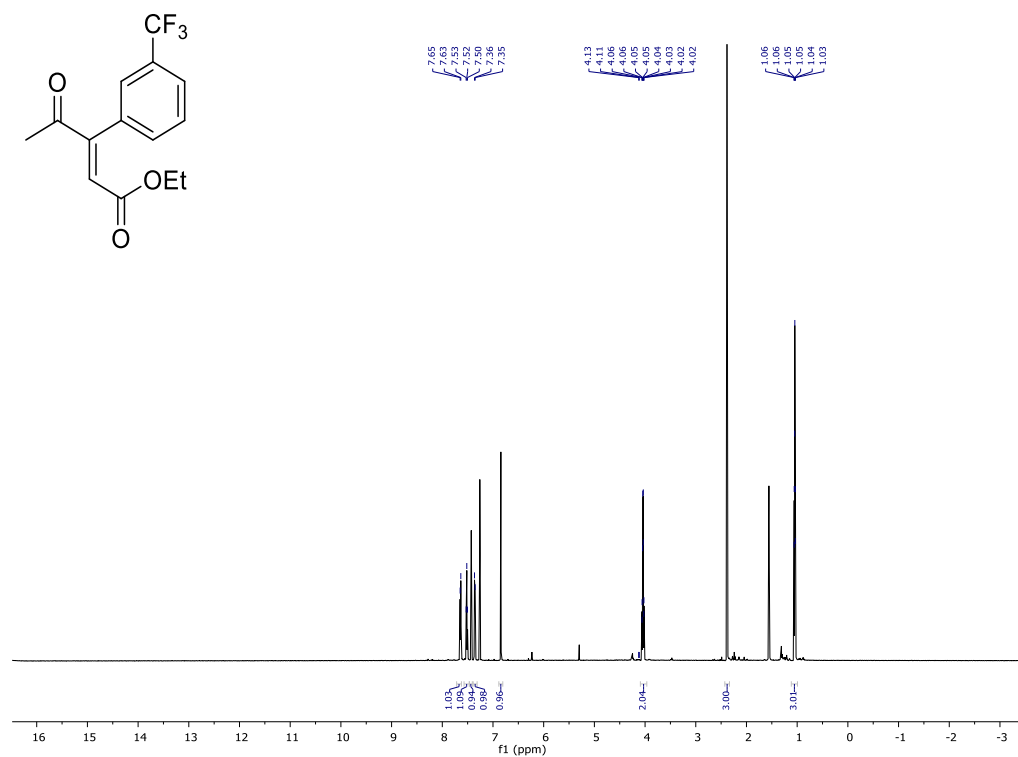


$^{13}\text{C}$  NMR (126 MHz, Chloroform-*d*)

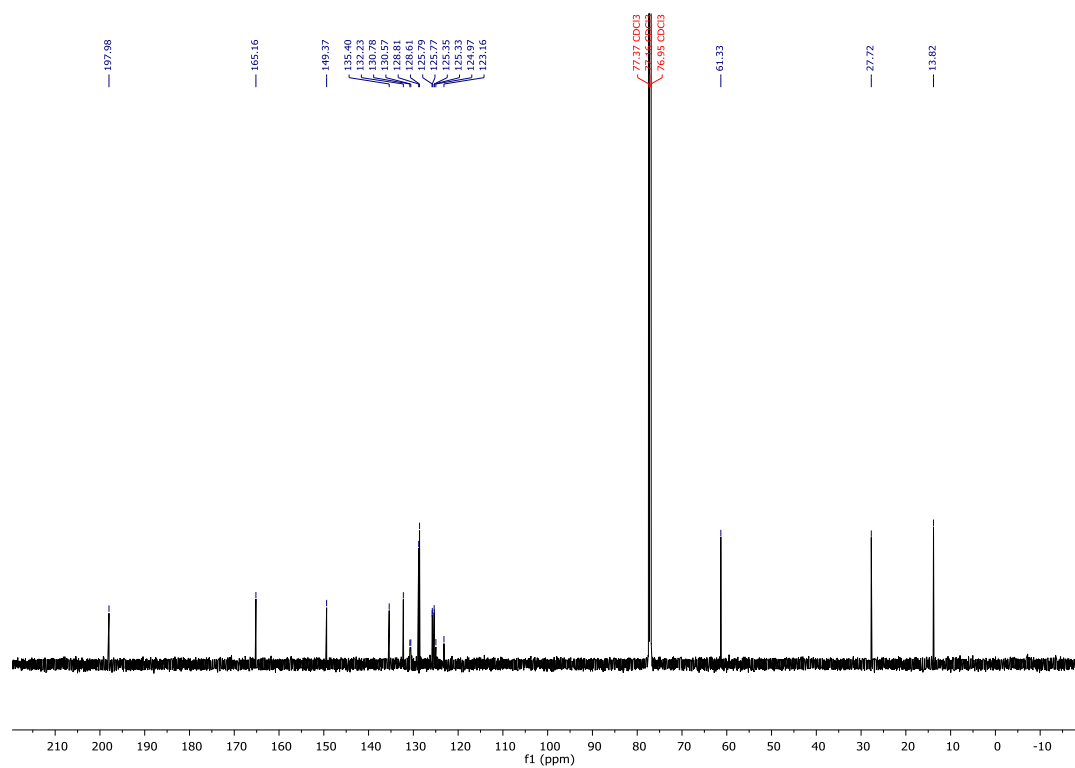


# Ethyl (E)-4-oxo-3-(3-(trifluoromethyl)phenyl)pent-2-enoate

$^1\text{H}$  NMR (600 MHz, Chloroform-*d*)

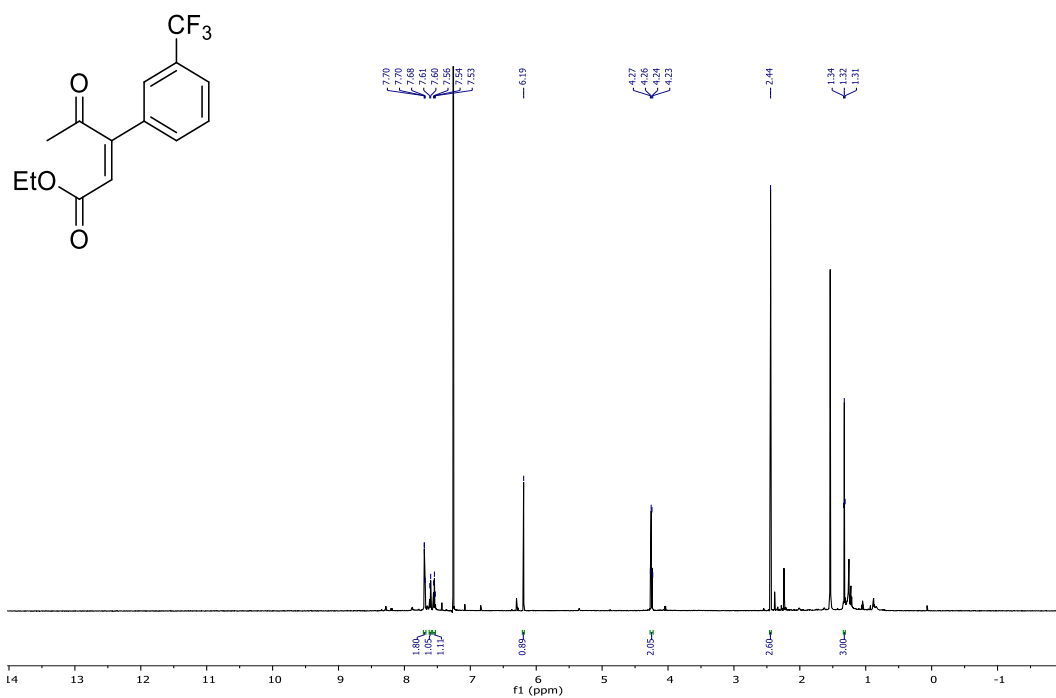


$^{13}\text{C}$  NMR (152 MHz, Chloroform-*d*)

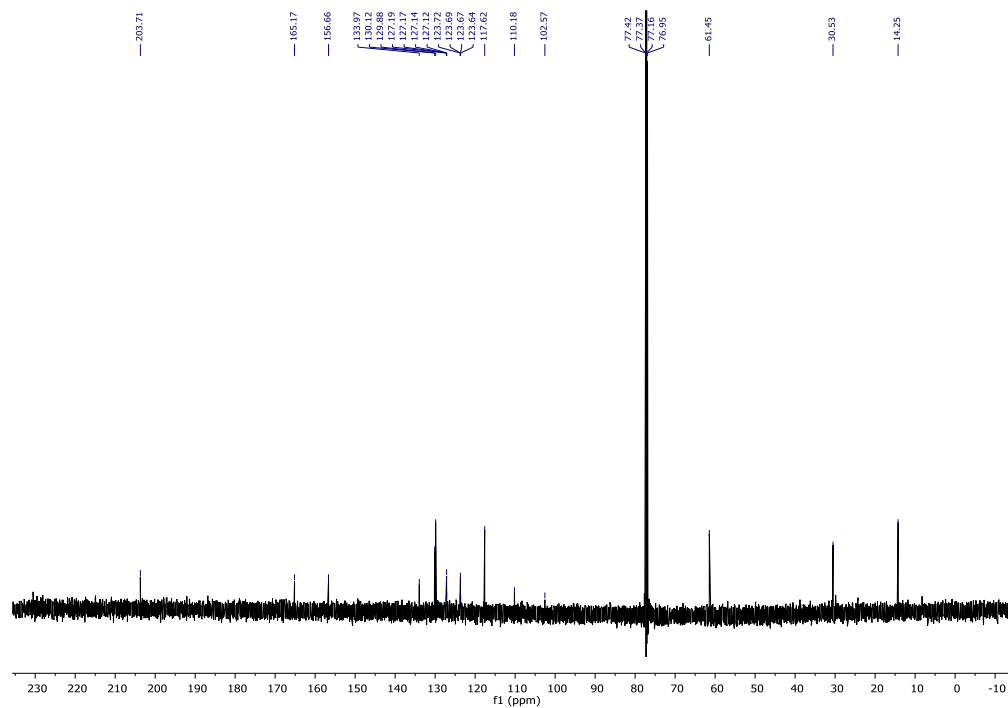


### Ethyl (Z)-4-oxo-3-(3-(trifluoromethyl)phenyl)pent-2-enoate

<sup>1</sup>H NMR (600 MHz, Chloroform-*d*)

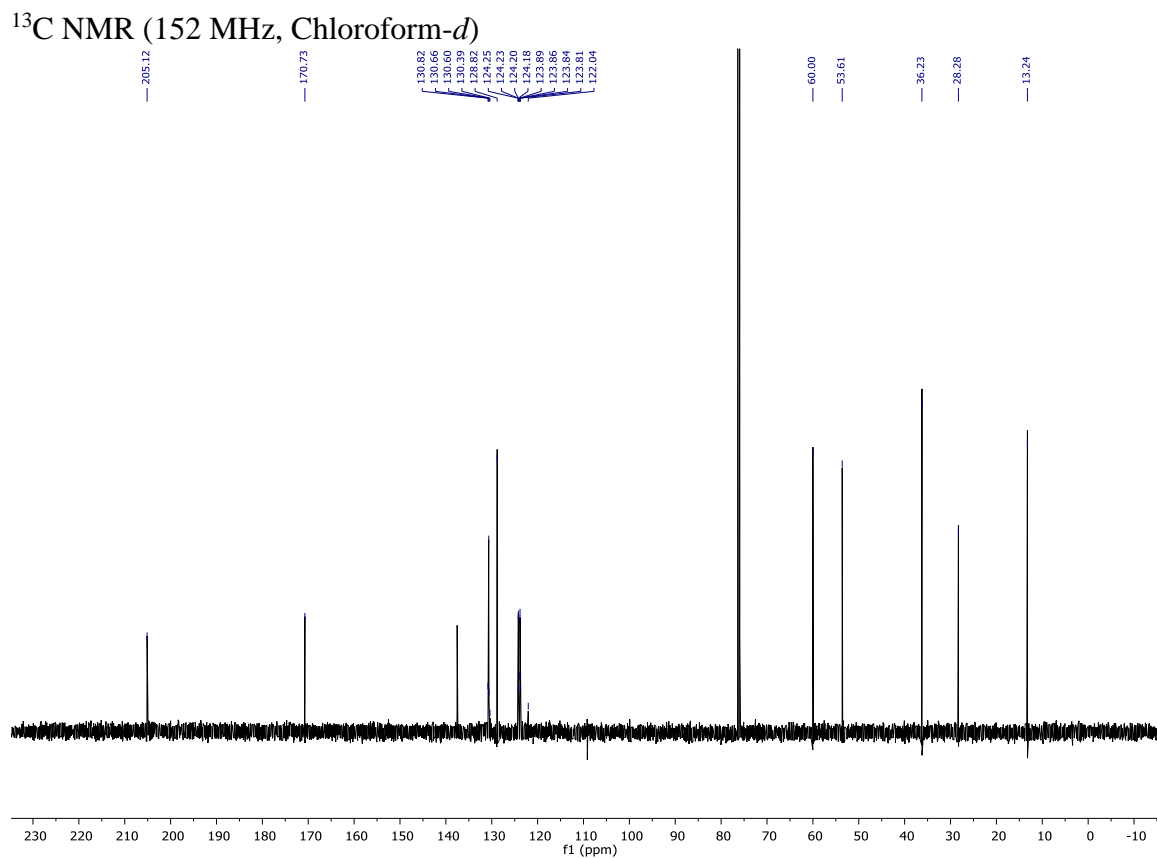
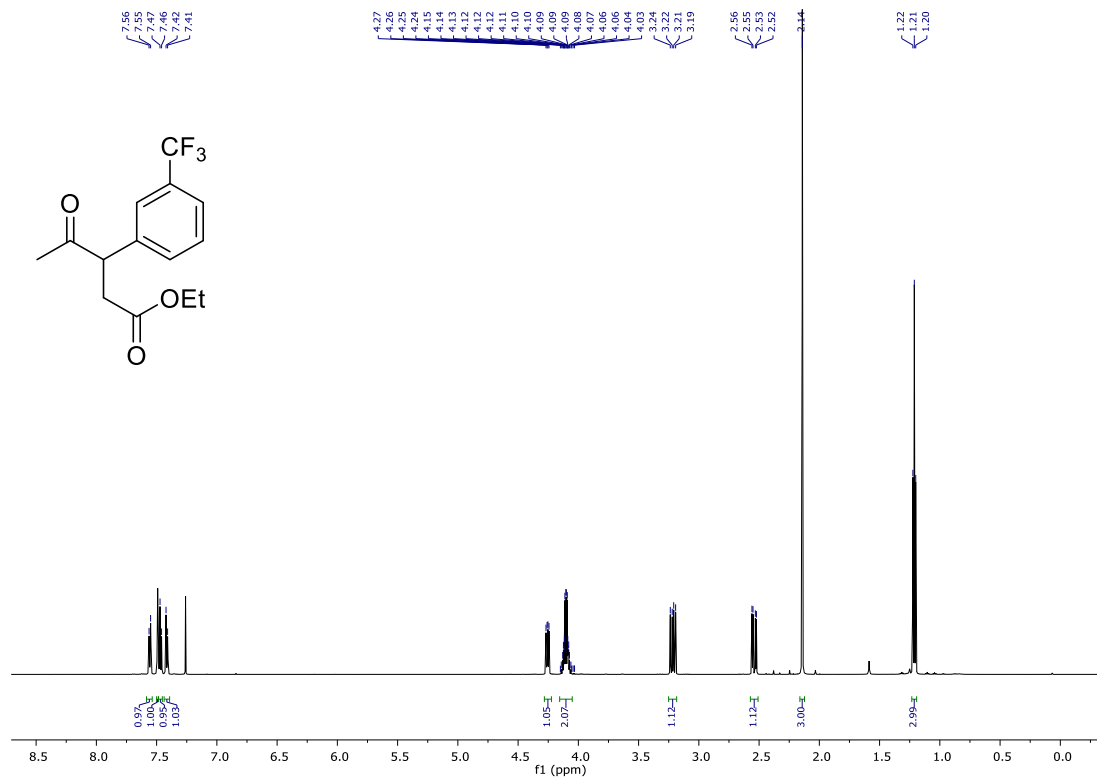


<sup>13</sup>C NMR (152 MHz, Chloroform-*d*)



### Ethyl 4-oxo-3-(3-(trifluoromethyl)phenyl)pentanoate

<sup>1</sup>H NMR (600 MHz, Chloroform-*d*)

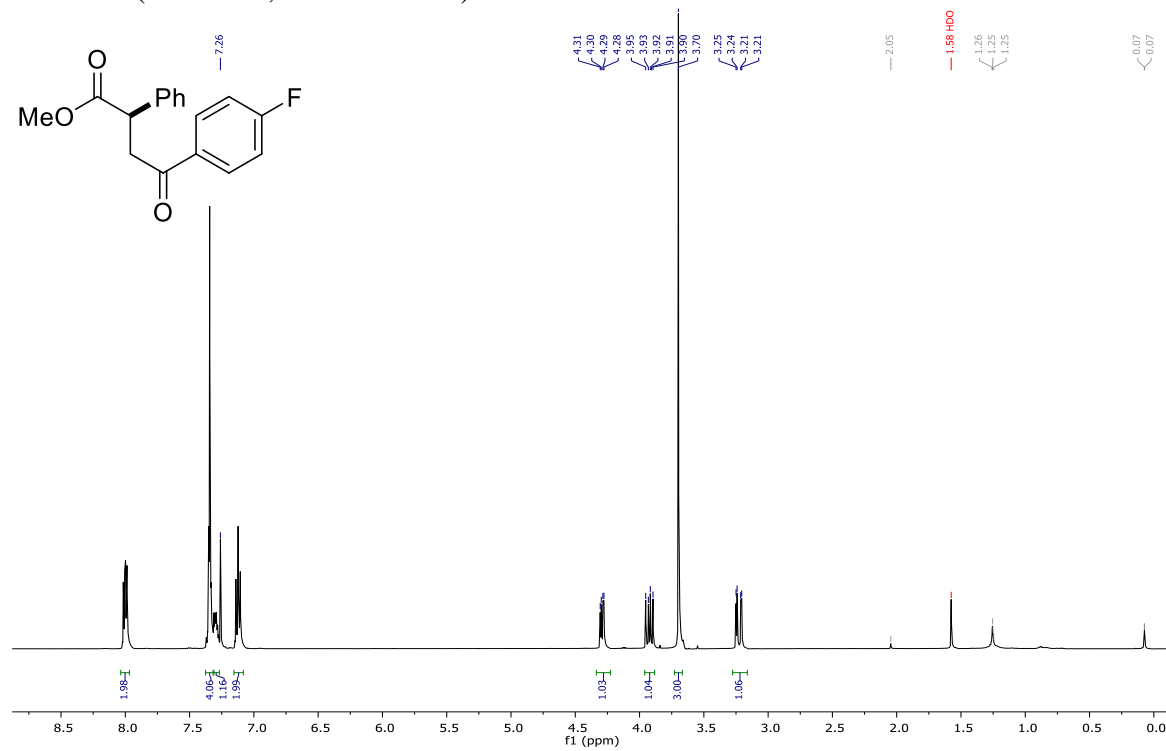




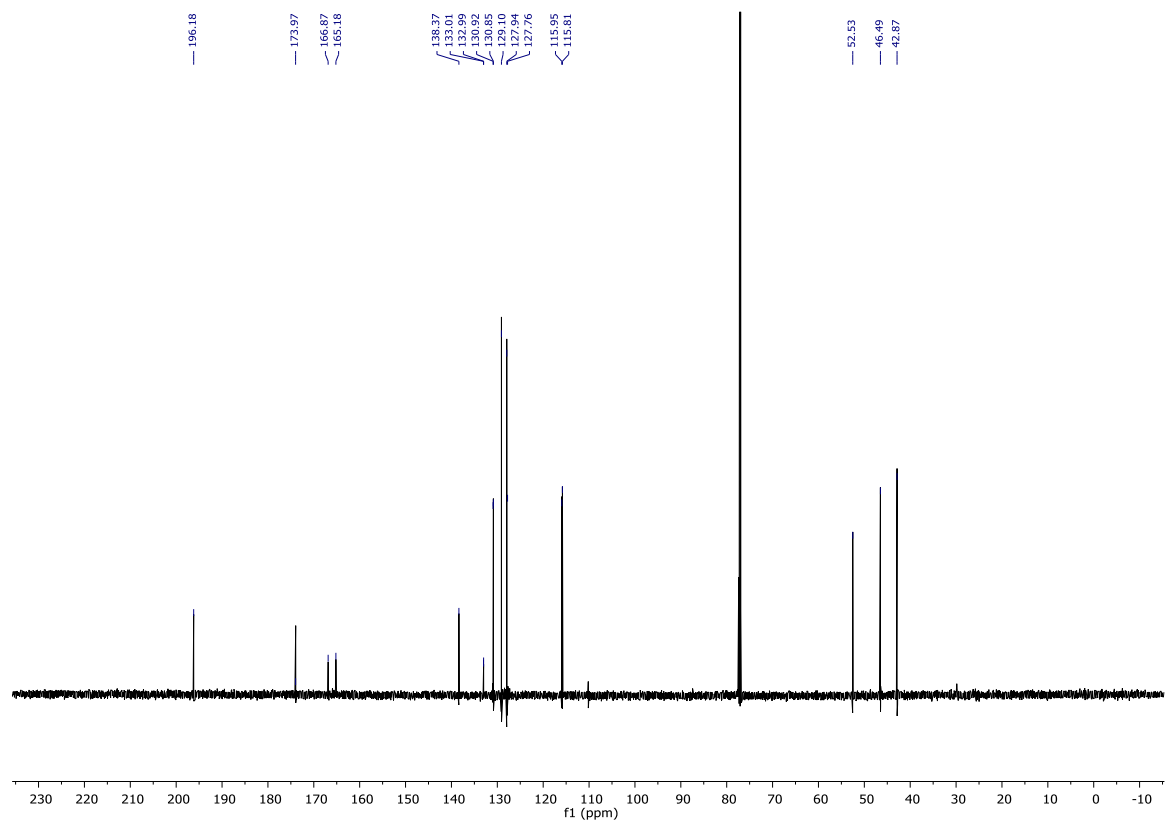


# Methyl (R)-4-(4-fluorophenyl)-4-oxo-2-phenylbutanoate

$^1\text{H}$  NMR (600 MHz, Chloroform-*d*)

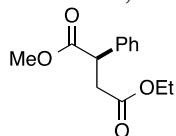


$^{13}\text{C}$  NMR (151 MHz, Chloroform-*d*)

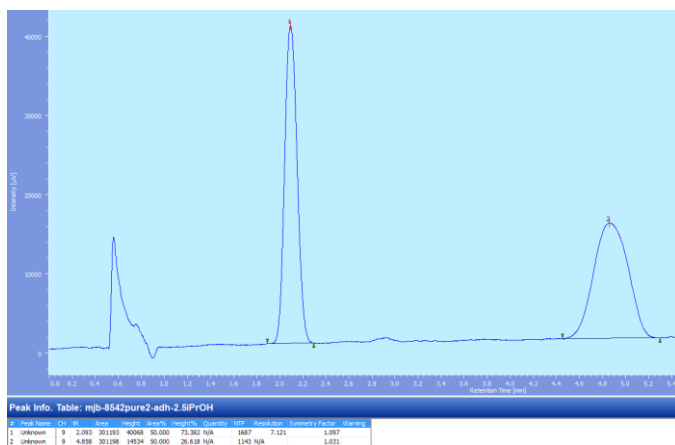


### 3.5.2. Representative HPLC and SFC Traces

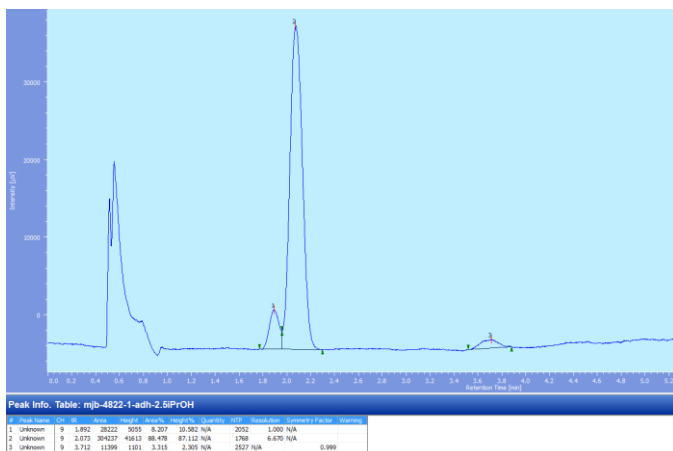
4-Ethyl 1-Methyl -2-Phenylsuccinate: SFC, AD-H column, 2.5% *i*PrOH, 2.5 mL/min, 220 nm.



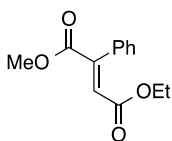
Racemate:  $t_R = 2.09, 4.86$  min (area = 50:50)

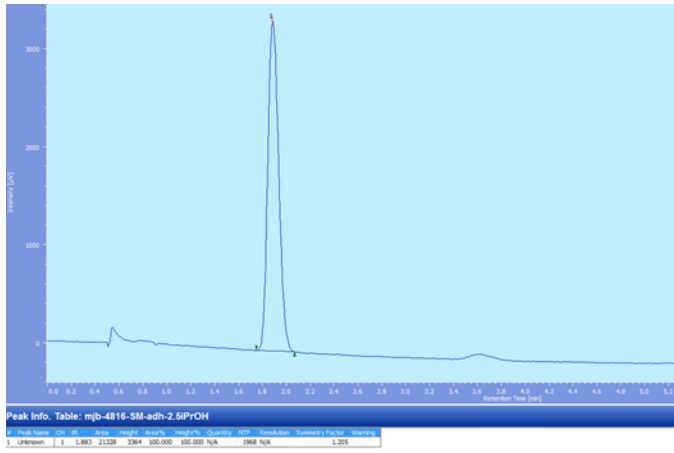


Reaction with YERS-ER:  $t_R = 2.07$  min, >99% *ee*

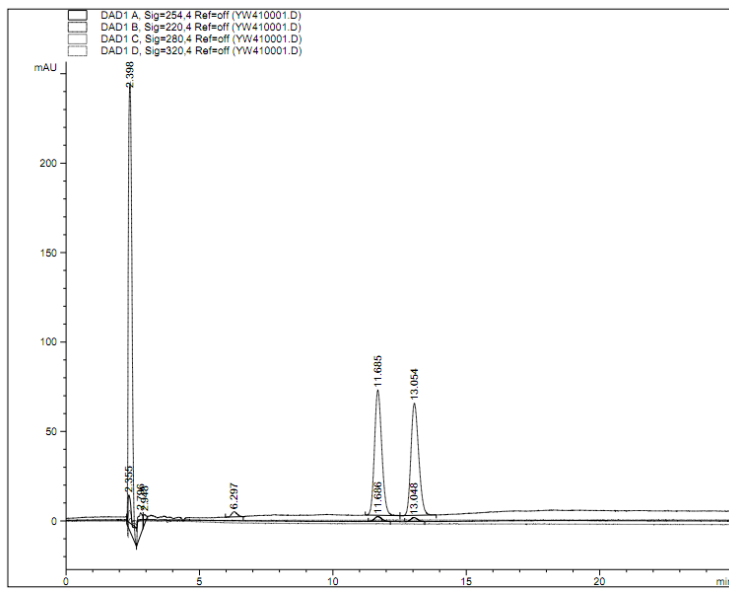


Starting Material:  $t_R = 1.88$  min



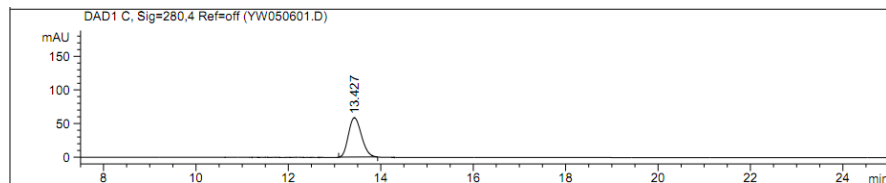


Racemate (By NP-HPLC OJH):  $t_R = 11.69, 13.05$  min (area = 50:50)



| Peak # | RetTime [min] | Type | Width [min] | Area [mAU*s] | Height [mAU] | Area %  |
|--------|---------------|------|-------------|--------------|--------------|---------|
| 1      | 2.355         | VV   | 0.1138      | 97.61587     | 15.18288     | 51.8042 |
| 2      | 11.686        | BB   | 0.2373      | 50.71163     | 2.71010      | 26.9124 |
| 3      | 13.048        | BB   | 0.2342      | 40.10501     | 2.27085      | 21.2835 |

Diazocoupling reaction followed by reduction with Yers-ER:  $t_R = 13.43\text{min}$ ,  $>99\%$  *ee*



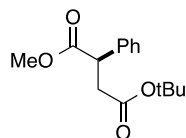
Signal 3: DAD1 C, Sig=280,4 Ref=off

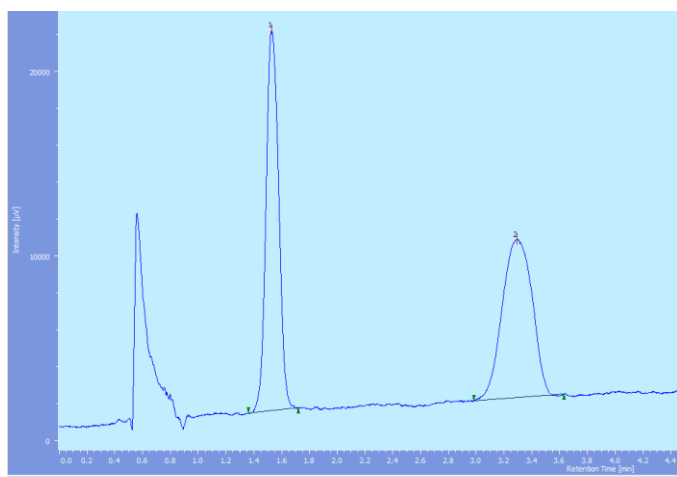
| Peak # | RetTime [min] | Type | Width [min] | Area [mAU*s] | Height [mAU] | Area %   |
|--------|---------------|------|-------------|--------------|--------------|----------|
| 1      | 13.427        | BB   | 0.3065      | 1145.42603   | 58.65222     | 100.0000 |

4-*tert*-Butyl 1-Methyl -2-Phenylsuccinate: SFC, AD-H column, 2.5% *i*PrOH, 2.5 mL/min, 220 nm.

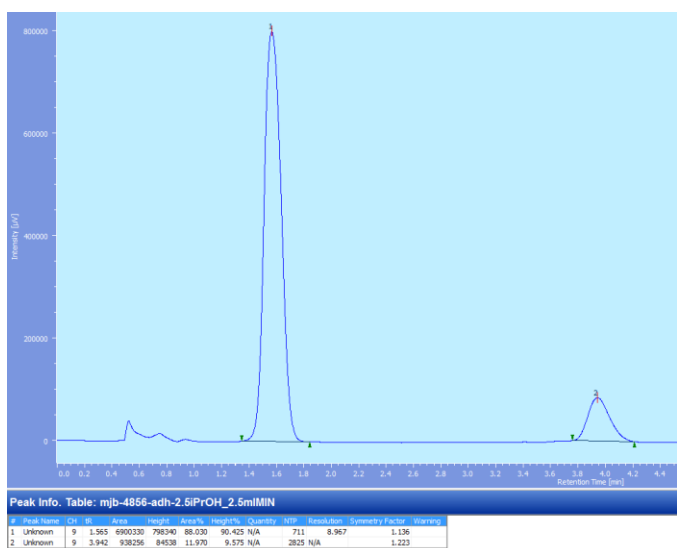
Full conversion of SM required for chiral SFC analysis.

Racemate:  $t_R = 1.53, 3.29\text{ min}$  (area = 50:50)

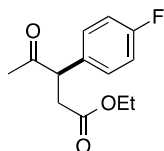




Reaction with OPR1:  $t_R = 1.57$  min, >99% *ee*

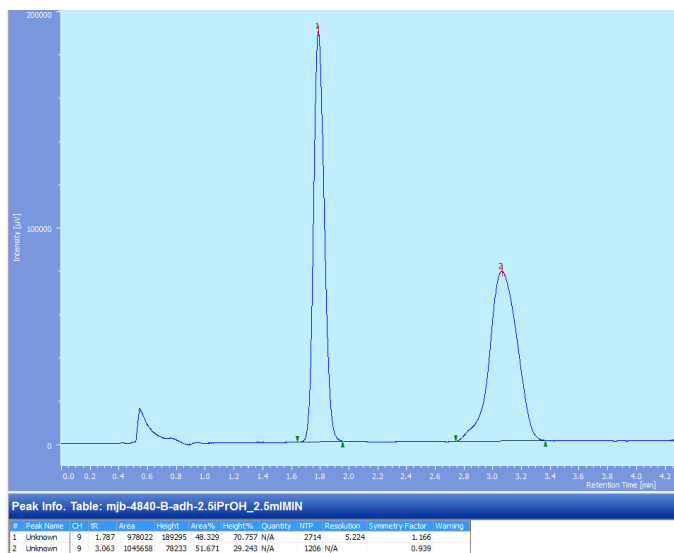


Ethyl 3-(4-Fluorophenyl)-4-oxopentanoate: SFC, AD-H column, 2.5% *i*PrOH, 2.5 mL/min, 220 nm.

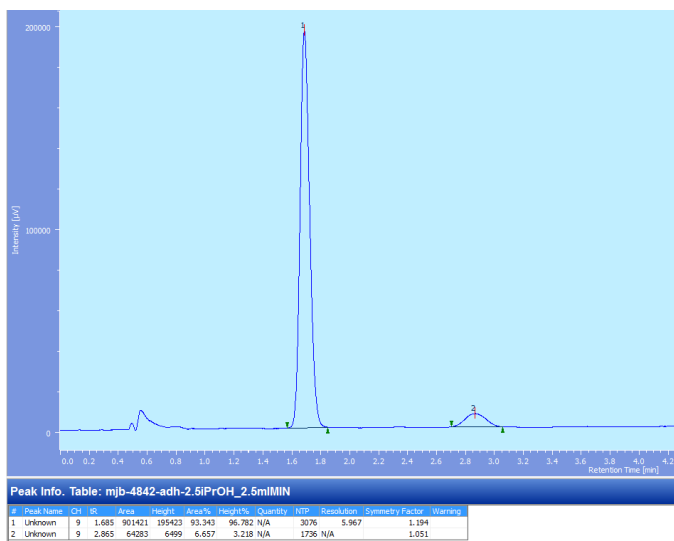


Full conversion of SM required for chiral SFC analysis.

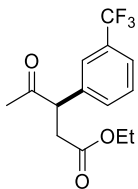
Racemate:  $t_R = 1.79, 3.06$  min (area = 50:50)



Reaction with Yers-ER:  $t_R = 1.69, 2.89$  min, 87% *ee*

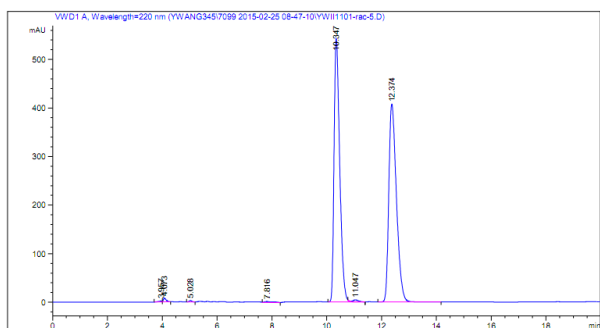


Ethyl (R)-4-oxo-3-(3-(trifluoromethyl)phenyl)pentanoate: NP HPLC, OJ-H column, 95:5 Hexanes: IPA, 0.8 mL/min, 220 nm



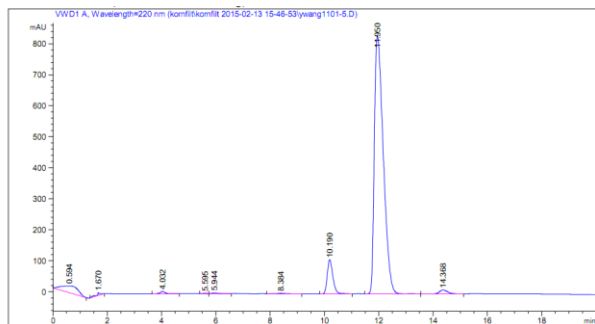
Full conversion of SM required for chiral HPLC analysis.

Racemate:  $t_R = 10.347, 12.347$  min (area = 50:50)



| Peak # | RetTime [min] | Type | Width [min] | Area [mAU*s] | Height [mAU] | Area %  |
|--------|---------------|------|-------------|--------------|--------------|---------|
| 5      | 10.347        | BV R | 0.2208      | 7754.53662   | 542.03766    | 49.0439 |
| 7      | 12.374        | BB   | 0.2982      | 7873.45410   | 407.49777    | 49.7960 |

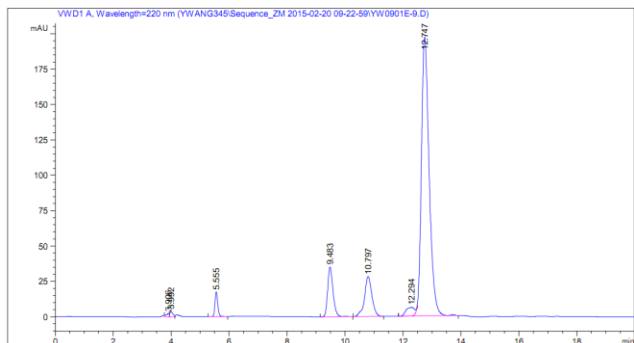
Reaction with Yers-ER:  $t_R = 10.190, 11.950$  min, 92% *ee*



Signal 1: VWD1 A, Wavelength=220 nm

| Peak # | RetTime [min] | Type | Width [min] | Area [mAU*s] | Height [mAU] | Area %  |
|--------|---------------|------|-------------|--------------|--------------|---------|
| 7      | 10.190        | BB   | 0.2191      | 1581.68030   | 110.72596    | 7.1363  |
| 8      | 11.950        | BV R | 0.3539      | 1.90192e4    | 832.42889    | 85.8123 |

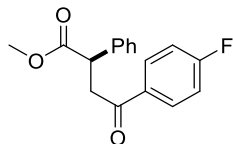
Diazocoupling reaction followed by reduction with Yers-ER:  $t_R = 10.797, 12.747$  min, 88% *ee*





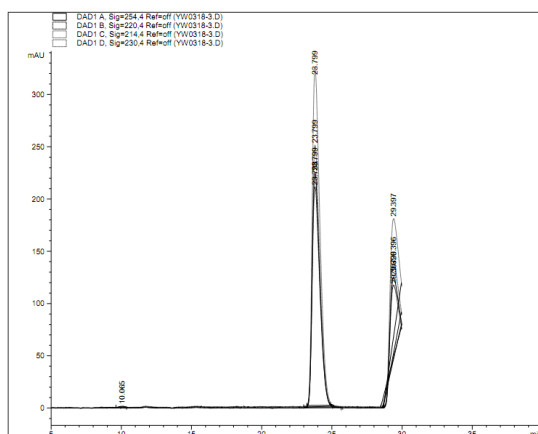
| Peak # | RetTime [min] | Type | Width [min] | Area [mAU*s] | Height [mAU] | Area %  |
|--------|---------------|------|-------------|--------------|--------------|---------|
| 5      | 10.797        | BB   | 0.2663      | 500.38501    | 28.26075     | 10.2150 |
| 7      | 12.747        | VV R | 0.2838      | 3661.28247   | 197.03004    | 74.7426 |

Methyl (R)-4-(4-fluorophenyl)-4-oxo-2-phenylbutanoate: NP HPLC, OJ-H column, 95:5 Hexanes : IPA, 0.8 mL/min, 220 nm.

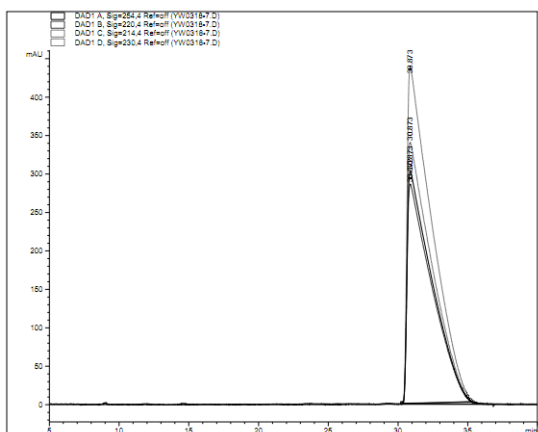


Full conversion of SM required for chiral HPLC analysis.

Racemate:  $t_R = 23.799, 29.397$  min (area = 50:50)

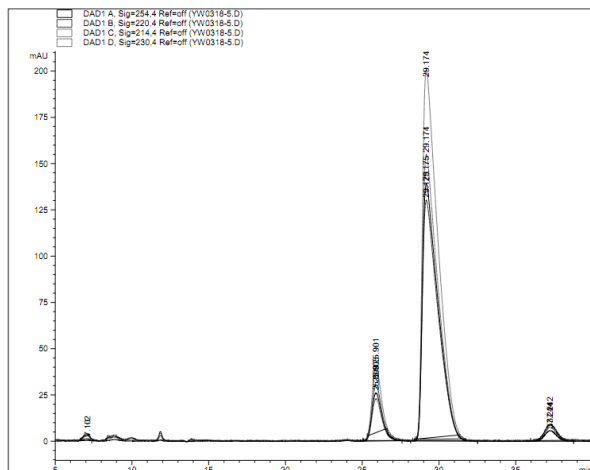


Reaction with OYE2:  $t_R = 30.873$  min, >99% *ee*



| Peak # | RetTime [min] | Type | Width [min] | Area [mAU*s] | Height [mAU] | Area %  |
|--------|---------------|------|-------------|--------------|--------------|---------|
| 1      | 2.371         | VV   | 0.0847      | 47.39185     | 7.60309      | 0.1260  |
| 2      | 2.710         | PB   | 0.0344      | 4.61297      | 2.03591      | 0.0123  |
| 3      | 30.873        | BB   | 1.5421      | 3.75682e4    | 302.82794    | 99.8618 |

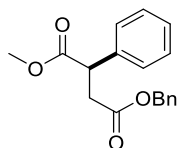
Diazocoupling reaction followed by reduction with OYE2:  $t_R = 29.174$  min, >99% *ee*. Other peaks are impurities.



Signal 2: DAD1 B, Sig=220,4 Ref=off

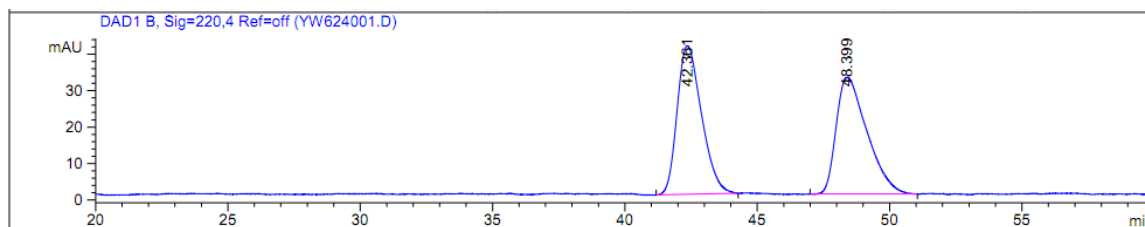
| Peak # | RetTime [min] | Type | Width [min] | Area [mAU*s] | Height [mAU] | Area %  |
|--------|---------------|------|-------------|--------------|--------------|---------|
| 1      | 25.903        | BB   | 0.6285      | 1403.19116   | 30.16465     | 12.6239 |
| 2      | 29.175        | BB   | 0.9885      | 9246.17090   | 130.00034    | 83.1836 |
| 3      | 37.242        | BB   | 0.8456      | 466.02106    | 8.45319      | 4.1926  |

4-Benzyl 1-methyl (R)-2-phenylsuccinate: NP HPLC, OJ-H column, 95:5 Hexanes: IPA, 0.8 mL/min, 220 nm.



Full conversion of SM required for chiral HPLC analysis.

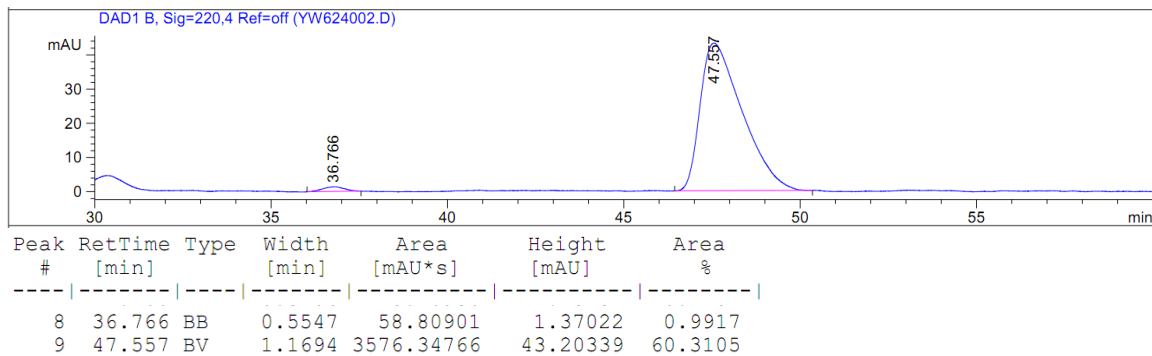
Racemate:  $t_R = 42.361, 48.399$  min (area = 50:50)



Signal 2: DAD1 B, Sig=220,4 Ref=off

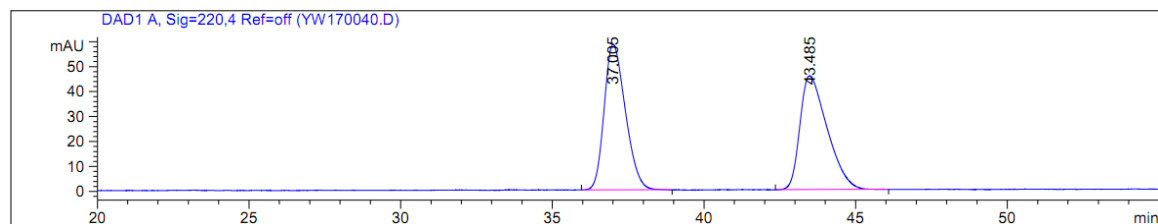
| Peak # | RetTime [min] | Type | Width [min] | Area [mAU*s] | Height [mAU] | Area %  |
|--------|---------------|------|-------------|--------------|--------------|---------|
| 1      | 42.361        | BB   | 0.9218      | 2606.61353   | 40.74746     | 50.0964 |
| 2      | 48.399        | BB   | 1.1987      | 2596.58569   | 32.04758     | 49.9036 |

Reaction with OPR1:  $t_R = 47.557$  min, >99% *ee*



Tandem reaction: OJ-H column (250 mm), 90:10 Hexanes: IPA, 1 mL/min, 220 nm.

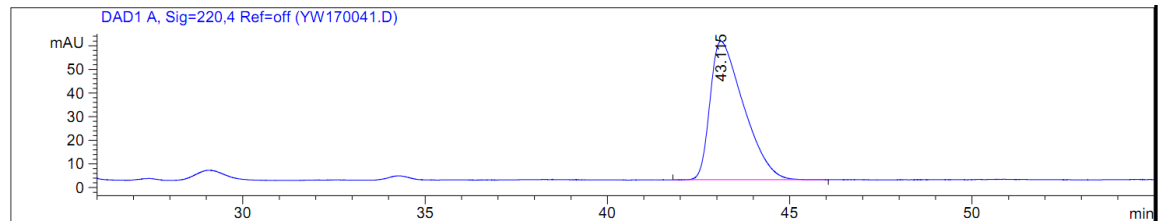
Racemate:  $t_R = 37.005, 43.485$  min (area = 50:50)



Signal 1: DAD1 A, Sig=220,4 Ref=off

| Peak # | RetTime [min] | Type | Width [min] | Area [mAU*s] | Height [mAU] | Area %  |
|--------|---------------|------|-------------|--------------|--------------|---------|
| 1      | 37.005        | BB   | 0.7553      | 2835.67798   | 58.32808     | 49.8747 |
| 2      | 43.485        | BB   | 0.9398      | 2849.92285   | 45.65257     | 50.1253 |

Diazocoupling reaction followed by reduction with OPR1:  $t_R = 43.115$  min, >99% *ee*. The product was confirmed by H NMR.



Signal 1: DAD1 A, Sig=220,4 Ref=off

| Peak # | RetTime [min] | Type | Width [min] | Area [mAU*s] | Height [mAU] | Area %  |
|--------|---------------|------|-------------|--------------|--------------|---------|
| 1      | 3.376         | BV   | 0.2061      | 1682.68750   | 141.15776    | 30.5108 |
| 2      | 3.775         | VV   | 0.0982      | 18.00277     | 3.05625      | 0.3264  |
| 3      | 4.444         | VV   | 0.0895      | 33.37144     | 6.21274      | 0.6051  |
| 4      | 13.370        | BB   | 0.2236      | 26.98635     | 1.87384      | 0.4893  |
| 5      | 43.115        | BB   | 0.9654      | 3753.99927   | 58.67488     | 68.0683 |

## 3.6 References

- 1 Saini, V., Stokes, B. J. & Sigman, M. S. Transition-metal-catalyzed laboratory-scale carbon-carbon bond-forming reactions of ethylene. *Angew. Chem. Int. Ed. Engl.* **52**, 11206-11220, (2013).
- 2 Lu, X., Xiao, B., Zhang, Z., Gong, T., Su, W., Yi, J., Fu, Y. & Liu, L. Practical carbon-carbon bond formation from olefins through nickel-catalyzed reductive olefin hydrocarbonation. *Nat Commun* **7**, (2016).
- 3 Hansen, J. H., Parr, B. T., Pelphrey, P., Jin, Q., Autschbach, J. & Davies, H. M. Rhodium(II)-catalyzed cross-coupling of diazo compounds. *Angew. Chem.* **50**, 2544-2548, (2011).
- 4 Denard, C. A., Hartwig, J. F. & Zhao, H. Multistep One-Pot Reactions Combining Biocatalysts and Chemical Catalysts for Asymmetric Synthesis. *ACS Catal.* **3**, 2856-2864, (2013).
- 5 Fesko, K. & Gruber-Khadjawi, M. Biocatalytic Methods for C-C Bond Formation. *Chemcatchem* **5**, 1248-1272, (2013).
- 6 Schmidt, N. G., Eger, E. & Kroutil, W. Building Bridges: Biocatalytic C-C-Bond Formation toward Multifunctional Products. *ACS Catalysis* **6**, 4286-4311, (2016).
- 7 Verho, O. & Backvall, J. E. Chemoenzymatic dynamic kinetic resolution: a powerful tool for the preparation of enantiomerically pure alcohols and amines. *J. Am. Chem. Soc.* **137**, 3996-4009, (2015).
- 8 Moroy, G., Denhez, C., El Mourabit, H., Toribio, A., Dassonville, A., Decarme, M., Renault, J.-H., Mirand, C., Bellon, G., Sapi, J., Alix, A. J. P., Hornebeck, W. & Bourguet, E. Simultaneous presence of unsaturation and long alkyl chain at of Ilomastat confers selectivity for gelatinase A (MMP-2) over gelatinase B (MMP-9) inhibition as shown by molecular modelling studies. *Bioorg. Med. Chem.* **15**, 4753-4766, (2007).
- 9 Chen, J. J., Zhang, Y. P., Hammond, S., Dewdney, N., Ho, T., Lin, X. H., Browner, M. F. & Castelhana, A. L. Design, synthesis, activity, and structure of a novel class of matrix metalloproteinase inhibitors containing a heterocyclic P-2'-P-3' amide bond isostere. *Bioorg. Med. Chem. Lett.* **6**, 1601-1606, (1996).
- 10 Galatsis, P., Caprathe, B., Gilmore, J., Thomas, A., Linn, K., Sheehan, S., Harter, W., Kostlan, C., Lunney, E., Stankovic, C., Rubin, J., Brady, K., Allen, H. & Talanian, R. Succinic acid amides as P2-P3 replacements for inhibitors of interleukin-1 beta converting enzyme (ICE or caspase 1). *Bioorg. Med. Chem. Lett.* **20**, 5184-5190, (2010).
- 11 Liu, J. C., Yang, Y. S. & Ji, R. Y. An effective and convenient method for the preparation of KAD-1229. *Helv. Chim. Acta* **87**, 1935-1939, (2004).

- 12 Korpak, M. & Pietruszka, J. Chemoenzymatic One-Pot Synthesis of  $\gamma$ -Butyrolactones. *Adv. Synth. Catal.* **353**, 1420-1424, (2011).
- 13 Barros, M. T., Maycock, C. D. & Ventura, M. R. Aldol reactions of dioxanes derived from tartaric acid. A total synthesis of (+)-nephrosteranic acid. *Org Lett* **5**, 4097-4099, (2003).
- 14 Furstner, A., Bouchez, L. C., Morency, L., Funel, J. A., Liepins, V., Poree, F. H., Gilmour, R., Laurich, D., Beaufils, F. & Tamiya, M. Total syntheses of amphidinolides B1, B4, G1, H1 and structure revision of amphidinolide H2. *Chemistry (Easton)* **15**, 3983-4010, (2009).
- 15 Tannert, R., Hu, T. S., Arndt, H. D. & Waldmann, H. Solid-phase based total synthesis of Jasplakinolide by ring-closing metathesis. *Chem. Commun. (Camb.)*, 1493-1495, (2009).
- 16 Tannert, R., Milroy, L. G., Ellinger, B., Hu, T. S., Arndt, H. D. & Waldmann, H. Synthesis and structure-activity correlation of natural-product inspired cyclodepsipeptides stabilizing F-actin. *J. Am. Chem. Soc.* **132**, 3063-3077, (2010).
- 17 Hekking, K. F. W., Lefort, L., de Vries, A. H. M., van Delft, F. L., Schoemaker, H. E., de Vries, J. G. & Rutjes, F. P. J. T. Synthesis of Versatile Building Blocks through Asymmetric Hydrogenation of Functionalized Itaconic Acid Mono-Esters. *Adv. Synth. Catal.* **350**, 85-94, (2008).
- 18 Liu, Y., Sandoval, C. A., Yamaguchi, Y., Zhang, X., Wang, Z., Kato, K. & Ding, K. Hydrogen Bonding Makes a Difference in the Rhodium-Catalyzed Enantioselective Hydrogenation Using Monodentate Phosphoramidites. *J. Am. Chem. Soc.* **128**, 14212-14213, (2006).
- 19 Tang, W., Liu, D. & Zhang, X. Asymmetric Hydrogenation of Itaconic Acid and Enol Acetate Derivatives with the Rh-TangPhos Catalyst. *Org Lett* **5**, 205-207, (2003).
- 20 Berens, U., Burk, M. J. & Gerlach, A. W., Hems. Chiral 1,1'-Diphosphetanylferrocenes: New Ligands for Asymmetric Catalytic Hydrogenation of Itaconate Derivatives. *Angew. Chem. Int. Ed.* **39**, 1981-1985, (2000).
- 21 Bernasconi, M., Muller, M. A. & Pfaltz, A. Asymmetric hydrogenation of maleic acid diesters and anhydrides. *Angew. Chem. Int. Ed. Engl.* **53**, 5385-5388, (2014).
- 22 Bernardi, L. & Fochi, M. A General Catalytic Enantioselective Transfer Hydrogenation Reaction of beta,beta-Disubstituted Nitroalkenes Promoted by a Simple Organocatalyst. *Molecules (Basel, Switzerland)* **21**, (2016).
- 23 Liu, Y., Chen, J., Zhang, Z., Qin, J., Zhao, M. & Zhang, W. One-pot sequential asymmetric hydrogenation of beta-aryl-beta-aryloxy acroleins. *Org. Biomol. Chem.* **14**, 7099-7102, (2016).
- 24 Kong, D., Li, M., Zi, G., Hou, G. & He, Y. Enantioselective Hydrogenation of Diarylmethanimines for Synthesis of Chiral Diarylmethylamines. *J. Org. Chem.*, (2016).
- 25 Pan, H. J., Zhang, Y., Shan, C., Yu, Z., Lan, Y. & Zhao, Y. Asymmetric Transfer Hydrogenation of Imines using Alcohol: Efficiency and Selectivity are Influenced by the Hydrogen Donor. *Angew. Chem. Int. Ed. Engl.* **55**, 9615-9619, (2016).
- 26 Reid, J. P. & Goodman, J. M. Goldilocks Catalysts: Computational Insights into the Role of the 3,3' Substituents on the Selectivity of BINOL-Derived Phosphoric Acid Catalysts. *J. Am. Chem. Soc.* **138**, 7910-7917, (2016).
- 27 Chen, Z. P., Hu, S. B., Chen, M. W. & Zhou, Y. G. Synthesis of Chiral Fluorinated Hydrazines via Pd-Catalyzed Asymmetric Hydrogenation. *Org Lett* **18**, 2676-2679, (2016).
- 28 Zhou, M., Xue, Z., Cao, M., Dong, X. Q. & Zhang, X. Rhodium-catalyzed asymmetric hydrogenation of unprotected beta-enamine phosphonates. *Org. Biomol. Chem.* **14**, 4582-4584, (2016).

- 29 Kita, Y., Hida, S., Higashihara, K., Jena, H. S., Higashida, K. & Mashima, K. Chloride-Bridged Dinuclear Rhodium(III) Complexes Bearing Chiral Diphosphine Ligands: Catalyst Precursors for Asymmetric Hydrogenation of Simple Olefins. *Angew. Chem. Int. Ed. Engl.* **55**, 8299-8303, (2016).
- 30 Kong, D., Li, M., Zi, G. & Hou, G. Synthesis of chiral lactams via asymmetric hydrogenation of alpha,beta-unsaturated nitriles. *Org. Biomol. Chem.* **14**, 4046-4053, (2016).
- 31 Stirling, M. J., Sweeney, G., MacRory, K., Blacker, A. J. & Page, M. I. The kinetics and mechanism of the organo-iridium-catalysed enantioselective reduction of imines. *Org. Biomol. Chem.* **14**, 3614-3622, (2016).
- 32 Kong, D., Li, M., Wang, R., Zi, G. & Hou, G. Highly efficient asymmetric hydrogenation of cyano-substituted acrylate esters for synthesis of chiral gamma-lactams and amino acids. *Org. Biomol. Chem.* **14**, 1216-1220, (2016).
- 33 Gao, W., Wang, Q., Xie, Y., Lv, H. & Zhang, X. Rhodium-catalyzed Asymmetric Hydrogenation of alpha-Dehydroamino Ketones: A General Approach to Chiral alpha-amino Ketones. *Chem. Asian J.* **11**, 231-233, (2016).
- 34 Li, Y., Wang, Z. & Ding, K. Minimizing Aryloxy Elimination in Rh(I) -Catalyzed Asymmetric Hydrogenation of beta-Aryloxyacrylic Acids using a Mixed-Ligand Strategy. *Chemistry (Easton)* **21**, 16387-16390, (2015).
- 35 Yan, Q., Kong, D., Li, M., Hou, G. & Zi, G. Highly Efficient Rh-Catalyzed Asymmetric Hydrogenation of alpha,beta-Unsaturated Nitriles. *J. Am. Chem. Soc.* **137**, 10177-10181, (2015).
- 36 Li, J.-Q., Quan, X. & Andersson, P. G. Highly Enantioselective Iridium-Catalyzed Hydrogenation of  $\alpha,\beta$ -Unsaturated Esters. *Chemistry – A European Journal* **18**, 10609-10616, (2012).
- 37 Chung, Y. C., Janmanchi, D. & Wu, H. L. Preparation of chiral 3-arylpyrrolidines via the enantioselective 1,4-addition of arylboronic acids to fumaric esters catalyzed by Rh(I)/chiral diene complexes. *Org Lett* **14**, 2766-2769, (2012).
- 38 Chen, Y. & Deng, L. Parallel Kinetic Resolutions of Monosubstituted Succinic Anhydrides Catalyzed by a Modified Cinchona Alkaloid. *J. Am. Chem. Soc.* **123**, 11302-11303, (2001).
- 39 Wang, M. H., Cohen, D. T., Schwamb, C. B., Mishra, R. K. & Scheidt, K. A. Enantioselective beta-Protonation by a Cooperative Catalysis Strategy. *J. Am. Chem. Soc.* **137**, 5891-5894, (2015).
- 40 Krauß, M., Winkler, T., Richter, N., Dommer, S., Fingerhut, A., Hummel, W. & Gröger, H. Combination of C=C Bond Formation by Wittig Reaction and Enzymatic C=C Bond Reduction in a One-Pot Process in Water. *Chemcatchem* **3**, 293-296, (2011).
- 41 Pace, V., Verniest, G., Sinisterra, J. V., Alcantara, A. R. & De Kimpe, N. Improved Arndt-Eistert synthesis of alpha-diazoketones requiring minimal diazomethane in the presence of calcium oxide as acid scavenger. *J. Org. Chem.* **75**, 5760-5763, (2010).
- 42 Martin, L. J., Marzinzik, A. L., Ley, S. V. & Baxendale, I. R. Safe and Reliable Synthesis of Diazoketones and Quinoxalines in a Continuous Flow Reactor. *Org Lett* **13**, 320-323, (2011).
- 43 Yanto, Y., Winkler, C. K., Lohr, S., Hall, M., Faber, K. & Bommarius, A. S. Asymmetric Bioreduction of Alkenes Using Ene-Reductases YersER and KYE1 and Effects of Organic Solvents. *Org Lett* **13**, 2540-2543, (2011).

- 44 Vidavsky, I., Mandelbaum, A., Tamiri, T. & Zitrin, S. Highly specific fragmentation processes of isomeric mixed esters of phenylsuccinic acid under electron impact. *Organic Mass Spectrometry* **26**, 287-292, (1991).
- 45 Felpin, F.-X. & Fouquet, E. A Useful, Reliable and Safer Protocol for Hydrogenation and the Hydrogenolysis of O-Benzyl Groups: The In Situ Preparation of an Active Pd0/C Catalyst with Well-Defined Properties. *Chemistry – A European Journal* **16**, 12440-12445, (2010).

# CHAPTER 4. Cooperative Asymmetric Reactions Combining Photocatalysis and Enzyme Catalysis

## 4.1 Introduction

Living organisms generate complex natural products from simple chemical precursors through simultaneous reactions that are catalyzed by mutually compatible enzymes. Many of these enzymes have been refined by evolution to be chemoselective, to react with high total turnover numbers, and to be highly selective. Enzymes, such as isomerases, work cooperatively with other enzymes, to generate products in yields and ee's that cannot be obtained from the sequential reactions of the individual catalysts on their respective substrates<sup>1,2</sup>. In contrast, artificial organic total syntheses of natural products consist of sequential reactions with intermediate purification steps that causes these syntheses to be labor intensive, to generate large quantities of waste, and to generate products in low overall yields. However, chemical catalysts enable valuable transformations that have no biological counterpart. But the selectivity of chemical catalysts is often lower than that of enzymes.

To combine the advantages of the biological systems with the reactivity of artificial chemical catalysts, chemists have devised sequential, concurrent, and cooperative chemoenzymatic reactions that combine enzymatic and artificial catalysts (Figure 4.1).<sup>3-11</sup>

Sequential Chemoenzymatic Reaction is a chemoenzymatic reaction that consists of at least two distinct steps that do not occur simultaneously. A solvent exchange may be required, and/or a catalyst, reagent, or enzyme may be added to the reaction mixture without intermediate purification



step. Similar (and sometimes superior) product yields and ee's of products can usually be achieved when the two reactions are conducted in different vessels.

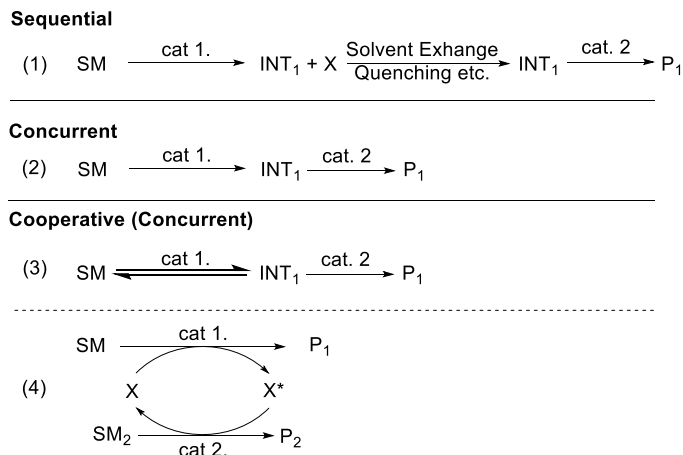


**Figure 4.1.** Schemes for different types of chemoenzymatic reactions

Concurrent chemoenzymatic reaction is a chemoenzymatic reaction that includes at least one catalyst and at least one enzyme that simultaneously catalyze two reactions in the same medium (biphasic and heterogeneous systems are included). Mutual catalyst deactivation must not occur for these systems to operate. Similar (and sometimes superior) yields and ee's of products can usually be achieved if the two reactions are conducted in a sequential manner or in different vessels.

Cooperative chemoenzymatic reaction is a chemoenzymatic reaction that includes at least one catalyst and at least one enzyme that simultaneously catalyze two reactions in the same medium (biphasic and heterogeneous systems are included). The catalysts in these systems must operate concurrently and be mutually compatible. Cooperative chemoenzymatic processes generate products in yield or selectivities or both that cannot be obtained from the sequential reactions of the individual catalytic reactions. This unique feature of cooperative processes makes

them the most valuable type of chemoenzymatic process. However, cooperative chemoenzymatic processes are difficult to develop because chemical and enzymatic catalysts generally operate in different media at different temperatures and can deactivate each other. As a result, the scope of cooperative chemoenzymatic processes that have been reported over the last 30 years has been narrow<sup>9,11,12</sup>.

The majority of cooperative chemoenzymatic processes that have been reported over the last 30 years can be divided into two categories: 1) chemoenzymatic dynamic kinetic resolutions of alcohols and amines, and 2) enzymatic reactions requiring the simultaneous regeneration of a cofactor<sup>6,7,13</sup>. The first category of reactions has been explored extensively because of the synthetic utility of the products and because the esterases employed in these reactions are unusually stable in organic solvent at elevated temperatures. The second category of reactions has been studied because of the need to recycle or replace expensive or unstable biological cofactors with inexpensive terminal oxidants or reductants. New approaches to the development of chemoenzymatic reactions are needed to enable valuable chemical transformations beyond kinetic resolutions and cofactor regenerations.

Chemoenzymatic transformations of alkenes would be valuable because alkenes are common reactants in chemical synthesis, and enantioselective reactions of alkenes are the most practiced class of enantioselective catalytic processes. Ene-reductases react with  $\alpha,\beta$ -unsaturated carbonyl compounds and nitriles to generate saturated products with high enantioselectivity. However, these enzymes often react with just one *E* or *Z* isomer of an alkene<sup>14</sup>. The limitations of my previous work (Chapter 3) on a (non-cooperative) sequential one-pot reaction in which a rhodium-catalyzed diazocoupling reaction generated alkenes which were reduced by ene-reductases to provide enantioenriched 2-substituted acid diesters, inspired efforts to develop a

conceptually new cooperative system. In cases in which the diastereoselectivity of the diazo-coupling reaction was low, and the ene-reductase only selectively reduced one of the isomers of substrate, the overall process was low yielding. Many of the most widely employed synthetic methods to form alkenes, including modern catalytic processes, like olefin metathesis, and traditional methods, like olefinations of carbonyl compounds, yield *E/Z* mixtures that must be separated before catalytic reduction to achieve high enantioselectivity. Other methods selectively generate an isomer of an alkene that is unreactive in the presence of common ene-reductases. Thus, we envisioned a chemoenzymatic reduction of olefin mixtures to highly enantioenriched products by combining a chemical catalyst to effect alkene isomerization and an ene-reductase to reduce one of the alkene isomers of the mixture. However, because thermal alkene isomerization is often a high-temperature process that is incompatible with enzymes, we considered the potential of a photocatalytic approach for the isomerization of alkenes. Here, we report a cooperative chemoenzymatic reaction that combines the photoisomerization of alkenes with an enzymatic reduction of one isomer of a mixture of *E* and *Z* alkenes (or pure *Z* alkenes). This system enables the stereoconvergent reduction of alkenes to form enantioenriched carbonyl compounds and nitriles (Figure 4.2) and shows the value of combining a photocatalyst with an enzyme catalyst to achieve cooperative processes beyond cofactor regeneration.

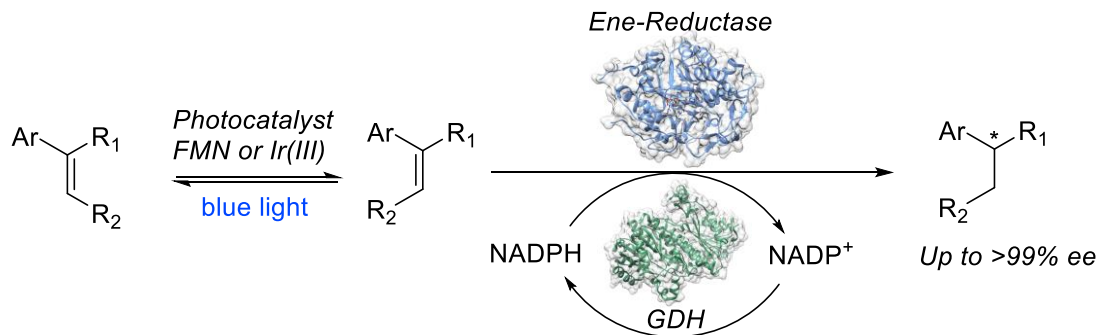


**Figure 4.2.** Combining of photocatalytic isomerization and enzymatic reduction of alkenes.

## 4.2 Results and Discussion

To develop a stereoconvergent enzymatic reduction of an isomeric mixture of alkenes, initial reactions were conducted with the model substrate 2-phenylbut-2-enedioic acid dimethyl ester (**1a**). YersER, an ene-reductase isolated from *Yersinia bercovieri*, exclusively reduces the *E* isomer of 2-phenylbut-2-enedioic acid dimethyl ester (*(E)*-**1a**) to dimethyl 2-phenylsuccinate (**2a**) in high yields with excellent ee's in the presence of a glucose dehydrogenase (GDH) enzyme for cofactor regeneration. To develop a stereoconvergent reduction reaction, a catalyst for the *E/Z* isomerization of olefins that is compatible with ene-reductases needed to be identified. An appropriate catalyst would 1) operate in aqueous solution at ambient temperature, 2) isomerize alkenes at rates that significantly exceed the rates of enzymatic reduction, 3) remain active in the presence of ene-reductases, substrates, and products in the reaction mixture, 4) isomerize olefins at the low substrate concentrations required for enzymatic reduction, and 5) generate the more reactive isomer of a substrate from the less reactive isomer. The isomerization catalyst must also 6) be mutually compatible with the ene-reductases, 7) be mutually compatible with a glucose dehydrogenase NADPH regeneration system, 8) and not racemize the product.

### 4.2.1. Development of Conditions for Cooperative Reaction

Negligible isomerization was observed in our initial attempts to isomerize *(E)*-**1a** or *(Z)*-**1b** in the presence of various metal salts and organic catalysts in Tris buffer at ambient temperature (Data were not shown). Inspired by the work of Gilmour et al. and Weaver et al., we considered that photocatalytic isomerization of alkenes<sup>15-18</sup> could be combined with enzymatic reduction to create the envisioned cooperative chemoenzymatic process. Gilmour et al. reported the photoisomerization of  $\alpha,\beta$ -unsaturated monoesters with riboflavin in the presence of UV (402 nm)

light in acetonitrile<sup>15</sup>. This reaction is proposed to proceed via preferential singlet or triplet energy transfer from a photocatalyst to one alkene isomer.

We began our investigation by assessing the photoisomerization of (*Z*)-**1a** in solvent mixtures appropriate for catalytic function of ene-reductases<sup>19</sup>. We found that limited isomerization of (*Z*)-**1a** was observed in the semi-aqueous media (1:9 DMSO:Tris buffer) in the presence of blue light (450-470 nm) and in the absence of a photocatalyst (Figure 4.3). However, extensive isomerization of (*Z*)-**1a** was observed when the reaction was conducted with riboflavin in the presence of blue light. A photostationary state (PS) consisting of a 9:1 ratio of (*E*) to (*Z*) **1a** was obtained after (*Z*)-**1a** was irradiated with blue light for 24 h in the presence of 5% riboflavin (Figure 4.3). However, only 18% yields of **2a** were obtained when YersER and riboflavin were employed concurrently in the presence of the blue light. This result demonstrated the importance of establishing compatibility between photocatalyst and enzymes.

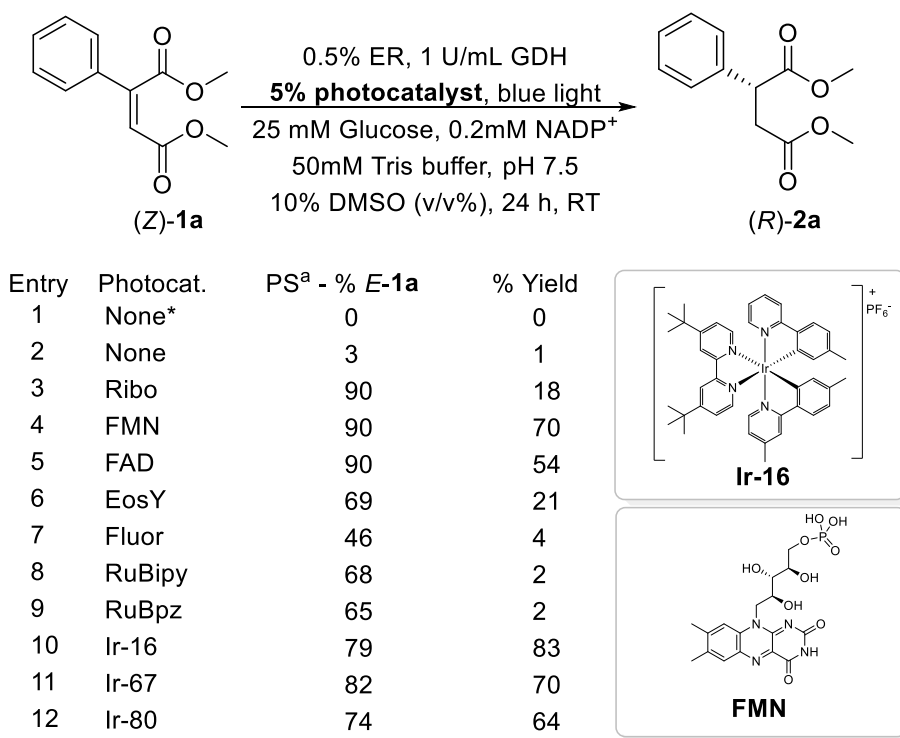


**Figure 4.3.** Isomerization and Reduction of (*Z*)-1a in the Presence of a Series of Photocatalysts and Blue Light. <sup>a</sup>PS is the % of (*E*)-1a present after (*Z*)-1a was irradiated with blue light in the presence of 5% photocatalyst for 24 h. The PS values for experiments labeled “None\*” and “None” in have been corrected for initial trace quantities of (*E*)-1a. Experiments labeled “None\*” were conducted in the presence of ambient light. Ribo: Riboflavin, FMN: Flavin Mononucleotide, FAD: Flavin Adenine Dinucleotide, EosY: Eosin Y, Fluor: Fluorescein, RuBipy: Ru(Bipy)<sub>3</sub>Cl<sub>2</sub>, RuBpz: [Ru(Bpz)<sub>3</sub>](PF<sub>6</sub>)<sub>2</sub>, **Ir-80**: CAS 808142-80-5, **Ir-67**: CAS 676525-77-2, **Ir-16**: CAS 1607469-49-7, Ac: Acridinium Salt CAS - 674783-97-2.

Before we evaluated the compatibility between various photocatalysts and ERs, we investigated the effects of DMSO concentration on the rate of alkene isomerization and enzymatic reduction. Higher (*E*)-1a:(*Z*)-1b ratios were obtained when the photoisomerization was conducted in semi-aqueous media with lower DMSO concentration within 15 minutes (Figure 4.4a). Isomerization rate in 5% DMSO was comparable with that in 10% DMSO and dropped tremendously when DMSO increased to 20%. The standard substrate cyclohexen-1-one of ERs was used to evaluate the catalytic activity of YersER. The depletion rate of reducing cofactor NADPH indicates the reducing rate of cyclohexen-1-one by YersER. The enzymatic activity will

be tremendously inhibited when DMSO more than 10% (Figure 4.4b). We chose 10% DMSO in Tris buffer as final solution to improve the solubility of substrate in aqueous solution.

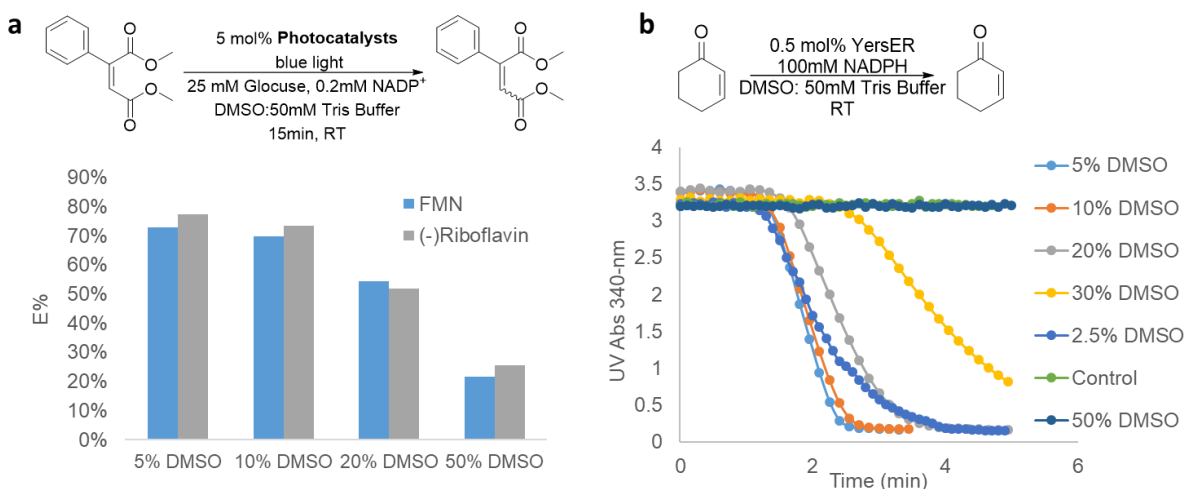


**Figure 4.4.** The effect of DMSO concentration on **a**) alkenes photoisomerization rate and **b**) enzymatic reducing rate. \*Control: the same reaction system without cyclohexen-1-one added. NADPH has strongest absorption at 340nm. 2-3 minutes lag in NADPH depletion may be due to the substrate-enzyme binding process.

We hypothesized that competitive binding of riboflavin to the flavin-binding site of YersER led to the inhibition of enzymatic activity<sup>20</sup>. Thus, we sought alternative photocatalysts that would lead to isomerization of (*Z*)-**1a** without inhibiting YersER or the cofactor regeneration system. The *E/Z* isomerization of (*Z*)-**1a** was evaluated in the presence of a series of organometallic and organic photocatalysts in 1:9 DMSO:50 mM Tris buffer, and the PS for each combination is recorded in Fig 3.3. Greater than 40% conversion of (*Z*)-**1a** to (*E*)-**1a** was observed when the substrate was irradiated in the presence of the majority of the photocatalysts, and the highest *E/Z* ratios exceeded 8:1 (Figure 4.3). Increasing catalyst loading and increasing light intensity enhanced the rate of photoisomerization of (*Z*)-**1a** (Figure 4.5 and Figure 4.6).

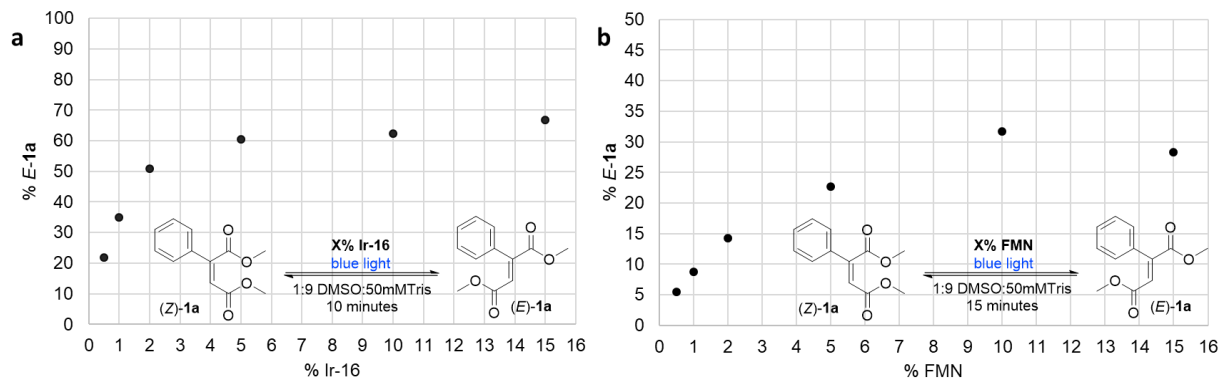


**Figure 4.5.** The effect of photocatalyst loading on the %(*E*)-**1a** at photostationary state. **a**) photoisomerization of (*Z*)-**1a** by Ir-16 and **b**) FMN. (Data provided by Zachary C. Litman)

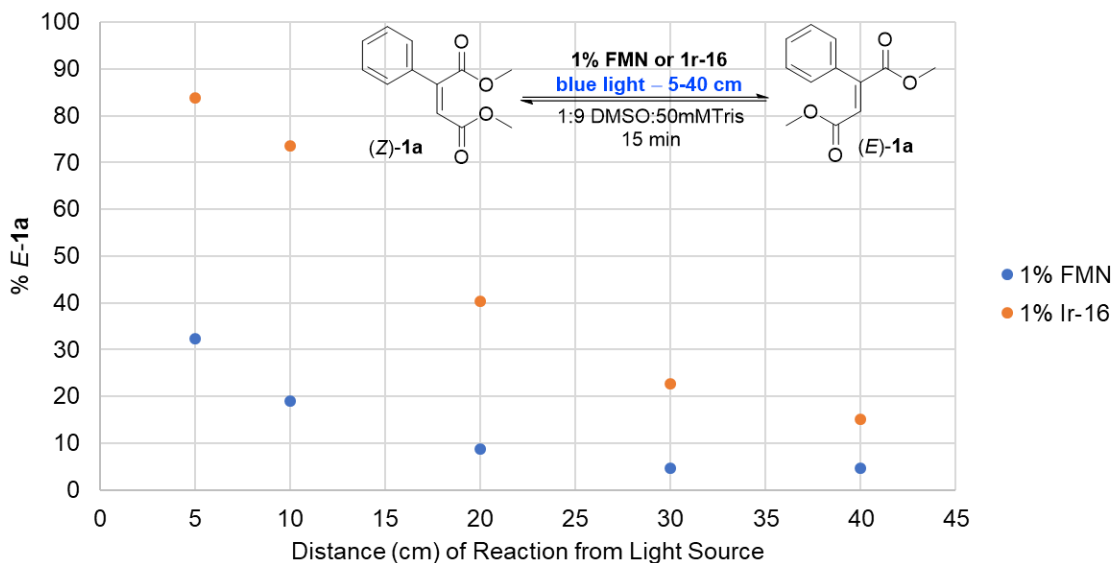


**Figure 4.6.** Light intensity (distance of reaction from light source) versus % (*E*)-**1a** After 15 min (Data provided by Zachary C. Litman)

Having identified a series of photocatalysts for the isomerization of (*Z*)-**1a** to (*E*)-**1a** in a semi-aqueous medium, we evaluated the “toxicity effect” of various photocatalysts on enzymatic system by reducing (*E*)-**1a** with YersER in the presence of photocatalysts with or without blue light. Riboflavin, Fluorescent and EosinY inhibited the enzymatic activity tremendously (Figure 4.7). Although ruthenium catalysts did not jeopardize the enzymatic function, they greatly inhibited the enzymatic activity in the presence of the blue light (Figure 4.7).



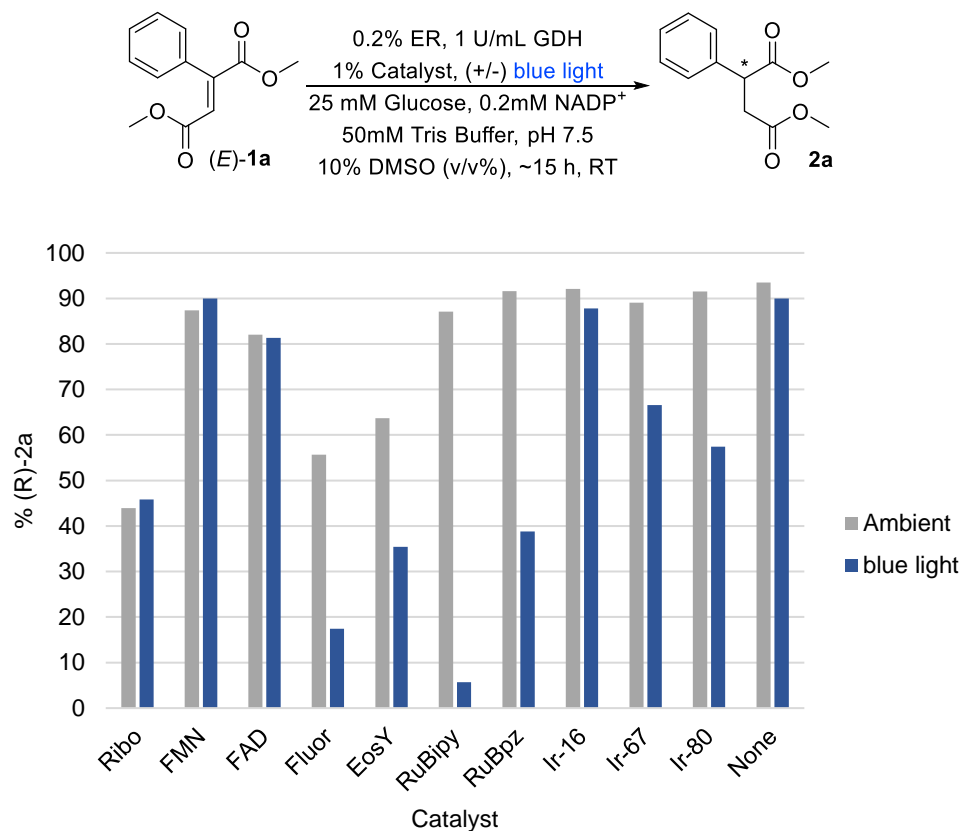


**Figure 4.7.** Enzymatic reduction of (*E*)-**1a** (more reactive isomer) in the presence of different photocatalysts with or without blue light

We further evaluated the concurrent cooperative photoisomerization and enzymatic reduction of (*Z*)-**1a** with the same photocatalysts (Figure 4.3). Moderate to high yields of **2a** were obtained when a range of catalysts were used in the cooperative process. The highest conversions and yields were obtained when the cooperative reaction was conducted with 5% of flavin mononucleotide (FMN) or 1% of the cationic iridium(III) complexes [Ir(dmppy)<sub>2</sub>(dtbbpy)]PF<sub>6</sub> (**Ir-16**), [Ir(dtbbpy)(ppy)<sub>2</sub>]PF<sub>6</sub> (**Ir-67**), and [Ir(dtbbpy)<sub>2</sub>(dtbbpy)]PF<sub>6</sub> (**Ir-80**). High isomerization rate was achieved by the same loading of Ir-16 compared with FMN (Figure 4.8)

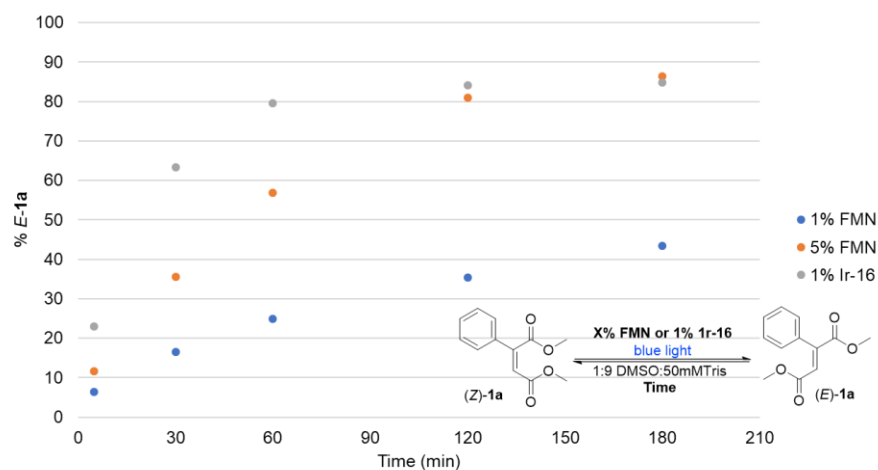


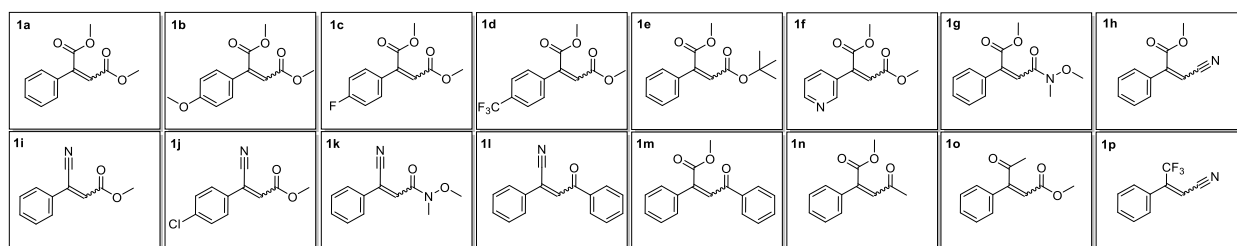
**Figure 4.8.** Photoisomerization of (*Z*)-**1a** with 5% FMN or 1% **Ir-16**

#### 4.2.2. Substrates Scope

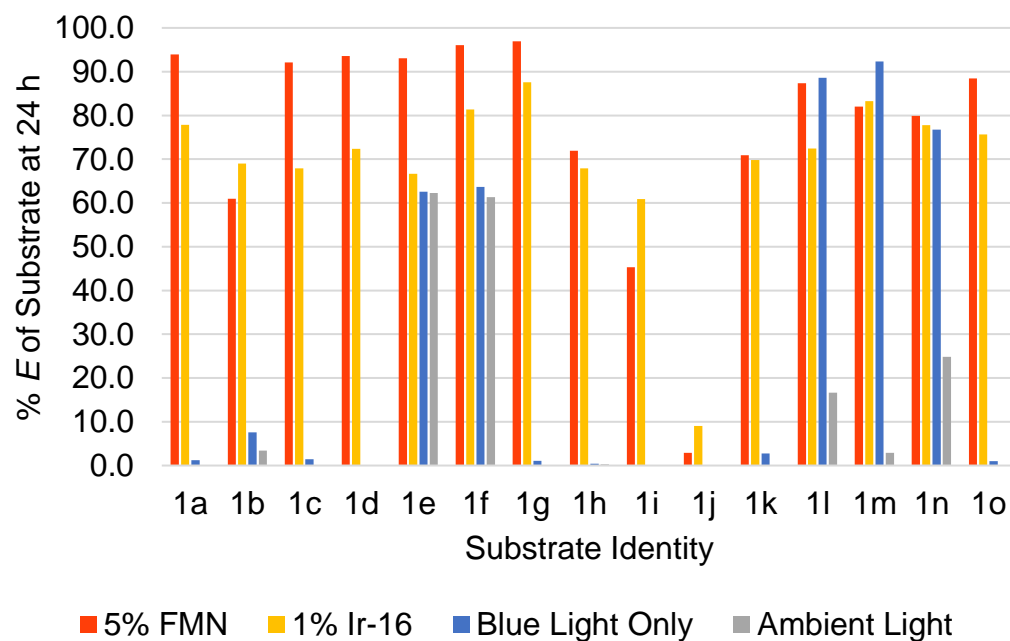
The high yields and ee's obtained from the cooperative reduction of the model diester (*Z*)-**1a** encouraged us to investigate the cooperative reduction of other aryl diesters. We identified enzymes that preferentially reduce the *E* isomers of diesters **1b-1f** in Figure 4.9 in high yields and ee's (Table 4.2). These enzymes were then employed in the cooperative reduction of the *Z* isomers of **1b-1d** with **Ir-16** or FMN as a photocatalyst in the presence of blue light. High yields of product were obtained from the cooperative isomerization and reduction of each of the diesters, including those containing electron-rich ((*Z*)-**1b**) and electron-poor aryl groups ((*Z*)-**1d**) with either FMN or **Ir-16** as photocatalysts and the enzymes YersER, XenB, or OPR1 (Table 4.2). The yields and ee's of the products obtained from the cooperative reductions of the *Z* isomers of **1b-1d** were equivalent to those obtained from the enzymatic reduction of the *E* isomers of substrates **1b-1d** in the absence of the photocatalyst. This result implies that the cooperative reduction of any *E/Z* mixture of these alkenes should give high yields and ee's of reduced products. This feature of the cooperative system was crucial for obtaining high yields and ee's for the reduction of **1e** and **1f**, which were synthesized as inseparable mixtures of *E* and *Z* alkenes. The cooperative chemoenzymatic

reduction of a 62:38 mixture of *E* and *Z* isomers of **1e** afforded **2e** in 74% yield and >99% ee, and the cooperative reduction of a 61:39 mixture of *E* and *Z* isomers of **1f** afforded **2f** in 94% yield and 91% ee. The yields and ee's from the cooperative reduction of (*E/Z*)-**1e** and (*E/Z*)-**1f** indicate that the reactions were stereoconvergent. The enzymatic reductions of **1e** and **1f** in the absence of a photocatalyst and light formed the reduced products in only 58% and 60% yield, reflecting the reaction with only the *E* isomer of the *E/Z* mixture (Table 4.1).

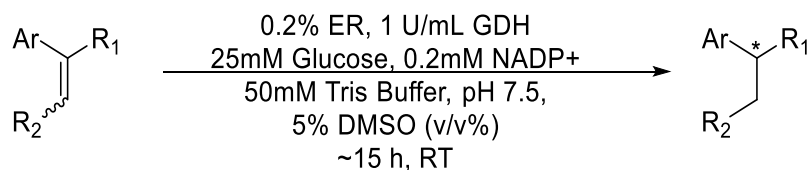
To determine if the cooperative reaction would give high yields and high enantioselectivities with alkenes other than diesters, the cooperative reduction of unsaturated compounds containing diverse combinations of functional groups was evaluated. The ene-reductases OPR1, TOYE, OYE2, YersER, and SYE1 preferentially reduced the *E* isomers of alkenes **1g-1o** to form **2g-2o** in high yields and ee's. The cooperative reactions of the *Z* isomers of **1g-1o** were then conducted with **Ir-16** or FMN in the presence of blue light. The results from the combination of photocatalyst and enzyme that generated the products in the highest yields and ee's from the *Z* isomers of **1g-1o** are shown in (Table 4.2). High yields and ee's were obtained for the cooperative reduction of  $\beta$ -cyano- $\alpha,\beta$ -unsaturated ester (*Z*)-**1h**,  $\alpha$ -cyano- $\alpha,\beta$ -unsaturated esters (*Z*)-**1i** and (*Z*)-**1j**, and amidocyanate (*Z*)-**1k**. High yields and ee's were also obtained from the reactions of cyanoketone (*Z*)-**1l**,  $\beta$ -keto- $\alpha,\beta$ -unsaturated esters (*Z*)-**1m** and (*Z*)-**1n**, and  $\alpha$ -keto- $\alpha,\beta$ -unsaturated ester (*Z*)-**1o**. The cooperative reductions of amidoacrylate (*Z*)-**1g** and amidocyanate (*Z*)-**1k** are noteworthy because enzymatic reductions of alkenes containing Weinreb amides have not been reported to our knowledge. Control experiments revealed that (*Z*)-**1l**, (*Z*)-**1m**, and (*Z*)-**1n** undergo enzymatic reduction to generate products in high yields and ee's in the presence of blue light but in the absence of an added photocatalyst (Table 4.2). In these cases, the alkenes (**1l-1n**) isomerize in the presence of blue light alone (Figure 4.10).



**Figure 4.9.** Scope of the cooperative photoisomerization and reduction and comparison to sequential reactions.

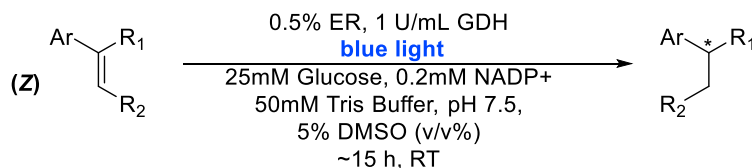
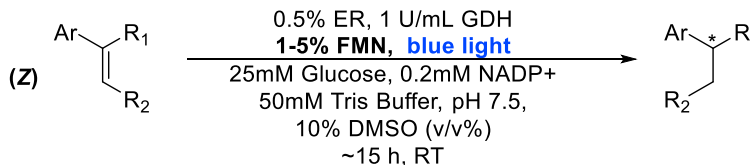
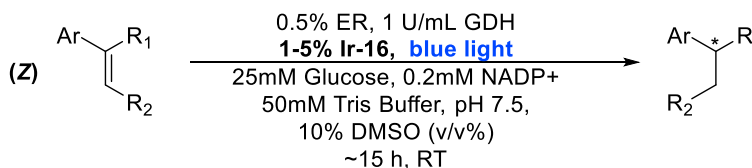


**Figure 4.10.** Photoisomerization of alkenes under different conditions. Red bar indicated the reactions conducted with 5% FMN, 50 mM Tris buffer at pH 7.5, and 5% DMSO at RT in the presence of blue light. Orange bar indicated the reactions conducted with 1% **Ir-16**, 50 mM Tris buffer at pH 7.5, and 5% DMSO at RT in the presence of blue light. Blue bar indicated reactions conducted with 50 mM Tris buffer at pH 7.5, and 5% DMSO at RT in the presence of blue light. Grey bar indicated reactions conducted with 50 mM Tris buffer at pH 7.5, and 5% DMSO at RT in the presence of ambient light. (The detailed of experimental setting and values are presented in section 3.4.6)

**Table 4.1.** Enantioselective enzymatic reduction of substrates **1a** to **1p**

| Entry | Substrate                    | Enzyme | % Conversion <sup>a</sup> | % Yield <sup>a</sup> | % ee <sup>b</sup> |
|-------|------------------------------|--------|---------------------------|----------------------|-------------------|
| 1     | <i>E</i> -1a                 | YersER | 100%                      | 88%                  | >99%              |
| 2     | <i>Z</i> -1a                 | YersER | 0%                        | 0%                   | -                 |
| 3     | <i>E</i> -1b                 | YersER | 100%                      | 87%                  | >99%              |
| 4     | <i>Z</i> -1b                 | YersER | 0%                        | 0%                   | -                 |
| 5     | <i>E</i> -1c                 | XenB   | 90%                       | 82%                  | >99%              |
| 6     | <i>Z</i> -1c                 | XenB   | 0%                        | 0%                   | -                 |
| 7     | <i>E</i> -1d                 | xenB   | 98%                       | 92%                  | 93%               |
| 8     | <i>Z</i> -1d                 | xenB   | 0%                        | 0%                   | -                 |
| 9     | (62/38)<br>( <i>E/Z</i> )-1e | OPR1   | 67%                       | 58%                  | >99%              |
| 10    | (61/39)<br>( <i>E/Z</i> )-1f | XenB   | 60%                       | 60%                  | 88%               |
| 11    | <i>E</i> -1g                 | OPR1   | 100%                      | 92%                  | >99%              |
| 12    | <i>Z</i> -1g                 | OPR1   | 0%                        | 0%                   | -                 |
| 13    | <i>E</i> -1h                 | TOYE   | 98%                       | 93%                  | >99%              |
| 14    | <i>Z</i> -1h                 | TOYE   | 0%                        | 0%                   | -                 |
| 15    | <i>E</i> -1i                 | OYE2   | 100%                      | 98%                  | 94%               |
| 16    | <i>Z</i> -1i                 | OYE2   | 7%                        | 3%                   | -                 |
| 17    | <i>E</i> -1j                 | OYE2   | 100%                      | 94%                  | 76%               |
| 18    | <i>Z</i> -1j                 | OYE2   | 0%                        | 0%                   | -                 |
| 19    | <i>E</i> -1k                 | YersER | 100%                      | 87%                  | 99%               |
| 20    | <i>Z</i> -1k                 | YersER | 10%                       | 6%                   | -                 |
| 21    | <i>E</i> -1l                 | OYE2   | 100%                      | 98%                  | >99%              |
| 22    | <i>Z</i> -1l                 | OYE2   | 0%                        | 0%                   | -                 |
| 23    | <i>E</i> -1m                 | OPR1   | 100%                      | 90%                  | >99%              |
| 24    | <i>Z</i> -1m                 | OPR1   | 30%                       | 26%                  | -                 |
| 25    | <i>E</i> -1n                 | SYE1   | 100%                      | 96%                  | 89%               |
| 26    | <i>Z</i> -1n                 | SYE1   | 0%                        | 6%                   | -                 |
| 27    | <i>E</i> -1o                 | YersER | 100%                      | 80%                  | 98%               |
| 28    | <i>Z</i> -1o                 | YersER | 0%                        | 0%                   | -                 |
| 29    | <i>Z</i> -1p                 | SYE1   | 100%                      | 78%                  | >99%              |
| 30    | <i>E</i> -1p                 | YersER | 14%                       | 14%                  | -                 |

Standard conditions: reactions were conducted with 0.5% ene-reductase, 1 U/mL GDH, 25 mM glucose, 0.2 mM NADP<sup>+</sup>, 50 mM Tris buffer at pH 7.5, and 10% DMSO at RT. <sup>a</sup> Yield and conversion determined by GC. <sup>b</sup> ee determined by chiral HPLC.

**Table 4.2.** Cooperative photoisomerization and reduction of substrates **1a** to **1p****Type I** - Enzymatic Reduction of (Z) Isomer of Substrate in the Presence of Blue Light**Type II** - Enzymatic Reduction of (Z) Isomer of Substrate in the Presence of Blue Light and FMN**Type III** - Enzymatic Reduction of (Z) Isomer of Substrate in the Presence of Blue Light and Ir-16

| Entry | Substrate           | Type | Enzyme | Photocat. | PS (%E) <sup>c</sup> | % Conversion <sup>a</sup> | % Yield <sup>a</sup> | % ee <sup>b</sup> |
|-------|---------------------|------|--------|-----------|----------------------|---------------------------|----------------------|-------------------|
| 1     | Z-1a                | I    | YersER | -         | -                    | 8%                        | 4%                   | -                 |
| 2     | Z-1a                | II   | YersER | 5% FMN    | 94%                  | 99%                       | 70%                  | >99%              |
| 3     | Z-1a                | III  | YersER | 1% Ir-16  | 78%                  | 88%                       | 87%                  | >99%              |
| 4     | (50/50)<br>(E/Z)-1a | II   | YersER | 5% FMN    | -                    | 99%                       | 86%                  | >99%              |
| 5     | (50/50)<br>(E/Z)-1a | III  | YersER | 1% Ir-16  | -                    | 96%                       | 89%                  | >99%              |
| 6     | Z-1b                | I    | YersER | -         | -                    | 7%                        | 7%                   | -                 |
| 7     | Z-1b                | II   | YersER | 5% FMN    | 61%                  | 72%                       | 63%                  | 92%               |
| 8     | Z-1b                | III  | YersER | 1% Ir-16  | 69%                  | 89%                       | 89%                  | >99%              |
| 9     | Z-1c                | I    | XenB   | -         | -                    | 15%                       | 14%                  | -                 |
| 10    | Z-1c                | II   | XenB   | 5% FMN    | 92%                  | 58%                       | 39%                  | -                 |
| 11    | Z-1c                | III  | XenB   | 1% Ir-16  | 68%                  | 89%                       | 89%                  | >99%              |
| 12    | Z-1d                | I    | XenB   | -         | -                    | 12%                       | 11%                  | -                 |
| 13    | Z-1d                | II   | XenB   | 5% FMN    | 94%                  | 70%                       | 58%                  | -                 |
| 14    | Z-1d                | III  | XenB   | 1% Ir-16  | 72%                  | 94%                       | 82%                  | >99%              |
| 15    | (62/38)<br>(E/Z)-1e | I    | OPR1   | -         | -                    | 73%                       | 56%                  | -                 |
| 16    | (62/38)<br>(E/Z)-1e | II   | OPR1   | 5% FMN    | 93%                  | 72%                       | 60%                  | >99%              |
| 17    | (62/38)<br>(E/Z)-1e | III  | OPR1   | 1% Ir-16  | 67%                  | 98%                       | 74%                  | >99%              |
| 18    | (61/39)<br>(E/Z)-1f | I    | XenB   | -         | -                    | 63%                       | 63%                  | -                 |

Table 4.2. cont.

|    |                     |                  |         |          |     |      |     |      |
|----|---------------------|------------------|---------|----------|-----|------|-----|------|
| 19 | (61/39)<br>(E/Z)-1f | II               | XenB    | 5% FMN   | 96% | 78%  | 60% | 87%  |
| 20 | (61/39)<br>(E/Z)-1f | III              | XenB    | 1% Ir-16 | 81% | 94%  | 94% | 91%  |
| 21 | Z-1g                | I                | OPR1    | -        | -   | 9%   | 9%  | -    |
| 22 | Z-1g                | II               | OPR1    | 5% FMN   | 97% | 28%  | 21% | -    |
| 23 | Z-1g                | III              | OPR1    | 1% Ir-16 | 88% | 98%  | 82% | >99% |
| 24 | Z-1h                | I                | TOYE*   | -        | -   | 7%   | 7%  | -    |
| 25 | Z-1h                | II               | TOYE*   | 1% FMN   | 69% | 99%  | 98% | >99% |
| 26 | Z-1h                | III              | TOYE*   | 1% Ir-16 | 68% | 88%  | 87% | >99% |
| 27 | Z-1i                | I                | OYE2*   | -        | -   | 10%  | 5%  | -    |
| 28 | Z-1i                | II               | OYE2*   | 1% FMN   | 46% | 100% | 94% | 99%  |
| 29 | Z-1i                | III              | OYE2*   | 1% Ir-16 | 61% | 98%  | 92% | 98%  |
| 30 | (50/50)<br>(E/Z)-1i | II               | OYE2*   | 1% FMN   | -   | 99%  | 94% | 98%  |
| 31 | (50/50)<br>(E/Z)-1i | III              | OYE2*   | 1% Ir-16 | -   | 99%  | 92% | 98%  |
| 32 | Z-1j                | I                | OYE2    | -        | -   | 3%   | 3%  | -    |
| 33 | Z-1j                | II               | OYE2    | 5% FMN   | 3%  | 78%  | 60% | 90%  |
| 34 | Z-1j                | III              | OYE2    | 5% Ir-16 | 9%  | 92%  | 80% | 92%  |
| 35 | Z-1k                | I                | YersER* | -        | -   | 26%  | 20% | -    |
| 36 | Z-1k                | II               | YersER* | 5% FMN   | 71% | 100% | 82% | 99%  |
| 37 | Z-1k                | III              | YersER* | 1% Ir-16 | 70% | 100% | 96% | 99%  |
| 38 | Z-1l                | I                | OYE2    | -        | 89% | 100% | 95% | >99% |
| 39 | Z-1l                | II               | OYE2    | 5% FMN   | 87% | 94%  | 46% | -    |
| 40 | Z-1l                | III              | OYE2    | 1% Ir-16 | 73% | 99%  | 86% | -    |
| 41 | Z-1m                | I                | OPR1    | -        | 92% | 100% | 80% | >99% |
| 42 | Z-1m                | II               | OPR1    | 5% FMN   | 82% | 100% | 73% | 95%  |
| 44 | Z-1m                | III              | OPR1    | 1% Ir-16 | 83% | 100% | 81% | >99% |
| 45 | Z-1n                | I                | SYE1    | -        | 77% | 78%  | 65% | -    |
| 46 | Z-1n                | II               | SYE1    | 5% FMN   | 80% | 39%  | 3%  | 76%  |
| 47 | Z-1n                | III              | SYE1    | 1% Ir-16 | 78% | 65%  | 60% | 88%  |
| 48 | Z-1o                | I                | YersER  | -        | -   | 24%  | 20% | -    |
| 49 | Z-1o                | II               | YersER  | 5% FMN   | 89% | 100% | 90% | 86%  |
| 50 | Z-1o                | III              | YersER  | 1% Ir-16 | 76% | 100% | 92% | 96%  |
| 51 | E-1p                | I <sup>d</sup>   | OYE2    | -        | -   | 48%  | 8%  | -    |
| 52 | E-1p                | II <sup>d</sup>  | OYE2    | 5% FMN   | 14% | 89%  | 22% | -    |
| 53 | E-1p                | III <sup>d</sup> | OYE2    | 1% Ir-16 | 14% | 98%  | 74% | >99% |

**Type I** reaction: reactions were conducted with 0.5% ene-reductase, 1 U/mL GDH, 25 mM glucose, 0.2 mM NADP<sup>+</sup>, 50 mM Tris buffer at pH 7.5, and 10% DMSO at RT in the presence of blue light. **Type II** reaction: reactions were conducted with 0.5% ene-reductase, 1 U/mL GDH, 5% FMN, 25 mM glucose, 0.2 mM NADP<sup>+</sup>, 50 mM Tris buffer at pH 7.5, and 10% DMSO at RT in the presence of blue light. **Type III** reaction: **Type II** reaction: reactions were conducted with 0.5% ene-reductase, 1 U/mL GDH, 1% Ir-16, 25 mM glucose, 0.2 mM NADP<sup>+</sup>, 50 mM Tris buffer at pH 7.5, and 10% DMSO at RT in the presence of blue light. <sup>a</sup>Year and conversion determined by GC. <sup>b</sup>ee determined by chiral HPLC. <sup>c</sup>PS is the % E of a substrate present after the Z isomer (or E/Z isomer mixture) was irradiated with light in the presence of either 5% FMN or 1% Ir-16 for 24 h. In the case of 1p, (E)-1p was irradiated with blue light in the presence of FMN and Ir-16 for 24 h, and the % of (Z)-1p was determined. <sup>d</sup>Isomers used in these experiments different from those depicted in formula. \*conducted with 0.2% ene-reductase.

### 4.2.3. Cooperative Concurrent Reaction Versus Sequential Reaction

The cooperative enzymatic reductions of alkenes **1i** and **1j** shown in Fig. 3.11 illustrate the benefits of a cooperative system over two sequential reactions. The photoisomerization of (*Z*)-**1i** and (*Z*)-**1j** with **Ir-16** or FMN result in *E/Z* mixtures in which the less reactive *Z* isomer is the major component. As a result, low yields were obtained from the sequential isomerization and reduction of (*Z*)-**1i** and (*Z*)-**1j**. The ee of **2i** obtained from the sequential isomerization and reduction of (*Z*)-**1i** was slightly lower than the ee obtained from the enzymatic reduction of the pure, more reactive isomer (*E*)-**1i**, and this difference likely results from the slow reduction of the *Z* isomer of **1i** after rapid consumption of the *E* isomer during the second stage of the sequential process Figure 4.11. In contrast, the simultaneous, cooperative reduction of (*Z*)-**1i** and (*Z*)-**1j** generated products **2i** and **2j** in both high yields and ee's.

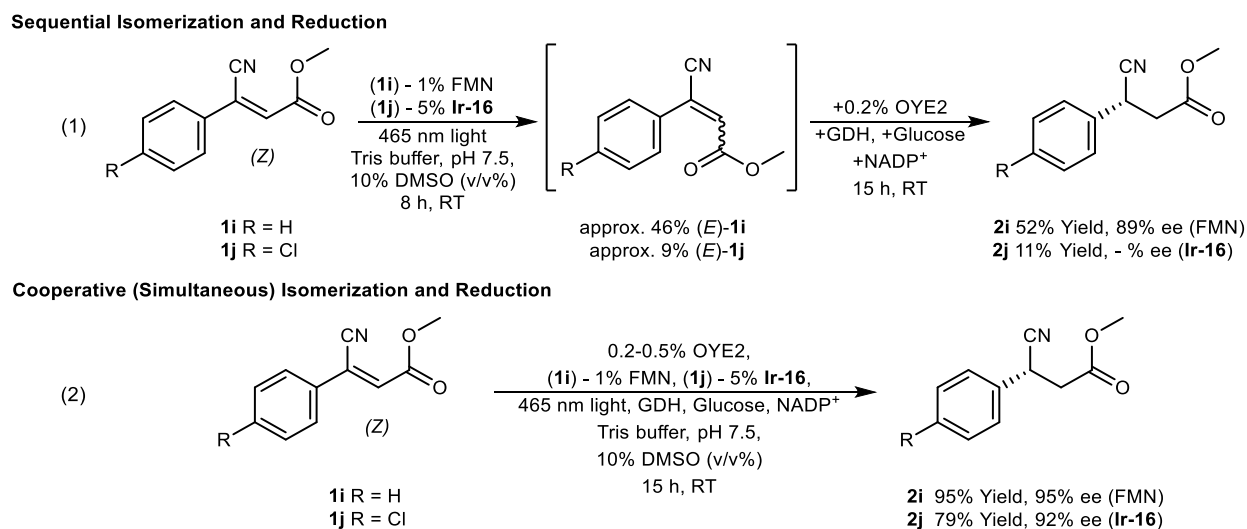


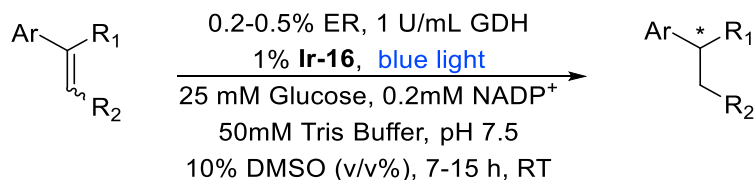
**Figure 4.11.** Comparison of sequential (1) vs. cooperative reduction (2) of cyanoacrylates **1i** and **1j** under standard conditions.



An enzyme that selectively reduces the *E* isomer of trifluoromethylcyanate **1p** in high yield and ee could not be identified, but OYE2 selectively reduces the *Z* isomer of **1p** in high yield and ee (Table 4.1). To determine if a cooperative reaction could convert (*E*)-**1p** to **2p** in high yield and ee, the ability of (*E*)-**1p** to undergo photoisomerization in the presence of **Ir-16** and blue light was evaluated. An 86:14 ratio of the *E/Z* isomers of **1p** was established after 24 h of irradiation with blue light in the presence of **Ir-16**. Although the photostationary state of **1p** favors the less reactive *E* isomer, the cooperative reaction of (*E*)-**1p** to **2p** occurred in high yield and ee with **Ir-16** as the photocatalyst and OYE2 as the reductase. This example illustrates an important benefit of the cooperative chemoenzymatic reaction: the system enables either the isomerization of a *Z* alkene with simultaneous enzymatic reduction of the *E* isomer or the isomerization of an *E* alkene with simultaneous enzymatic reduction of the *Z* isomer. The conversion of (*E*)-**1p** to **2p** is also noteworthy because enzymatic reduction to generate a product containing a stereogenic center substituted with a trifluoromethyl group is rare.

#### 4.2.4. Derivatization of Synthesized Enantioenriched Products

To demonstrate the synthetic value of this new method, preparative scale cooperative reactions were conducted with 1% **Ir-16** and 40-60 mg of (*Z*)-**1a**, a 62:38 mixture of the *E* and *Z* isomers of **1e**, (*Z*)-**1g**, (*Z*)-**1h**, and (*Z*)-**1o**. Product **2a** was isolated in 87% yield and >99% ee, product **2e** was isolated in 79% yield and >99% ee, product **2g** was isolated in 71% yield and >99% ee, product **2h** was isolated in 96% yield and 92% ee, and product **2o** was isolated in 79% yield and >99% ee (Table 4.3).

**Table 4.3.** Summary of prep scale cooperative reactions

| Entry | Substrate           | Enzyme            | Time | % Conversion <sup>a</sup> | % Yield <sup>a</sup> | % ee <sup>b</sup> |
|-------|---------------------|-------------------|------|---------------------------|----------------------|-------------------|
| 1     | Z-1a                | YersER            | 7 h  | 100%                      | 87%                  | >99%              |
| 2     | (62/38)<br>(E/Z)-1e | OPR1 <sup>c</sup> | 24h  | 96%                       | 79%                  | >99%              |
| 3     | Z-1g                | OPR1              | 24h  | 92%                       | 71%                  | >99%              |
| 4     | Z-1h                | TOYE              | 24h  | 100%                      | 96%                  | 92%               |
| 5     | Z-1o                | YersER            | 24h  | 98%                       | 79%                  | >99%              |

<sup>a</sup> Isolated yield. <sup>b</sup> ee determined by chiral HPLC. <sup>c</sup> Conducted with 0.2% OPR1.

The enantioenriched compounds that were obtained from the cooperative isomerization and enzymatic reduction system can be transformed into a variety of biologically active molecules and valuable synthetic intermediates (Fig. 3.12). For example, the selective hydrolysis of the *tert*-butyl ester in compound **2e** followed by a Curtius rearrangement yielded **3e**, a  $\beta^2$ -amino ester. The  $\beta$ -amino ester was isolated in 90% yield without significant erosion of enantiomeric excess (98% ee). The selective reduction of the Weinreb amide in compound **2g** with Schwartz's reagent yielded methyl 4-oxo-2-phenylbutanoate (**3g**) in 74% isolated yield and 99% ee. This compound is an intermediate in the synthesis of protein kinase inhibitors and microsomal triglyceride transfer protein inhibitors.<sup>21,22</sup> Acid-catalyzed hydrolysis of the nitrile in **2p** yielded 4,4,4-trifluoro-3-phenylbutanoic acid (**3p**) in 96% yield and >99% ee. This versatile synthetic intermediate has previously been employed in the synthesis of inhibitors of beta amyloid production.<sup>23,24</sup> Reduction of **2a** with lithium aluminum hydride formed 2-phenylbutane-1,4-diol (**3a**) in 93% yield and >99% ee. This diol is a synthetic precursor to inhibitors of matrix metalloproteases.<sup>25</sup> Other products of

the cooperative reactions are known precursors to biologically active compounds. For example, **2i** and **2j** have been converted previously to  $\gamma$ -amino acids (including balcofen and phenibut) and  $\gamma$ -lactams,<sup>26</sup> **2h** has been converted into a  $\gamma^2$  amino ester and a  $\gamma^2$  lactam,<sup>27</sup> and **2m** has been converted into calyxolanes, which are cyclic ether natural products.<sup>28</sup> Thus, the products of the cooperative chemoenzymatic reduction are precursors to valuable synthetic intermediates by both newly disclosed and previously reported transformations. (Derivatizations were performed by Zachary Litman. The detailed steps were presented in SI of publication: *Nature*, volume 560, pages355–359 (2018)).

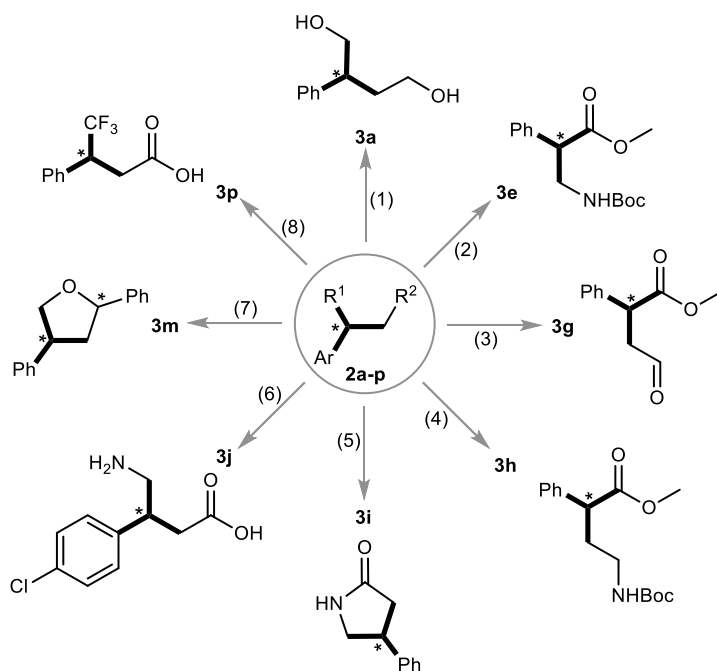


**Figure 4.12.** Derivatization of enantioenriched products.

A short summary of the previously reported and newly disclosed transformations of the products of the chemoenzymatic cooperative reduction of alkenes are follows. (1) Conversion **2a** to **3a**: 4.0 equiv LiAlH<sub>4</sub>, THF, 5 h, RT. (2) Conversion of **2e** to **3e**: i. 1:1 TFA:DCM, 3 h, RT. ii.

1.7 equiv NEt<sub>3</sub>, DCE, and 1.5 equiv DPPA, 65 °C, 2 h. iii. 0.10 equiv of Mo(O)<sub>2</sub>Cl<sub>2</sub>, *t*-BuOH, 65 °C, 1 h 10 min. (3) Conversion of **2g** to **3g**: 1.4 equiv Cp<sub>2</sub>Zr(H)Cl, 1.0 equiv ZrF<sub>4</sub>, 1:1 THF:DCM, 3 h, RT. (4) Conversion of **2h** to **3h** was previously reported.<sup>27</sup> (5) Conversion of **2i** to **3i** was previously reported.<sup>26</sup> (6) Conversion of **2j** to **3j** was previously reported.<sup>26</sup> (7) Conversion of **2m** to **3m** was previously reported.<sup>28</sup> (8) Conversion of **2p** to **3p**: 1:1 H<sub>2</sub>O:H<sub>2</sub>SO<sub>4</sub>, 6 h, 120 °C.

## 4.3 Conclusion

The combination of a photocatalytic process and an enzymatic reaction enables transformations that combine the reactivity of chemical catalysts with the selectivity of enzymes. Two features of photocatalytic reactions make them, in general, suitable for chemoenzymatic processes: 1) photochemical reactions typically occur at or near room temperature, making them compatible with thermal requirements of enzymatic systems, and 2) photocatalysts often react by mechanisms, such as outer-sphere electron transfer or energy transfer, that involve intermediates that are stable to water and the functional groups in proteins. These considerations, in combination with the renewed interest in photocatalysis and the rapidly advancing tools of molecular biology, should create opportunities for the development of a wide range of new cooperative chemoenzymatic transformations.

## 4.4 Experimental procedures

### 4.4.1. General Materials

All air-sensitive manipulations were conducted in a nitrogen-filled glovebox or by standard Schlenk technique under nitrogen. All glassware was heated in an oven and cooled under an inert atmosphere prior to use. Vials (4 mL) were used as reaction vessels and were sealed with Teflon-lined caps. Products were visualized on TLC plates with an anisaldehyde stain and a heat

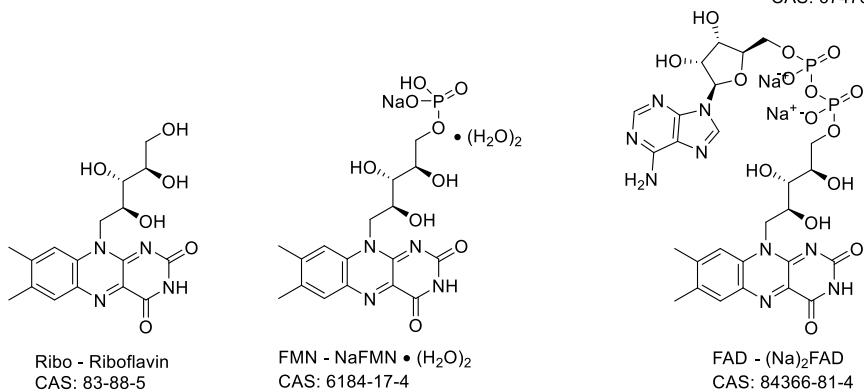
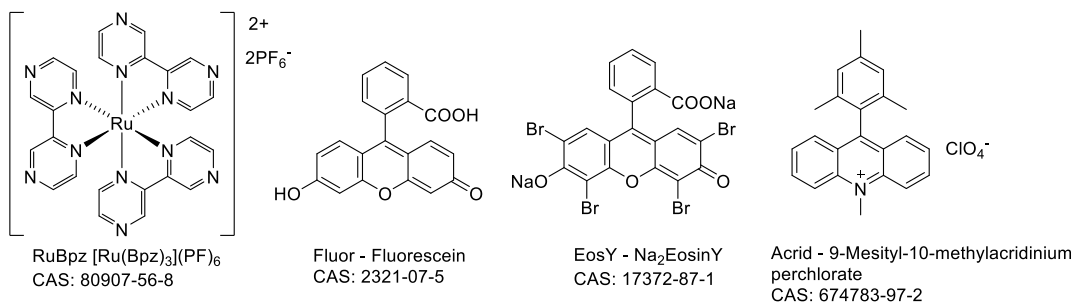
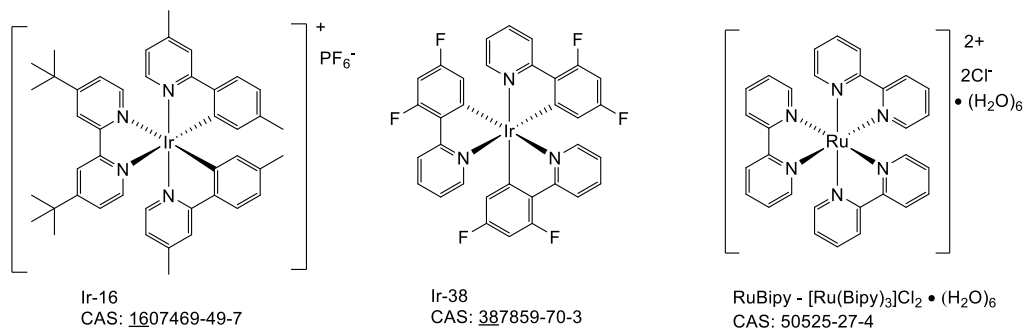
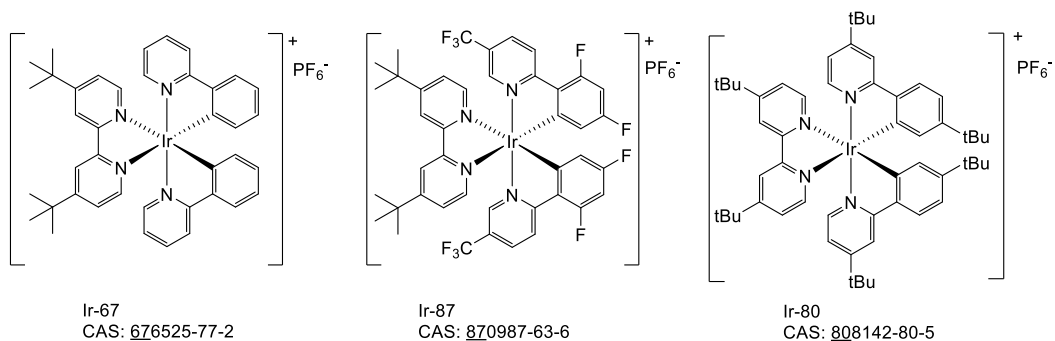
gun.  $^1\text{H}$  and  $^{13}\text{C}$  NMR spectra were acquired on 300 MHz, 400 MHz, 500 MHz, or 600 MHz Bruker instruments at the University of California.  $^{19}\text{F}$  NMR spectra were obtained at 376 MHz on a 400 MHz instrument – chemical shifts relative to  $\text{CFCl}_3$  at 0 ppm. NMR spectra were processed with MestReNova 5.0 (Mestrelab Research SL). Chemical shifts are reported in ppm and referenced to residual solvent peaks ( $\text{CHCl}_3$  in  $\text{CDCl}_3$ : 7.26 ppm for  $^1\text{H}$  and 77.16 ppm for  $^{13}\text{C}$ ). Coupling constants are reported in hertz. Flash chromatography was performed with a Teledyne ISCO CombiFlash RF 200 with Gold-Top silica. *E/Z* ratios were determined by  $^1\text{H}$  NMR spectroscopy and corrected values obtained from GC analysis. High-resolution mass spectra were obtained via the Micro-Mass/Analytical Facility operated by the College of Chemistry, University of California, Berkeley. Organometallic photocatalysts were purchased from Aspira Scientific. Organic photocatalysts were purchased from Sigma Aldrich.

Chiral HPLC analyses were performed 3 instruments: HPLC1 - GL science GL-7400 instrument using Daicel Chiracel columns at 35 °C, HPLC2 - Agilent 1100 series, HPLC3 - Shimadzu Prominence HPLC system with SPD-M20A UV/VIS Photodiode array detector. A mixture of HPLC-grade hexanes and isopropanol were used as eluents. Chiral SFC analyses were performed on a Jasco instrument using Daicel Chiracel columns at 40 °C and HPLC-grade isopropanol as the co-eluent. Optical rotations were measured on Perkin Elmer 241 and JASCO P-1030 polarimeters equipped with sodium vapor lamps at 589 nm and sample concentrations are denoted as *c.* (in g/100 mL).

*E. coli* DH5 $\alpha$  cells were purchased from the Cell Media Facility at the University of Illinois at Urbana-Champaign (Urbana, IL). *Escherichia coli* BL21 (DE3) and plasmid pET28a<sup>+</sup> were purchased from Novagen (Madison, WI). Oligonucleotides for cloning were purchased from Integrated DNA Technologies (IDT) (Coralville, IO). Restriction enzymes were purchased from

New England Biolabs (Ipswich, MA). NADPH was purchased from Enzo Life Sciences (Farmingdale, NY). NADP<sup>+</sup> was purchased from Roche Diagnostics (Indianapolis, IN). Isopropyl- $\beta$ -D-thiogalactoside (IPTG) was purchased from GoldBio (St. Louis, MO). The strain *Bacillus megaterium* (B14308) was obtained from the NRRL culture collection (Peoria, IL).

## 4.4.2. Photocatalyst Abbreviations, CAS Numbers, and Structures



### 4.4.3. Experimental Apparatus

Blue Light Source (Blue LED Lamp): 34 W Kessil KSH150B Blue LED Grow Light with cooling fan. Unless otherwise indicated, all reactions requiring blue light were conducted with the Kessil blue lamp positioned 20 cm from the base of the stir plate. Both 4 mL and 20 mL vials were placed horizontally on the stir-plate (Figure 4.13). <http://kessil.com/photoredox/Products.php>

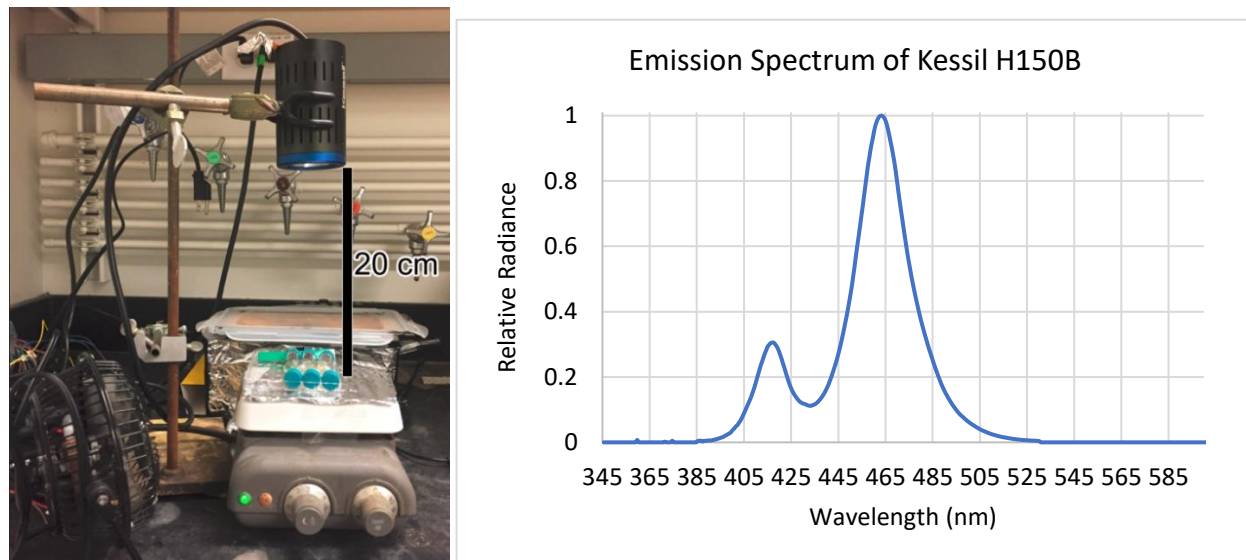


**Figure 4.13.** Blue LED Light Setup and Emission Spectrum of Blue LED Light

### 4.4.4. Cloning, Expression and Purification of Enzymes

#### **YersER**

The YersER employed in this research was originally isolated from *Yersinia bercovieri*. The codon-optimized gene was synthesized by IDT and cloned in pET28a with N-terminal His-tag. For expression of YersER, a BL21 colony harboring pET28a-YersER was inoculated in 5 mL LB containing 100  $\mu$ g/mL ampicillin and grown overnight at 37  $^{\circ}$ C. This overnight culture was used to inoculate 500 mL of TB medium containing 100  $\mu$ g/mL ampicillin, which was grown at 37  $^{\circ}$ C until an OD of  $\sim$ 0.6 was reached. Protein expression was subsequently induced with the addition of 0.3 mM IPTG. The induced culture was placed at 25  $^{\circ}$ C, 250 rpm, for 16 h for protein production.



YersER Sequence:

MKTAKLFSPLKVGALTLPNRVFMAPLTRLRSIEPGDIPTPLMAEYYRQRASAGLIITEAT  
QISFQAKGYAGAPGLHTQEQLNAWKKITQAVHEEGGHIAVQLWHVGRISHSSLQPGQQ  
APVAPSAIAADTRTTVRDENGAWVRVPCSTPRALETEEIPGIINDFRQATANAREAGFDY  
IELHAAHGYLLHQFMSPASNQRTDQYGGSIENRTRLTLEVVDATAAQWSAERIGIRISPL  
GPFNGLDNGEDQEEAALYLIDELNKRHIAYLHISEPDWAGGKPYSEAFRDAVRARFKGV  
IIGAGAYTAEKAEELIEKGFIDAVAFGRSYISNPDLVARLQQHAPLNEPDGETFYGGGAK  
GYTDYPTL

### **OYE1/OYE2/OYE3**

The OYE1/2/3 ene-reductases employed in this research were originally isolated from baker's yeast. The plasmids pET30a-OYE1/2/3 with N-terminal His tag were gifts from Dr. Francesco G. Gatti's lab. The plasmids were transformed into *E. coli* BL21. For expression of OYE1/2/3, BL21 colonies harboring pET30a-OYE1/2/3 respectively were inoculated in 5 mL LB containing 50 µg/mL kanamycin and grown overnight at 37 °C. These overnight cultures were used to inoculate 500 mL of LB medium containing 50 µg/mL kanamycin, which were grown at 37 °C until ODs of ~0.6 were reached. Protein expression was subsequently induced with the addition of 0.1 mM IPTG. The induced cultures were placed at 25 °C, 250 rpm, for 16 h for protein production.

OYE1 Sequence:

MSFVKDFKPKQALGDTNLFKPIKIGNNELLHRAVIPPLTRMRALHPGNIPNRDWAVEYYT  
QRAQRPGTMIITEGAFISPQAGGYDNAPGVWSEEQMVWTKIFNAIHEKKSFWVWQLW  
VLGWAAPDNLARDGLRYDSASDNVFMDAEQEAKAKKANNPQHSLTKDEIKQYIKEY  
VQAAKNSIAAGADGVEIHSANGYLLNQFLDPHSNTRTDEYGGSIENRARFTLEVVDALV  
EAIGHEKVGLRLSPYGVFNSMSGGAETGIVAQYAYVAGELEKRAKAGKRLAFVHLVEP  
RVTNPFLTEGEGEYEGGSNDFVYSIWKGPVIRAGNFALHPEVVREEVKDKRTLIGYGRF  
FISNPDLVDRLEKGLPLNKYDRDTFYQMSAHGYIDYPTYEEALKLGWDKK

OYE2 Sequence:

MPFVKDFKPKQALGDTNLFKPIKIGNNELLHRAVIPPLTRMRAQHPGNIPNRDWAVEYYA  
QRAQRPGTLIITEGTFPSPQSGGYDNAPGIWSEEQIKEWTKIFKAIHENKSFAWVQLWVL  
GWAAPDNLARDGLRYDSASDNVYMNAEQEEKAKKANNPQHSITKDEIKQYVKEYVQ  
AAKNSIAAGADGVEIHSANGYLLNQFLDPHSNTRTDEYGGSIENRARFTLEVVDVAVDA  
IGPEKVGLRLSPYGVFNSMSGGAETGIVAQYAYVLGELERRAKAGKRLAFVHLVEPRVT

NPFLTEGEGEYNGGSNKFAYSIWKGPIIRAGNFALHPEVVREEVKDPRTLIGYGRFFISNP  
DLVDR

OYE3 Sequence:

MPFVKGFEPISLRDTNLFEPKIGNTQLAHRAVMPPLTRMRATHPGNIPNKEWAAVYYG  
QRAQRPGTMIITEGTFISPAAGGYDNAPGIWSDEQVAEWKNIFLAIHDCQSFAWVQLWS  
LGWASFPDVLARDGLRYDCASDRVYMNATLQEKAKDANNLEHSLTKDDIKQYIKDYIH  
AAKNSIAAGADGVEIHSANGYLLNQFLDPHSNKRTDEYGGTIENRARFTLEVVDALIETI  
GPERVGLRLSPYGTFSMSGGAEPGIIAQYSYVLGELEKRAKAGKRLAFVHLVEPRVTD  
PSLVEGEGEYSEGTFNDFAYSIWKGPIIRAGNYALHPEVVREQVKDPRTLIGYGRFFISNP  
LVYRLEEGLPLNKYDRSTFYTMSAEGYTDYPTYEEAVDLGWNKN

### **OPR1**

The OPR1 employed in this research was originally isolated from *Lycopersicon esculentum* (tomato). The plasmid pET21b-OPR1 with C-terminal His tag was a gift from Dr. Kurt Faber's group. The plasmid was transformed into *E. coli* BL21. For expression of OPR1, a BL21 colony harboring pET21b-OPR1 was inoculated in 5 mL LB containing 100 µg/mL ampicillin and grown overnight at 37 °C. This overnight culture was used to inoculate 500 mL of TB medium containing 100 µg/mL ampicillin, which was grown at 37 °C until an OD of ~0.6 was reached. Protein expression was subsequently induced with the addition of 1 mM IPTG. The induced culture was placed at 25 °C, 250 rpm, for 16 h for protein production.

OPR1 Sequence:

MENKVVEEKQVDKIPLMSPCKMGKFELCHR VVLAPLTRQRSYGYIPQPHAILHYSQRST  
NGLLIGEATVISETGIGYKDVPGIWTKEQVEAWKPIVDAVHAKGGIFFCQIWHVGRVS  
NKDFQPNGEDPISCTDRGLTPQIRSNIDIAHFTRPRRLTTDEIPQIVNEFRVAARNAIEAG  
FDGVEIHGAHG YLIDQFMKDQVND RSDKYGG SLENRCRFALEIVEAVANEIGSDRVGIRI  
SPFAHYNEAGDTNPTALGLYMVESLNKYDLAYCHVVEPRMKTAWEKIECTESLVPMR  
KAYKGT FIVAGGYDREDGNRALIEDRADLVAYGRLFISNPDLPKRFELNAPLNKYNRDT  
FYTSDPIVGYTDYPFLETMT

### **XenB**

The XenB employed in this research is from *Pseudomonas putida* ATCC 17453. The plasmid pGaston-XenB with C-terminal His-tag was a gift from Dr. Uwe T. Bornscheuer's group. The

plasmid was transformed into *E. coli* BL21. For expression of *XenB*, a BL21 colony harboring pGaston-XenB was inoculated in 5 mL LB containing 100 µg/mL ampicillin and grown overnight at 37 °C. This overnight culture was used to inoculate 500 mL of LB medium containing 100 µg/mL ampicillin, which was grown at 37 °C at 180 rpm until an OD of ~0.6-0.8 was reached. Protein expression was subsequently induced with the addition of 0.2% (w/v) r-rhamnose. The induced culture was placed at 25 °C XenB for 8 h.

XenB Sequence:

METTTLFDPI TLGDLQLPNRIIMETAPLTRCRADEGRVPNALMETAEYYVQRASAGLILS  
EATSVSAMETGVGYPDTPGIWNDEQVRGWNNVTKAVHAAGGRIFLQLWHVGRISHPS  
YLNGLPVPAPSAIQPKGHVSLVRPLSDYPTPRALETEEIIDIVEAYRSGAENAKAAGFDG  
VEIHGANGYLLDQFLQSSTNQR TD RYGG SLENRARLLLEVTDA AIEVWG ANRVGVHLA  
PRADAHDMETGDADRAETFTYVARELGKRGIAFICSREREADDSIGPLIKEAFGGPYIVN  
ERFDKASANAALASGKADAVAFGVPFIANPDLPARLAADAPLNEARPETFYGRGPVGYI  
DYPRLGSHHHHHH

**TOYE**

The TOYE employed in this research was originally isolated from *Thermoanaerobacter pseudotahnolicus* E39. The plasmid pET21b-TOYE with C-terminal His tag was a gift from Dr. Uwe T. Bornscheuer's group. The plasmid was transformed into *E. coli* BL21. For expression of TOYE, a BL21 colony harboring pET21b-TOYE was inoculated in 5 mL LB containing 100 µg/mL ampicillin and grown overnight at 37 °C. This overnight culture was used to inoculate 500 mL of LB medium containing 100 µg/mL ampicillin, which was grown at 25 °C at 250 rpm until an OD of ~0.5 was reached. Protein expression was subsequently induced with the addition of 0.4 mM IPTG. The induced culture was placed at 25 °C for 12 h.

TOYE Sequence:

MSILHMPLKIKDITIKNRIMMSPMCMYSASTDGMPNDWHIVHYATRAIGGVGLIMQEAT  
AVESRGRITDHD LGIWNDEQVKELKKIVDICKANGAVMGIQLAHAGRKCNI SYEDVVGP  
SPIKAGDRYKLPRELSVEEIKSIVKAFGEAAKRANLAGYDVVEIHAAHGYLIHEFLSPLSN

KRKDEYGN SIENRARFLIEVIDEVRKNWPENKPIFVRVSADDYMEGGINIDMMVEYINMI  
KDKVDLIDVSSGGLLNVDINLYPGYQVKYAETIKKRCNIKTSAVGLITTQELAEELSNER  
ADLVALGRELLRNPYWVLHTYTSKEDWPKQYERAFKK

## **SYE1**

The SYE1 employed in this research was originally isolated from *Shewanella*. The codon-optimized gene was synthesized by IDT and cloned in pET28a with N-terminal His-tag. For expression of SYE1, a BL21 colony harboring pET28a-SYE1 was inoculated in 5 mL LB containing 100 µg/mL ampicillin and grown overnight at 37 °C. This overnight culture was used to inoculate 500 mL of TB medium containing 100 µg/mL ampicillin, which was grown at 37 °C until an OD of ~0.6 was reached. Protein expression was subsequently induced with the addition of 0.1 mM IPTG. The induced culture was placed at 25 °C, 250 rpm, for 16 h for protein production.

SYE1 Sequence:

MTQSLFQPITLGALTLKNRIVMPPMTRSRASQPGDVANHMMAIYYAQRASAGLIVSEGT  
QISPTAKGYAWTPGIYTPEQIAGWRIVTEAVHAKGCAIFAQLWHVGRVTHPDNIDGQQP  
ISSSTLKAENVKVFVDNGSDEPGFVDVAVPRAMTKADIAQVIADYRQAALNAMEAGFG  
IELHAANGYLINQFIDSEANNRSDEYGGSLNRLRFLDEVVAALVDAIGAERVGVR LAPL  
TTLNGTV DADPILTYTAAAALLNKHRIVYLHIAEVDWDDAPDTPVSFKRALREAYQGV I  
YAGRYNAEKAEQAIN DGLADMIGFGRPFIANPDLPERLRHGYPLAEHVPATLFGGGEKL  
TDYPTYQA

## **GDH from *Bacillus megaterium***

*Bacillus megaterium* B14308 was inoculated in 5 mL TGY medium and grown at 30 °C for 18 h. Genomic DNA was isolated using the Wizard<sup>®</sup> Genomic DNA purification kit from Promega according to the manufacturer's protocol. The gene encoding the *gdh* was amplified from the genome of *B. megaterium* using primers *gdh*-NdeI-for and *gdh*-HindIII-rev. Restriction sites are underlined. The gene was ligated into pET28a<sup>+</sup> and transformed in *E. coli* DH5α.

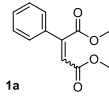
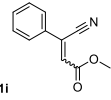
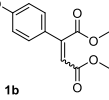
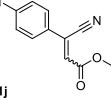
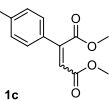
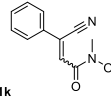
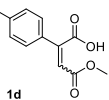
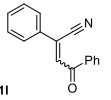
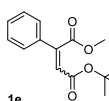
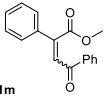
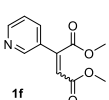
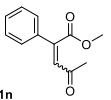
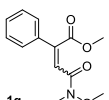
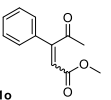
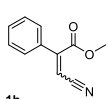
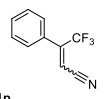
The plasmid pET28a-*gdh* was transformed into *E. coli* BL21. For expression of GDH, a BL21 colony harboring pET28a-*gdh* was inoculated in 5 mL LB containing 50 µg/mL kanamycin and grown overnight at 37 °C. This overnight culture was used to inoculate 500 mL of TB medium containing 50 µg/ml kanamycin, which was grown at 37 °C until an OD of ~0.7 was reached. Protein expression was subsequently induced with the addition of 0.3 mM IPTG. The induced culture was placed at 25 °C for 16 h for protein production.

Following expression, BL21 cells were recovered by centrifugation (6000 x *g* for 15 min), lysed by sonication and clarified by centrifugation (18 000 x *g* for 30 min). The protein was subsequently purified by affinity chromatography using a HisTrap column fitted to an AKTA FPLC system (GE Health Life Sciences, Pittsburgh, PA). The purified protein was buffer exchanged against 100 mM KPi buffer, pH 8.1 using an Amicon Ultra concentration tube (10 kDa cut-off) before being stored in 15% glycerol as 100 µL aliquots at -80 °C

#### 4.4.5. GC/MS Methods and Calibration Curve

Instrument 1: 1 µL was injected in a split mode (20:1) into the GC-MS system consisting of an Agilent 6890 (Agilent Inc, Palo Alto, CA, USA) gas chromatograph, an Agilent 5973 mass selective detector, and Agilent 7683B autosampler. Gas chromatography was performed on a 30 m HP-5MS with 0.25 mm inner diameter (I.D.) and 0.25 µm film thickness (Agilent, USA) with an injection temperature of 250 °C, MSD transfer line of 250 °C, and the ion source adjusted to 230 °C. The helium carrier gas was set at a constant flow rate of 1 ml min<sup>-1</sup>. The temperature program for different samples is listed below. The mass spectrometer was operated in positive electron impact mode (EI) at 69.9 eV ionization energy in m/z 30-500 scan range. The spectra of all chromatogram peaks were evaluated using the HP Chemstation (Agilent, Palo Alto, CA, USA).

*Instrument 2:* 1  $\mu\text{L}$  was injected in a split mode (20:1) into the GC-MS system consisting of an Agilent 6890N (Agilent Inc, Palo Alto, CA, USA) gas chromatograph, an Agilent 5975B mass selective detector, and Agilent 7683B autosampler. Gas chromatography was performed on a 30 m DB-5MS column with 0.25 mm inner diameter (I.D.) and 0.25  $\mu\text{m}$  film thickness (Agilent Technologies, USA) with an injection temperature of 300  $^{\circ}\text{C}$ , MSD transfer line of 230  $^{\circ}\text{C}$ , and the ion source adjusted to 230  $^{\circ}\text{C}$ . The helium carrier gas was set at a constant flow rate of 1 ml  $\text{min}^{-1}$ . The temperature program was different for different samples. The mass spectrometer was operated in positive electron impact mode (EI) at 69.9 eV ionization energy in  $m/z$  30-500 scan range. The spectra of all chromatogram peaks were evaluated using the HP Chemstation (Agilent, Palo Alto, CA, USA).

| Compound  | GC-Instrument | Program  | Retention Time   | Compound  | GC-Instrument | Program  | Retention Time   |
|---|---------------|--|--|---|---------------|--|--|
| <br>1a   | Instrument 1  | 100 °C (2 min, iso),<br>8 °C/min to 200 °C<br>(4 min, iso) | $t_R[(E)] = 15.29$ min,<br>$t_R[(Z)] = 15.51$ min,<br>$t_R[(P)] = 15.29$ min | <br>1i   | Instrument 1  | 100 °C (2 min, iso),<br>6 °C/min to 200 °C<br>(3 min, iso) | $t_R[(E)] = 13.09$ min,<br>$t_R[(Z)] = 15.96$ min,<br>$t_R[(P)] = 13.82$ min |
| <br>1b   | Instrument 1  | 100 °C (2 min, iso),<br>8 °C/min to 250 °C<br>(3 min, iso) | $t_R[(E)] = 16.50$ min,<br>$t_R[(Z)] = 18.05$ min,<br>$t_R[(P)] = 16.18$ min | <br>1j   | Instrument 1  | 100 °C (2 min, iso),<br>8 °C/min to 200 °C<br>(0 min, iso) | $t_R[(E)] = 14.03$ min,<br>$t_R[(Z)] = 16.18$ min,<br>$t_R[(P)] = 14.72$ min |
| <br>1c   | Instrument 1  | 100 °C (2 min, iso),<br>8 °C/min to 200 °C<br>(0 min, iso) | $t_R[(E)] = 12.80$ min,<br>$t_R[(Z)] = 14.00$ min,<br>$t_R[(P)] = 12.57$ min | <br>1k   | Instrument 2  | 100 °C (2 min, iso),<br>8 °C/min to 220 °C<br>(3 min, iso) | $t_R[(E)] = 14.35$ min,<br>$t_R[(Z)] = 16.92$ min,<br>$t_R[(P)] = 14.83$ min |
| <br>1d   | Instrument 1  | 100 °C (2 min, iso),<br>3 °C/min to 175 °C<br>(3 min, iso) | $t_R[(E)] = 20.91$ min,<br>$t_R[(Z)] = 23.81$ min,<br>$t_R[(P)] = 20.75$ min | <br>1l   | Instrument 2  | 100 °C (2 min, iso),<br>6 °C/min to 230 °C<br>(3 min, iso) | $t_R[(E)] = 17.57$ min,<br>$t_R[(Z)] = 20.75$ min,<br>$t_R[(P)] = 18.88$ min |
| <br>1e   | Instrument 2  | 100 °C (2 min, iso),<br>8 °C/min to 280 °C<br>(2 min, iso) | $t_R[(E)] = 13.74$ min,<br>$t_R[(Z)] = 15.09$ min,<br>$t_R[(P)] = 13.47$ min | <br>1m   | Instrument 2  | 100 °C (2 min, iso),<br>8 °C/min to 280 °C<br>(2 min, iso) | $t_R[(E)] = 18.44$ min,<br>$t_R[(Z)] = 20.16$ min,<br>$t_R[(P)] = 19.03$ min |
| <br>1f   | Instrument 2  | 100 °C (2 min, iso),<br>6 °C/min to 200 °C<br>(3 min, iso) | $t_R[(E)] = 15.06$ min,<br>$t_R[(Z)] = 16.19$ min,<br>$t_R[(P)] = 14.82$ min | <br>1n   | Instrument 2  | 80 °C (2 min, iso),<br>6 °C/min to 130 °C<br>(2 min, iso)  | $t_R[(E)] = 12.87$ min,<br>$t_R[(Z)] = 14.51$ min,<br>$t_R[(P)] = 12.32$ min |
| <br>1g  | Instrument 1  | 100 °C (2 min, iso),<br>8 °C/min to 280 °C<br>(0 min, iso) | $t_R[(E)] = 16.60$ min,<br>$t_R[(Z)] = 17.83$ min,<br>$t_R[(P)] = 16.40$ min | <br>1o  | Instrument 1  | 100 °C (3 min, iso),<br>8 °C/min to 220 °C<br>(2 min, iso) | $t_R[(E)] = 13.11$ min,<br>$t_R[(Z)] = 14.47$ min,<br>$t_R[(P)] = 12.89$ min |
| <br>1h | Instrument 1  | 100 °C (2 min, iso),<br>8 °C/min to 200 °C<br>(3 min, iso) | $t_R[(E)] = 11.98$ min,<br>$t_R[(Z)] = 12.94$ min,<br>$t_R[(P)] = 12.15$ min | <br>1p | Instrument 2  | 80 °C (2 min, iso),<br>6 °C/min to 130 °C<br>(2 min, iso)  | $t_R[(E)] = 6.45$ min,<br>$t_R[(Z)] = 9.62$ min,<br>$t_R[(P)] = 8.55$ min    |

**Figure 4.14.** The summary of GC methods and the retention times.

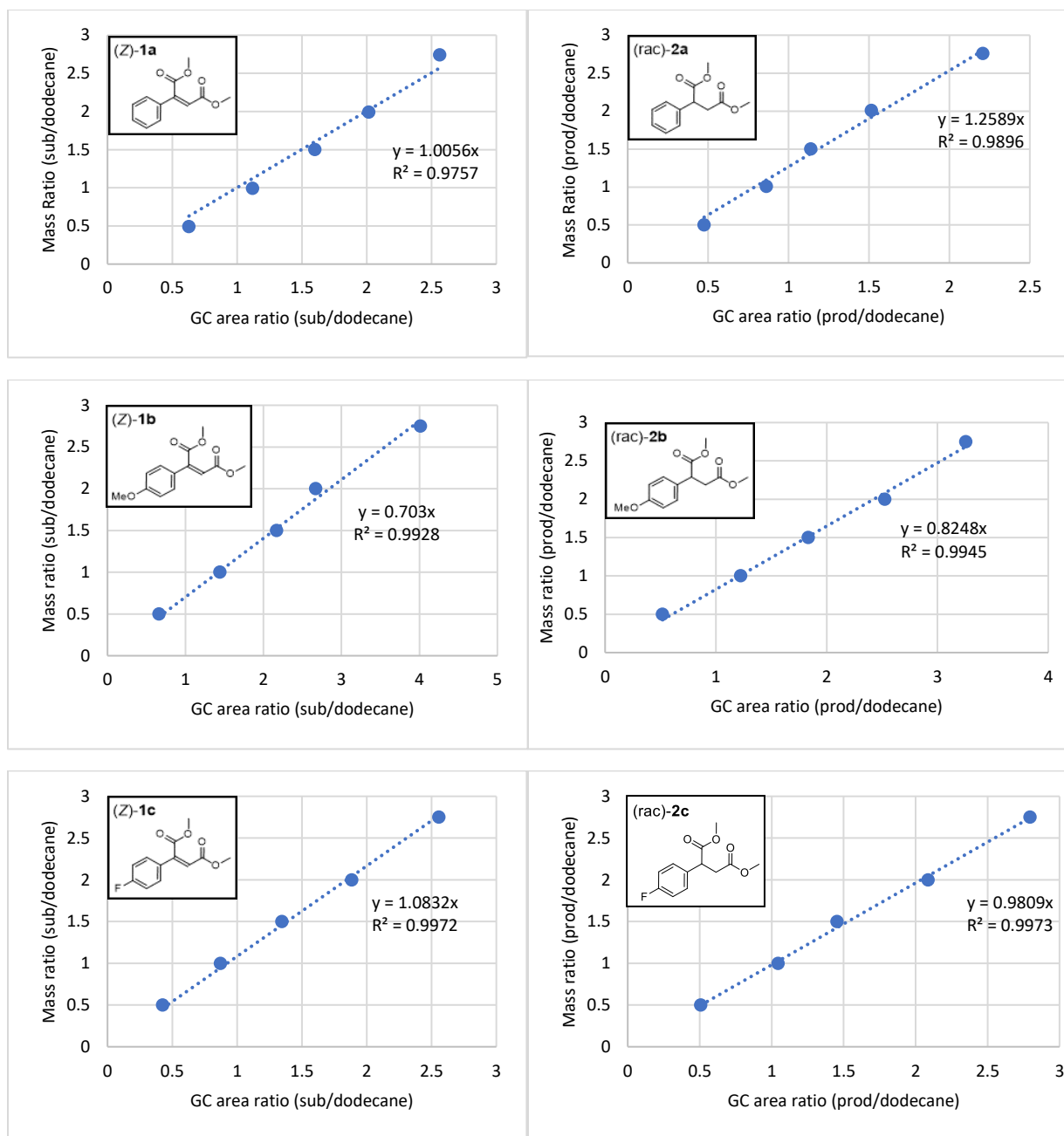


**Figure 4.15.** The representative of GC calibration curve



Figure 4.15. cont.

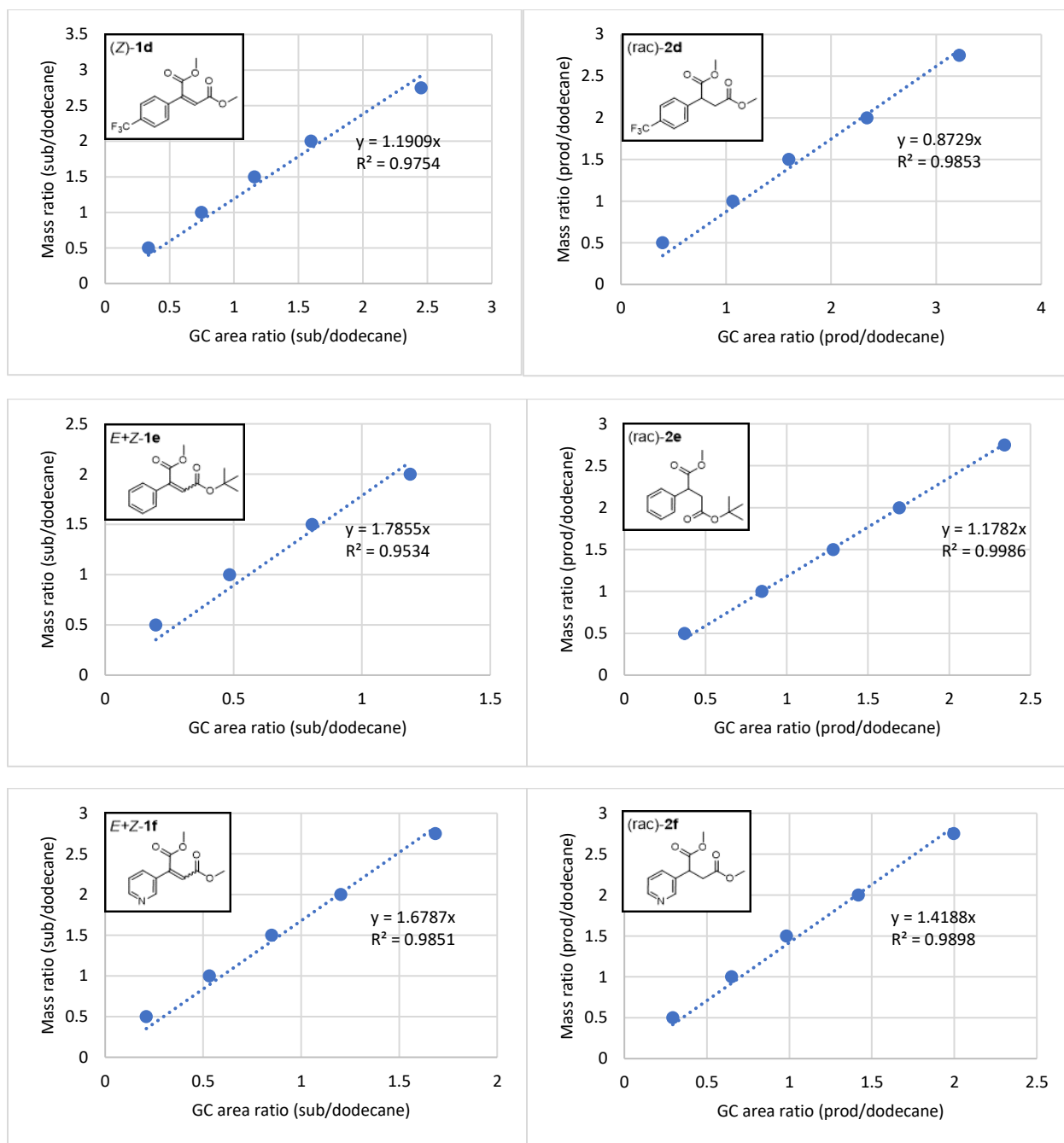


Figure 4.15. cont.

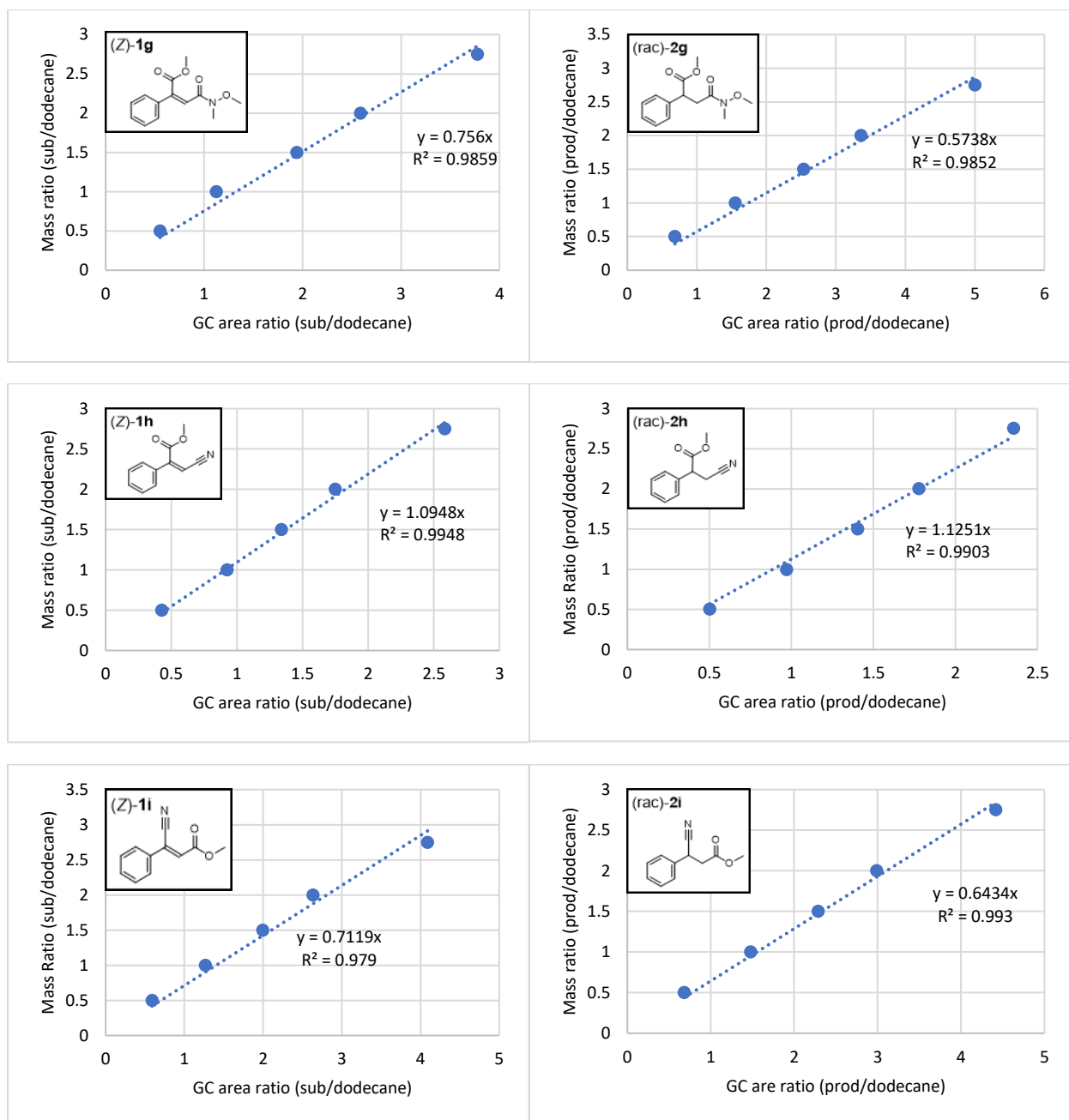


Figure 4.15. cont.

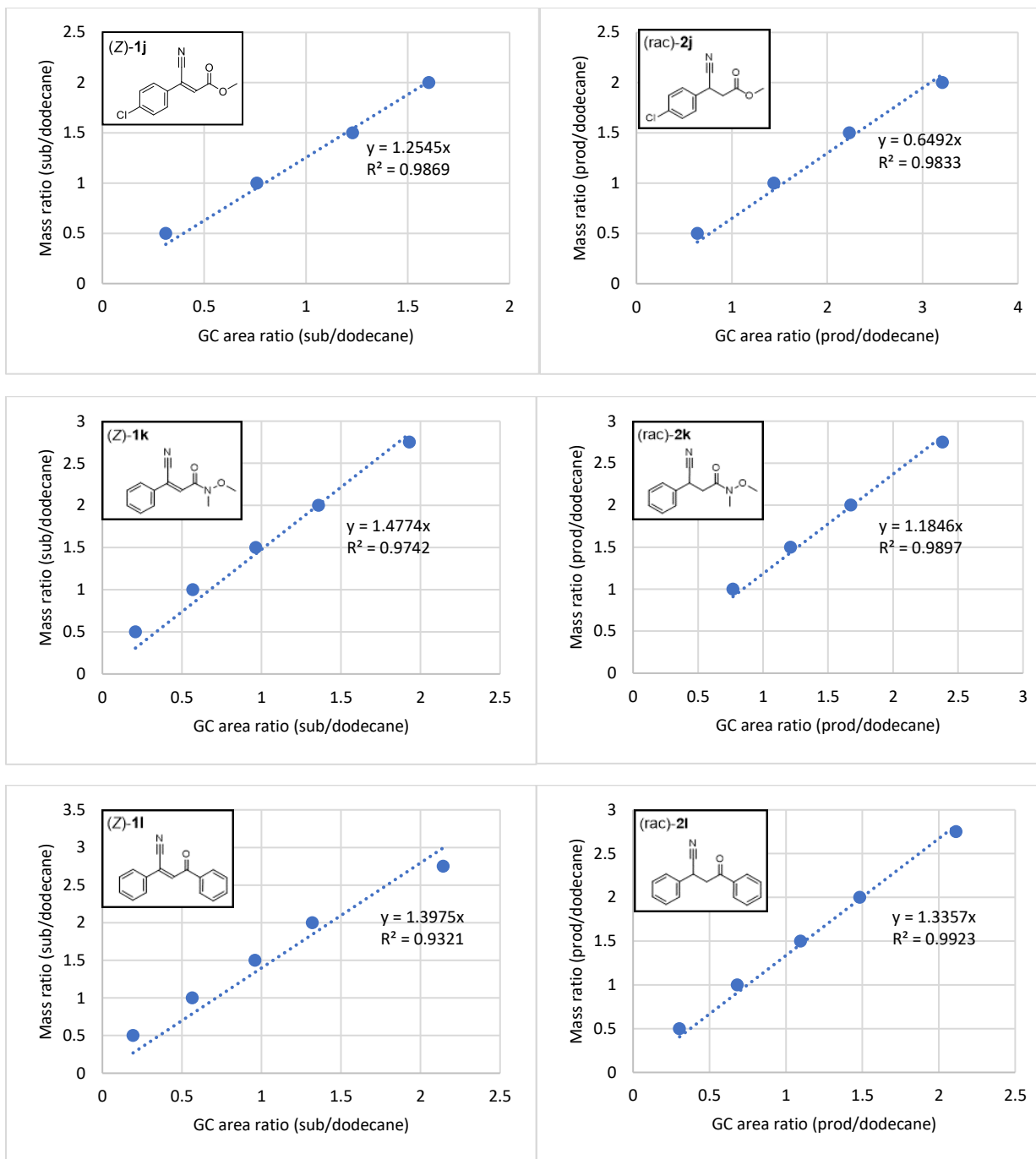


Figure 4.15. cont.

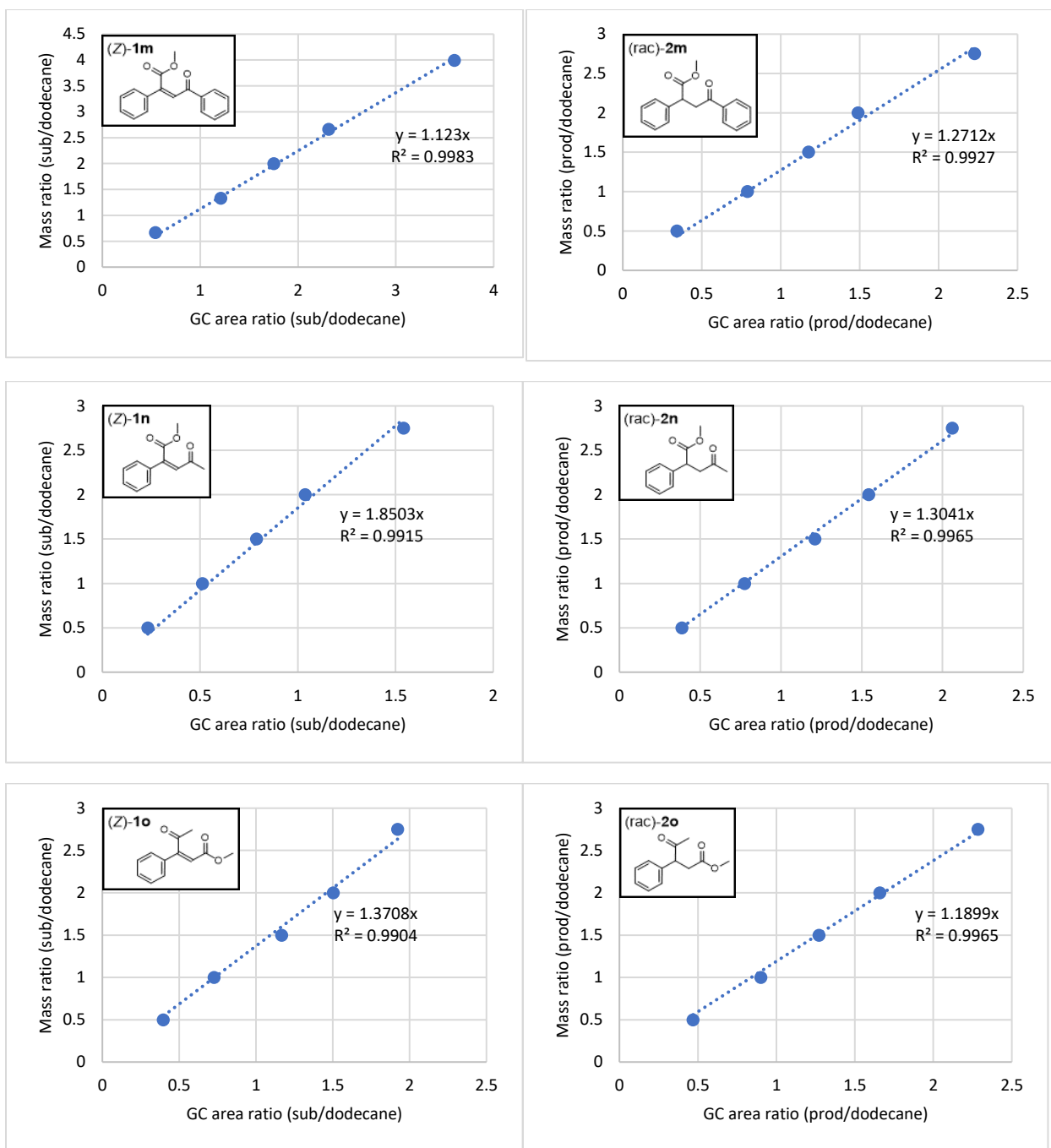
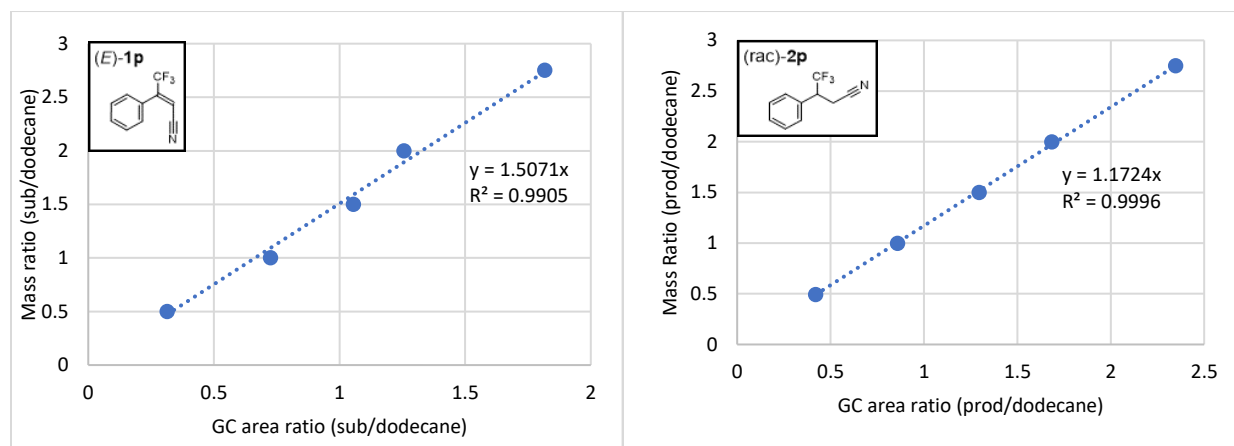


Figure 4.15. cont.



#### 4.4.6. Photocatalyzed Isomerization of Alkenes and Control Experiments

The isomerization reactions presented in Figure 4.3 were conducted on a 0.5 mL scale in the absence of an ene-reductase, GDH, NADP<sup>+</sup>, and glucose. *E/Z* ratios were determined by GC analysis. The experiment labeled “None\*” was conducted in the absence of a photocatalyst under ambient light. The experiment labeled “None” was conducted in the presence of blue light, but in the absence of a photocatalyst. Both “None” and “None\*” were corrected for initial trace quantities of (*E*)-**1a** present in the starting material (*Z*)-**1a**.

The isomerization reactions presented in Figure 4.10 were conducted on a 0.5 mL scale in the absence of an ene-reductase. The PS values (photostationary states) for the isomerization of substrates in the presence of **Ir-16** and FMN are listed on the table below. (62/38) (*E/Z*)-**1e**, and (61/39) (*E/Z*)-**1f** were used in these reactions in place of the pure *Z* isomers of **1e** and **1f**.

**Table 4.4.** Tabulated Results of Figure 4.10 for the Photoisomerization of Alkenes Under Different Conditions (Photostationary States - PS)

| Sub. | Abbrev       | % E<br>X<br>Ambient | % E<br>X<br>blue light | % E<br>5% FMN<br>blue light | % E<br>1% Ir- 16<br>blue light |
|------|--------------|---------------------|------------------------|-----------------------------|--------------------------------|
| 1a   | Ph Est       | 0.1 <sup>a</sup>    | 1.2 <sup>a</sup>       | 93.9                        | 77.9                           |
| 1b   | p-OMe Est    | 3.4 <sup>a</sup>    | 7.6 <sup>a</sup>       | 60.9                        | 69.0                           |
| 1c   | p-F Est      | 0.0 <sup>a</sup>    | 1.4 <sup>a</sup>       | 92.1                        | 67.9                           |
| 1d   | p-CF3 Est    | 0.0                 | 0.0                    | 93.5                        | 72.3                           |
| 1e   | tBu Est      | 62.3                | 62.5                   | 93.1                        | 66.6                           |
| 1f   | Py Est       | 61.3                | 63.7                   | 96.0                        | 81.3                           |
| 1g   | Est Wein     | 0.0 <sup>a</sup>    | 1.1 <sup>a</sup>       | 96.9                        | 87.6                           |
| 1h   | Est CN       | 0.3 <sup>a</sup>    | 0.4 <sup>a</sup>       | 71.9                        | 67.9                           |
| 1i   | CN Est       | 0.0                 | 0.0                    | 45.3                        | 60.9                           |
| 1j   | p-Cl CN Est  | 0.0                 | 0.0                    | 2.9                         | 9.0                            |
| 1k   | CN Wein      | 0.0 <sup>a</sup>    | 2.8 <sup>a</sup>       | 70.9                        | 69.8                           |
| 1l   | CN Ph Keto   | 16.7                | 88.6                   | 87.3                        | 72.5                           |
| 1m   | Est Ph Keto  | 2.9                 | 92.3                   | 82.0                        | 83.3                           |
| 1n   | Est Me Keto  | 24.8                | 76.8                   | 79.9                        | 77.8                           |
| 1o   | top Keto Est | 0.0 <sup>a</sup>    | 1.0 <sup>a</sup>       | 88.5                        | 75.7                           |

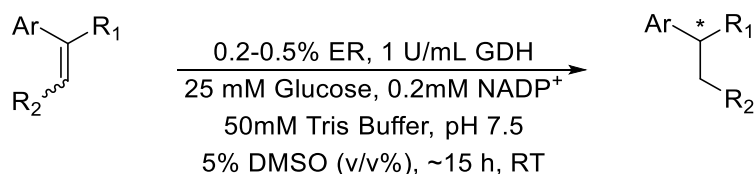
<sup>a</sup> Initial trace quantities of *E* substrate were subtracted from values obtained after subjecting (*Z*)-**1x** to various conditions. <sup>b</sup> 1% FMN. <sup>c</sup> 1% FMN, 2h. <sup>d</sup> 5% **Ir-16**.

It is unlikely that substrates **1e** and **1f** undergo isomerization in the presence of ambient light (the *E/Z* ratios obtained from the reactions conducted in ambient light closely match the initial *E/Z* ratios). Because of **1e**'s structural similarity to **1a** and other related diesters, and the high yields obtained in the cooperative experiments (see section G), it is highly likely that **1e** undergoes rapid isomerization in the presence of blue light and 1% **Ir-16** (even though the final photostationary ratio with **Ir-16** closely resembles the initial *E/Z* ratio). Substrates **1l**, **1m**, and **1n** undergo some isomerization in the presence of ambient light at room temperature. The *Z* isomers of **1l**, **1m**, and **1n**, could be isomerized in the presence of blue light alone. However, the reduction of the *Z* isomer of these substrates could only be accomplished in high yields when the reactions were conducted in the presence of blue light (with or without a catalyst).

Since (*Z*)-**1p** is the more reactive isomer for OYE2, (*E*)-**1p** was used as the starting material for isomerization experiments involving **1p**. All other experimental details were identical to the ones described above.

#### 4.4.7. General Synthetic Procedures for the Cooperative and Non-Cooperative Enzymatic Reduction of Alkenes

##### General Procedure 1: Enzymatic Reduction of Alkenes

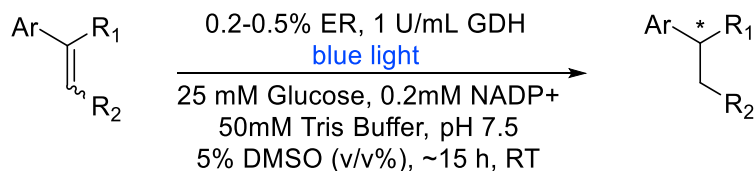


To a 4 mL vial containing a magnetic stir bar, a solution of NADP<sup>+</sup> (5.00 μL of 20.0 mM stock, 0.0400 equiv), glucose (12.5 μL of a 1.00 M stock, 5.00 equiv), GDH (1.00 U/mL) and ene-reductase (0.200 or 0.500 mol %) in 50 mM pH 7.5 Tris buffer (~450 μL) was added a solution of alkene (0.00250 mmol, 1.00 equiv, in 25.0 μL DMSO) at room temperature. The final solution volume was ~500 μL. The final reagent and catalyst concentrations were as follows: 0.200 mM NADP<sup>+</sup>, 25.0 mM glucose, 1 U/mL GDH, 10 or 25 μM ene-reductase, 5.00 mM substrate, 5.00 v/v% DMSO. The reaction was incubated for ~15 h at 24 °C on a magnetic stirrer. At the end of this period, EtOAc (1 mL) and dodecane (10.0 μL of 0.0200 g/mL stock in EtOAc) were added. An aliquot was removed from the organic layer, and the yield and conversion of the reaction were determined by GC analysis with dodecane as the internal standard.

The ee of the product was obtained from a separate reaction conducted on a 5 mL scale (10 X scale of the general procedure listed above) in a 20 mL vial. Concentrations of all reagents and catalysts were identical to those listed above. After the reaction was incubated for ~15 h at 24 °C, EtOAc was added, and the organic layer was extracted three times. The combined organic

layers were concentrated under vacuum and purified by preparative TLC. The ee of the product was determined by Chiral HPLC or SFC.

### General Procedure 2: Reactions Conducted in the Absence of a Photocatalyst but in the Presence of Light



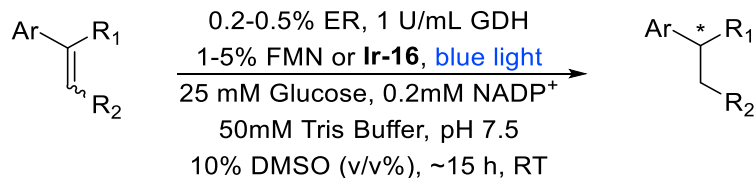
To a 4 mL vial containing a magnetic stir bar, a solution of NADP<sup>+</sup> (5.00 μL of 20.0 mM stock, 0.0400 equiv), glucose (12.5 μL of a 1.00 M stock, 5.00 equiv), GDH (1.00 U/mL) and ene-reductase (0.200 or 0.500 mol %) in 50 mM pH 7.5 Tris buffer (~450 μL) was added a solution of alkene (0.00250 mmol, 1.00 equiv, in 25.0 μL DMSO) at room temperature. The final solution volume was ~500 μL. The final reagent and catalyst concentrations were as follows: 0.200 mM NADP<sup>+</sup>, 25.0 mM glucose, 1 U/mL GDH, 10 or 25 μM ene-reductase, 5.00 mM substrate, 5.00 v/v% DMSO. The reaction was irradiated with a with a blue LED lamp positioned 20 cm above the reaction vial for ~15 h at 24 °C on a magnetic stirrer. At the end of this period, EtOAc (1 mL) and dodecane (10.0 μL of 0.0200 g/mL stock in EtOAc) were added. An aliquot was removed from the organic layer, and the yield and conversion of the reaction were determined by GC analysis with dodecane as the internal standard.

The ee of the product was obtained from a separate reaction conducted on a 5 mL scale (10 X scale of the general procedure listed above) in a 20 mL vial. Concentrations of all reagents and catalysts were identical to those listed above. After the reaction was incubated for ~15 h at 24 °C, EtOAc was added, and the organic layer was extracted three times. The combined organic



layers were concentrated under vacuum and purified by preparative TLC. The ee of the product was determined by Chiral HPLC or SFC.

### General Procedure 3: Cooperative Enzymatic Reduction of Alkenes in the Presence of a Photocatalyst and Light

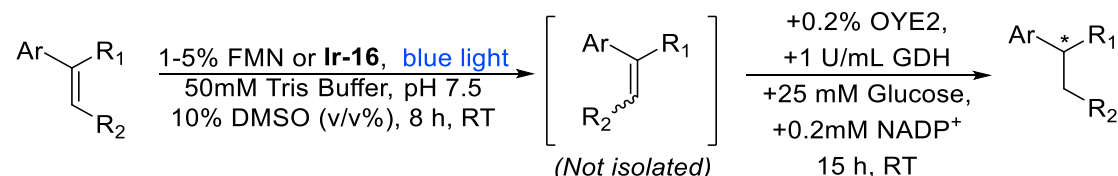


To a 4 mL vial containing a magnetic stir bar, a solution of NADP<sup>+</sup> (5.00 μL of 20.0 mM stock, 0.0400 equiv), glucose (12.5 μL of a 1.00 M stock, 5.00 equiv), GDH (1.00 U/mL) and ene-reductase (0.200 or 0.500 mol %) in 50 mM pH 7.5 Tris buffer (~425 μL) was added a solution of alkene (0.00250 mmol, 1.00 equiv, in 25.0 μL DMSO) at room temperature. A solution containing FMN or **Ir-16** (1.00 or 5.00 mol %) and 25.0 μL of DMSO was added. The final solution volume was ~500 μL. The final reagent and catalyst concentrations were as follows: 0.200 mM NADP<sup>+</sup>, 25.0 mM glucose, 1 U/mL GDH, 10 or 25 μM ene-reductase, 5.00 mM substrate, 0.250-0.0500 mM FMN or **Ir-16**, and 10.0 v/v% DMSO. The reaction was irradiated with a with a blue LED lamp positioned 20 cm above the reaction vial for ~15 h at 24 °C on a magnetic stirrer. At the end of this period, EtOAc (1 mL) and dodecane (10.0 μL of 0.0200 g/mL stock in EtOAc) were added. An aliquot was removed from the organic layer, and the yield and conversion of the reaction were determined by GC analysis with dodecane as the internal standard.

The ee of the product was obtained from a separate reaction conducted on a 5 mL scale (10 X scale of the general procedure listed above) in a 20 mL vial. Concentrations of all reagents and catalysts were identical to those listed above. After the reaction was incubated for ~15 h at 24 °C,

EtOAc was added, and the organic layer was extracted three times. The combined organic layers were concentrated under vacuum and purified by preparative TLC. The ee of the product was determined by Chiral HPLC or SFC.

#### 4.4.8. Procedure for Sequential Isomerization and Reduction of Alkenes



To a 4 mL vial containing a magnetic stir bar, a solution of alkene (0.00250 mmol, 1.00 equiv, in 25.0  $\mu\text{L}$  DMSO), a solution containing FMN or **Ir-16** (1.00 or 5.00 mol %) and 25.0  $\mu\text{L}$  of DMSO, and 50 mM pH 7.5 Tris buffer ( $\sim$ 425  $\mu\text{L}$ ) were added at room temperature. The vial was sealed with a Teflon cap, and the solution was irradiated with a with a blue LED lamp positioned 20 cm above the reaction vial for 8 h at 24  $^{\circ}\text{C}$  on a magnetic stirrer. At the end of this period, the vial was uncapped and a solution of  $\text{NADP}^+$  (5.00  $\mu\text{L}$  of 20.0 mM stock, 0.0400 equiv), glucose (12.5  $\mu\text{L}$  of a 1.00 M stock, 5.00 equiv), GDH (1.00 U/mL), and OYE2 (0.200 mol %) were added. The final solution volume was  $\sim$ 500  $\mu\text{L}$ . The reaction mixture was re-sealed and incubated for 15 h at 24  $^{\circ}\text{C}$  on a magnetic stirrer under ambient conditions and light. At the end of this period, EtOAc (1 mL) and dodecane (10.0  $\mu\text{L}$  of 0.0200 g/mL stock in EtOAc) were added. An aliquot was removed from the organic layer, and the yield and conversion of the reaction were determined by GC analysis with dodecane as the internal standard.

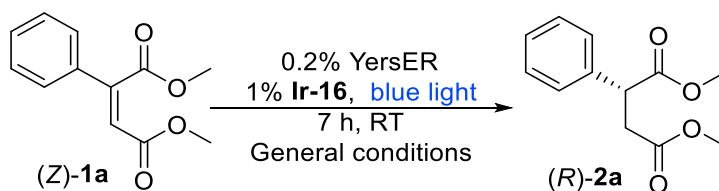
The ee of the product was obtained from a separate reaction conducted on a 5 mL scale (10 X scale of the general procedure listed above) in a 20 mL vial. Concentrations of all reagents and catalysts were identical to those listed above. After the reaction was incubated for  $\sim$ 15 h at 24  $^{\circ}\text{C}$ , EtOAc was added, and the organic layer was extracted three times. The combined organic

layers were concentrated under vacuum and purified by preparative TLC. The ee of the product was determined by Chiral HPLC or SFC

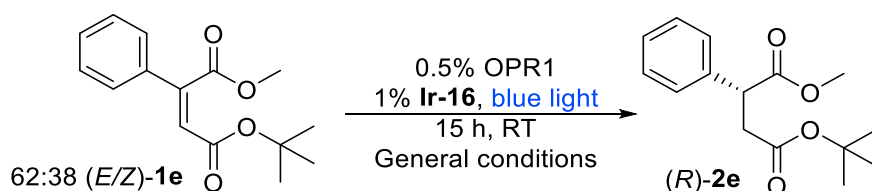
#### 4.4.9. Preparative Scale Cooperative Reactions

Preparative scale cooperative reactions were conducted with the same relative concentrations of reagents as those listed in General Procedure 3 on a 100 X scale.

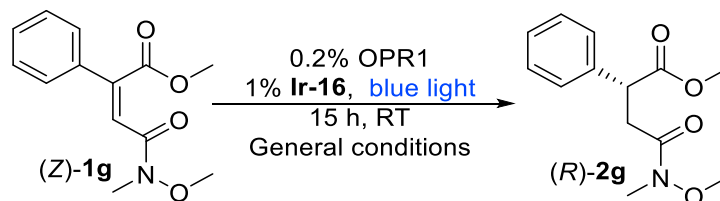
To a 125 mL Erlenmeyer flask containing a magnetic stir bar, a solution of NADP<sup>+</sup> (0.500 mL of 20.0 mM stock, 0.0400 equiv), glucose (1.25 mL of a 1.00 M stock, 5.00 equiv), GDH (1.00 U/mL), and ene-reductase (0.200 or 0.500 mol %) in 50 mM pH 7.5 Tris buffer (42.5 mL) was added a solution of alkene (0.250 mmol, 1.00 equiv) in 2.50 mL of DMSO. A solution containing **Ir-16** (1.00 mol %) and 2.50 mL of DMSO was added. The final concentrations were as follows: 0.200 mM NADP<sup>+</sup>, 25.0 mM glucose, 1 U/mL GDH, 10.0 or 25.0 μM enoate reductase, 5.00 mM substrate, 0.0500 mM **Ir-16**, 10.0 v/v% DMSO. The reaction flask was placed inside a dewar containing 300 mL of water at room temperature on a stirplate. A blue LED lamp was placed 20 cm above the base of the stirplate and a thermometer was inserted in the water bath. The reaction was irradiated with light for 7-15 h, and the temperature of the water bath was maintained at 24 °C. At the end of this period, the reaction mixture was transferred to a separatory funnel containing brine and extracted with EtOAc. The organic layers were combined and concentrated under vacuum and purified by automated silica gel chromatography (combiflash), eluting with a mixture of ethyl acetate and hexanes.



The substrate (*Z*)-**1a** (0.250 mmol, 1.00 equiv) was allowed to react according to the general procedure for preparative scale reactions with 0.2% YersER and 1% **Ir-16**. The reaction time was 7 h. The product was purified by automated silica gel chromatography (combiflash), eluting with a mixture of ethyl acetate and hexanes (gradient 0:100 to 15:95 EtOAc:Hexanes). The product (*R*)-**2a** was obtained as a clear oil (0.0481 g, 0.217 mmol, 87% yield, >99% ee). The spectra of the product matched those of (*rac*)-**2a**. For relevant HPLC traces see section K.

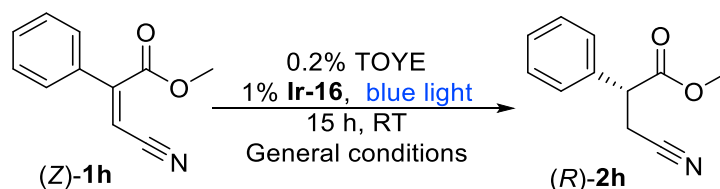


A (62:38) mixture of (*E/Z*)-**1e** (0.250 mmol, 1.00 equiv) was allowed to react according to the general procedure for preparative scale reactions with 0.5% OPR1 and 1% **Ir-16**. The reaction time was 24 h. The product was purified by automated silica gel chromatography (combiflash), eluting with a mixture of ethyl acetate and hexanes (gradient 0:100 to 10:90 EtOAc:Hexanes). The product (*R*)-**2e** was obtained as a clear oil (0.0520 g, 0.197 mmol, 79% yield, >99% ee). The spectra of the product matched those of (*rac*)-**2e**. For relevant HPLC traces see section K.

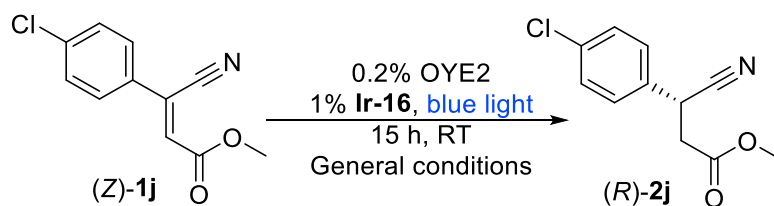


The substrate (*Z*)-**1g** (0.200 mmol, 1.00 equiv) was allowed to react according to the general procedure for preparative scale reactions with 0.2% OPR1 and 1% **Ir-16**. The reaction

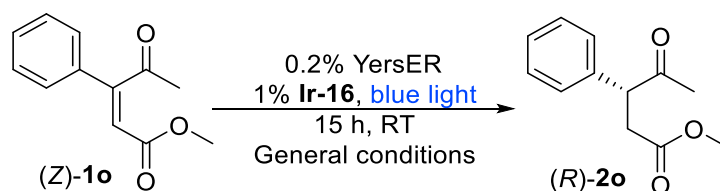
time was 24 h. The product was purified by automated silica gel chromatography (combiflash), eluting with a mixture of ethyl acetate and hexanes (gradient 0:100 to 40:60 EtOAc:Hexanes). The product (*R*)-**2g** was obtained as a clear oil (0.0356 g, 0.142 mmol, 71% yield, >99% ee). The spectra of the product matched those of (*rac*)-**2g**. For relevant HPLC traces see section K.



The substrate (*Z*)-**1h** (0.241 mmol, 1.00 equiv) was allowed to react according to the general procedure for preparative scale reactions with 0.2% TOYE and 1% **Ir-16**. The reaction time was 24 h. The product was purified by automated silica gel chromatography (combiflash), eluting with a mixture of ethyl acetate and hexanes (gradient 0:100 to 20:80 EtOAc:Hexanes). The product (*R*)-**2h** was obtained as a clear oil (0.0438 g, 0.231 mmol, 96% yield, 92% ee). The spectra of the product matched those of (*rac*)-**2h**. For relevant HPLC traces see section K.



The substrate-**1j** (0.150 mmol, 1.00 equiv) was allowed to react according to the general procedure for preparative scale reactions with 0.2% OYE2 and 1% **Ir-16**. The reaction time was 24 h. The product was purified by automated silica gel chromatography (combiflash), eluting with a mixture of ethyl acetate and hexanes (gradient 0:100 to 20:80 EtOAc:Hexanes). The product (**R**)-**2j** was obtained as a clear oil (0.0205 g, 0.0917 mmol, 61% yield, 91% ee). The spectra of the product matched those of (*rac*)-**2j**. For relevant HPLC traces see section K.



The substrate-**1o** (0.200 mmol, 1.00 equiv) was allowed to react according to the general procedure for preparative scale reactions with 0.2% YersER and 1% **Ir-16**. The reaction time was 24 h. The product was purified by automated silica gel chromatography (combiflash), eluting with a mixture of ethyl acetate and hexanes (gradient 0:100 to 20:80 EtOAc:Hexanes). The product (**R**)-**2o** was obtained as a clear oil (0.0326 g, 0.158 mmol, 79% yield, >99% ee). The spectra of the product matched those of (*rac*)-**2o**. For relevant HPLC traces see section K.

#### 4.4.10. Investigating the Plausibility of Direct Photoreduction of (Z)-1a and the Photoracemization of (R)-2a

Reactions 1 and 2 were conducted on a 0.5 mL scale with 5mM (R)-2a

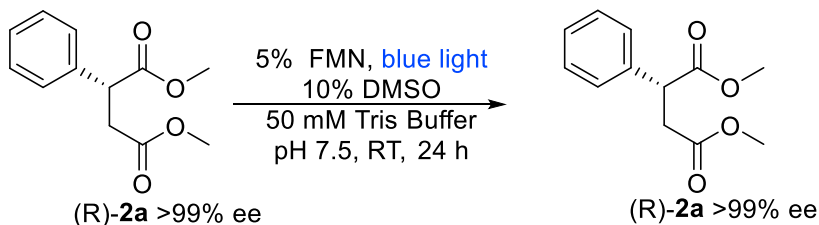
**Scheme 1.** Subjecting (R)-2a to Photoisomerization Conditions to Determine if Racemization of 2a Occurs

##### Reaction 1



No erosion of ee observed

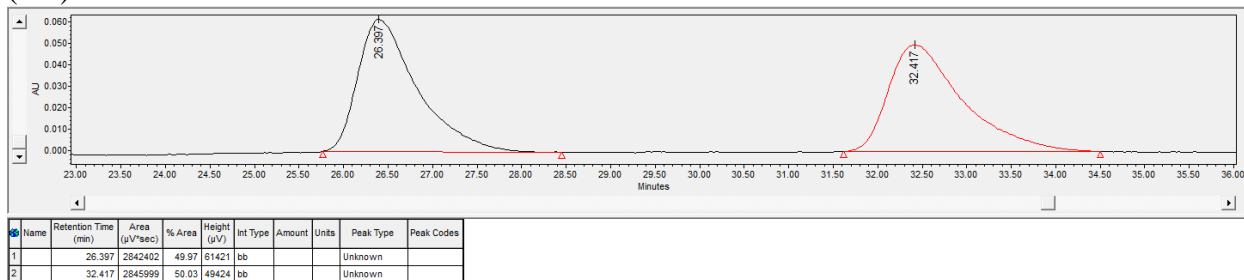
##### Reaction 2



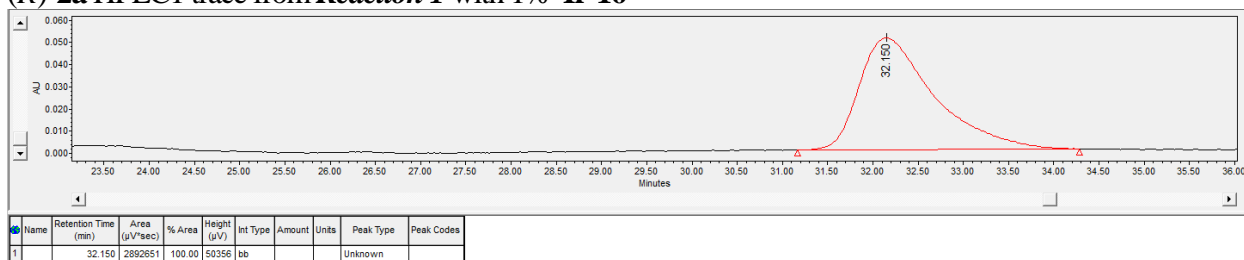
No erosion of ee observed

HPLC1 - OJ-H column, 5% iPrOH, 95% hexanes 1.0 mL/min, 220 nm;  $t_R$  (minor): 26.397 min,  $t_R$ (major): 32.417

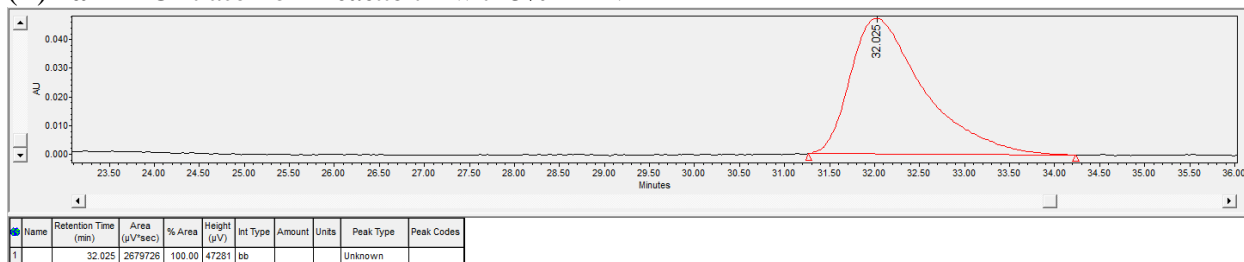
##### (rac)-2a HPLC1 trace



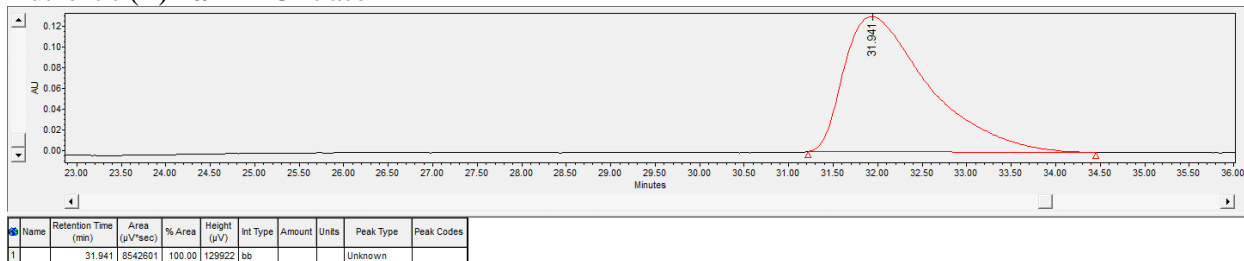
**(R)-2a HPLC1 trace from Reaction 1 with 1% Ir-16**



**(R)-2a HPLC1 trace from Reaction 2 with 5% FMN**

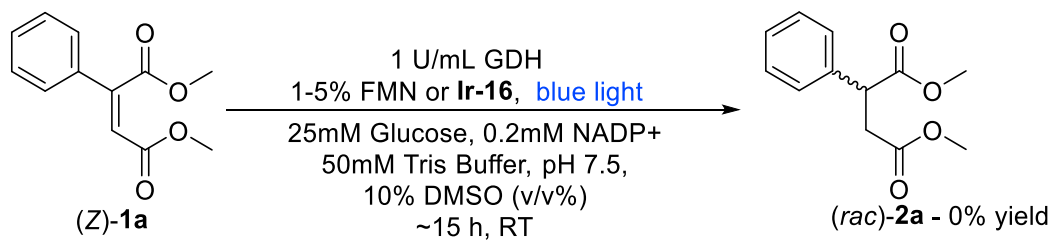


**Authentic (R)-2a HPLC1 trace**



**Scheme 2. Testing for Photoreduction of (Z)-1a**

**Reaction 3** - Photocatalytic Reduction of (Z)-1a in the Presence of Blue Light and FMN or Ir-16 - Only GDH Present



| Sub. | Type | Photocat. | Conv. | Yield |
|------|------|-----------|-------|-------|
| Z-1a | X    | 5% FMN    | 0%    | 0%    |
| Z-1a | X    | 1% Ir-16  | 0%    | 0%    |

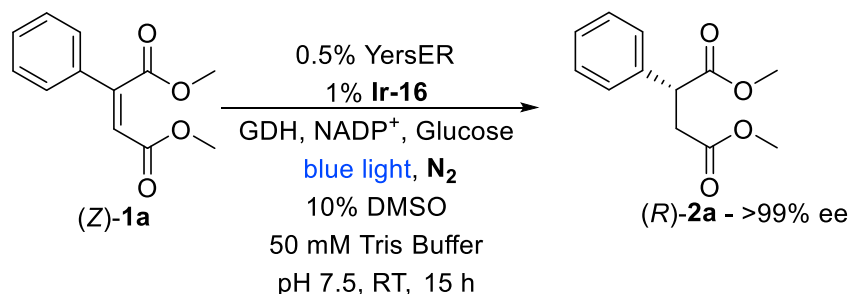


Reaction 3 was conducted on a 0.5 mL scale with 5 Mm (Z)-**1a**. The Z isomer of a substrate was allowed to react in the presence of GDH, NADP<sup>+</sup>, and glucose. No ene-reductase was present in this type of experiment. In the absence of an ene-reductase, only direct photoreduction of the substrate (with NADPH) should generate saturated products. Any products generated by photoreduction should be racemic since no ene-reductase is present in this type of experiment

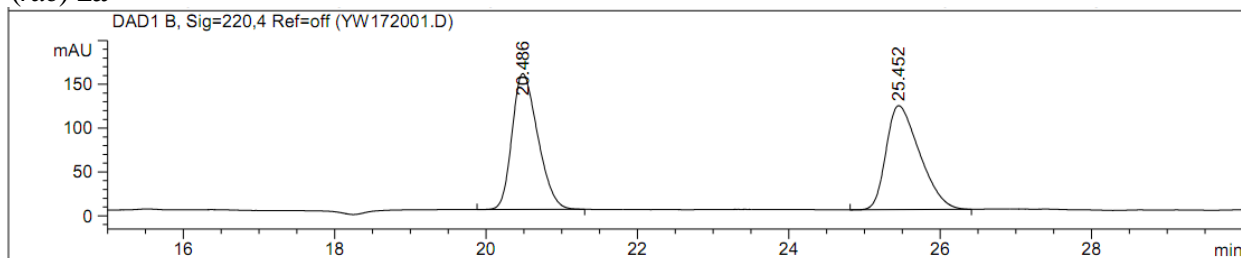
Reaction 4 was conducted on a 5 mL scale according to General Procedure 1 for the cooperative reduction of alkenes with (Z)-**1a**. The % ee of (R)-**2a** in Reaction 4 matched that obtained in the same reaction conducted in air. This suggests that neither photoracemization of the product nor photoreduction of the substrate occurs in a nitrogen atmosphere.

### Scheme 3. Cooperative Reduction of (Z)-**1a** Under a Nitrogen Atmosphere

#### Reaction 4



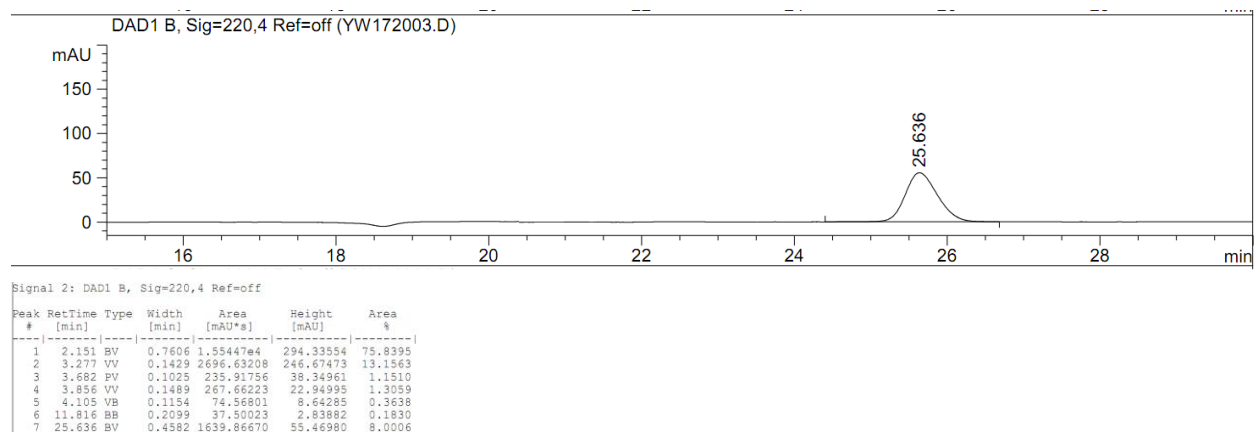
#### (rac)-**2a**



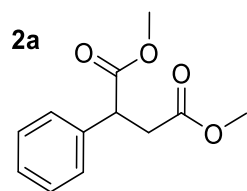
Signal 2: DAD1 B, Sig=220,4 Ref=off

| Peak # | RetTime [min] | Type | Width [min] | Area [mAU*s] | Height [mAU] | Area %  |
|--------|---------------|------|-------------|--------------|--------------|---------|
| 1      | 20.486        | BV   | 0.3585      | 3656.63794   | 155.00519    | 50.0095 |
| 2      | 25.452        | BV   | 0.4688      | 3655.24731   | 118.68571    | 49.9905 |

#### (R)-**2a**



## 4.5 HPLC Traces for the Cooperative Enzymatic Reduction of Alkenes and Control Experiments



Separation Method/Eluent:

HPLC2 - OJ-H (150mm), 5% iPrOH, 95% hexanes 0.8 mL/min, 220 nm;  $t_R$  (minor): 15.752 min,  $t_R$ (major): 19.953

(*rac*)-**2a** HPLC2 trace

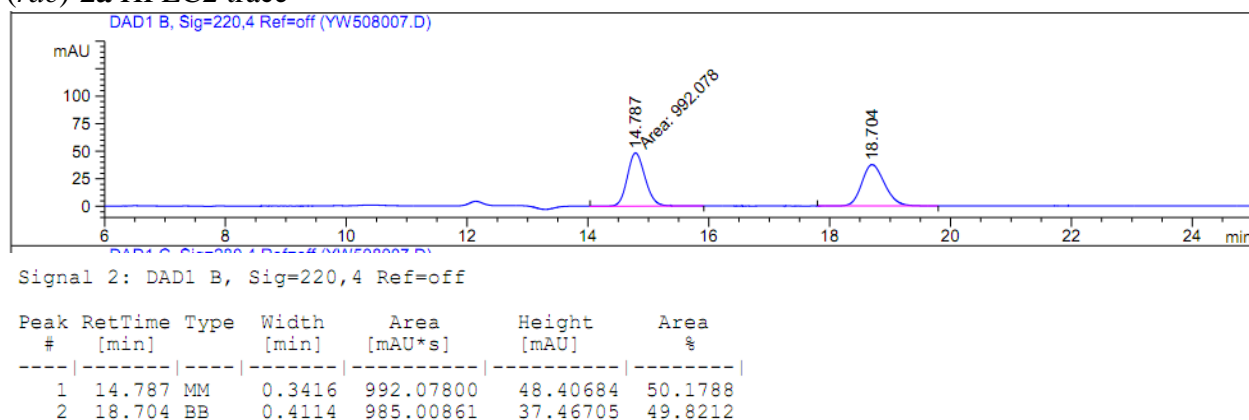
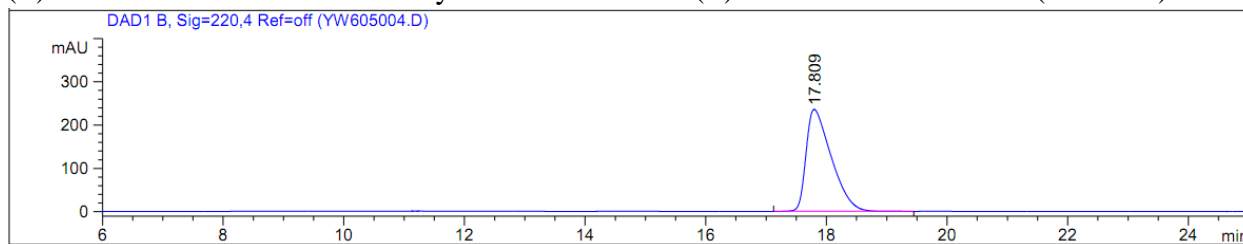


Table 4.1 Entry 1

(R)-2a HPLC2 trace from the enzymatic reduction of (E)-1a with 0.2% YersER (>99% ee)



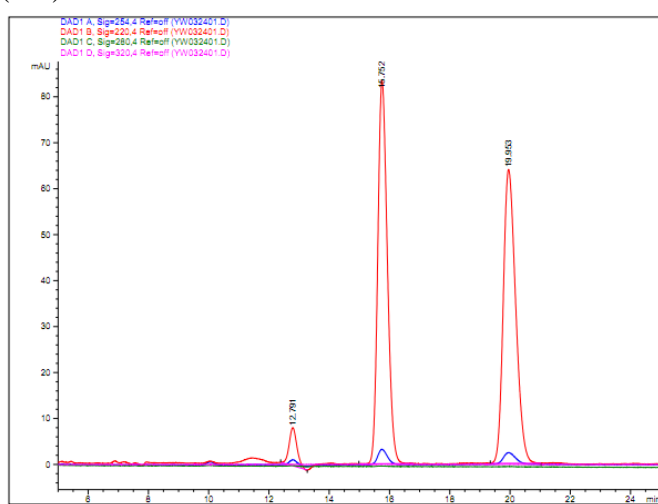
Signal 1: DAD1 A, Sig=254,4 Ref=off

| Peak # | RetTime [min] | Type | Width [min] | Area [mAU*s] | Height [mAU] | Area %   |
|--------|---------------|------|-------------|--------------|--------------|----------|
| 1      | 3.508         | BB   | 0.7085      | 997.26764    | 21.42810     | 100.0000 |

Totals : 997.26764 21.42810

HPLC2 - OJ-H (150mm), 5% iPrOH, 95% hexanes 0.8 mL/min, 220 nm; t<sub>R</sub> (minor): 14.787 min, t<sub>R</sub>(major): 18.704

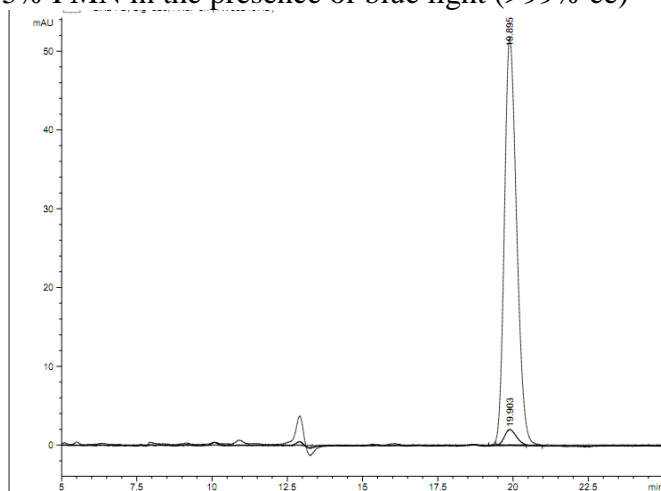
(rac)-2a HPLC2 trace



| Peak # | RetTime [min] | Type | Width [min] | Area [mAU*s] | Height [mAU] | Area %  |
|--------|---------------|------|-------------|--------------|--------------|---------|
| 1      | 2.384         | BV   | 0.1171      | 262.62579    | 30.51068     | 6.2520  |
| 2      | 3.694         | FV   | 0.2209      | 44.97707     | 2.76421      | 1.0707  |
| 3      | 4.079         | VV   | 0.1110      | 46.50237     | 5.98219      | 1.1070  |
| 4      | 4.427         | VV   | 0.1897      | 40.21054     | 3.01840      | 0.9572  |
| 5      | 12.791        | BV   | 0.2662      | 149.70363    | 8.31669      | 3.5638  |
| 6      | 15.752        | BB   | 0.3396      | 1831.71143   | 83.31888     | 43.6051 |
| 7      | 19.953        | BB   | 0.4415      | 1824.94690   | 63.94482     | 43.4441 |

Table 4.2 Entry 2

(R)-**2a** HPLC2 trace from the cooperative enzymatic reduction of (Z)-**1a** with 0.5% YersER and 5% FMN in the presence of blue light (>99% ee)

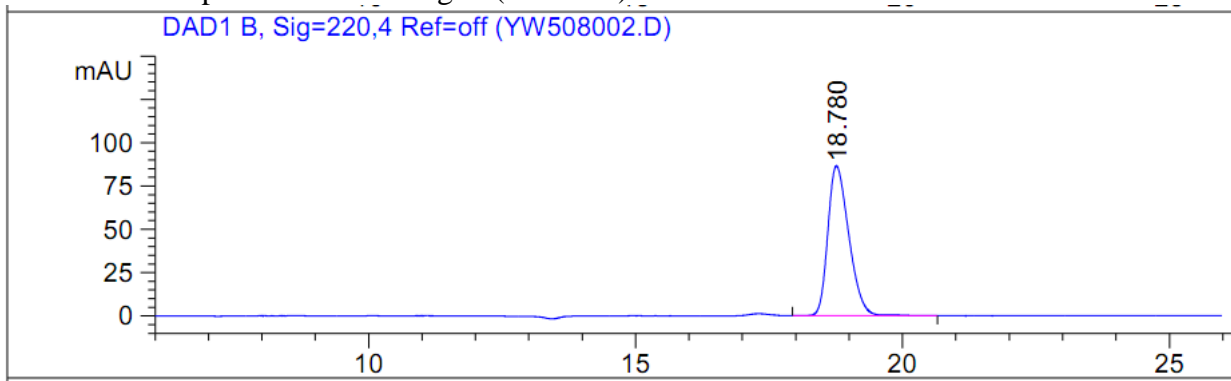


Signal 2: DAD1 B, Sig=220,4 Ref=off

| Peak # | RetTime [min] | Type | Width [min] | Area [mAU*s] | Height [mAU] | Area %   |
|--------|---------------|------|-------------|--------------|--------------|----------|
| 1      | 19.895        | BB   | 0.4264      | 1467.80945   | 51.68619     | 100.0000 |

Table 4.2 Entry 3

(R)-**2a** HPLC2 trace from the cooperative enzymatic reduction of (Z)-**1a** with 0.5% YersER and 1% Ir-**16** in the presence of blue light (>99% ee)

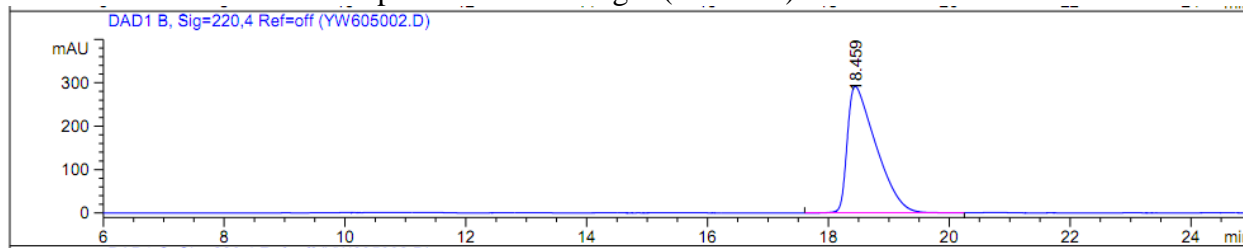


Signal 2: DAD1 B, Sig=220,4 Ref=off

| Peak # | RetTime [min] | Type | Width [min] | Area [mAU*s] | Height [mAU] | Area %   |
|--------|---------------|------|-------------|--------------|--------------|----------|
| 1      | 18.780        | VB   | 0.4445      | 2374.46289   | 85.03007     | 100.0000 |

Table 4.2 Entry 4

(*R*)-**2a** HPLC2 trace from the cooperative enzymatic reduction of (50/50) (*E/Z*)-**1a** with 0.5% YersER and 5% FMN in the presence of blue light (>99% ee)

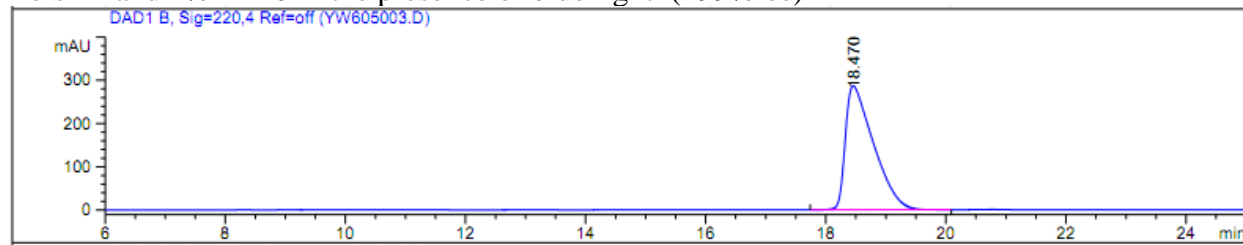


Signal 2: DAD1 B, Sig=220,4 Ref=off

| Peak # | RetTime [min] | Type | Width [min] | Area [mAU*s] | Height [mAU] | Area %   |
|--------|---------------|------|-------------|--------------|--------------|----------|
| 1      | 18.459        | BV   | 0.4964      | 9612.51758   | 289.63583    | 100.0000 |

Table 4.2 Entry 5

(*R*)-**2a** HPLC2 trace from the cooperative enzymatic reduction of (50/50) (*E/Z*)-**1a** with 0.5% YersER and 1% **Ir-16** in the presence of blue light (>99% ee)



Signal 2: DAD1 B, Sig=220,4 Ref=off

| Peak # | RetTime [min] | Type | Width [min] | Area [mAU*s] | Height [mAU] | Area %  |
|--------|---------------|------|-------------|--------------|--------------|---------|
| 1      | 2.427         | BV   | 0.2299      | 2240.26416   | 221.93233    | 11.7533 |
| 2      | 3.432         | PB   | 0.7581      | 7479.92334   | 148.64032    | 39.2427 |
| 3      | 18.470        | BV   | 0.4892      | 9340.48242   | 285.24960    | 49.0040 |

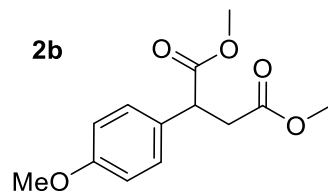


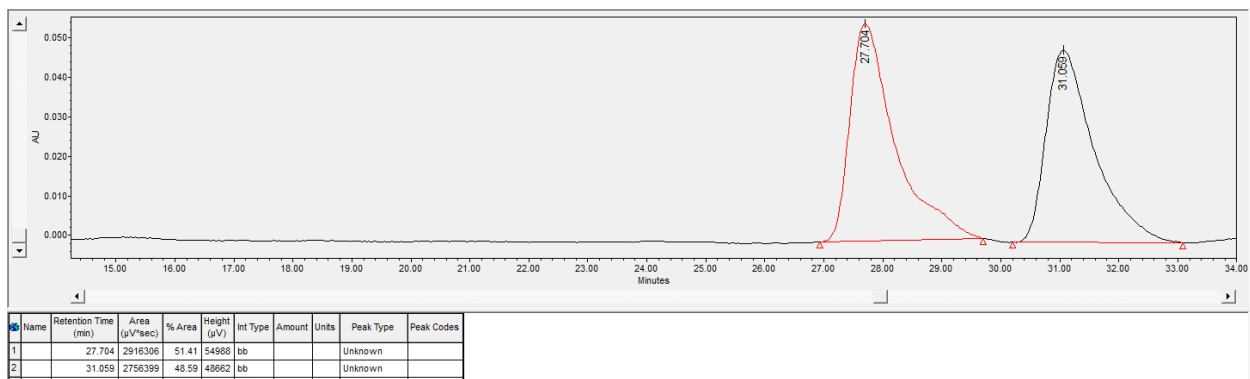
Table 4.1 Entry 3

Separation Method/Eluent:

HPLC1 - OJ-H column, 10% iPrOH, 90% hexanes 1.0 mL/min, 220 nm;  $t_R$  (major): 27.704 min,  $t_R$ (minor): 31.059 min

Enantiomeric Excess = >99% ee

(*rac*)-**2b** HPLC1 trace



(*R*)-**2b** HPLC1 trace from enzymatic reduction of (*E*)-**1b** with YersER (>99% ee) (0.0351 g scale)

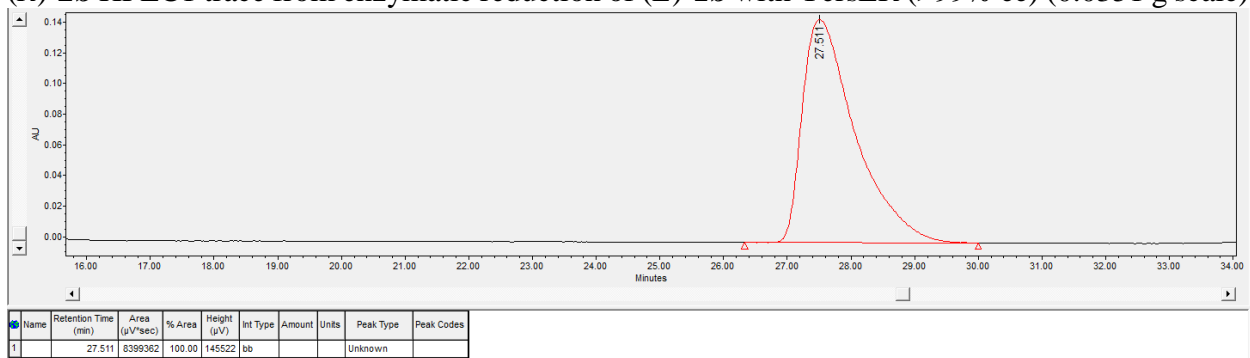
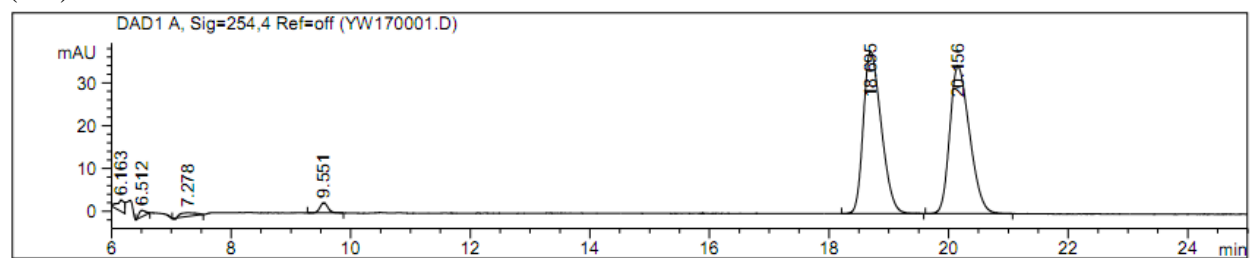


Table 4.2 Entry 7

Separation Method/Eluent:

HPLC2 - OJ-H (250mm), 50% iPrOH, 50% hexanes 0.5 mL/min, 254 nm;  $t_R$  (major): 18.695 min,  $t_R$ (minor): 20.156

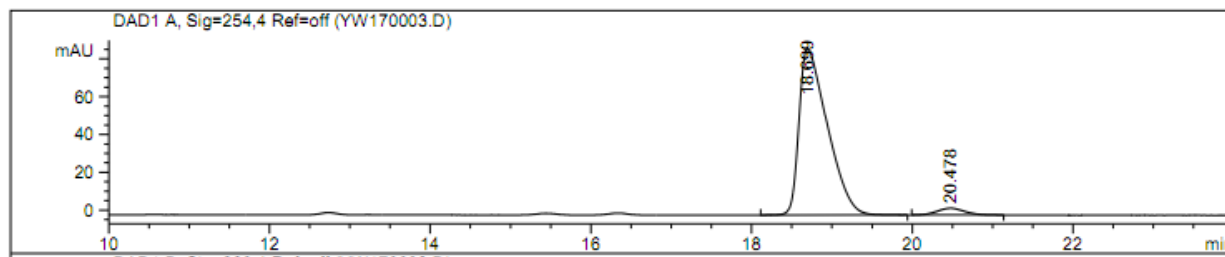
(*rac*)-**2b** HPLC2 trace



Signal 1: DAD1 A, Sig=254,4 Ref=off

| Peak # | RetTime [min] | Type | Width [min] | Area [mAU*s] | Height [mAU] | Area %  |
|--------|---------------|------|-------------|--------------|--------------|---------|
| 5      | 18.695        | BB   | 0.3218      | 789.31238    | 37.89428     | 47.7130 |
| 6      | 20.156        | BB   | 0.3584      | 792.90363    | 34.36451     | 47.9301 |

(*R*)-**2b** HPLC2 trace from the cooperative enzymatic reduction of (*Z*)-**1b** with 0.5% YersER and 5% FMN in the presence of blue light (92% ee)

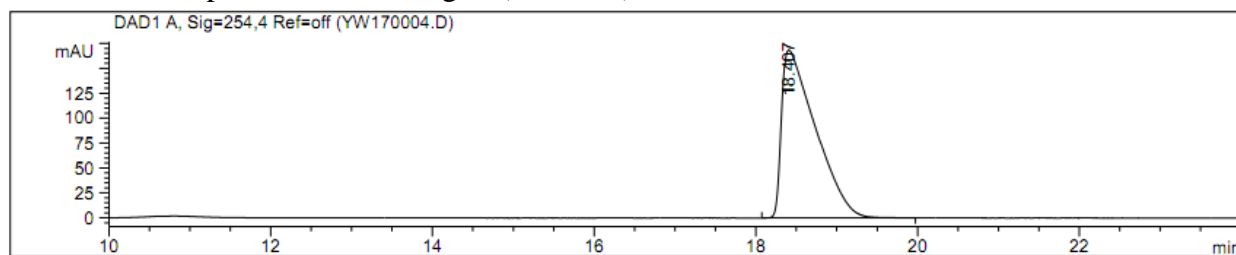


Signal 1: DAD1 A, Sig=254,4 Ref=off

| Peak # | RetTime [min] | Type | Width [min] | Area [mAU*s] | Height [mAU] | Area %  |
|--------|---------------|------|-------------|--------------|--------------|---------|
| 1      | 18.699        | BB   | 0.3602      | 2159.59619   | 88.04809     | 96.1779 |
| 2      | 20.478        | BB   | 0.3510      | 85.82156     | 3.58227      | 3.8221  |

Table 4.2 Entry 8

(*R*)-**2b** HPLC2 trace from the cooperative enzymatic reduction of (*Z*)-**1b** with 0.5% YersER and 1% **Ir-16** in the presence of blue light (>99% ee)



Signal 1: DAD1 A, Sig=254,4 Ref=off

| Peak # | RetTime [min] | Type | Width [min] | Area [mAU*s] | Height [mAU] | Area %   |
|--------|---------------|------|-------------|--------------|--------------|----------|
| 1      | 18.307        | BB   | 0.4161      | 4895.33545   | 168.59383    | 100.0000 |

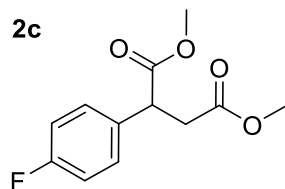


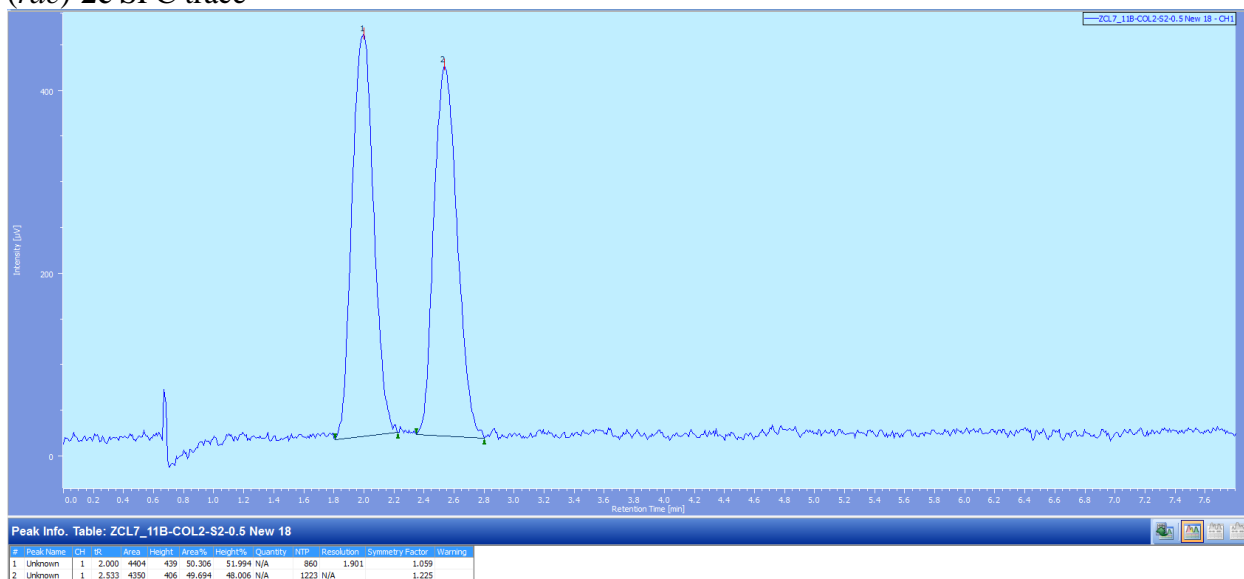
Table 4.1 Entry 5

Separation Method/Eluent:

SFC – OD-H column, 0.5% iPrOH, 2.5 mL/min, 220 nm;  $t_R$  (minor): 2.000 min,  $t_R$ (major): 2.533

Enantiomeric Excess: >99 % ee

(rac)-2c SFC trace



(R)-2c SFC trace from enzymatic reduction of (E)-1c with XenB (>99% ee) (0.0357 g scale – Entry 13)

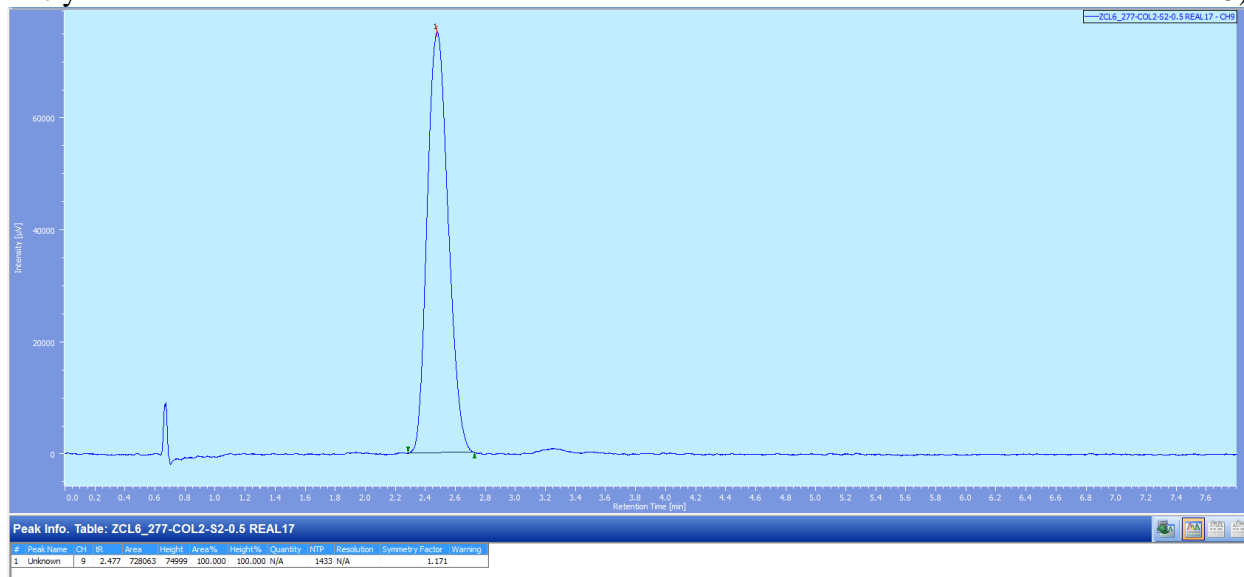


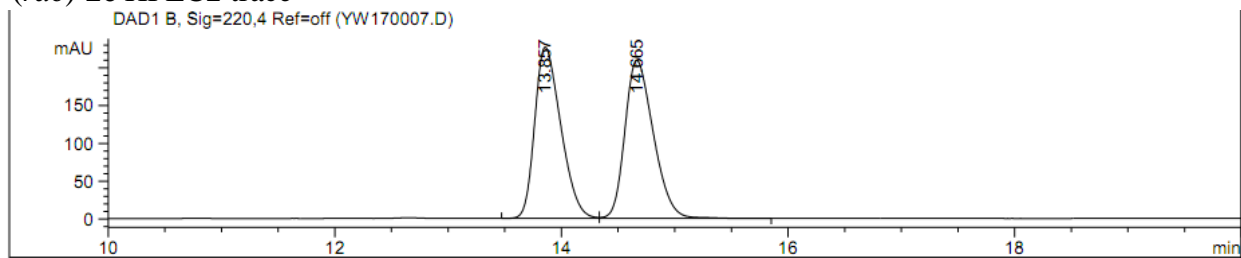
Table 4.2 Entry 11

Separation Method/Eluent:

HPLC2 - OJ-H (250mm), 5% iPrOH, 95% hexanes 1.0 mL/min, 220 nm;  $t_R$  (major): 13.857 min,  $t_R$ (minor): 14.665



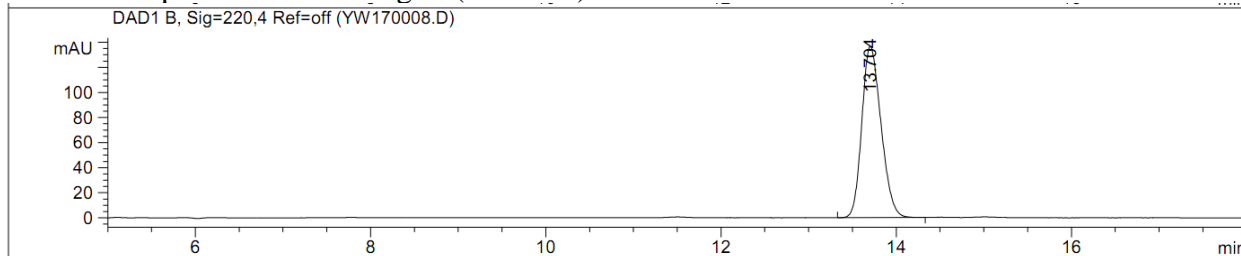
**(rac)-2c HPLC2 trace**



Signal 1: DAD1 A, Sig=254,4 Ref=off

| Peak # | RetTime [min] | Type | Width [min] | Area [mAU*s] | Height [mAU] | Area %  |
|--------|---------------|------|-------------|--------------|--------------|---------|
| 1      | 13.857        | BV   | 0.2454      | 422.77051    | 26.50725     | 49.9927 |
| 2      | 14.665        | VB   | 0.2653      | 422.89365    | 24.37929     | 50.0073 |

**(R)-2c HPLC2 trace from the cooperative enzymatic reduction of (Z)-1c with 0.5% XenB and 1% Ir-16 in the presence of blue light (>99% ee)**



| Peak # | RetTime [min] | Type | Width [min] | Area [mAU*s] | Height [mAU] | Area %   |
|--------|---------------|------|-------------|--------------|--------------|----------|
| 1      | 13.704        | BB   | 0.3522      | 4862.21338   | 213.97617    | 100.0000 |

**2d**

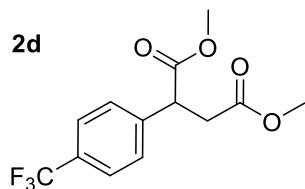


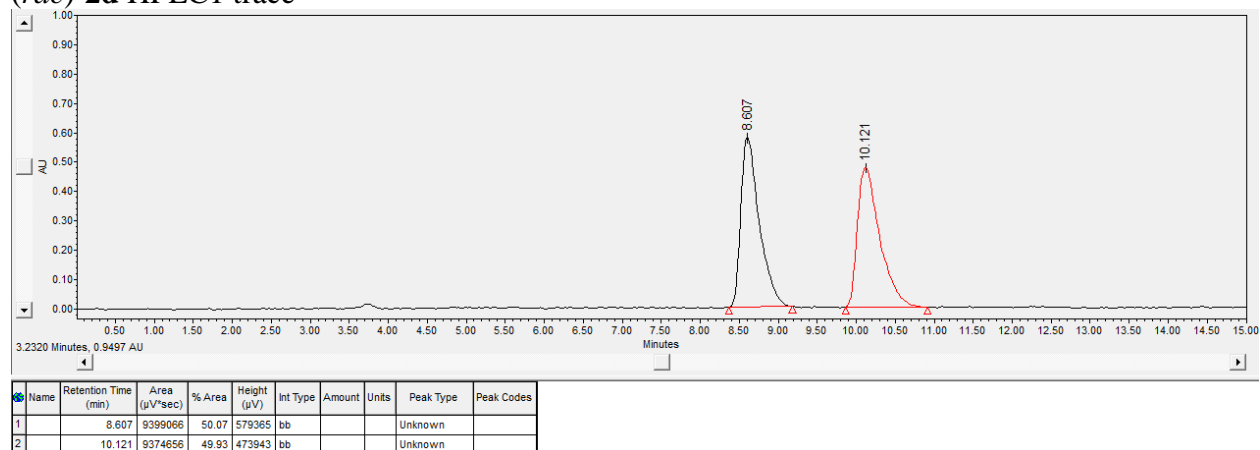
**Table 4.1 Entry 7**

Separation Method/Eluent:

HPLC1 - OJ-H column, 5% iPrOH, 95% hexanes 1.0 mL/min, 220 nm; t<sub>R</sub> (major): 8.607 min, t<sub>R</sub>(minor): 10.121

Enantiomeric Excess = 93% ee

**(rac)-2d HPLC1 trace**



**(R)-2d HPLC1 trace from enzymatic reduction of (E)-1d with XenB (93% ee) (**

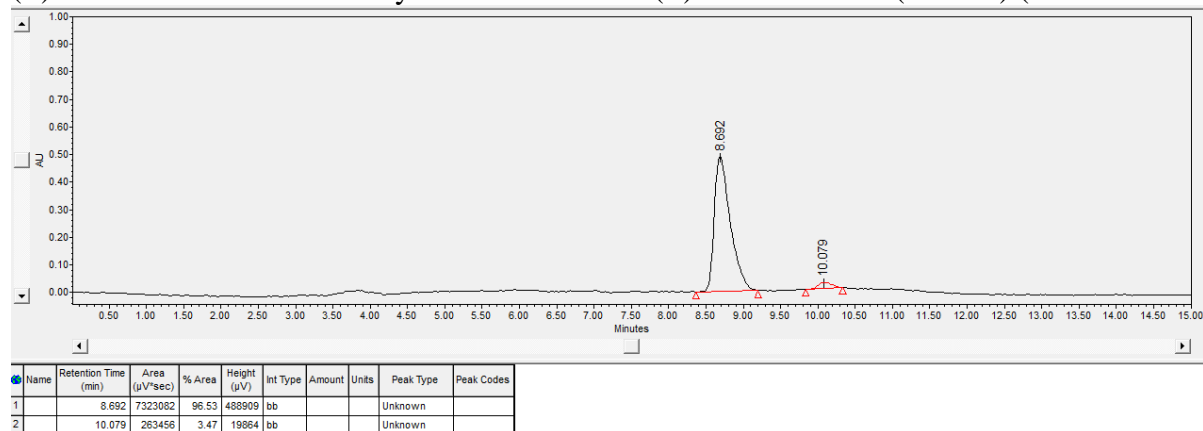
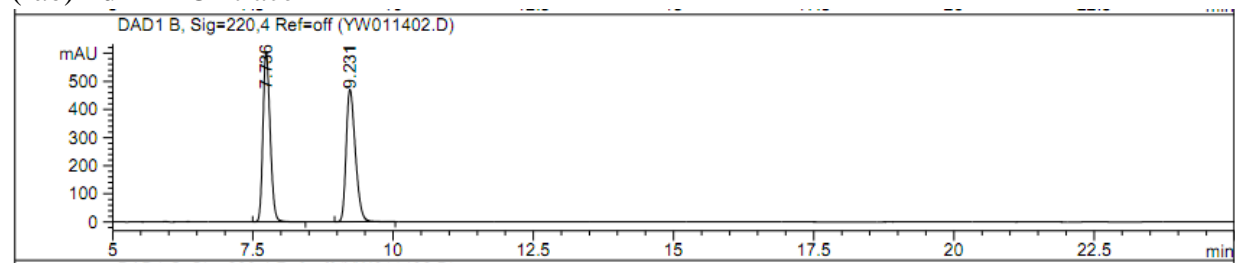


**Table 4.2 Entry 14**

Separation Method/Eluent:

HPLC2 - OJ-H (250mm), 5% iPrOH, 95% hexanes 1.0 mL/min, 220 nm;  $t_R$  (major): 7.736 min,  $t_R$ (minor): 9.231

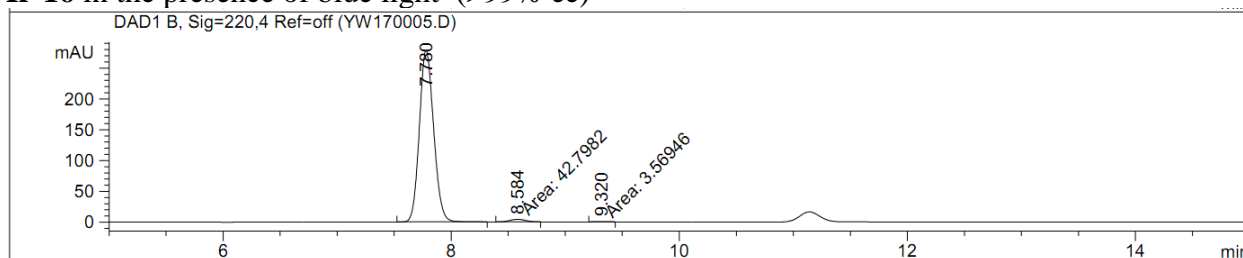
**(rac)-2d HPLC2 trace**



Signal 2: DAD1 B, Sig=220,4 Ref=off

| Peak # | RetTime [min] | Type | Width [min] | Area [mAU*s] | Height [mAU] | Area %  |
|--------|---------------|------|-------------|--------------|--------------|---------|
| 6      | 7.736         | BB   | 0.1382      | 5369.75586   | 603.03467    | 42.2993 |
| 7      | 9.231         | BB   | 0.1764      | 5384.77979   | 470.61526    | 42.4176 |

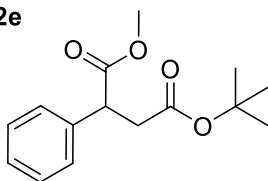
**(R)-2d** HPLC2 trace from the cooperative enzymatic reduction of **(Z)-1d** with 0.5% XenB and 1% **Ir-16** in the presence of blue light (>99% ee)



Signal 2: DAD1 B, Sig=220,4 Ref=off

| Peak # | RetTime [min] | Type | Width [min] | Area [mAU*s] | Height [mAU] | Area %  |
|--------|---------------|------|-------------|--------------|--------------|---------|
| 1      | 7.780         | BB   | 0.1355      | 2426.10132   | 278.49316    | 98.1246 |
| 2      | 8.584         | MM   | 0.1652      | 42.79824     | 4.31700      | 1.7310  |
| 3      | 9.320         | MM   | 0.1493      | 3.56946      | 3.98533e-1   | 0.1444  |

**2e**

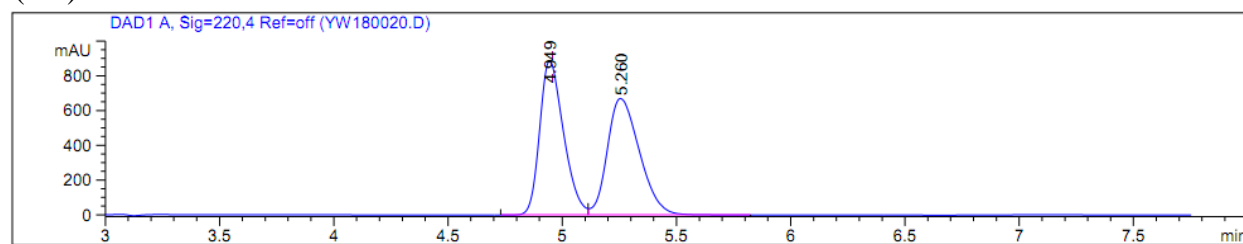


Separation Method/Eluent:

HPLC2 - OJ-H (250mm), 10% iPrOH, 90% hexanes 1.0 mL/min, 220 nm;  $t_R$  (minor): 6.916 min,  $t_R$ (major): 7.450

HPLC2 - OJ-H (150mm), 10% iPrOH, 90% hexanes 1.0 mL/min, 220 nm;  $t_R$  (major): 4.949 min,  $t_R$ (minor): 5.260

**(rac)-2e** HPLC2 trace

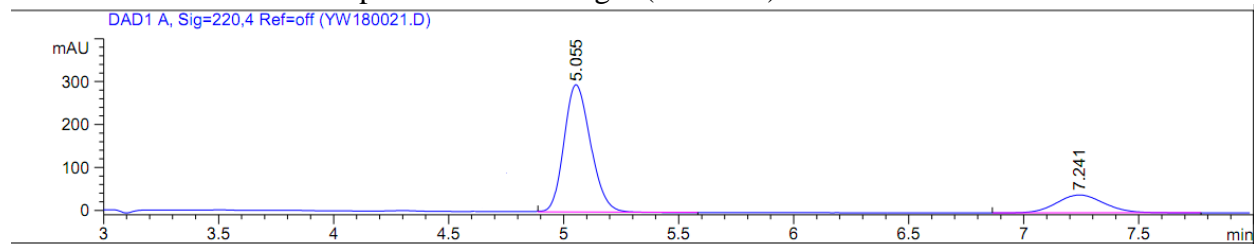


Signal 1: DAD1 A, Sig=220,4 Ref=off

| Peak # | RetTime [min] | Type | Width [min] | Area [mAU*s] | Height [mAU] | Area %  |
|--------|---------------|------|-------------|--------------|--------------|---------|
| 1      | 4.949         | BV   | 0.1159      | 6412.54297   | 882.71112    | 49.4165 |
| 2      | 5.260         | VB   | 0.1563      | 6563.97852   | 663.74268    | 50.5835 |

Table 4.2 Entry 16

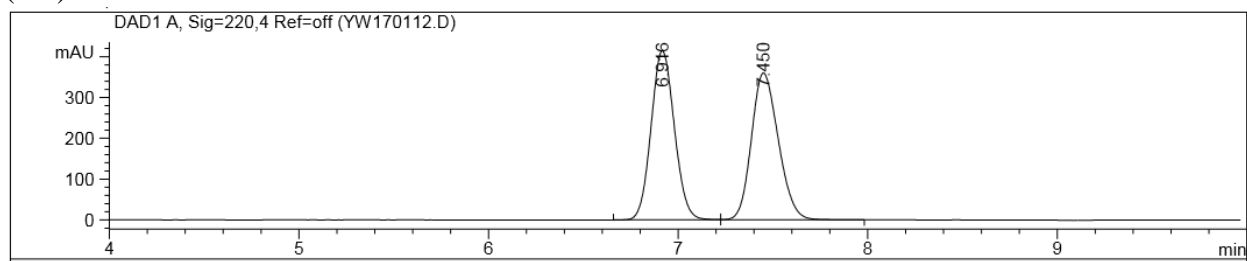
(*R*)-**2e** HPLC2 trace from the cooperative enzymatic reduction of (62/38) (*E/Z*)-**1e** with 0.5% OPR1 and 5% FMN in the presence of blue light (>99% ee)



Signal 1: DAD1 A, Sig=220,4 Ref=off

| Peak # | RetTime [min] | Type | Width [min] | Area [mAU*s] | Height [mAU] | Area %  |
|--------|---------------|------|-------------|--------------|--------------|---------|
| 1      | 5.055         | VB   | 0.1291      | 2387.07275   | 296.07584    | 79.9053 |
| 2      | 7.241         | BB   | 0.2257      | 600.30426    | 41.70131     | 20.0947 |

(*rac*)-**2e** HPLC2 trace

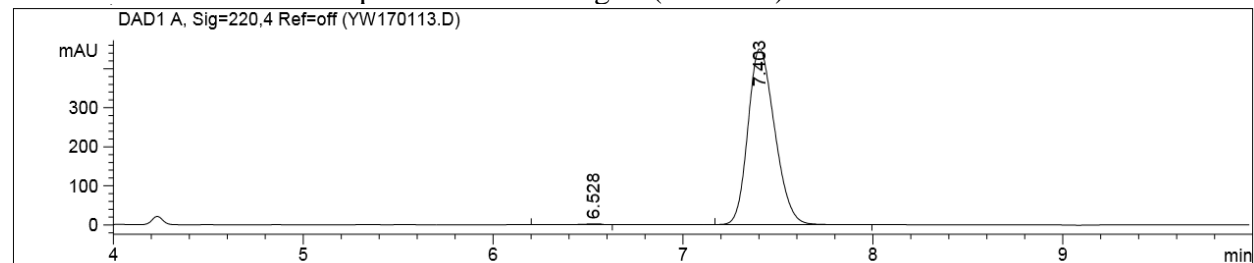


Signal 1: DAD1 A, Sig=220,4 Ref=off

| Peak # | RetTime [min] | Type | Width [min] | Area [mAU*s] | Height [mAU] | Area %  |
|--------|---------------|------|-------------|--------------|--------------|---------|
| 1      | 3.331         | BV   | 0.1014      | 718.39062    | 118.07276    | 8.3133  |
| 2      | 3.417         | VB   | 0.0828      | 811.55774    | 136.54472    | 9.3914  |
| 3      | 3.791         | BB   | 0.0559      | 8.58430      | 2.37522      | 0.0993  |
| 4      | 6.916         | BV   | 0.1332      | 3546.56641   | 415.06689    | 41.0413 |
| 5      | 7.450         | VB   | 0.1536      | 3556.35791   | 359.98453    | 41.1546 |

Table 4.2 Entry 17

(*R*)-**2e** HPLC2 trace from the cooperative enzymatic reduction of (62/38) (*E/Z*)-**1e** with 0.5% OPR1 and 1% **Ir-16** in the presence of blue light (>99% ee)



Signal 1: DAD1 A, Sig=220,4 Ref=off

| Peak # | RetTime [min] | Type | Width [min] | Area [mAU*s] | Height [mAU] | Area %  |
|--------|---------------|------|-------------|--------------|--------------|---------|
| 1      | 6.528         | BV   | 0.1219      | 14.56322     | 1.59437      | 0.3299  |
| 2      | 7.403         | VB   | 0.1519      | 4400.37158   | 450.33319    | 99.6701 |

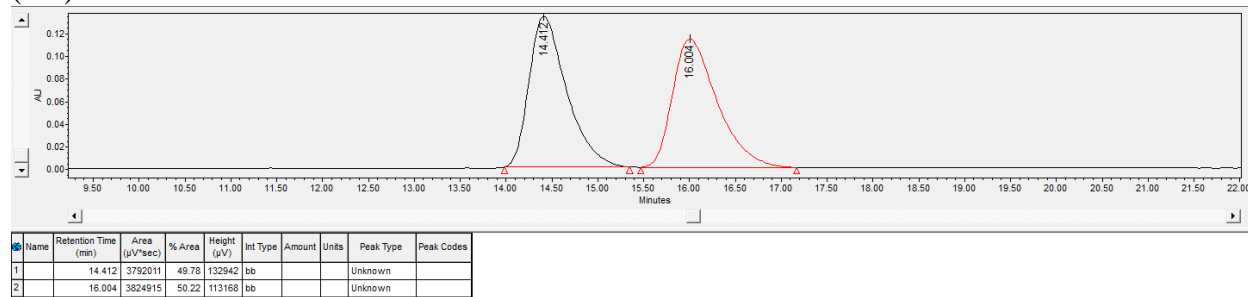
Table 4.1 Entry 9

Separation Method/Eluent:

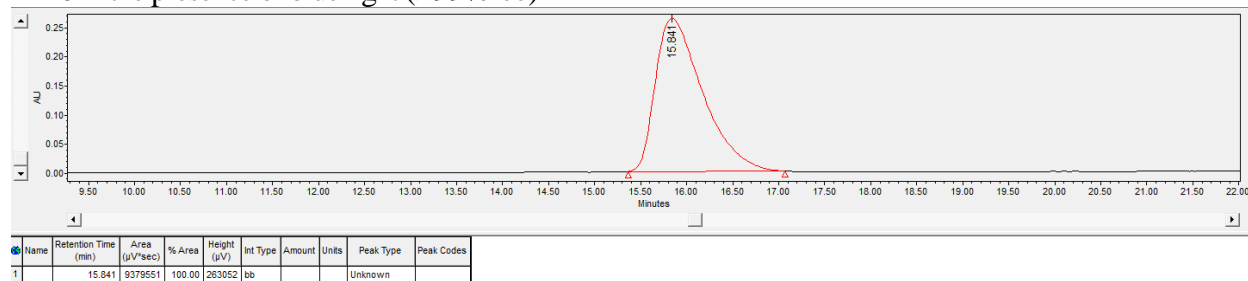
HPLC1 OJ-H, 1% iPrOH, 99% hexanes 1.0 mL/min, 220 nm;  $t_R$  (minor): 14.412 min,  $t_R$ (major): 16.004 min

Enantiomeric Excess = >99% ee

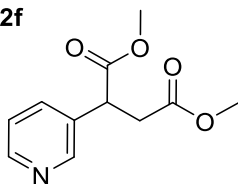
(rac)-2e HPLC1 trace



(R)-2e HPLC1 trace from prep-scale cooperative enzymatic reduction of 62:38 (E/Z)-1e with OPR1 and 1% Ir-16 in the presence of blue light (>99% ee)



2f



Separation Method/Eluent:

HPLC2 - OJ-H (250mm), 5% iPrOH, 95% hexanes 1.0 mL/min, 220 nm;  $t_R$  (minor): 28.321 min,  $t_R$ (major): 38.119

(rac)-**2f** HPLC2 trace

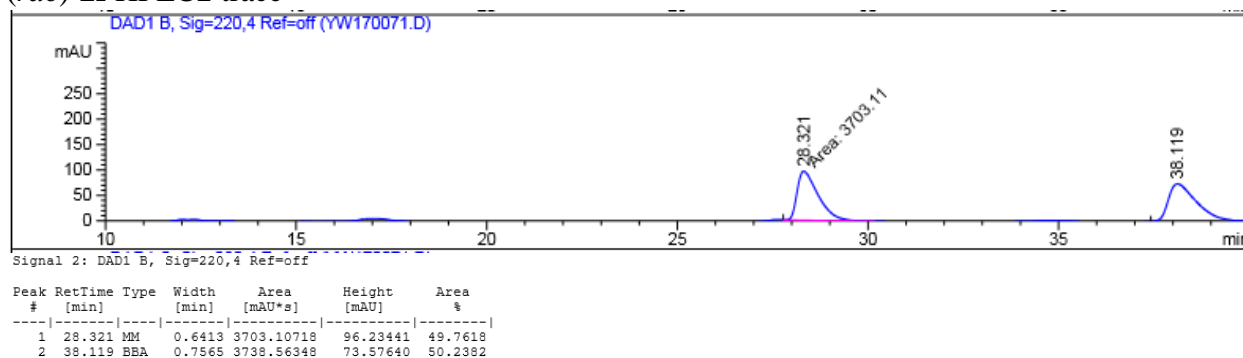


Table 4.2 Entry 19

(R)-**2f** HPLC2 trace from the cooperative enzymatic reduction of (61/39) (*E/Z*)-**1f** with 0.5% XenB and 5% FMN in the presence of blue light (87% ee)

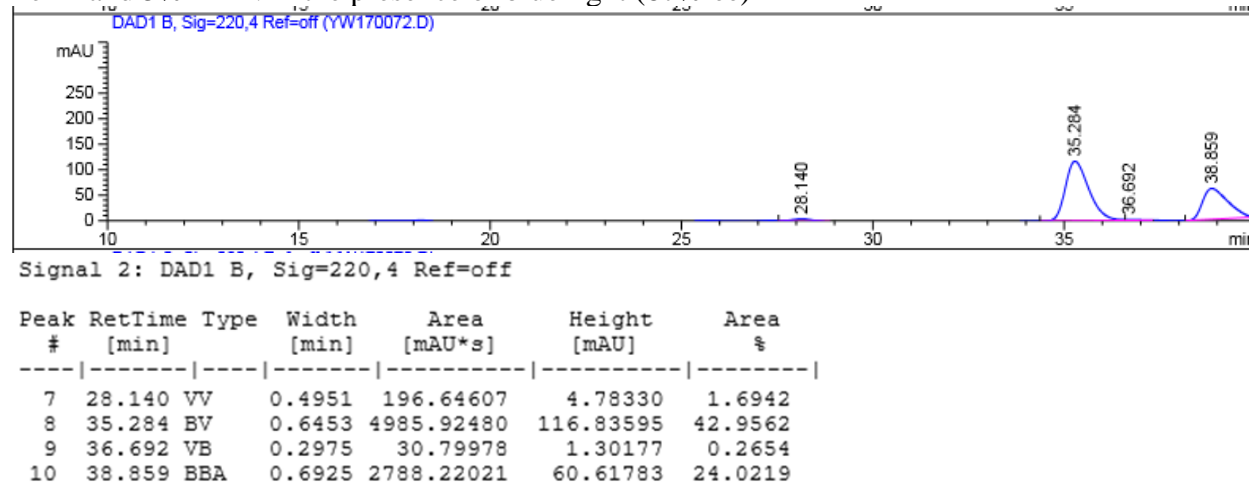


Table 4.2 Entry 20

(R)-**2f** HPLC2 trace from the cooperative enzymatic reduction of (61/39) (*E/Z*)-**1f** with 0.5% XenB and 1% **Ir-16** in the presence of blue light (91% ee)

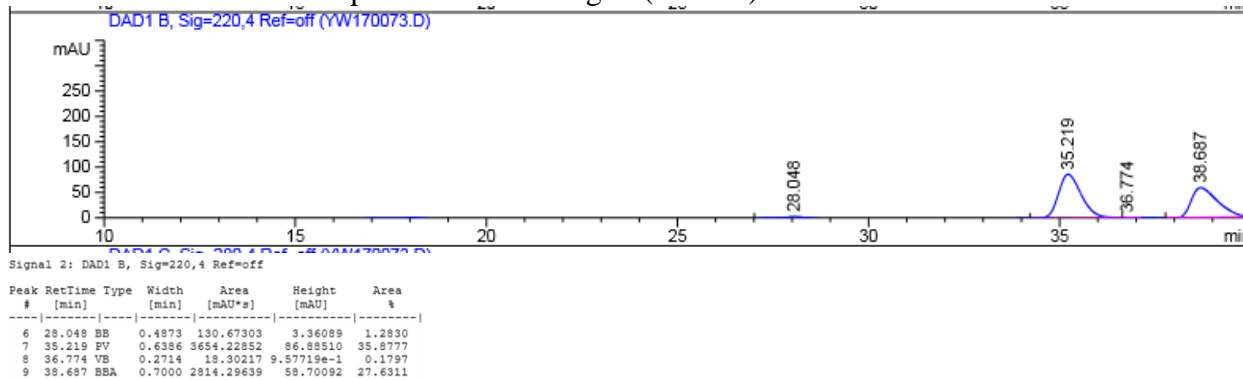


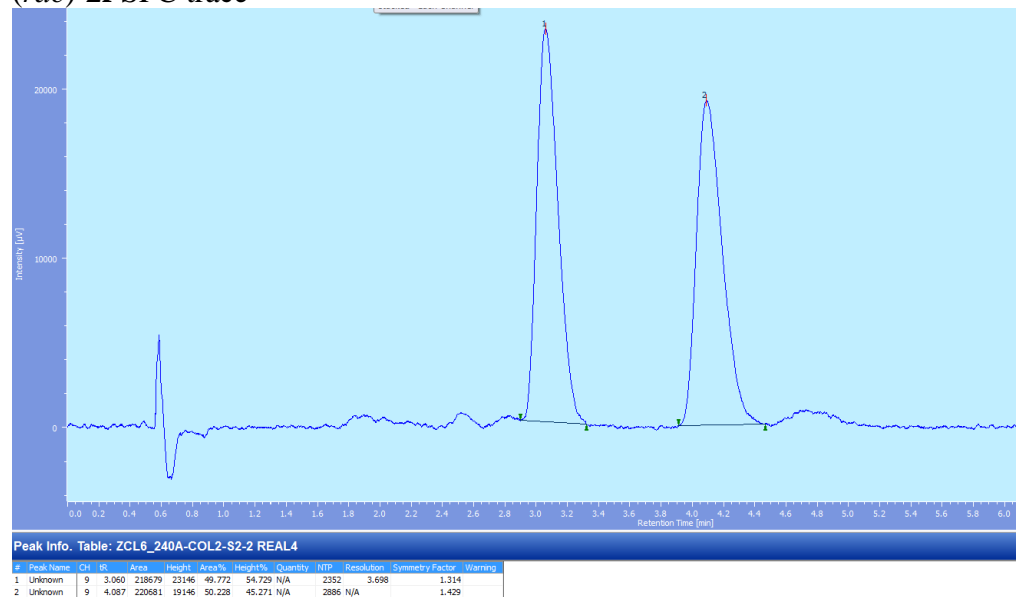
Table 4.1 Entry 10

Separation Method/Eluent:

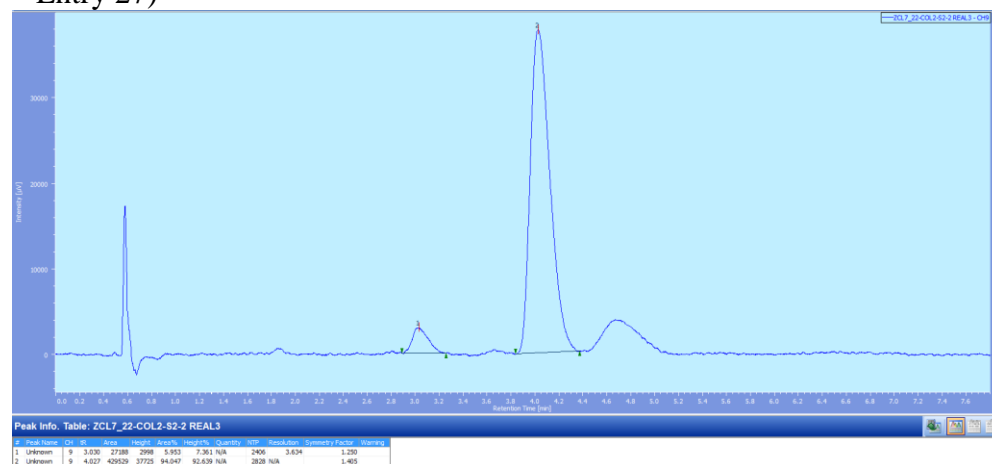
Chiral SFC - OD-H column, 2% iPrOH, 2.5 mL/min, 220 nm;  $t_R$  (minor): 3.060 min,  $t_R$ (major): 4.087

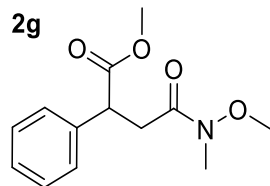
Enantiomeric Excess = 88% ee

(rac)-**2f** SFC trace



(*R*)-**2f** SFC trace from enzymatic reduction of 61:39 (*E/Z*)-**1f** with XenB (88% ee) (0.0330 g scale – Entry 27)

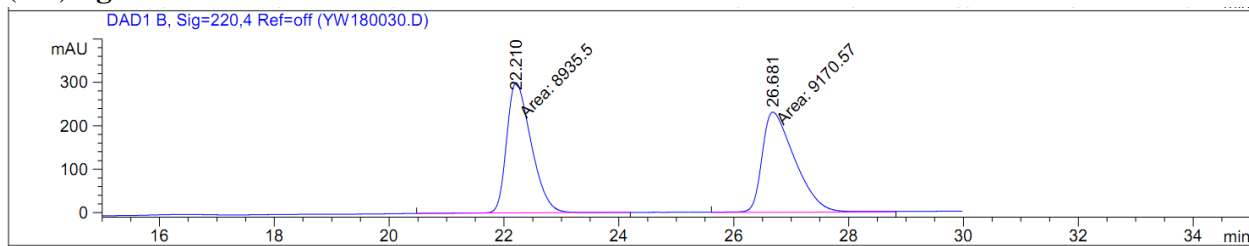




Separation Method/Eluent:

HPLC2 - OJ-H (250mm), 5% iPrOH, 95% hexanes 1.0 mL/min, 220 nm;  $t_R$  (minor): 22.210 min,  $t_R$ (major): 26.681

(rac)-**2g** HPLC2 trace

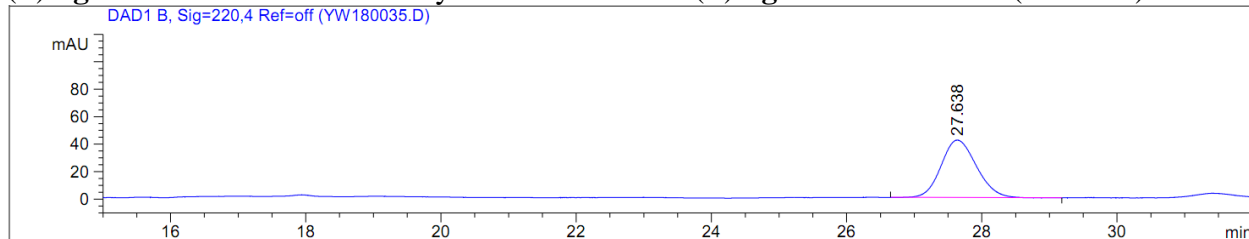


Signal 2: DAD1 B, Sig=220,4 Ref=off

| Peak # | RetTime [min] | Type | Width [min] | Area [mAU*s] | Height [mAU] | Area %  |
|--------|---------------|------|-------------|--------------|--------------|---------|
| 1      | 22.210        | MM   | 0.4963      | 8935.49512   | 300.04407    | 49.3508 |
| 2      | 26.681        | MM   | 0.6623      | 9170.57422   | 230.78772    | 50.6492 |

Table 4.1 Entry 11

(*R*)-**2g** HPLC2 trace from the enzymatic reduction of (*E*)-**1g** with 0.2% OPR1 (>99% ee)



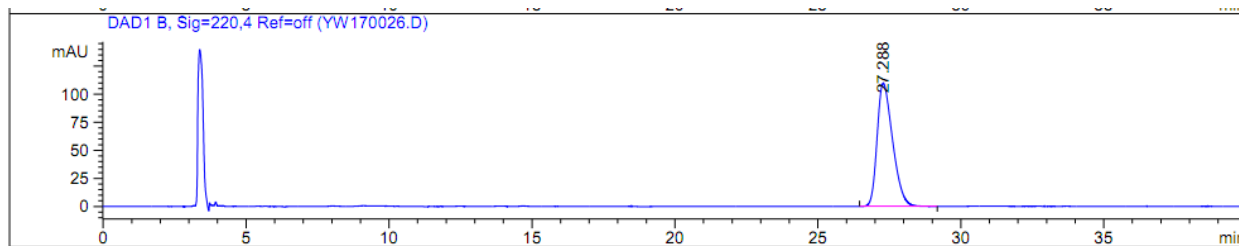
Signal 2: DAD1 B, Sig=220,4 Ref=off

| Peak # | RetTime [min] | Type | Width [min] | Area [mAU*s] | Height [mAU] | Area %   |
|--------|---------------|------|-------------|--------------|--------------|----------|
| 1      | 27.638        | BB   | 0.5687      | 1525.98437   | 41.84188     | 100.0000 |



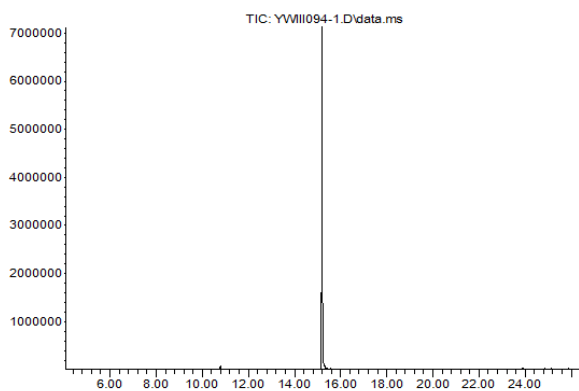
Table 4.2 Entry 23

(*R*)-**2g** HPLC2 trace from the cooperative enzymatic reduction of (*Z*)-**1g** with 0.5% OPR1 and 1% **Ir-16** in the presence of blue light (>99% ee)



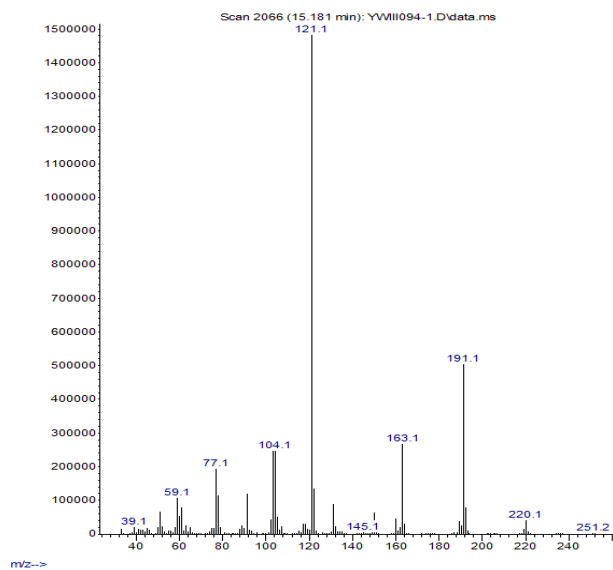
There is a shift in retention time of the major enantiomer compared to the same enantiomer on the HPLC trace of the racemic product. The identity of the product was confirmed by GC-MS:  
The GC trace of reaction:

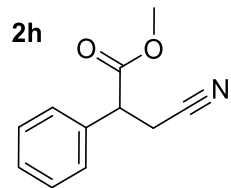
Abundance



The MS trace of the peak

Abundance

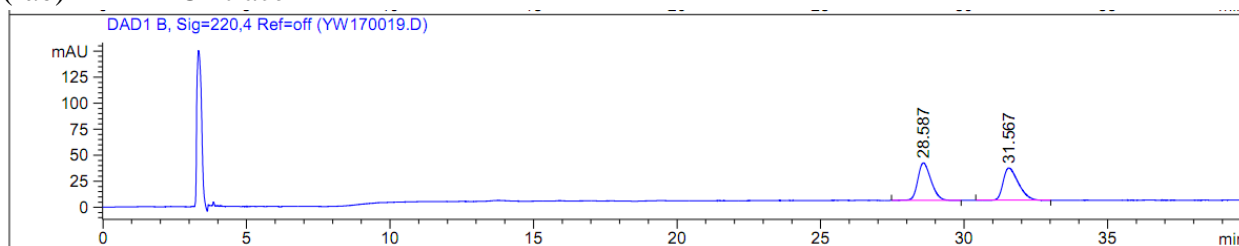




Separation Method/Eluent:

HPLC2 - OJ-H (250mm), 5% iPrOH, 95% hexanes 1.0 mL/min, 220 nm;  $t_R$  (minor): 28.587 min,  
 $t_R$ (major): 31.567

(*rac*)-**2h** HPLC2 trace

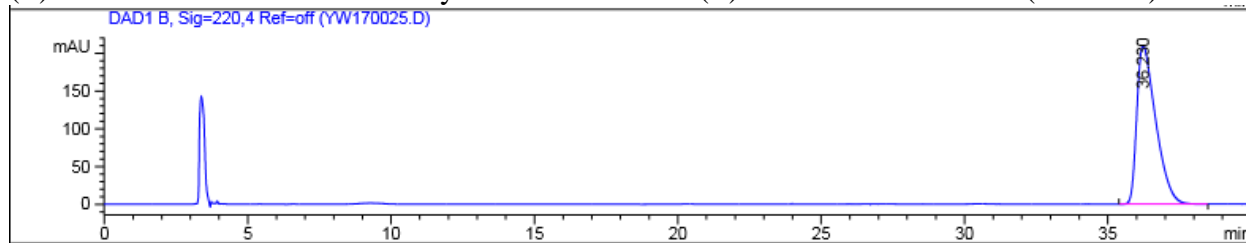


Signal 2: DAD1 B, Sig=220,4 Ref=off

| Peak # | RetTime [min] | Type | Width [min] | Area [mAU*s] | Height [mAU] | Area %  |
|--------|---------------|------|-------------|--------------|--------------|---------|
| 1      | 28.587        | BB   | 0.4975      | 1148.25806   | 35.90205     | 50.1490 |
| 2      | 31.567        | BB   | 0.5679      | 1141.43457   | 31.02990     | 49.8510 |

Table 4.1 Entry 13

(*R*)-**2h** HPLC2 trace from the enzymatic reduction of (*E*)-**1h** with 0.2% TOYE (>99% ee)



Signal 1: DAD1 A, Sig=254,4 Ref=off

| Peak # | RetTime [min] | Type | Width [min] | Area [mAU*s] | Height [mAU] | Area %   |
|--------|---------------|------|-------------|--------------|--------------|----------|
| 1      | 36.231        | BB   | 0.6471      | 406.29218    | 8.96259      | 100.0000 |

Table 4.2 Entry 25

(*R*)-**2h** HPLC2 trace from the cooperative enzymatic reduction of (*Z*)-**1h** with 0.2% TOYE and 1% FMN in the presence of blue light (>99% ee)

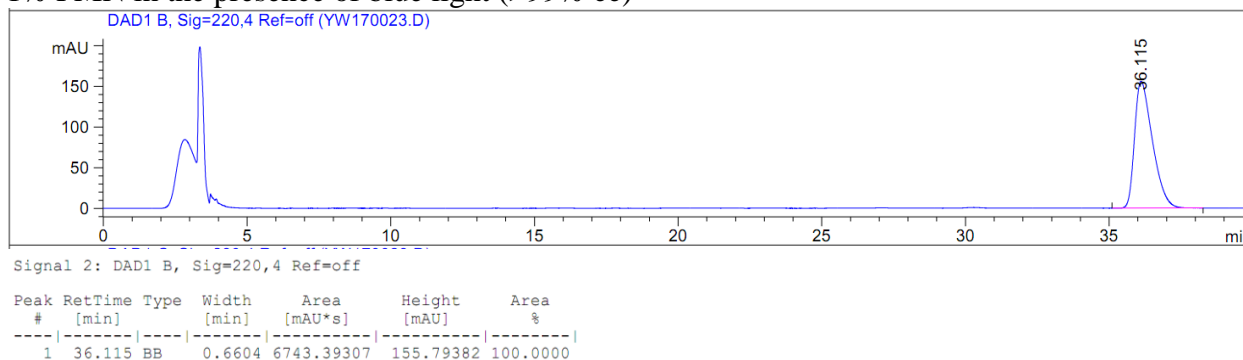
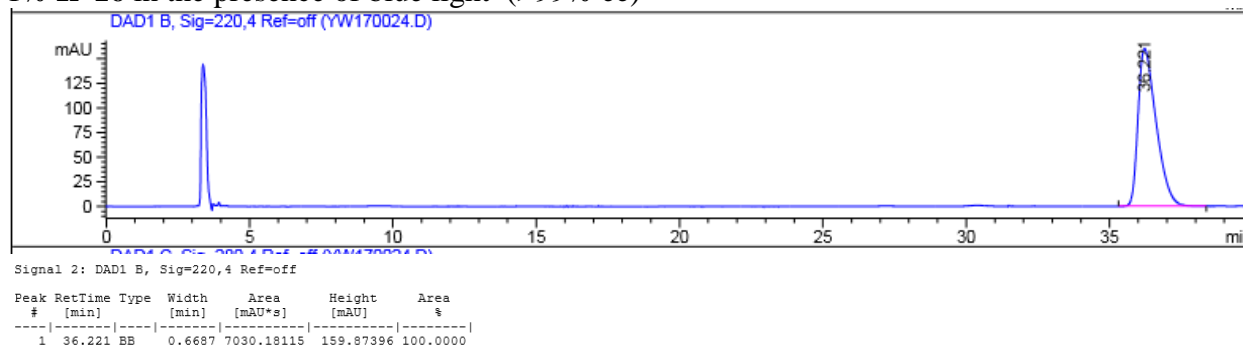


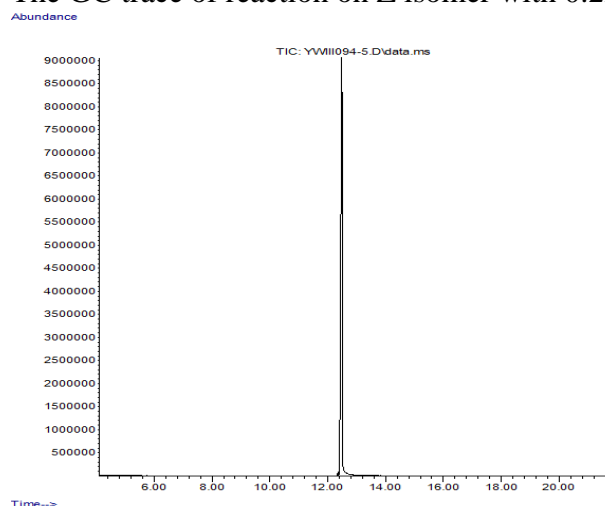
Table 4.2 Entry 26

(*R*)-**2h** HPLC2 trace from the cooperative enzymatic reduction of (*Z*)-**1h** with 0.2% TOYE and 1% **Ir-16** in the presence of blue light (>99% ee)

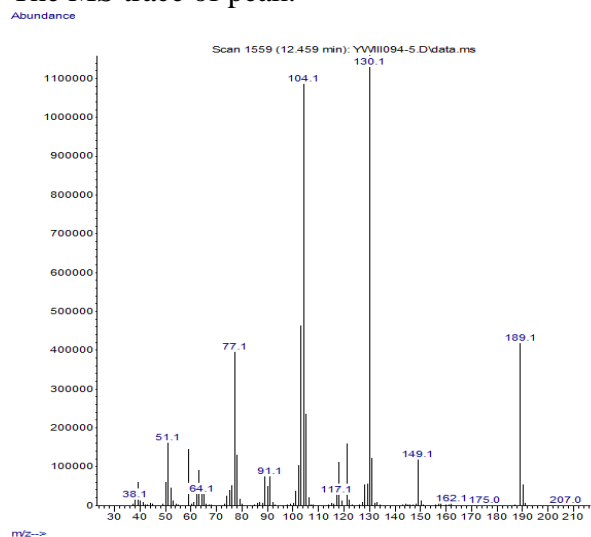


There is a significant shift in retention time of the major enantiomer compared to the same enantiomer on the HPLC trace of the racemic product. The identity of the product was confirmed by GC-MS:

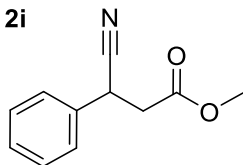
The GC trace of reaction on Z isomer with 0.2mol% TOYE/1mol% Ir-16



## The MS trace of peak:



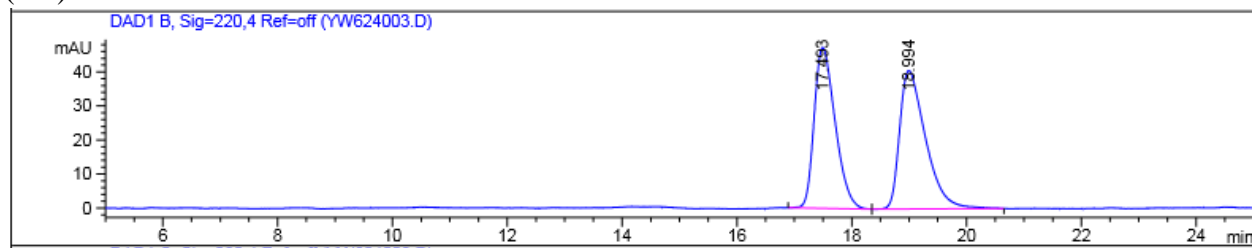
2i



## Separation Method/Eluent:

HPLC2 - OJ-H (150mm), 5% iPrOH, 95% hexanes 0.8 mL/min, 220 nm;  $t_R$  (minor): 17.493 min,  
 $t_R$ (major): 18.994

## (rac)-2i HPLC2 trace

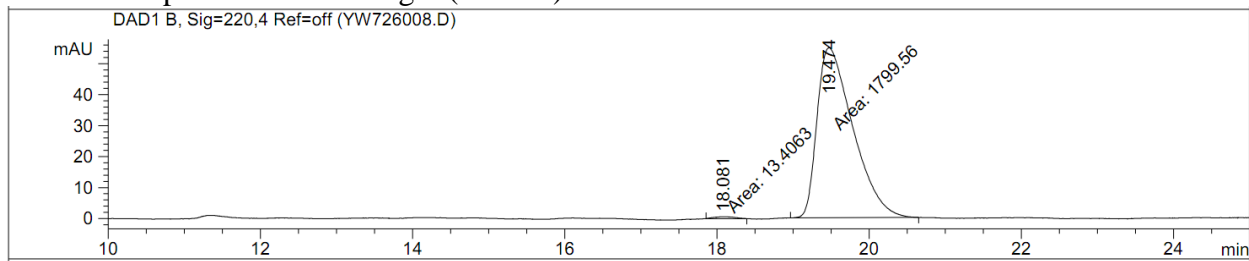


Signal 2: DAD1 B, Sig=220,4 Ref=off

| Peak # | RetTime [min] | Type | Width [min] | Area [mAU*s] | Height [mAU] | Area %  |
|--------|---------------|------|-------------|--------------|--------------|---------|
| 1      | 17.493        | BV   | 0.3895      | 1200.27295   | 47.25861     | 48.4886 |
| 2      | 18.994        | PB   | 0.4675      | 1275.09692   | 40.62315     | 51.5114 |

Table 4.2 Entry 28

(R)-**2i** HPLC2 trace from the cooperative enzymatic reduction of (Z)-**1i** with 0.2% OYE2 and 1% FMN in the presence of blue light (99% ee)

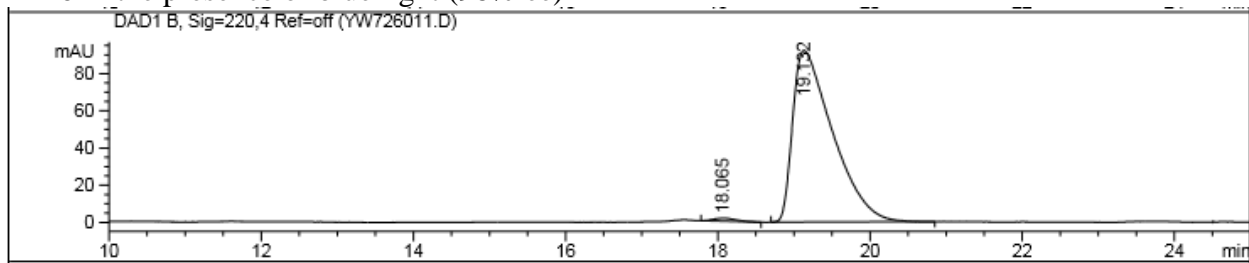


Signal 2: DAD1 B, Sig=220,4 Ref=off

| Peak # | RetTime [min] | Type | Width [min] | Area [mAU*s] | Height [mAU] | Area %  |
|--------|---------------|------|-------------|--------------|--------------|---------|
| 1      | 18.081        | MM   | 0.3287      | 13.40635     | 6.79728e-1   | 0.7395  |
| 2      | 19.474        | MM   | 0.5464      | 1799.56384   | 54.88877     | 99.2605 |

Table 4.2 Entry 29

(R)-**2i** HPLC2 trace from the cooperative enzymatic reduction of (Z)-**1i** with 0.2% OYE2 and 1% **Ir-16** in the presence of blue light (98% ee)

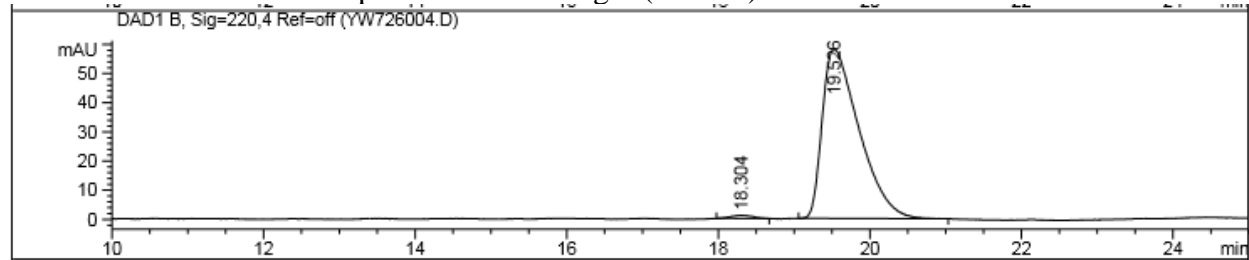


Signal 2: DAD1 B, Sig=220,4 Ref=off

| Peak # | RetTime [min] | Type | Width [min] | Area [mAU*s] | Height [mAU] | Area %  |
|--------|---------------|------|-------------|--------------|--------------|---------|
| 1      | 18.065        | BB   | 0.2611      | 32.63350     | 1.62785      | 0.9601  |
| 2      | 19.132        | BB   | 0.5146      | 3366.23413   | 92.22581     | 99.0399 |

Table 4.2 Entry 30

(R)-**2i** HPLC2 trace from the cooperative enzymatic reduction of (50/50) (E/Z)-**1i** with 0.2% OYE2 and 1% FMN in the presence of blue light (98% ee)

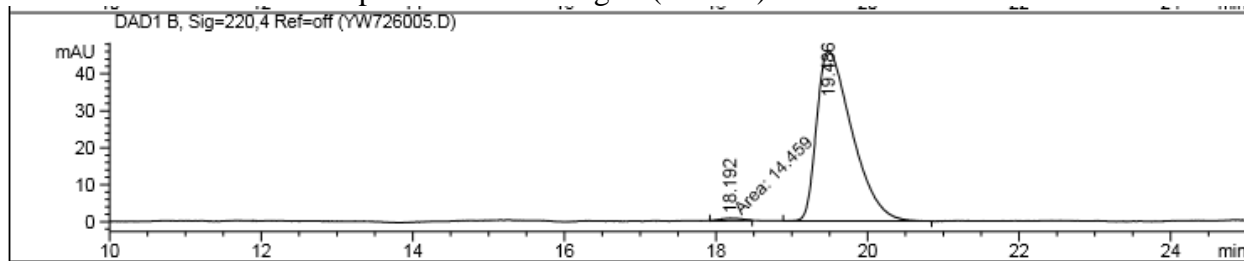


Signal 2: DAD1 B, Sig=220,4 Ref=off

| Peak # | RetTime [min] | Type | Width [min] | Area [mAU*s] | Height [mAU] | Area %  |
|--------|---------------|------|-------------|--------------|--------------|---------|
| 1      | 18.304        | BB   | 0.2690      | 22.94963     | 1.11192      | 1.1542  |
| 2      | 19.526        | BB   | 0.4934      | 1965.46912   | 58.13927     | 98.8458 |

Table 4.2 Entry 31

(*R*)-**2i** HPLC2 trace from the cooperative enzymatic reduction of (50/50) (*E/Z*)-**1i** with 0.2% OYE2 and 1% **Ir-16** in the presence of blue light (98% ee)



Signal 2: DAD1 B, Sig=220,4 Ref=off

| Peak # | RetTime [min] | Type | Width [min] | Area [mAU*s] | Height [mAU] | Area %  |
|--------|---------------|------|-------------|--------------|--------------|---------|
| 1      | 18.192        | MM   | 0.3357      | 14.45899     | 7.17812e-1   | 0.9598  |
| 2      | 19.486        | BV   | 0.4506      | 1491.97351   | 45.96968     | 99.0402 |

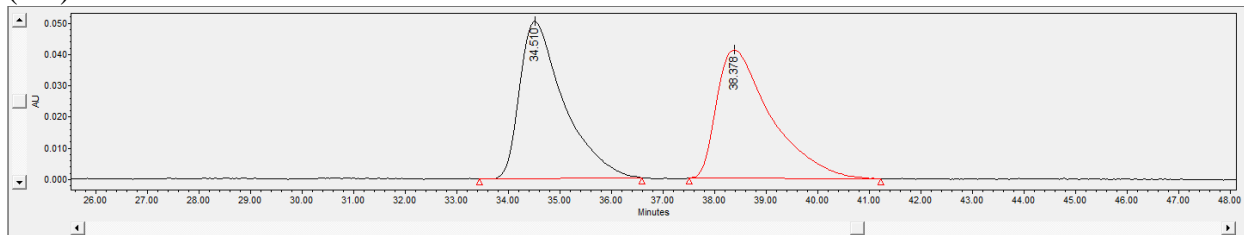
Table 4.1 Entry 15

Separation Method/Eluent:

HPLC1 - OJ-H column, 5% iPrOH, 95% hexanes 1.0 mL/min, 220 nm;  $t_R$  (minor): 34.510 min,  $t_R$  (major): 38.378

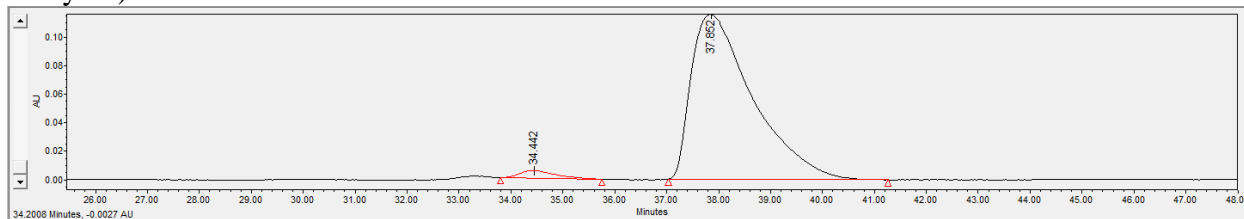
Enantiomeric Excess = 94%

(*rac*)-**2i** HPLC1 trace

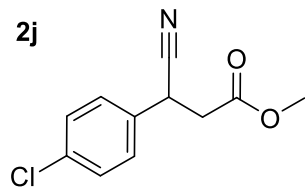


| Name | Retention Time (min) | Area (μV*sec) | % Area | Height (μV) | Int Type | Amount | Units | Peak Type | Peak Codes |
|------|----------------------|---------------|--------|-------------|----------|--------|-------|-----------|------------|
| 1    | 34.510               | 2989913       | 49.93  | 50293       | bb       |        |       | Unknown   |            |
| 2    | 38.378               | 2995162       | 50.07  | 41041       | bb       |        |       | Unknown   |            |

(*R*)-**2i** HPLC1 trace from enzymatic reduction of (*E*)-**1i** with OYE2 (94% ee) (0.0234 g scale – Entry 41)

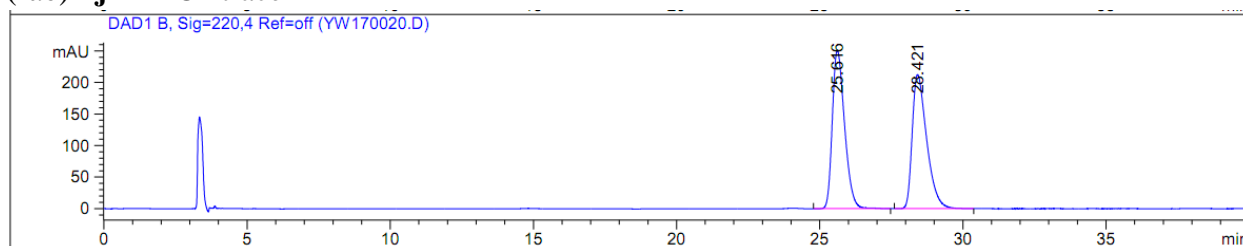


| Name | Retention Time (min) | Area (μV*sec) | % Area | Height (μV) | Int Type | Amount | Units | Peak Type | Peak Codes |
|------|----------------------|---------------|--------|-------------|----------|--------|-------|-----------|------------|
| 1    | 34.442               | 268352        | 2.76   | 5471        | bb       |        |       | Unknown   |            |
| 2    | 37.852               | 9450282       | 97.24  | 115484      | bb       |        |       | Unknown   |            |

**2j**

Separation Method/Eluent:

HPLC2 - OJ-H (250mm), 5% iPrOH, 95% hexanes 1.0 mL/min, 220 nm;  $t_R$  (minor): 25.616 min,  
 $t_R$ (major): 28.421

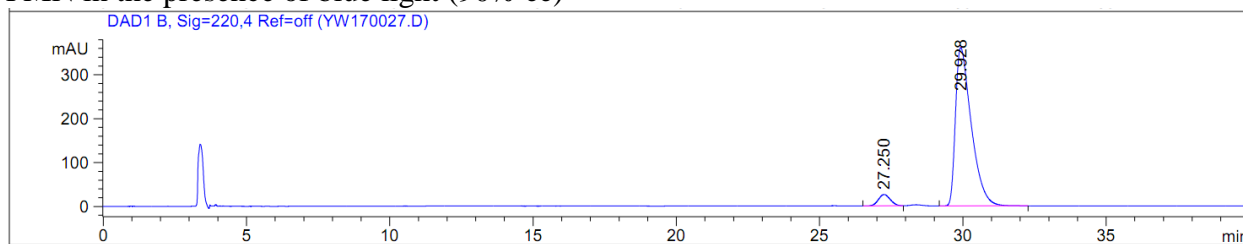
**(rac)-2j** HPLC2 trace

Signal 2: DAD1 B, Sig=220,4 Ref=off

| Peak # | RetTime [min] | Type | Width [min] | Area [mAU*s] | Height [mAU] | Area %  |
|--------|---------------|------|-------------|--------------|--------------|---------|
| 1      | 25.616        | BB   | 0.4601      | 7464.79687   | 250.73517    | 50.0733 |
| 2      | 28.421        | BB   | 0.5349      | 7442.94482   | 212.52840    | 49.9267 |

**Table 4.2 Entry 33**

**(R)-2j** HPLC2 trace from the cooperative enzymatic reduction of **(Z)-1j** with 0.5% OYE2 and 5% FMN in the presence of blue light (90% ee)



Signal 2: DAD1 B, Sig=220,4 Ref=off

| Peak # | RetTime [min] | Type | Width [min] | Area [mAU*s] | Height [mAU] | Area %  |
|--------|---------------|------|-------------|--------------|--------------|---------|
| 1      | 27.250        | BV   | 0.4509      | 746.38000    | 25.95320     | 5.1280  |
| 2      | 29.928        | BB   | 0.5760      | 1.38087e4    | 361.02124    | 94.8720 |

Table 4.2 Entry 34

(*R*)-**2j** HPLC2 trace from the cooperative enzymatic reduction of (*Z*)-**1j** with 0.5% OYE2 and 5% Ir-16 in the presence of blue light (91% ee)

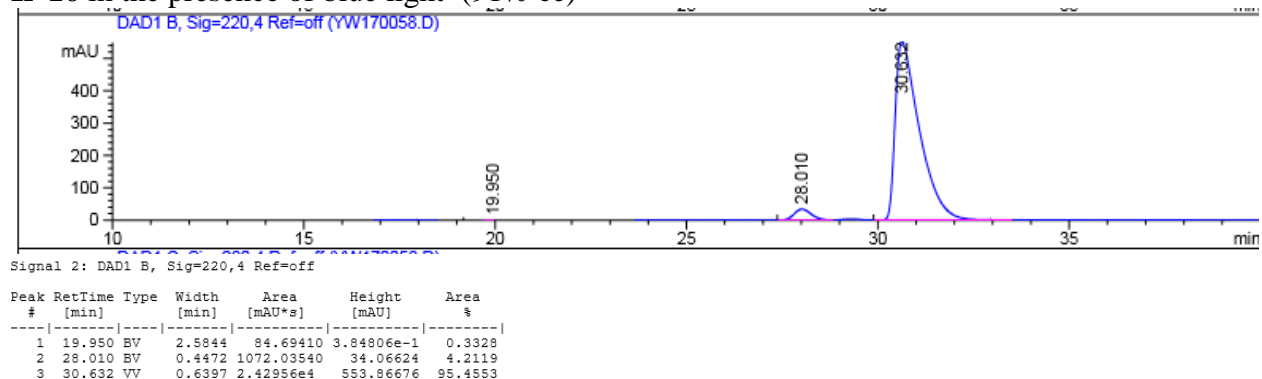
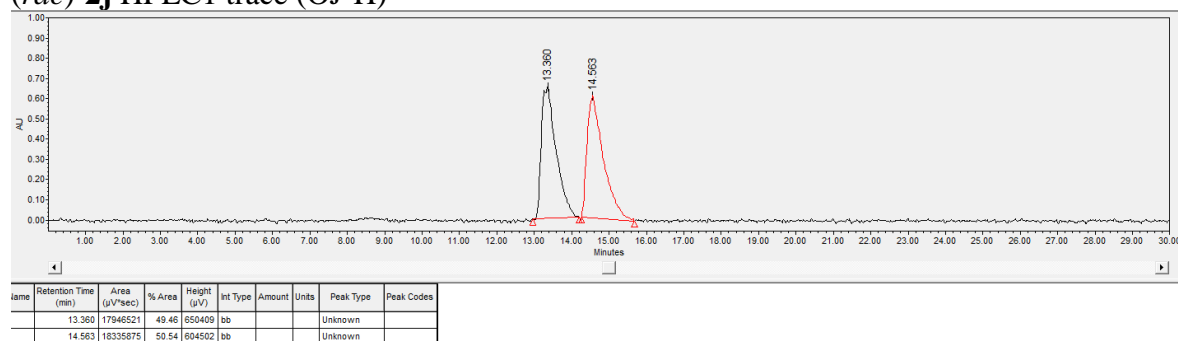


Table 4.1 Entry 17

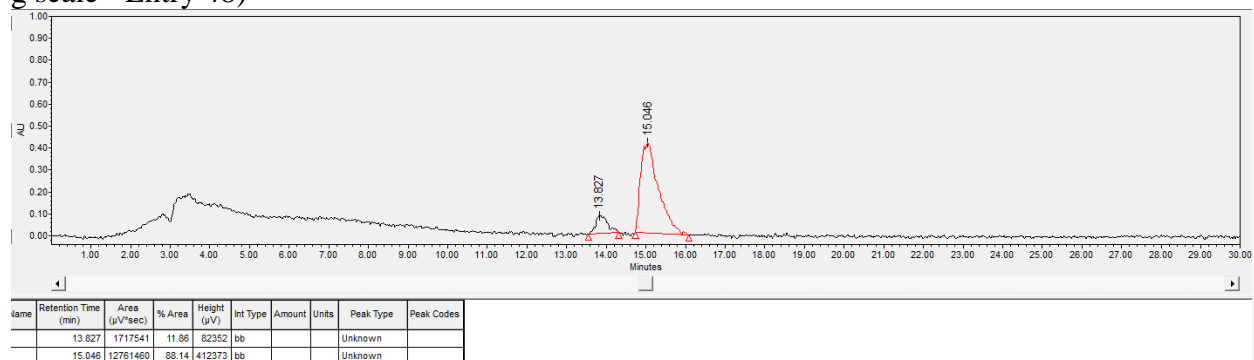
Separation Method/Eluent:

HPLC1 – OJ-H, 10% iPrOH, 90% hexanes 1.0 mL/min, 220 nm;  $t_R$  (minor): 13.360 min,  $t_R$ (major): 14.563

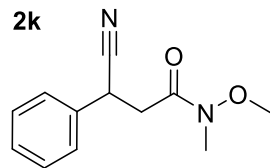
(*rac*)-**2j** HPLC1 trace (OJ-H)



(*R*)-**2j** HPLC1 (OD-H) trace from the enzymatic reduction of (*E*)-**1j** with OYE2 (76% ee) (0.0221 g scale - Entry 48)







Separation Method/Eluent:

HPLC2 - OJ-H (250mm), 5% iPrOH, 95% hexanes 1.0 mL/min, 220 nm;  $t_R$  (minor): 33.103 min,  $t_R$ (major): 35.794

(*rac*)-**2k** HPLC2 trace

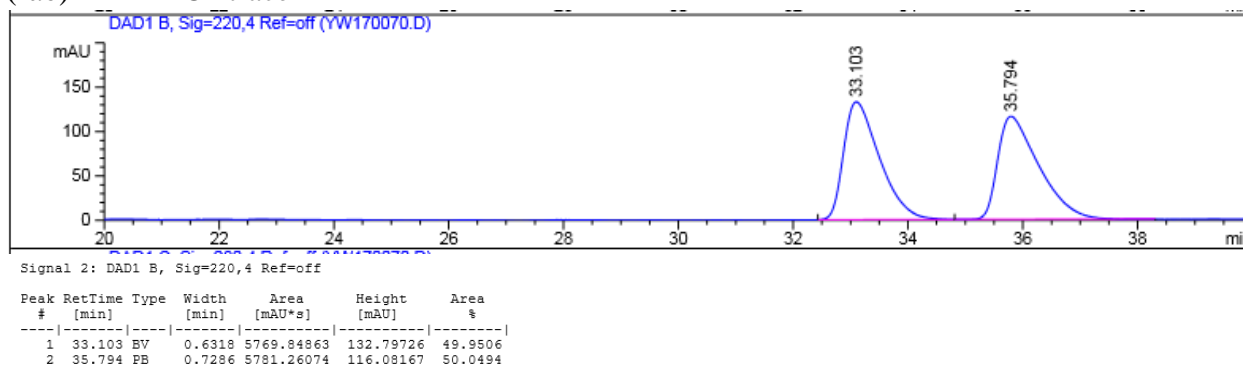


Table 4.1 Entry 19

(*R*)-**2k** HPLC2 trace from the enzymatic reduction of (*E*)-**1k** with 0.2% YersER (99% ee)

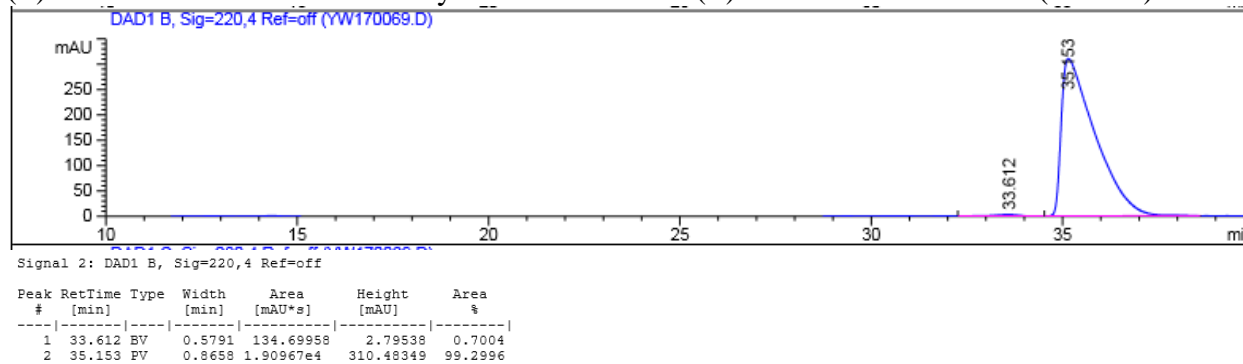


Table 4.2 Entry 36

(*R*)-**2k** HPLC2 trace from the cooperative enzymatic reduction of (*Z*)-**1k** with 0.2% YersER and 5% FMN in the presence of blue light (99% ee)

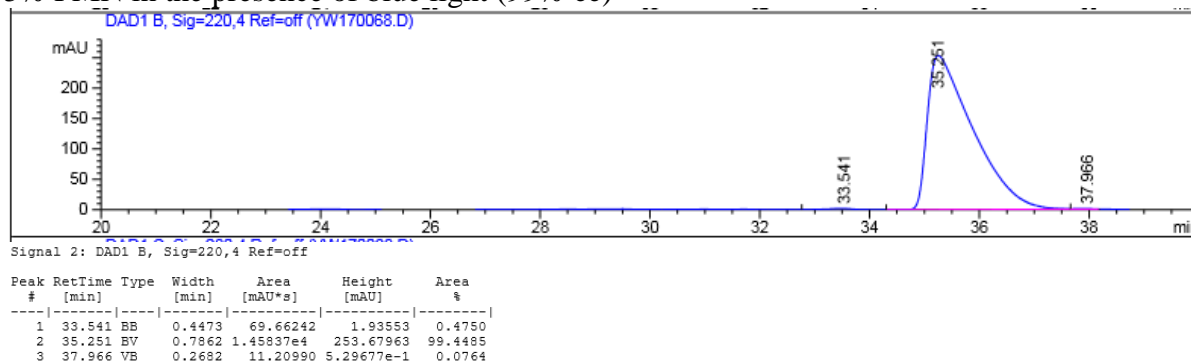
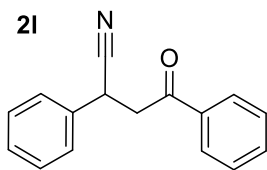
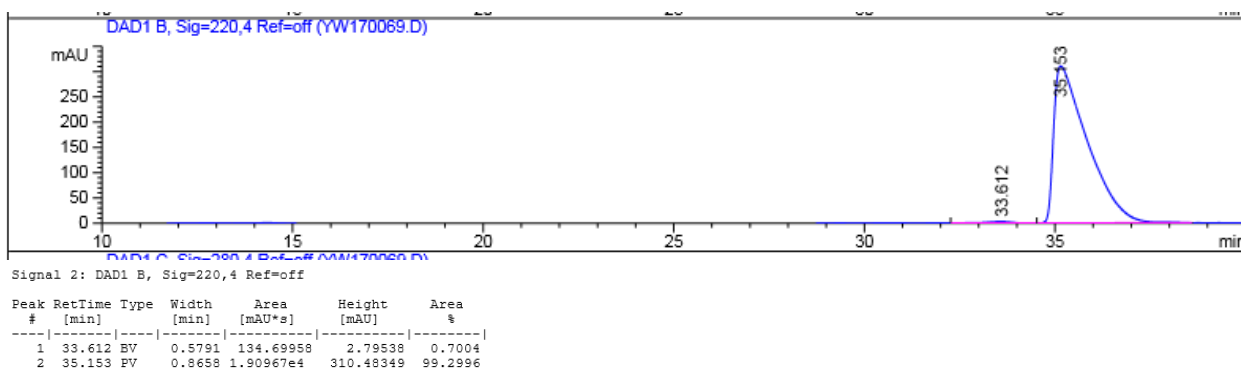


Table 4.2 Entry 37

(*R*)-**2k** HPLC2 trace from the cooperative enzymatic reduction of (*Z*)-**1k** with 0.2% YersER and 1% **Ir-16** in the presence of blue light (99% ee)



Separation Method/Eluent:

HPLC2 - OJ-H (250mm), 10% iPrOH, 90% hexanes 1.0 mL/min, 220 nm;  $t_R$  (minor): 33.295 min,  $t_R$ (major): 39.70

(*rac*)-**21** HPLC2 trace

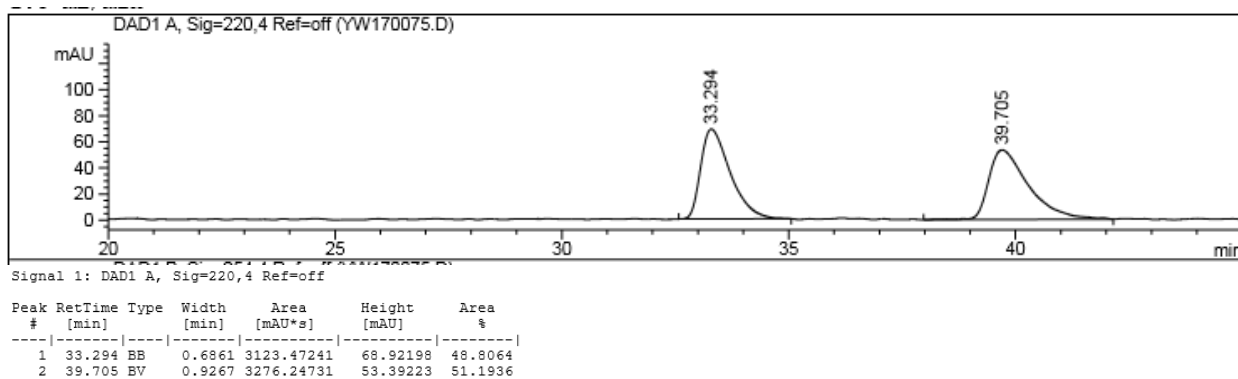


Table 4.2 Entry 37

(R)-**21** HPLC2 trace from the stereoconvergent enzymatic reduction of (Z)-**11** with 0.2% OYE2 in the presence of blue light (>99% ee)

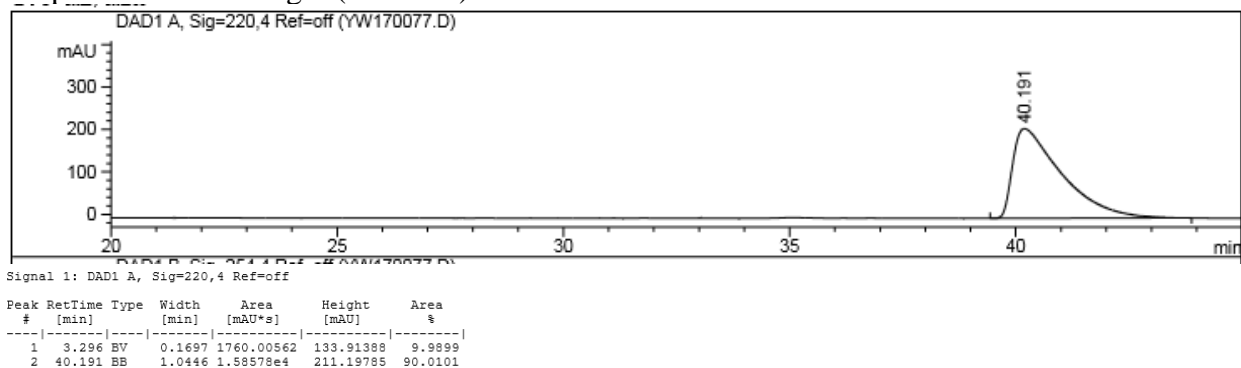


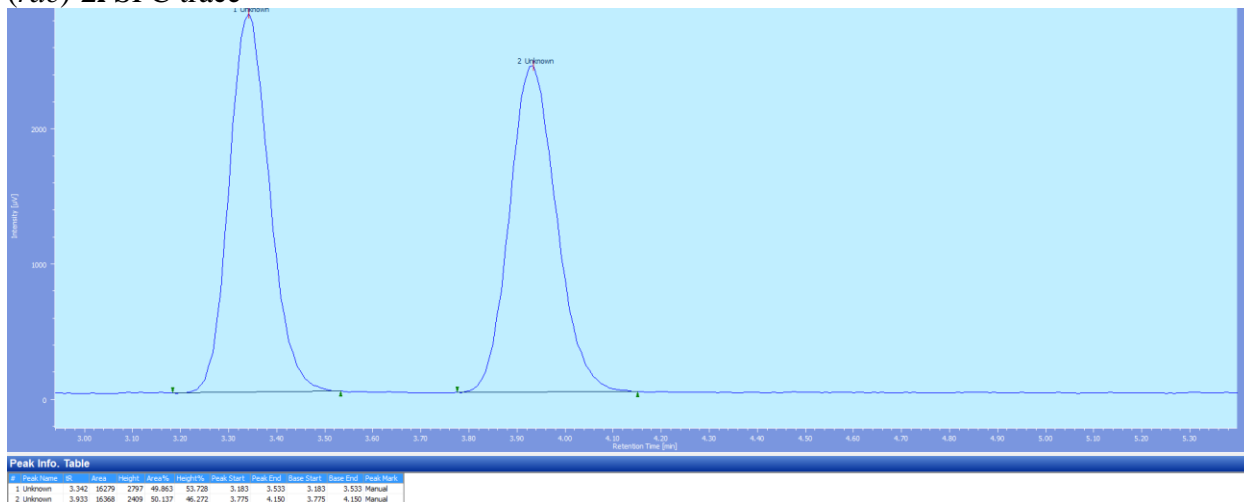
Table 4.1 Entry 21

Separation Method/Eluent:

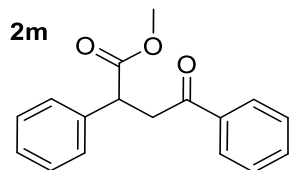
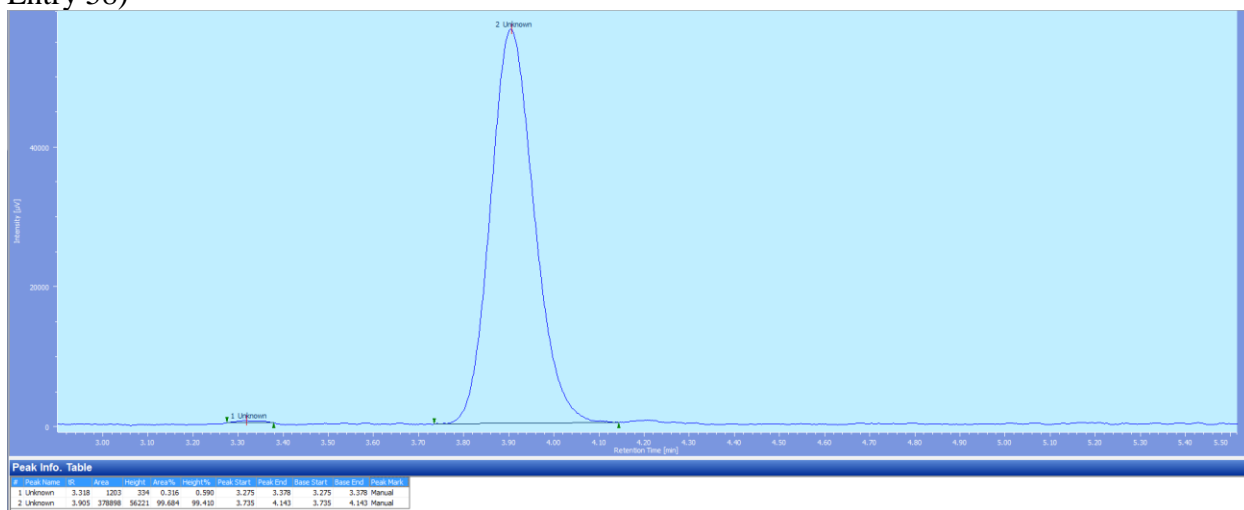
SFC - OD-H column, 10% MeOH, 2.5 mL/min, 220 nm;  $t_R$  (minor): 3.342 min,  $t_R$ (major): 3.933 min

Enantiomeric Excess = 99%

(rac)-**21** SFC trace



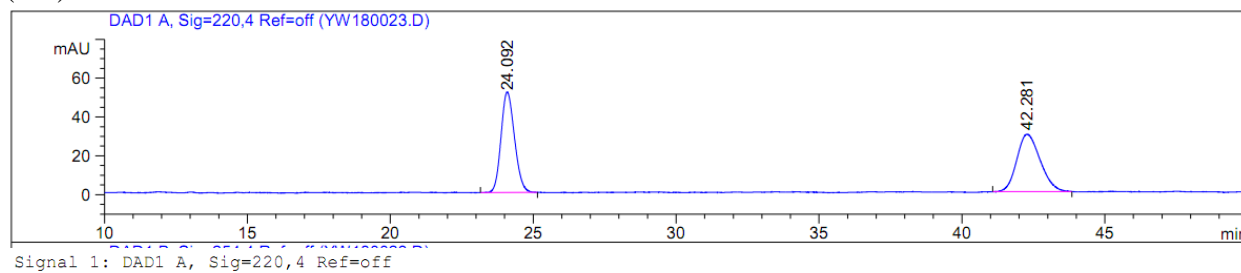
(*R*)-**2l** SFC trace from the enzymatic reduction of (*E*)-**1l** with OYE2 (99% ee) (0.0175 g scale – Entry 58)



Separation Method/Eluent:

HPLC2 - OJ-H (250mm), 10% iPrOH, 90% hexanes 1.0 mL/min, 254 nm/220 nm;  $t_R$  (major): 24.092 min,  $t_R$ (minor): 42.281

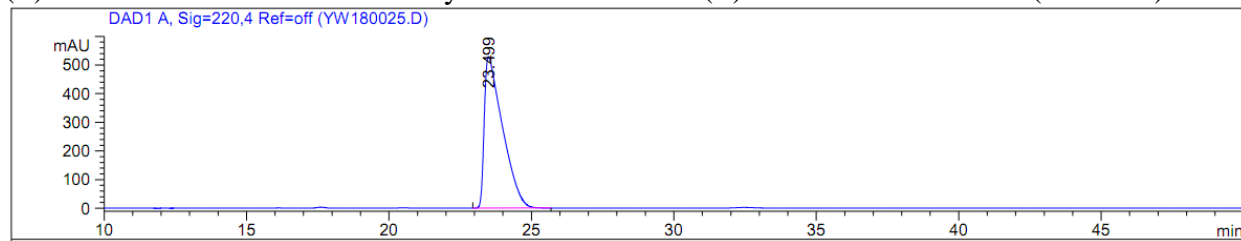
(*rac*)-**2m** HPLC2 trace



| Peak # | RetTime [min] | Type | Width [min] | Area [mAU*s] | Height [mAU] | Area %  |
|--------|---------------|------|-------------|--------------|--------------|---------|
| 1      | 24.092        | BB   | 0.5112      | 1698.27173   | 51.71969     | 50.1899 |
| 2      | 42.281        | BB   | 0.8837      | 1685.42236   | 29.59173     | 49.8101 |

Table 4.1 Entry 23

(*R*)-**2m** HPLC2 trace from the enzymatic reduction of (*E*)-**1m** with 0.2% OPR1 (>99% ee)

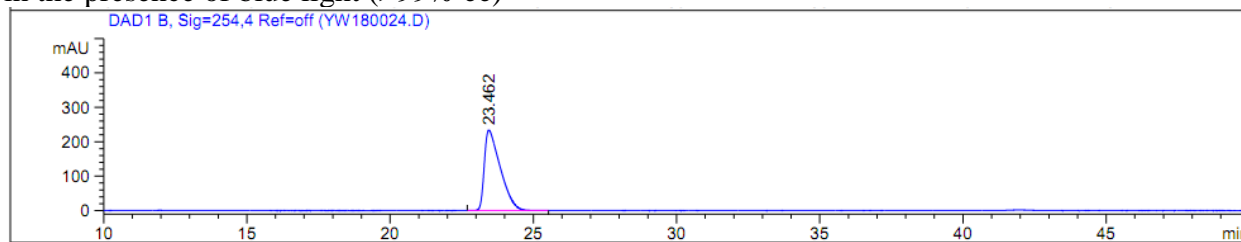


Signal 1: DAD1 A, Sig=220,4 Ref=off

| Peak # | RetTime [min] | Type | Width [min] | Area [mAU*s] | Height [mAU] | Area %   |
|--------|---------------|------|-------------|--------------|--------------|----------|
| 1      | 23.499        | BB   | 0.6447      | 2.35440e4    | 528.33453    | 100.0000 |

Table 4.2 Entry 41

(*R*)-**2m** HPLC2 trace from the stereoconvergent enzymatic reduction of (*Z*)-**1m** with 0.5% OPR1 in the presence of blue light (>99% ee)

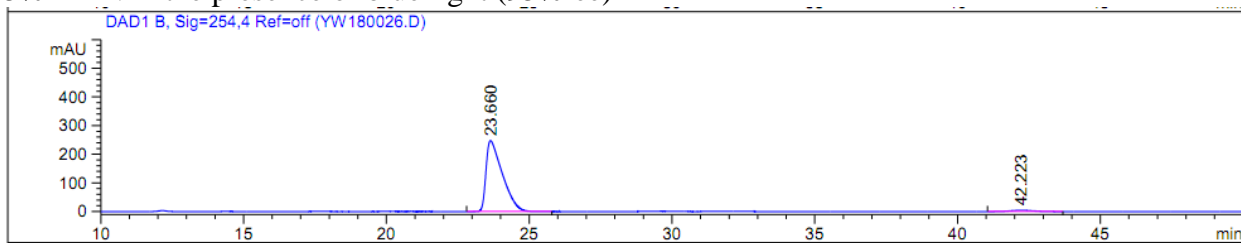


Signal 1: DAD1 A, Sig=220,4 Ref=off

| Peak # | RetTime [min] | Type | Width [min] | Area [mAU*s] | Height [mAU] | Area %  |
|--------|---------------|------|-------------|--------------|--------------|---------|
| 1      | 3.185         | BB   | 0.1597      | 289.13483    | 41.55252     | 2.0723  |
| 2      | 23.455        | BB   | 0.5663      | 1.36629e4    | 356.74902    | 97.9277 |

Table 4.2 Entry 42

(*R*)-**2m** HPLC2 trace from the cooperative enzymatic reduction of (*Z*)-**1m** with 0.5% OPR1 and 5% FMN in the presence of blue light (95% ee)

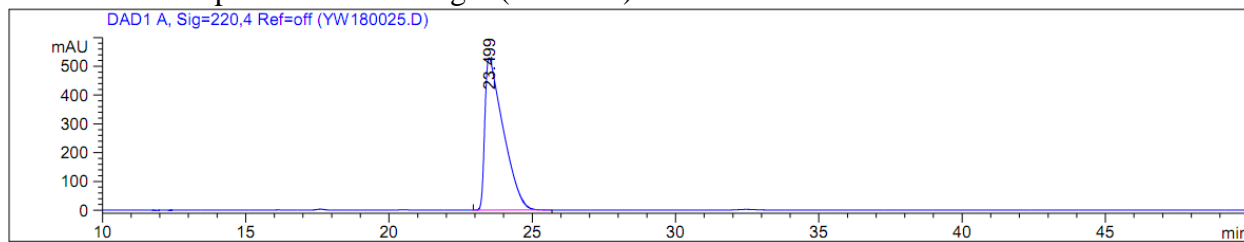


Signal 2: DAD1 B, Sig=254,4 Ref=off

| Peak # | RetTime [min] | Type | Width [min] | Area [mAU*s] | Height [mAU] | Area %  |
|--------|---------------|------|-------------|--------------|--------------|---------|
| 1      | 23.660        | BB   | 0.5894      | 9806.12695   | 246.48622    | 97.7189 |
| 2      | 42.223        | BB   | 0.8695      | 228.90616    | 4.12153      | 2.2811  |

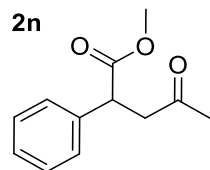
Table 4.2 Entry 43

(*R*)-**2m** HPLC2 trace from the cooperative enzymatic reduction of (*Z*)-**1m** with 0.5% OPR1 and 1% **Ir-16** in the presence of blue light (>99% ee)



Signal 1: DAD1 A, Sig=220,4 Ref=off

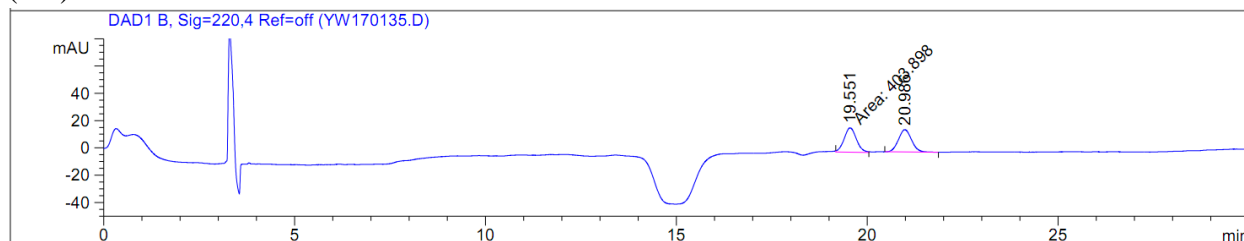
| Peak # | RetTime [min] | Type | Width [min] | Area [mAU*s] | Height [mAU] | Area %   |
|--------|---------------|------|-------------|--------------|--------------|----------|
| 1      | 23.499        | BB   | 0.6447      | 2.35440e4    | 528.33453    | 100.0000 |



Separation Method/Eluent:

HPLC2 - OJ-H (250mm), 5% iPrOH, 95% hexanes 1.0 mL/min, 220 nm;  $t_R$  (major): 19.551 min,  $t_R$  (minor): 20.986

(*rac*)-**2n** HPLC2 trace



Signal 2: DAD1 B, Sig=220,4 Ref=off

| Peak # | RetTime [min] | Type | Width [min] | Area [mAU*s] | Height [mAU] | Area %  |
|--------|---------------|------|-------------|--------------|--------------|---------|
| 1      | 19.551        | MM   | 0.3759      | 403.89783    | 17.91004     | 50.5874 |
| 2      | 20.986        | BV   | 0.3756      | 394.51770    | 16.38863     | 49.4126 |

Table 4.1 Entry 25

(*S*)-**2n** HPLC2 trace from the enzymatic reduction of (*E*)-**1n** with 0.2% SYE1 (89% ee)

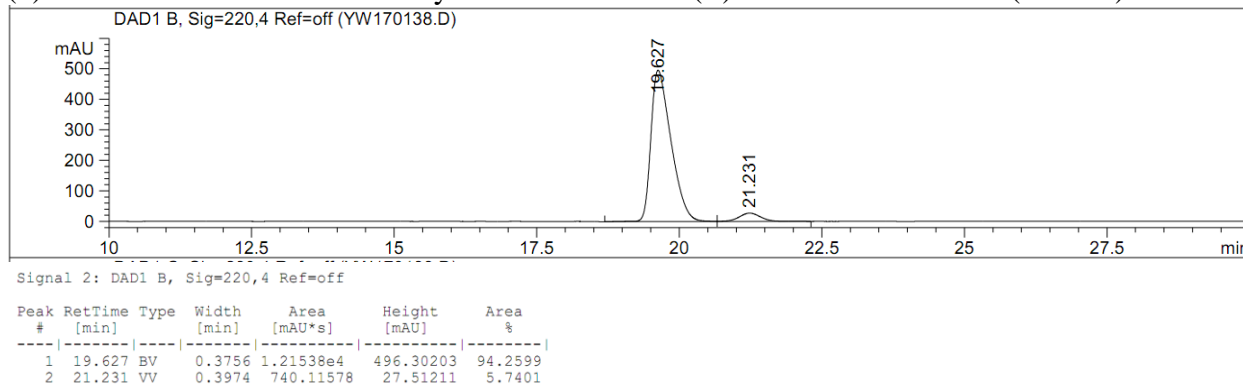


Table 4.2 Entry 45

(*S*)-**2n** HPLC2 trace from the cooperative enzymatic reduction of (*Z*)-**1n** with 0.5% SYE1 and 5% FMN in the presence of blue light (76% ee)

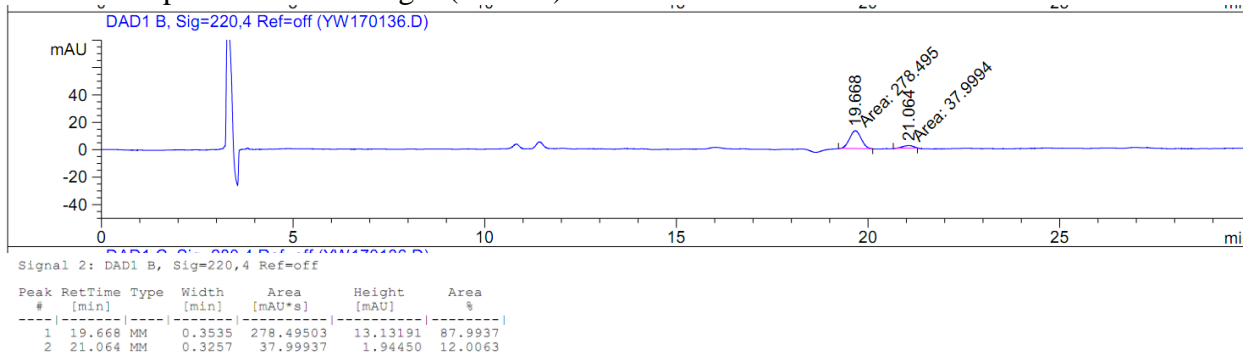
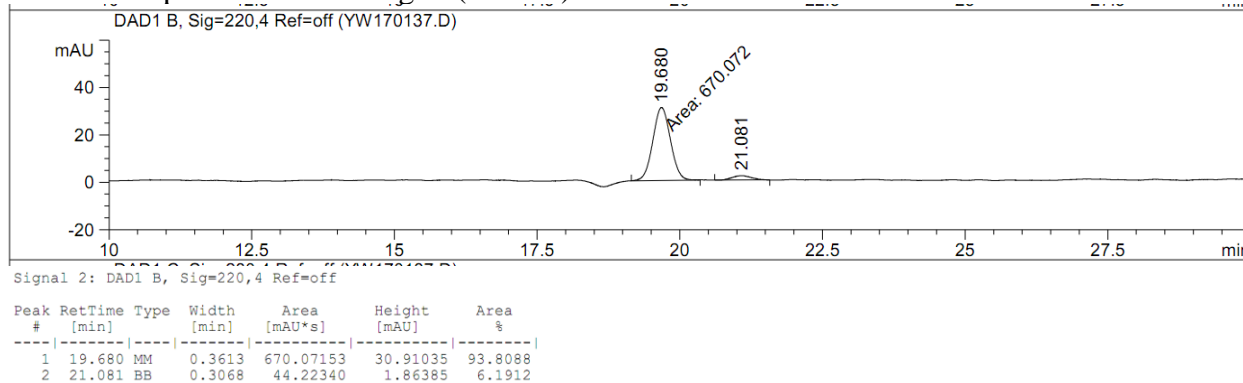
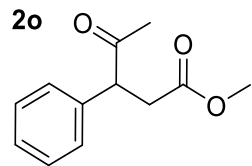


Table 4.2 Entry 46

(*S*)-**2n** HPLC2 trace from the cooperative enzymatic reduction of (*Z*)-**1n** with 0.5% SYE1 and 1% **Ir-16** in the presence of blue light (88% ee)



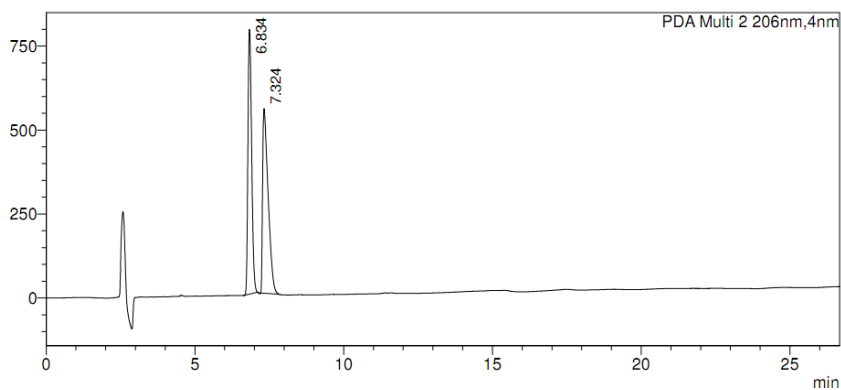


Separation Method/Eluent:

HPLC2 – ID-3 (150mm), 5% iPrOH, 95% hexanes 0.8 mL/min, 220 nm;  $t_R$  (major): 6.834 min,  $t_R$ (minor): 7.324

(*rac*)-**2o** HPLC3 trace

mAU



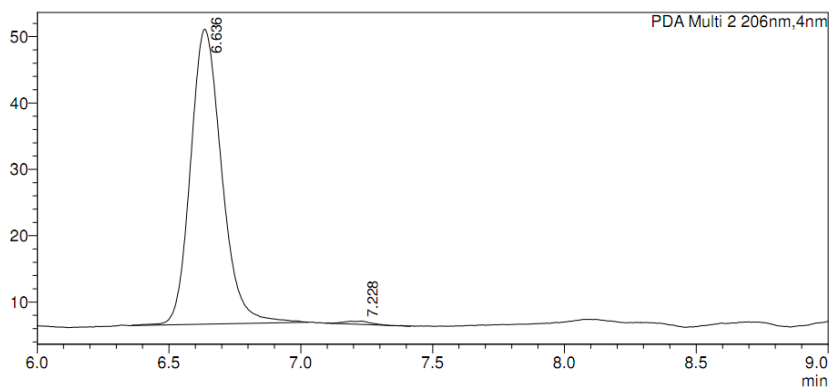
PDA Ch2 206nm

| Peak# | Ret. Time | Area     | Height  | Area%   |
|-------|-----------|----------|---------|---------|
| 1     | 6.834     | 6839974  | 786336  | 49.154  |
| 2     | 7.324     | 7075305  | 549501  | 50.846  |
| Total |           | 13915279 | 1335837 | 100.000 |

Table 4.1 Entry 27

(*R*)-**2o** HPLC3 trace from the enzymatic reduction of (*E*)-**1o** with 0.2% YersER (98% ee)

mAU



PDA Ch2 206nm

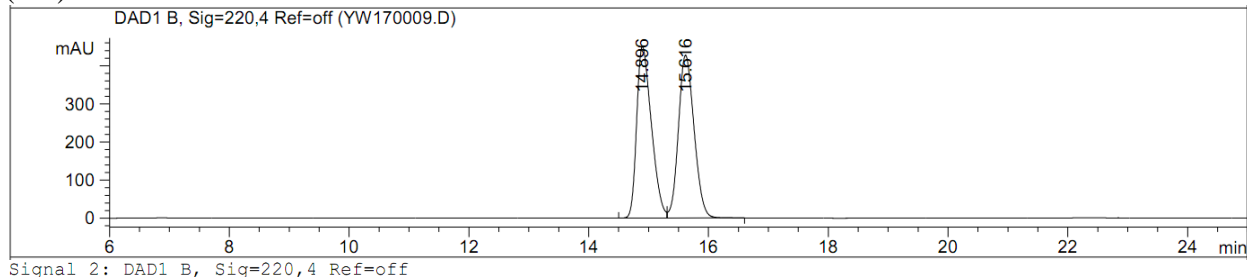
| Peak# | Ret. Time | Area   | Height | Area%   |
|-------|-----------|--------|--------|---------|
| 1     | 6.636     | 365541 | 44385  | 99.085  |
| 2     | 7.228     | 3374   | 506    | 0.915   |
| Total |           | 368915 | 44891  | 100.000 |



Separation Method/Eluent:

HPLC2 – OJ-H (250mm), 5% iPrOH, 95% hexanes 1.0 mL/min, 220 nm;  $t_R$  (major): 14.896 min,  $t_R$ (minor): 15.616

**(rac)-2o** HPLC2 trace

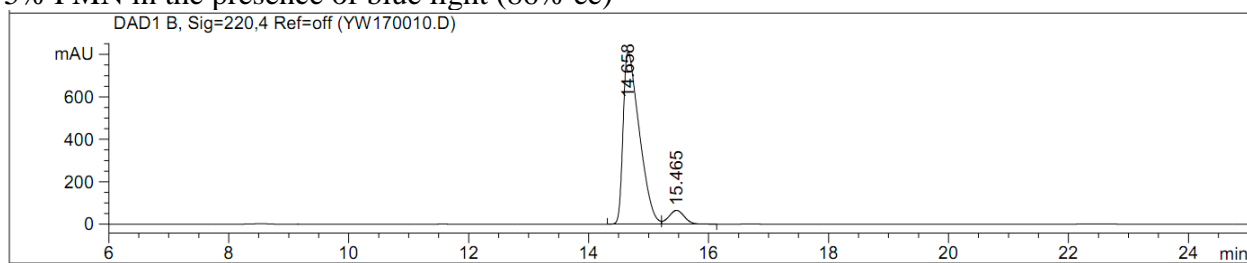


Signal 2: DAD1 B, Sig=220,4 Ref=off

| Peak # | RetTime [min] | Type | Width [min] | Area [mAU*s] | Height [mAU] | Area %  |
|--------|---------------|------|-------------|--------------|--------------|---------|
| 1      | 14.896        | BV   | 0.2635      | 7684.47656   | 450.50885    | 49.7283 |
| 2      | 15.616        | VB   | 0.2837      | 7768.45410   | 427.28354    | 50.2717 |

**Table 4.2 Entry 48**

**(R)-2o** HPLC2 trace from the cooperative enzymatic reduction of **(Z)-1o** with 0.5% YersER and 5% FMN in the presence of blue light (86% ee)

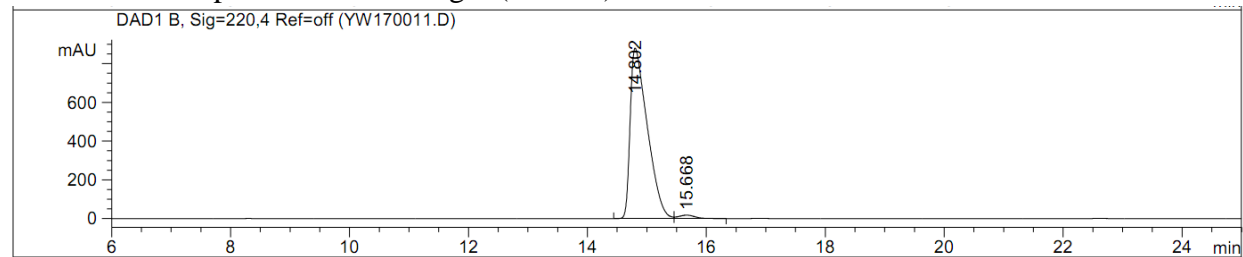


Signal 2: DAD1 B, Sig=220,4 Ref=off

| Peak # | RetTime [min] | Type | Width [min] | Area [mAU*s] | Height [mAU] | Area %  |
|--------|---------------|------|-------------|--------------|--------------|---------|
| 1      | 14.658        | BV   | 0.2832      | 1.51595e4    | 812.42603    | 92.8806 |
| 2      | 15.465        | VB   | 0.2769      | 1161.99194   | 64.87752     | 7.1194  |

Table 4.2 Entry 49

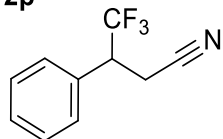
(*R*)-**2o** HPLC2 trace from the cooperative enzymatic reduction of (*Z*)-**1o** with 0.5% YersER and 1% **Ir-16** in the presence of blue light (96% ee)



Signal 2: DAD1 B, Sig=220,4 Ref=off

| Peak # | RetTime [min] | Type | Width [min] | Area [mAU*s] | Height [mAU] | Area %  |
|--------|---------------|------|-------------|--------------|--------------|---------|
| 1      | 3.202         | BV   | 0.1565      | 1811.68152   | 158.00452    | 9.1146  |
| 2      | 3.522         | PV   | 0.0961      | 68.00956     | 10.06243     | 0.3422  |
| 3      | 3.713         | VV   | 0.0903      | 57.84493     | 8.73820      | 0.2910  |
| 4      | 3.861         | VV   | 0.0985      | 24.64186     | 3.35626      | 0.1240  |
| 5      | 3.964         | VB   | 0.0762      | 10.57669     | 1.99354      | 0.0532  |
| 6      | 14.802        | BV   | 0.2984      | 1.75775e4    | 880.22412    | 88.4329 |
| 7      | 15.668        | VB   | 0.2803      | 326.40430    | 17.54132     | 1.6421  |

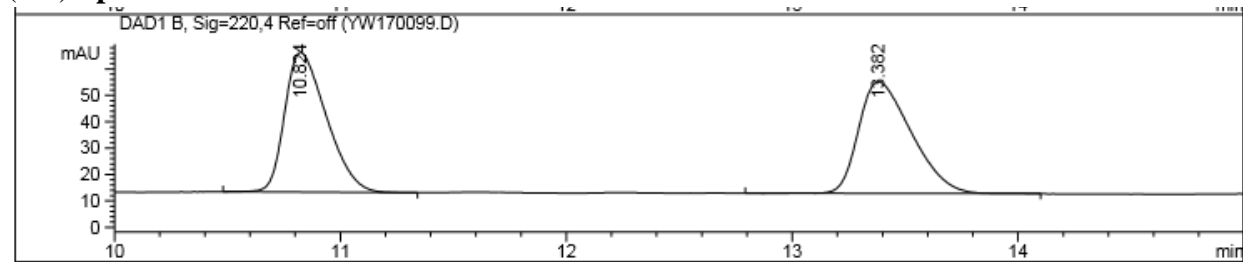
**2p**



Separation Method/Eluent:

HPLC2 – OJ-H (250mm), 20% iPrOH, 80% hexanes 1.0 mL/min, 220 nm;  $t_R$  (minor): 10.824 min,  $t_R$ (major): 13.382

(*rac*)-**2p** HPLC2 trace



| Peak # | RetTime [min] | Type | Width [min] | Area [mAU*s] | Height [mAU] | Area %  |
|--------|---------------|------|-------------|--------------|--------------|---------|
| 6      | 6.003         | BB   | 0.0847      | 5.65184      | 1.01606      | 0.5614  |
| 7      | 10.823        | BB   | 0.1907      | 435.28937    | 34.76490     | 43.2367 |
| 8      | 13.382        | BB   | 0.2462      | 426.22931    | 27.12449     | 42.3368 |

Table 4.1 Entry 29

(*S*)-**2p** HPLC trace from the enzymatic reduction of (*Z*)-**1p** with 0.2% OYE2 (>99% ee)

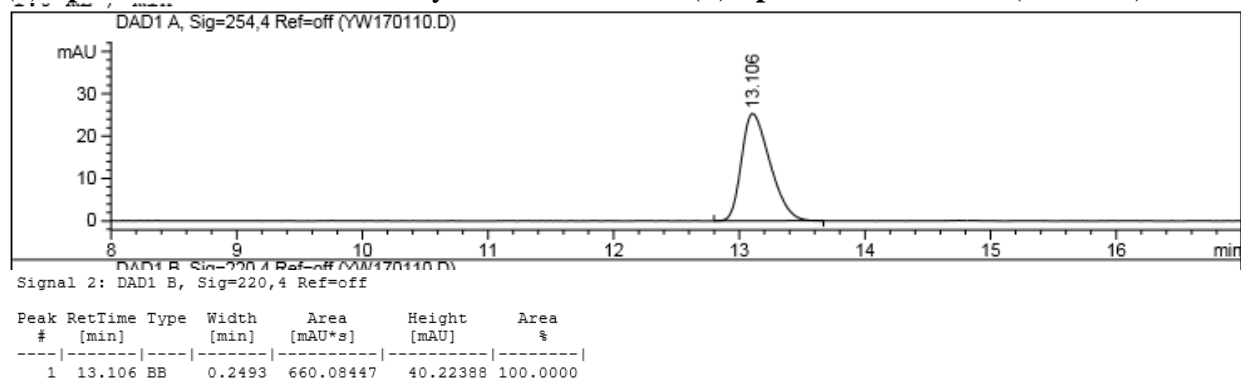
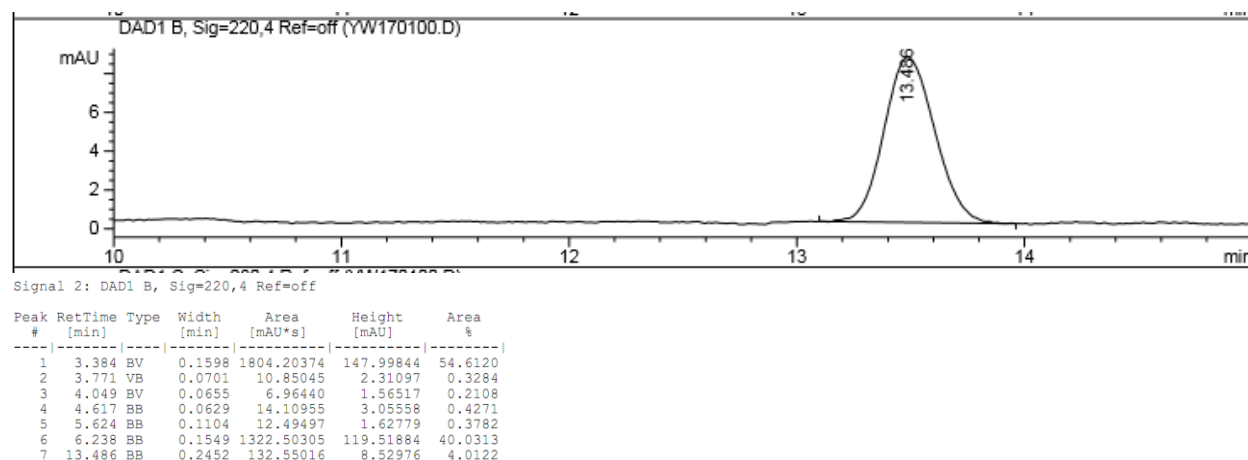


Table 4.2 Entry 52

(*S*)-**2p** HPLC2 trace from the cooperative enzymatic reduction of (*E*)-**1p** with 0.5% OYE2 and 1% **Ir-16** in the presence of blue light (>99% ee)



## 4.6 References

- 1 Bugg, T. D. H. in *Introduction to Enzyme and Coenzyme Chemistry* Ch. Isomerases, 213-224 (John Wiley & Sons, Ltd, 2012).
- 2 Martínez Cuesta, S., Rahman, S. A. & Thornton, J. M. Exploring the chemistry and evolution of the isomerases. *P. Natl. Acad. Sci. U.S.A.* **113**, 1796-1801, (2016).
- 3 Rudroff, F. *et al.* Opportunities and challenges for combining chemo- and biocatalysis. *Nature Catalysis* **1**, 12-22, (2018).
- 4 Köhler, V. & Turner, N. J. Artificial concurrent catalytic processes involving enzymes. *Chem. Commun.* **51**, 450-464, (2015).
- 5 Denard, C. A., Hartwig, J. F. & Zhao, H. Multistep One-Pot Reactions Combining Biocatalysts and Chemical Catalysts for Asymmetric Synthesis. *ACS Catalysis* **3**, 2856-2864, (2013).
- 6 Peters, R. *Cooperative Catalysis: Designing Efficient Catalysts for Synthesis.* (Wiley, 2015).

- 7 Verho, O. & Bäckvall, J.-E. Chemoenzymatic Dynamic Kinetic Resolution: A Powerful Tool for the Preparation of Enantiomerically Pure Alcohols and Amines. *J. Am. Chem. Soc.* **137**, 3996-4009, (2015).
- 8 Wang, Y., Ren, H. & Zhao, H. Expanding the boundary of biocatalysis: design and optimization of in vitro tandem catalytic reactions for biochemical production. *Crit. Rev. Biochem. Mol. Biol.* **53**, 115-129, (2018).
- 9 Denard, C. A. *et al.* Cooperative Tandem Catalysis by an Organometallic Complex and a Metalloenzyme. *Angew. Chem. Int. Ed.* **53**, 465-469, (2014).
- 10 Köhler, V. *et al.* Synthetic cascades are enabled by combining biocatalysts with artificial metalloenzymes. *Nat Chem* **5**, 93-99, (2013).
- 11 Haak, R. M. *et al.* Dynamic Kinetic Resolution of Racemic  $\beta$ -Haloalcohols: Direct Access to Enantioenriched Epoxides. *J. Am. Chem. Soc.* **130**, 13508-13509, (2008).
- 12 KöhlerV *et al.* Synthetic cascades are enabled by combining biocatalysts with artificial metalloenzymes. *Nat Chem* **5**, 93-99, (2013).
- 13 Kohler, V. & Turner, N. J. Artificial concurrent catalytic processes involving enzymes. *Chem. Commun.* **51**, 450-464, (2015).
- 14 Wohlgemuth, R. in *Synthetic Methods for Biologically Active Molecules* Ch. Synthetic Strategies Based on C=C Bioreductions, 49-82 (Wiley-VCH Verlag GmbH & Co. KGaA, 2013).
- 15 Metternich, J. B. & Gilmour, R. A Bio-Inspired, Catalytic E  $\rightarrow$  Z Isomerization of Activated Olefins. *J. Am. Chem. Soc.* **137**, 11254-11257, (2015).
- 16 Singh, K., Staig, S. J. & Weaver, J. D. Facile Synthesis of Z-Alkenes via Uphill Catalysis. *J. Am. Chem. Soc.* **136**, 5275-5278, (2014).
- 17 Metternich, J. B. *et al.* Photocatalytic E  $\rightarrow$  Z Isomerization of Polarized Alkenes Inspired by the Visual Cycle: Mechanistic Dichotomy and Origin of Selectivity. *J. Org. Chem.*, (2017).
- 18 Metternich, J. B. & Gilmour, R. Photocatalytic E  $\rightarrow$  Z Isomerization of Alkenes. *Synlett* **27**, 2541-2552, (2016).
- 19 Yanto, Y. *et al.* Asymmetric Bioreduction of Alkenes Using Ene-Reductases YersER and KYE1 and Effects of Organic Solvents. *Org Lett* **13**, 2540-2543, (2011).
- 20 Chaparro-Riggers, J. F., Rogers, T. A., Vazquez-Figueroa, E., Polizzi, K. M. & Bommarius, A. S. Comparison of Three Enoate Reductases and their Potential Use for Biotransformations. *Adv. Synth. Catal.* **349**, 1521-1531, (2007).
- 21 Bamaung, N. Y. *et al.* Imidazo-thiazole derivatives as protein kinase inhibitors. 2009/WO2009070516 A1 (2009).
- 22 Meerpoel, L. *et al.* MTP Inhibiting Aryl Piperidines or Piperazines Substituted with 5-Membered Heterocycles. 2005/WO2005085226 A1 (2005).
- 23 Caggiano, T. J. *et al.* Inhibitors of Beta Amyloid Production. 2009/WO2009012205 A1 (2009).
- 24 Dong, K., Li, Y., Wang, Z. & Ding, K. Catalytic Asymmetric Hydrogenation of  $\alpha$ -CF<sub>3</sub>- or  $\beta$ -CF<sub>3</sub>-Substituted Acrylic Acids using Rhodium(I) Complexes with a Combination of Chiral and Achiral Ligands. *Angew. Chem. Int. Ed.* **52**, 14191-14195, (2013).
- 25 Chung, Y.-C., Janmanchi, D. & Wu, H.-L. Preparation of Chiral 3-Arylpyrrolidines via the Enantioselective 1,4-Addition of Arylboronic Acids to Fumaric Esters Catalyzed by Rh(I)/Chiral Diene Complexes. *Org. Lett.* **14**, 2766-2769, (2012).

- 26 Brenna, E. *et al.* Opposite Enantioselectivity in the Bioreduction of (Z)- $\beta$ -Aryl- $\beta$ -cyanoacrylates Mediated by the Tryptophan 116 Mutants of Old Yellow Enzyme 1: Synthetic Approach to (R)- and (S)- $\beta$ -Aryl- $\gamma$ -lactams. *Advanced Synthesis & Catalysis* **357**, 1849-1860, (2015).
- 27 Kong, D., Li, M., Wang, R., Zi, G. & Hou, G. Highly efficient asymmetric hydrogenation of cyano-substituted acrylate esters for synthesis of chiral  $\gamma$ -lactams and amino acids. *Org. Biomol. Chem.* **14**, 1216-1220, (2016).
- 28 Zhao, F. *et al.* Enantioselective Aza-Ene-type Reactions of Enamides with Gold Carbenes Generated from  $\alpha$ -Diazoesters. *Angew. Chem. Int. Ed.* **56**, 3247-3251, (2017).

# CHAPTER 5. Automated Cellular Engineering of *Saccharomyces cerevisiae* Strains with High Resistance and Production of Lactic Acid

## 5.1 Introduction

Lactic acid (LA) has broad applications in the food, cosmetics, pharmaceutical and chemical industries. Recently, LA demand has grown dramatically, mainly due to its potential as a building block of poly-lactic acid materials.<sup>1</sup> Poly-lactic acid is a biodegradable alternative to petroleum-based plastics, preferably synthesized from optically pure monomers. Given this prerequisite of LA optical purity in PLA synthesis, microbial fermentation is the optimum choice since chemical synthesis generally generates racemic LA.<sup>2,3</sup>

Mainly thanks to its high acid tolerance, *Saccharomyces cerevisiae* serves as a promising host for LA production under acidic fermentation condition. Increasing the acid tolerance of LA producing *S. cerevisiae* could reduce the usage of neutralizing reagents such as CaCO<sub>3</sub> and simplify the downstream purification steps, thus reducing the cost of LA production. Coupled with metabolic engineering efforts, heterologous expression of stereospecific lactate dehydrogenase (LDH) gene in *S. cerevisiae* enables the production of optically pure L- or D-LA with titer as high as 142 g/L, albeit at an industrially non-preferred pH (pH 4.7).<sup>4</sup> Adaptive evolution was also applied to create a *S. cerevisiae* mutant producing up to 82.6 g/L LA at a lower pH (pH 3.5).<sup>5</sup>

Recently, we developed two advanced genome-scale engineering tools in *S. cerevisiae*: CRISPR-AID,<sup>6</sup> and RNA interference-assisted genome evolution (RAGE)<sup>7</sup>. CRISPR-AID is a combinatorial metabolic engineering strategy based on an orthogonal tri-functional CRISPR system that combines transcriptional activation, transcriptional interference and gene deletion in the *S. cerevisiae* in a high-throughput manner. RAGE is based on RNA interference for genome-

scale overexpression and downregulation in *S. cerevisiae*. Standardized genetic parts encoding overexpression and knockdown mutations of >90% yeast genes could be created in a single step from a full-length cDNA library.<sup>7</sup> Through iterative cycles of creating a library of mutants with high throughput screening or selection, RAGE can continuously improve target traits by accumulation multiplex beneficial genetic modification in an evolving yeast genome. Particularly, we also developed an automated cellular engineering (ACE) platform for yeast multiplex genome engineering by combining RAGE and a robotic system called Illinois Biological Foundry for Advanced Biomanufacturing (iBioFAB).<sup>7</sup> This platform is capable of creating and screening massive genomic variants in a fully automated manner and we have used it to optimize diverse phenotype of *S. cerevisiae* including cellulase expression, isobutanol production, glycerol utilization, and furfural tolerance.<sup>7,8</sup>

In this study, I applied RAGE and CRISPR-AID methods to identify a few single mutants with improved LA resistance and production at an industrially preferred low pH (pH 3). To adapt the selection process into an ACE platform for high throughput screening, I developed a growth-based LA biosensor and an automated quantification assay based on industry-standard BioProfile Analyzer. Based on the single round screening, I created a few mutants with up to 3 times improved acid tolerance and 1.5 times LA production compared with the parent strain. The best candidate could produce 52 g/L LA in fed-batch fermentation at pH 3 with SC medium.

## 5.2 Results and Discussion

### 5.2.1. Creation of L-LA Producing Mutants with RNAi and CRISPR-AID Machinery

Hahn and co-workers recently created a D-LA producing strain JHY5610 with good D-LA productivity of 26.8 g/L by expressing a D-lactate dehydrogenase gene while deleting alcohol

dehydrogenases, glycerol-3-phosphate dehydrogenase and D-lactate dehydrogenase involved in ethanol production (ADH1, ADH2, ADH3, ADH4 and ADH5), glycerol production (GPD1 and GPD2), and degradation of D-LA (DLD1) respectively (Figure 5.1). Further adaptive evolution and metabolic engineering led to the mutant JHY 5730 producing up to 82.6 g/L of D-LA with a yield of 0.83g/g glucose and a productivity of 1.5 g/(L.h) in fed-batch fermentation at pH 3.5.<sup>9</sup> We obtained JHY5610 and JHY5617 from Dr. Hahn’s lab as positive controls in this study (Table 5.1).

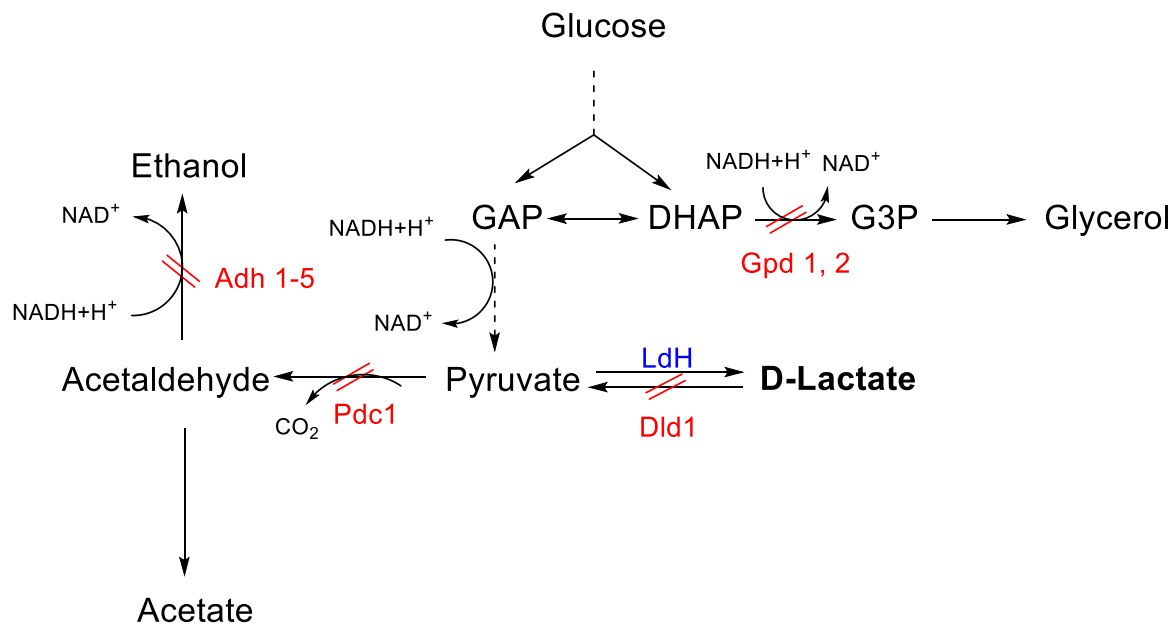


**Figure 5.1.** Metabolic engineering to produce lactic acid in *S. cerevisiae*.

Instead of starting with the wild type CEN.PK2-1C, we first created several L-LA mutants by replacing *ADH5* with four different L-lactate dehydrogenase genes, *Lp-ldh* from *Lactobacillus plantarum*, *Lpm-ldh*, a mutant of *Lp-ldh*, *Lb-ldh* from *Lactobacillus brevis*, and *Ro-ldh* from *Rhizopus oryzae*, while deleting *ADH1*, *ADH4*, *GPD1* and *GPD2*, resulting mutants PK2M2, PK2M3, PK2M4 and PK2M5 respectively (Table 5.1). Among them, PK2M2, PK2M3 and PK2M4 showed a L-LA productivity that is comparable to that of JHY5610 (Figure 5.2).



**Table 5.1.** Summary of CEN.PK2 mutants and their genome types

| <b>Mutants</b> | <b>Genome type</b>   |
|----------------|--|
| JHY5610        | <i>Adh 1-5Δ, gpd1-2Δ, dld1Δ, P<sub>TDH3</sub>-Lm.ldhA-T<sub>CYC1</sub>-kanMX</i> |
| JHY5617*       | Based on JHY 5610: <i>erf2Δ, SUR<sup>I245S</sup>-kanMX</i>                       |
| PK2-M1         | <i>Adh1,4Δ, gpd1-2Δ</i>  |
| PK2-M2         | <i>Adh1,4,5Δ, gpd1-2Δ, P<sub>TEF1p</sub>-Lp.ldh-T<sub>TEF1p</sub>-kanMX</i>      |
| PK2-M3         | <i>Adh1,4,5Δ, gpd1-2Δ, P<sub>TEF1p</sub>-Lpm.ldh-T<sub>TEF1p</sub>-kanMX</i>     |
| PK2-M4         | <i>Adh1,4,5Δ, gpd1-2Δ, P<sub>TEF1p</sub>-LB.ldh-T<sub>TEF1p</sub>-kanMX</i>      |
| PK2-M5         | <i>Adh1,4,5Δ, gpd1-2Δ, P<sub>TEF1p</sub>-Ro.ldh-T<sub>TEF1p</sub>-kanMX</i>      |
| PK2-M6         | <i>Adh1,2,3,4Δ, gpd1-2Δ</i>  |

The four newly created mutants (PK2M2, PK2M3, PK2M4 and PK2M5) together with JHY 5610 and JHY 5617 were grown in YPG medium and a small amount of cells (OD<sub>600</sub>=1) were serially diluted and spotted onto YPD solid medium supplemented with or without LA at different pH (Figure 5.3). Increasing LA concentration with pH unchanged or decreasing pH alone inhibited the cell growth. Further deletion of *ADH2* and *AHD3* may improve the LA production (Figure 5.1, PK2M2-M4 versus JHY5610), but it led to worse acid tolerance (Figure 5.3). PK2M3 was selected as a good parent strain for genome-scale engineering due to its moderate LA production and acid tolerance compared with JHY5610 and JHY5617. PK2M3 was largely inhibited at pH 3.0 with 2% LA (Figure 5.3) and failed to grow at pH lower than 3 (data were not shown). Thus, medium supplemented with 2.5% LA at pH 3.0 would be chosen as selection medium to identify mutants with improved acid tolerance.

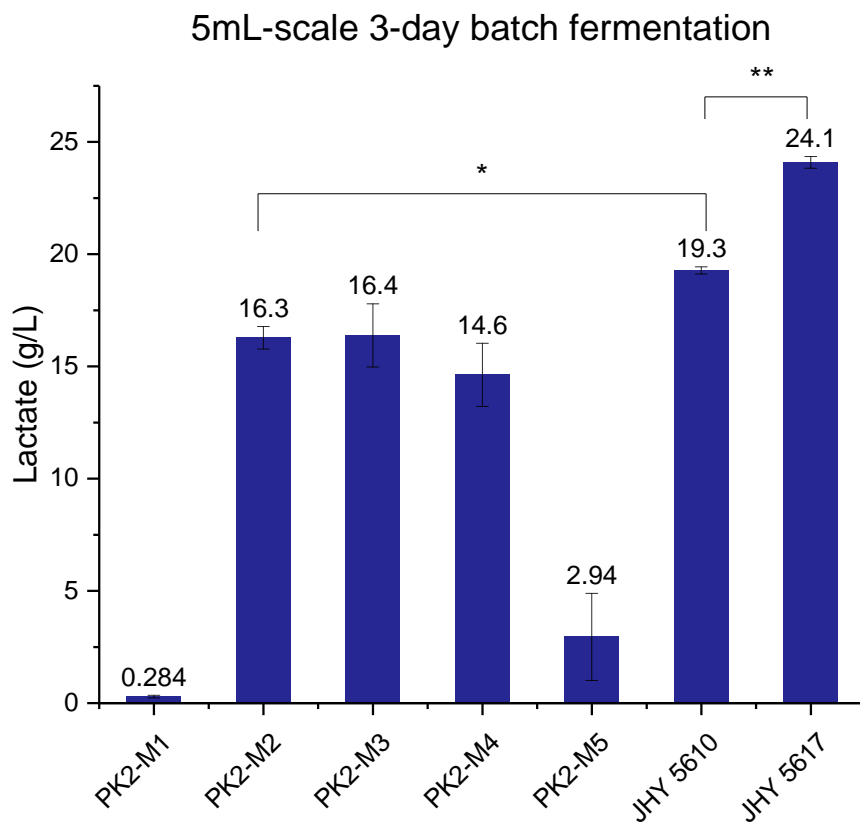


**Figure 5.2.** L-LA production in PK2M2, PK2M3, PK2M4, PK2M5 and D-LA production in JHY5610 and JHY5617. The mutants were grown in YPD medium with 50 g/L glucose in a 50 mL bioreaction tube from CELLTREAT, at 30 °C with shaking at 250 rpm. The error bars indicate standard deviations of three independent experiments.

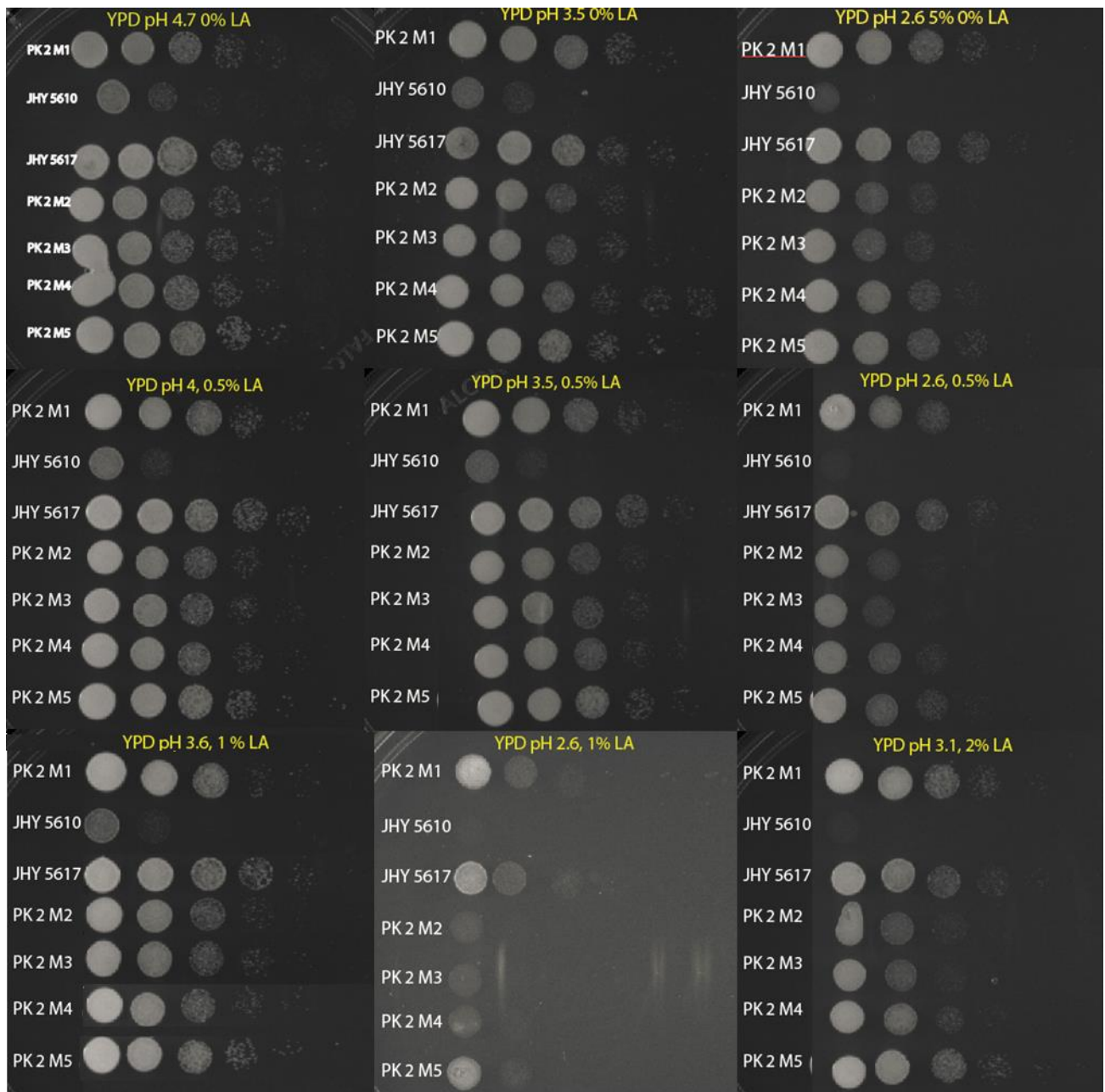


**Figure 5.3.** Effects of pH and LA concentration on the mutant's growth.

The RNAi machinery originated from *S. castellii* was reconstructed into PK2M3 using the same protocol as described elsewhere.<sup>10</sup> Green fluorescent protein (GFP) was selected as the reporter to test the RNAi machinery. The reporter system consisted of an *GFP* expression cassette on yeast centromere plasmid (YCp) pRS414 and an anti-sense *GFP* cassette (GFPrC) on YCp

pRS416 (Figure 5.4). The RNAi machinery cassette consisting of *ago1* and *dcr1* genes that were driven by the constitutive promoters  $P_{TEF1}$  and  $P_{TPII}$  respectively was transformed into PK2M3 together with a delta-integration cassette. Since the location and the copy number of integrations will affect the performance of the RNAi machinery. 36 mutants were screened to identify the best candidate with the weakest GFP expression when both *GFP* and *GFPrc* were expressed (Figure 5.5). *GFP* and *GFPrc* were removed from the selected mutant by using the 5-fluoroorotic acid (5-FOA) and 5-fluoroanthranilic acid (5-FAA) counterselection system. The resulting strain was named as PK2M3-RNAi and it was used for transformation of genome-wide single gene overexpression and knockdown library, RAGE 2.0.<sup>10</sup>

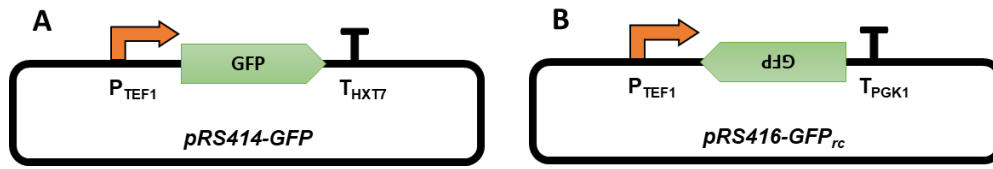


**Figure 5.4.** GFP reporter system: A) *GFP* is overexpressed by strong constitutive promoter  $P_{TEF1}$  and B) anti-sense *GFP* is overexpressed by  $P_{TEF1}$ .

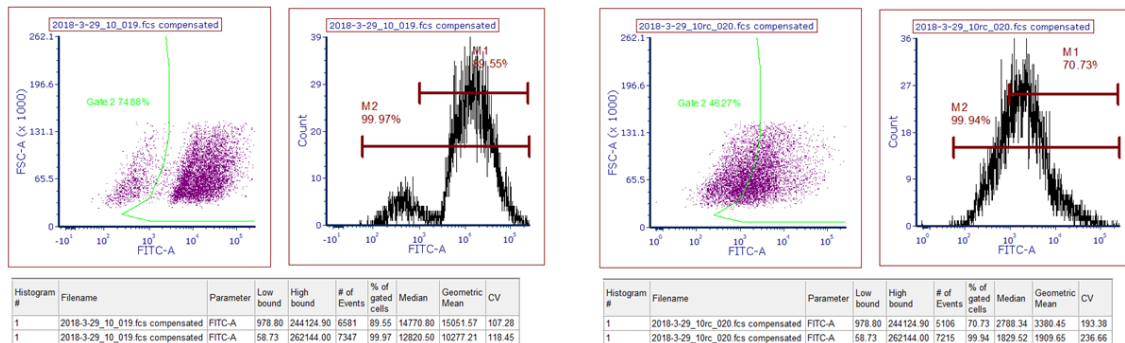


**Figure 5.5.** Flow cytometry analysis of mutants: A) PK2M3-RNAi-pRS414\_ *GFP*, B) PK2M3-RNAi-pRS414\_ *GFP*-pRS416\_ *GFPrc*.

The orthogonal tri-functional CRISPR system, CRISPR-AID, was also reconstructed in PK2M3 based on Lian J. et. al's work.<sup>6</sup> CRISPR-guided deletion in the final strain PK2M3-PAID6

was verified by *ADE2* deletion efficiency. PK2M3-PAID6 was used as the parent strain to create a CRISRP-AID library.

### 5.2.2. Establishing Screening Methods for L-LA Overproduction

For high-throughput screening, we proposed two automated quantification assays using BioProfile Analyze, including pH indicator-based quantification assay and lactate oxidase-based quantification assay (LOD). We also developed a cell growth-based LA biosensor and designed a high-throughput system combined with the biosensor technique for screening ultracellular metabolites.

#### 5.2.2.1. Bromocresol Green Assay

The pH indicator with no side-effect on yeast growth could be used to identify the mutant with high LA production in a high throughput way. We firstly aimed at making the agar plate containing pH indicator that enabled the obvious color change around the colony producing more LA than others. Since our aim was “creation a yeast strain that can produce 50 g/L LA at pH 3”, we tested a few pH indicators working at pHs ranging from 0.2 to 5.4 (Table 5.2). However, they are either not stable under the light or have poor solubility in aqueous medium. More importantly, the pH indicators working at low pH range are not sensitive to the small changes of LA concentration. We then decided to develop a pH indicator assay in 96-well plates that could be analyzed quantitatively by the plate reader.

Bromocresol green was chosen as the pH indicator since it has relatively linear color changes with decreasing PH. A calibration curve of LA concentration versus absorbance change at 616 nm was built by adding 2 ul SC liquid medium with different amount of LA into 200 ul 60 mg/L bromocresol blue solution at pH 5.5 (Figure 5.6 A). Bromocresol green assay (BG) works for LA ranging from 0.01 g/L to 1 g/L. LA concentration is reverse proportional to the absorbance

at 616 nm and a linear correlation can be established between LA concentration versus Abs ( $A_{616nm}$ )<sup>-1</sup>. 2 ul 12-hr SC fermentation broth of different mutants was evaluated using BG assay (Figure 5.6 B). The lighter the color or lower the absorbance value of the culture broth, the higher the concentration of LA. The calculated concentration is comparable with the values measured by HPLC. BG assay could be integrated in iBioFAB to evaluate LA concentration from fermentation broth of different mutants in a high-throughput manner.

**Table 5.2.** pH Indicators tested for agar plate-based screening

| Indicator         | Acid color | Transition range | Base color | Comments                     |
|-------------------|------------|------------------|------------|------------------------------|
| Cresol red        | Red        | pH 0.2-pH 1.8    | Yellow     | Unstable, poor solubility,   |
| Thymol blue       | Red        | pH 1.2-pH2.8     | Yellow     | Poor solubility, insensitive |
| Methyl yellow     | Red        | pH 2.9-pH 4.0    | Yellow     | Insensitive                  |
| Bromophenol blue  | Yellow     | pH 3.0-pH 4.6    | Green      | Insensitive, outside range   |
| Bromocresol green | Yellow     | pH 3.8-pH 5.4    | Blue       | Outside range                |

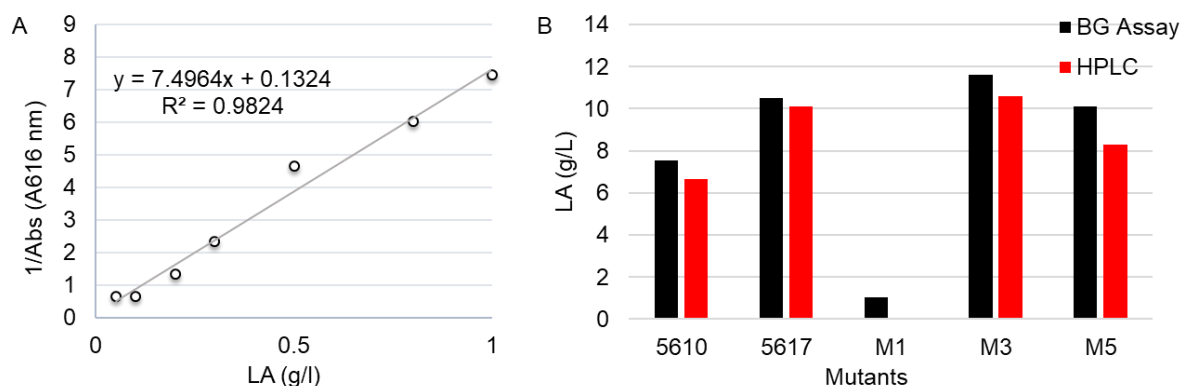


**Figure 5.6.** Bromocresol green (BG) assay development and verification. A) calibration curve of LA concentration versus absorbance at  $A_{616nm}$ , B) LA production of different mutants measured by BG assay and HPLC.

#### 5.2.2.2. Lactate Oxidase Assay

The BG assay is not specific to L-LA measurements and it can also be used for D-LA screening. However false-positives may also occur if the mutants produce more acids other than LA resulting

in low fermentation pH. To overcome this shortcoming, we developed a LOD assay specific for L-LA measurements.

L-LA can be oxidized by lactate oxidase (LOD) to pyruvate and H<sub>2</sub>O<sub>2</sub>. There are several methods available to quantitatively measure the amount of H<sub>2</sub>O<sub>2</sub>. I selected the lactate oxidase from *Aerococcus viridans* (L9795) and the fluorometric hydrogen peroxide assay kit (MAK165-1KT) from sigma. The LOD reaction was successfully integrated with the fluorometric hydrogen peroxide assay kit. The reaction protocol was established for creating the calibration curve of LA (uM) versus RFU (Ex/Em = 540/590 nm) (Figure 5.7A) and for measuring the fermentation sample (Figure 5.7B). The fermentation supernatant should be diluted 1000 times before the measurements since the active interval of LOD assay is 5 uM to 30 uM. Although the concentration measured by LOD was about 20%~50% less than the actual concentration, the relative concentration of different mutants was consistent with the HPLC measurements. This assay was done in 96-well plates and the absorbance change was detected at 590 nm using fluorescent plate reader. LOD assay could be used to directly measure the L-LA concentration in fermentation supernatant and the process could be adapted to iBioFAB easily for high-throughput screening. The assay costs US\$1.22/reaction.

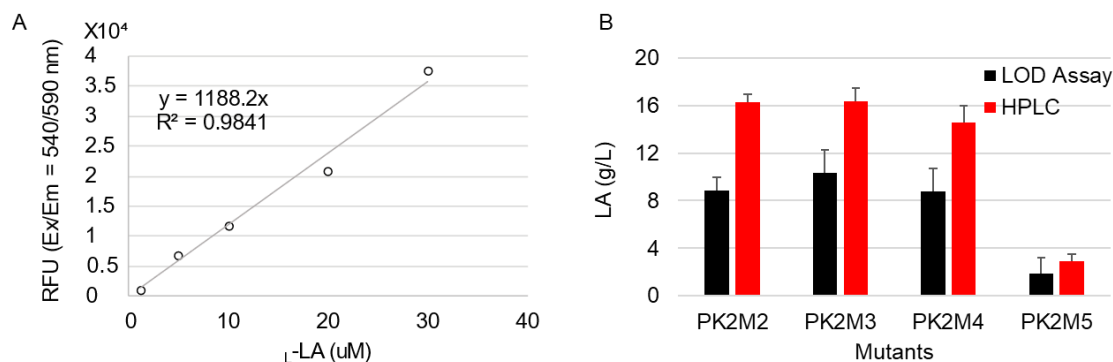


**Figure 5.7.** LOD assay development and verification. A) The calibration curve of L-LA (uM) versus the RFU (Ex/Em=540/590 nm). B) Measurements of fermentation samples by LOD assay and HPLC. The error bars represent the standard deviation of biologically triplicate experiments.

### 5.2.2.3. L-Lactic Acid Biosensor

Inspired by L-LA biosensor constructed in *E. coli*,<sup>11</sup> I planned to develop a genetic sensor responsive to L-LA concentration in CEN.PK2.1C, so that we would be able to rapidly screen the high L-LA producing strain in a high throughput manner. We designed the yeast biosensor based on a bacterial transcription factor LIdR and its corresponding operator O1 and O2, involved in L-LA metabolism in *E. coli*.<sup>12</sup> LIdR undergoes a conformational change when it specifically binds to L-LA and dissociates from its operator O1 (design 1) or O2 (design 2), allowing access of the RNA polymerase (Figure 5.8A). *LidR* was fused with a strong NLS SV40 at the C-terminus to enable nuclear import. The *LidR*-NLS SV40 was assembled in a YCp with TEF1 promoter and PGK1 terminator. To provide a quantitative readout of LIdR-O behavior, a YIp harboring the GFP as a reporter was constructed. The O1 or O2 regulated fluorescent protein expression cassette was constructed by inserting O1 or O2 into an engineered promoter *GPM1* in front of *GFP*. The *GPM1* promoter was modified with only one upstream activation sequence conserved to eliminate native transcriptional regulation (Figure 5.8B). The operator sequence was inserted immediately in front of the TATA box.



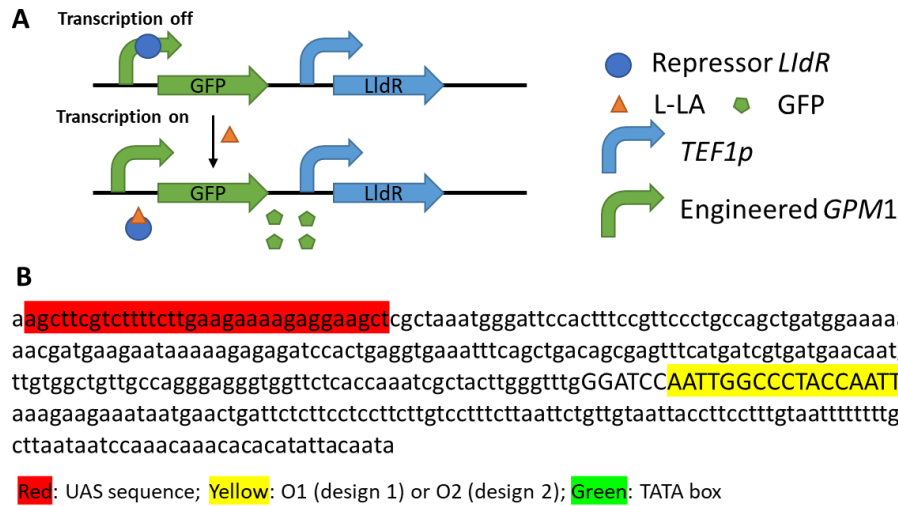


**Figure 5.8.** Design of L-LA sensor/regulating circuits: (A) scheme (B) sequence

I first evaluated the GFP expression level in PK2M1-LAb1 (PK2M1\_pRS405-*GPM1*(O1)-*GFP-PGK1t\_pRS416*) and PK2M1-LAb2 (PK2M1\_pRS405-*GPM1*(O1)-*GFP-PGK1t\_pRS416*) in SC-Ura liquid medium supplemented with 20 g/L glucose and different L-LA concentration or at different pHs. The GFP intensity increased when L-LA concentration was increased from 0% to 1% while decreased at 2% (Figure 5.9A). It was interesting to find that pH value alone had regulation effect on GFP expression. The fluorescence intensity increased when the pH decreased from 6.7 to 2.7. Further decrease in pH inhibited the GFP expression (Figure 5.9B). Since SC-Ura liquid medium with 2% L-LA is at pH 2.4, cellular stress response to low pH maybe the reason of decreased GFP intensity at 2% L-LA.

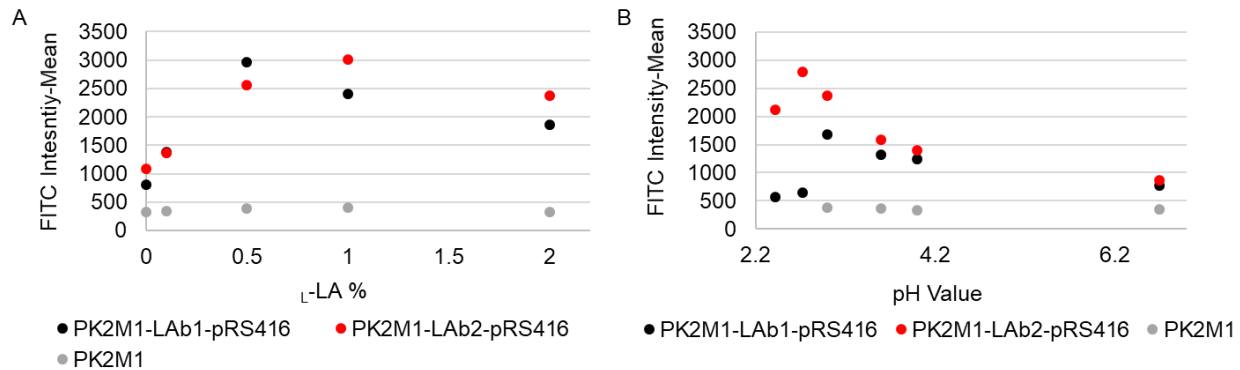


**Figure 5.9.** A) Dynamic response of L-LA-sensing/regulating gene circuits in SC-Ura liquid medium supplemented with 20 g/L glucose at A) different L-LA concentrations; B) at different pHs. Sensor activity was measured by fluorescence intensity of 24-hr cell culture by flow cytometry.

To test the regulation effect of L-LA on GFP expression alone, I measured the GFP intensity of PK2M1-*Lab1* and PK2M1-*Lab2* individually in SC-Ura liquid medium with different L-LA concentration at pH 5.6. The sensor activity was measured at 6hr, 12hr, 18hr, 24hr, 24hr and 48hr respectively. The induction ratio was maximum at 24 hr after L-LA being added. The fluorescence intensity was proportional to the L-LA concentrations from 0.2% to 2% and there was no substantial background fluorescence change in PK2M1 (Figure 5.10). Native repressor of O1 and O2 may present and could interact with L-LA. Introducing LldR in PK2M1-*Lab1-LldR* (PK2M1\_ pRS405-*GPM1*(O1)-*GFP-PGK1t\_pRS416-TEF1p-LldR-PGK1t*) and PK2M1-*Lab2-LldR* (PK2M1\_ pRS405-*GPM1*(O2)-*GFP-PGK1t\_pRS416-TEF1p-LldR-PGK1t*) improved the sensitivity of L-LA-sensing/regulating gene circuit to different L-LA concentrations. Higher induction ratio was achieved for gene circuit containing *LldR*: around 4-fold in PK2M1-*Lab1-LldR* and PK2M1-*Lab2-LldR*, 2-fold in PK2M1-*Lab1* and PK2M1-*Lab2*). In both cases, O2 has stronger basal level expression than O1.

I further optimized the L-LA-sensing/regulating gene circuit by adjusting the ratio of O1(O2)/LldR by using a high copy number plasmid to express LldR. I also used a codon-optimized

LldR to replace the original LldR from *E. coli* to theoretically achieve higher expression level. More LldR in the system reduced the induction ratio of L-LA-sensing/regulating gene circuits within the working range (0~4% L-LA) (Figure 5.11). So, use of single copy repressor is enough to achieve the best regulation effect.

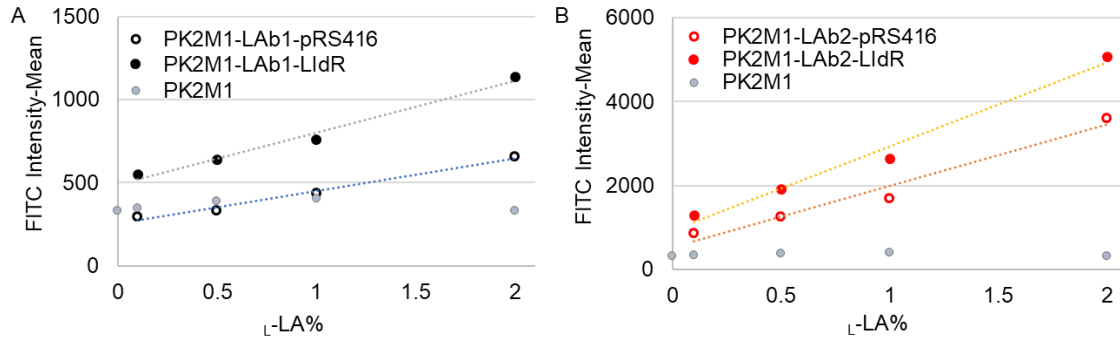


**Figure 5.10.** Dose-response curves of L-LA-sensing/regulating gene circuits. Dynamic response of sensors designed with different operator A) *Lab1* or B) *Lab2* with or without *LldR* being expressed in SC-Ura liquid medium supplemented with 20 g/L glucose and different L-LA concentration at pH 5.6. The average fluorescence intensity of 24-hr liquid culture was measured by flowcytometry.

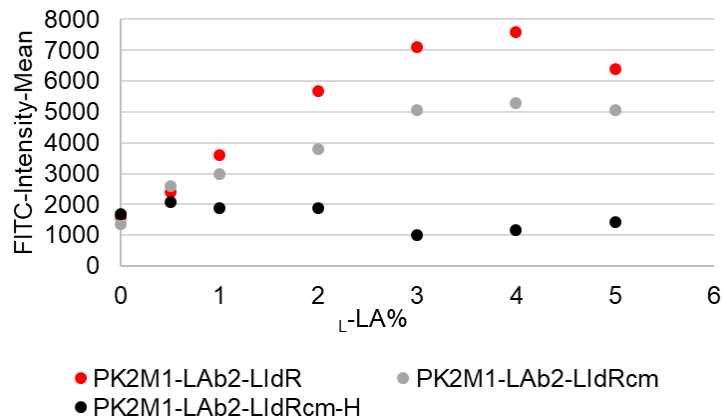


**Figure 5.11.** Dose-response curves of L-LA-sensing/regulating gene circuits designed with different Operator/repressor ratio. Sensor activities were compared by fluorescence intensity of cells cultured in SC-Ura liquid medium with 20 g/L glucose and different L-LA concentrations (%) at pH 5.6. LldRcm indicates codon-optimized LldR. LldRcm-H indicates that LldRcm was expressed on high copy number plasmid.

The designed L-LA-sensors could respond to different amount of extracellular L-LA. To use the sensor as a high throughput screening method to identify mutants with improved LA production. I must confirm that L-LA-sensing/regulating gene circuit can work well in the yeast strains producing different amount of L-LA. I built different L-LA-sensing/regulating gene circuits, basically *Lab1-LldR*, *Lab2-LldR* and *Lab3-LldR* in PK2M3, PK2M4 and PK2M5 that produced different amount of L-LA in flask-fermentation (Figure 5.2). *Lab3-LldR* is a new design which placed O1 behind the UAS region and O2 just before the TATA box. A small amount of PK2M3-sensor, PK2M4-sensor and PK2M5-sensor strains (OD<sub>600</sub>=1) were inoculated in SC-Ura liquid medium supplemented with 20 g/L glucose and 100 mM citrate phosphate at pH 5.6. The fluorescence intensity and L-LA production of 24-hr culture were analyzed by flowcytometry and HPLC respectively. In *Lab2-LldR* design, mutants produced more L-LA have stronger fluorescence intensity too (Figure 5.12A, B). The mutants produced more L-LA after 24-hr fermentation also have higher titer at the end of 3-day fermentation (Figure 5.12 and Figure 5.2). Although the *Lab1-LldR* sensing/regulating gene circuits worked well in Pk2M1 that does not produce LA, it did not show good correlation between L-LA production and fluorescent intensity in those strains producing LA. The L-LA sensor works well in other two common liquid mediums used in this study SC-Ura and YPD, and the sensor activity assay is performed after 24 hrs (Figure 5.12C, D).

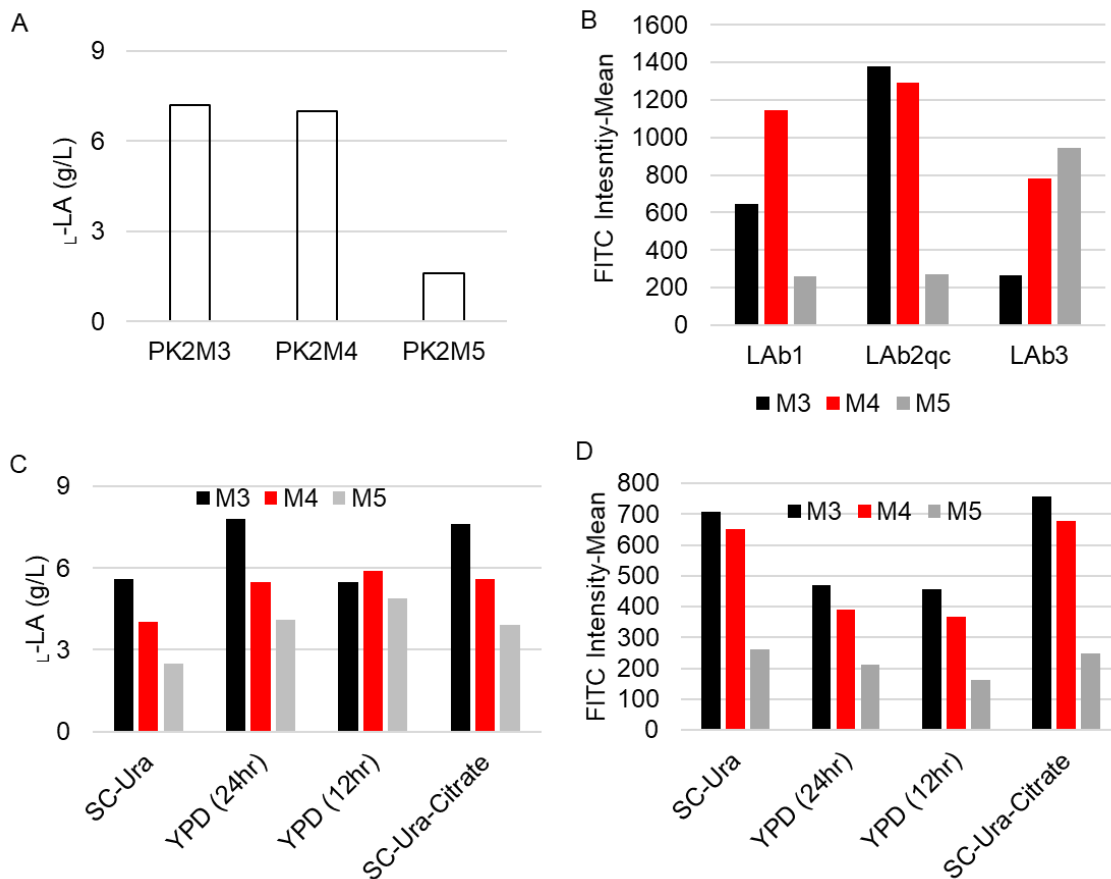


**Figure 5.12.** A) and B) Different L-LA sensor activity in PK2M3, PK2M4 and Pk2M5 produced different amount of LA after 24-hr fermentation in SC-Ura liquid medium supplemented with 20 g/L glucose and 100 mM citrate phosphate at pH 5.6 C) and D) *LAB2qc-LldR* L-LA sensor activity in PK2M3, PK2M4 and PK2M5 produced different amount of LA after 24-hr fermentation in SC-Ura liquid medium supplemented with 20g/L glucose, 12-hr and 24-hr fermentation in YPD medium.

### 5.2.3. Establishing Screening Methods for Low pH Tolerance

RAGE 2.0 library and CRISPR-AID library were constructed on the plasmid pRS416 and pRS426 respectively.<sup>6,10</sup> SC-Ura solid/ liquid medium supplemented with 20 g/L galactose and LA at low pH was chosen as the selecting medium for acid tolerance screening. To identify the optimum pH and LA concentration for selection purpose, 1ul (OD<sub>600</sub> = 1) PK2M3 (approximately 10<sup>4</sup> cells) were plated on SC-Ura solid medium at pH ranging from 2.6 to 5 with LA ranging from 1% to 4%

respectively. SC-Ura supplemented with 20 g/L glucose and 3% LA at pH 3.0 showed around 100 small colonies after 4-day growth and it was chosen as the selection plate for screening mutants with improved acid tolerance.

Based on later study, there is no absolute relationship between strong acid tolerance and high LA production. The tolerance screening was coupled with the production screening based on the bromocresol assay since it can be applied to the iBioFAB platform more easily compared with other screening methods. As shown in Figure 5.13, following the transformation, the yeast library was plated on SC-Ura solid medium supplemented with 20 g/L galactose and 3% LA at pH 3.0. The first appeared colonies or those sizes were bigger than the largest colonies on the control plates were inoculated in deep-round 96-well plates dispensed with SC-Ura liquid medium supplemented with 20 g/L galactose. The saturated culture was sub-cultured one time to synchronize the growth. The subculture was used to do growth profile evaluation in the selecting medium and fermentation test. For growth profile evaluation, mutants and control strain with the initial  $OD_{600}$  of 0.2~0.8 were grown in SC-Ura liquid medium supplemented with 20 g/L glucose with 3% LA at pH 3. The  $OD_{600}$  was measured at 4h intervals for the first 24hs and 12h intervals for the next 2 days. For fermentation, mutants and control strain with the initial  $OD_{600}$  of 1 were started in SC-Ura supplemented with 50g/L glucose. The bromocresol green assay was applied on 3-day fermentation culture to estimate the LA production. The top candidates from both tolerance screening and LA production screening were chosen for further verification and analysis. The plasmids from those candidates were extracted, sequenced and re-transformed back into fresh-background parent strain confirm the improvements. The improved strain can be used as new parent strain for the next round of engineering.

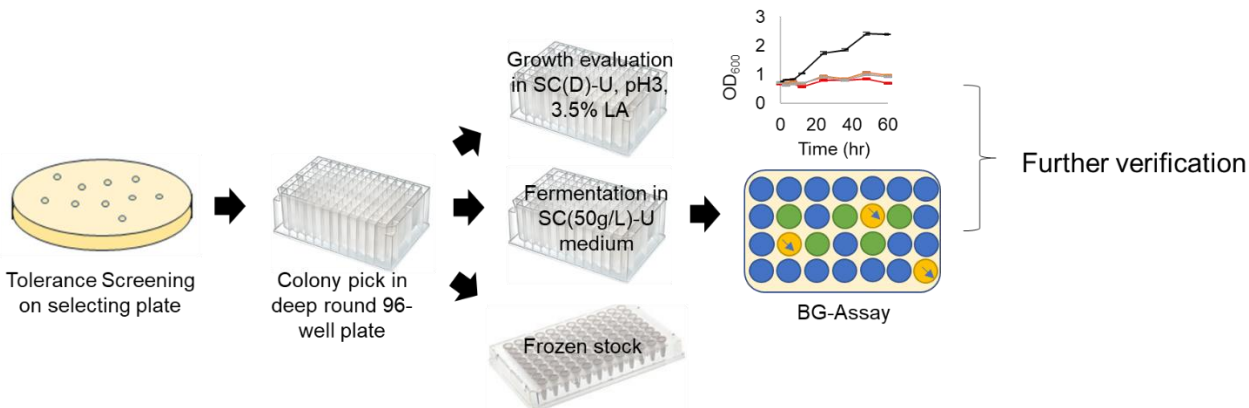


**Figure 5.13.** Schematic of library screening and verification.

#### 5.2.4. CADnm-RNAi RAGE 2.0 Library

CADnm is the mutant of CEN.PK2-1C with an reconstructed functional RNAi machinery. We first created CADnm-RNAi-RAGE 2.0 library to demonstrate the outperformance of RAGE 2.0 library in terms of improving the strain tolerance at low pH compared with the wild type. To ensure the adequate coverage,  $>10^6$  independent clones were obtained for both overexpression library CADnm-pRS416-TEF1p-RAGE2.0-Forward and (library size:  $1.1 \times 10^6$ ) and knockdown library CADnm-pRS416-TEF1p-RAGE2.0-Reverse (library size:  $4.4 \times 10^6$ ). We performed the enrichment selection of the overexpression and the knockdown libraries in SC-Ura liquid medium supplemented with 20 g/L glucose and 0% to 4% LA at pH 3.0. Both libraries outperformed the control strain in the first round of enrichment (Figure 5.14A)

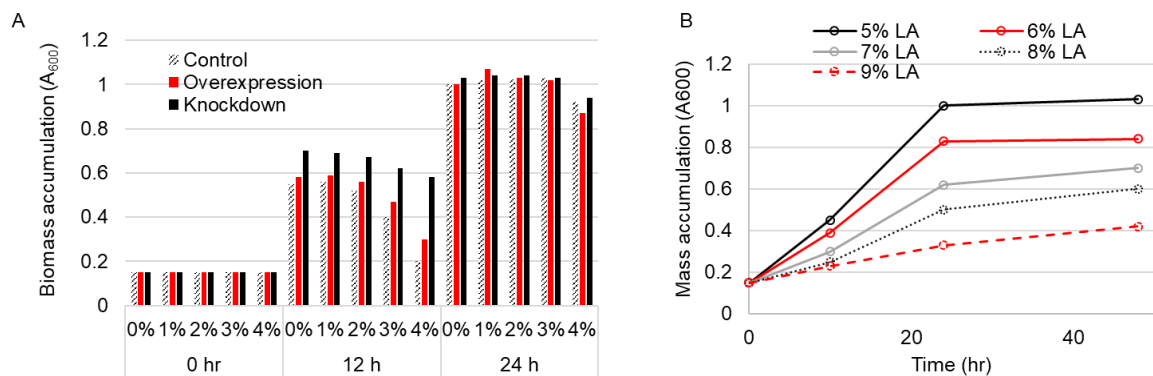


**Figure 5.14.** A) Comparison of RAGE 2.0 libraries with the control strain CADnm-pRS416 in SC-Ura liquid medium supplemented with 20 g/L glucose and 0~4% LA at pH 3. B) The growth profile of CADnm-pRS416 in SC-Ura liquid medium supplemented with 20 g/L glucose and 5~9% LA at pH 3.

Since the control strain also reached the same OD as the library at 4% LA. I evaluated the growth rate of the control strain at higher LA concentration (5% to 9%) (Figure 5.14B). CADnm has higher LA tolerance compared with PK2M3. The growth rate and maximum OD were reduced while increasing the LA concentration. Libraries in SC-Ura (20 g/L glucose, 7% LA, pH 3) were further enriched in the same medium four to five rounds to reach 625 to 3125-fold total enrichment. For each round enrichment, 2% inoculum was transformed into fresh SC-Ura (20 g/L glucose, 7% LA, pH 3) when the OD<sub>600</sub> exceeded 1 in a previous round. The enrichment was also performed on CADnm-pRS416 as a control. After enrichment, single colonies were obtained by streaking the library onto a SC-Ura plate containing 5% LA at pH 3. Fifty randomly picked colonies from each library were examined for growth in SC-Ura (20 g/L glucose, 5% LA, pH 3) (Figure 5.15). 35 candidates with either higher final OD<sub>600</sub> or faster exponential growth rate compared with the enriched control strain CADnm-pRS416 (enriched) were selected for further verification.

Plasmid library was isolated from the positive candidates and sequenced to elucidate the target gene information. 21 candidates down regulated the expression of *tup1*, encoding a chromatin-silencing transcriptional regulator. Interestingly, five candidates upregulated the expression of



*tup1* too. Other up- or downregulated candidates are summarized in Table 5.3. We transformed those isolated plasmids into fresh background CADnm and PK2M3-RNAi strain to confirm the improvements on the acid tolerance. Since CADnm strain has very strong tolerance to LA, the mutants did not show obvious improvements of growth in acid medium (Figure 5.16A,B). However, the final OD<sub>600</sub> of mutants PK2M3-RNAi-*tup1* (down), *tma10* (down), *tup1* (up), *bmh1* (up), *stf1*(down) was much larger than that of the parent strain PK2M3-RNAi-pRS416 in acidic medium with galactose as carbon source. Although PK2M3 has glucose “toxicity” due to gene modification, mutants with *tup1* being overexpressed, *tup1* (up), or knockdown, *tup1* (down), still overperformed the parent strain PK2M3 in terms of growth rate and final OD<sub>600</sub> (Figure 5.16C,D).

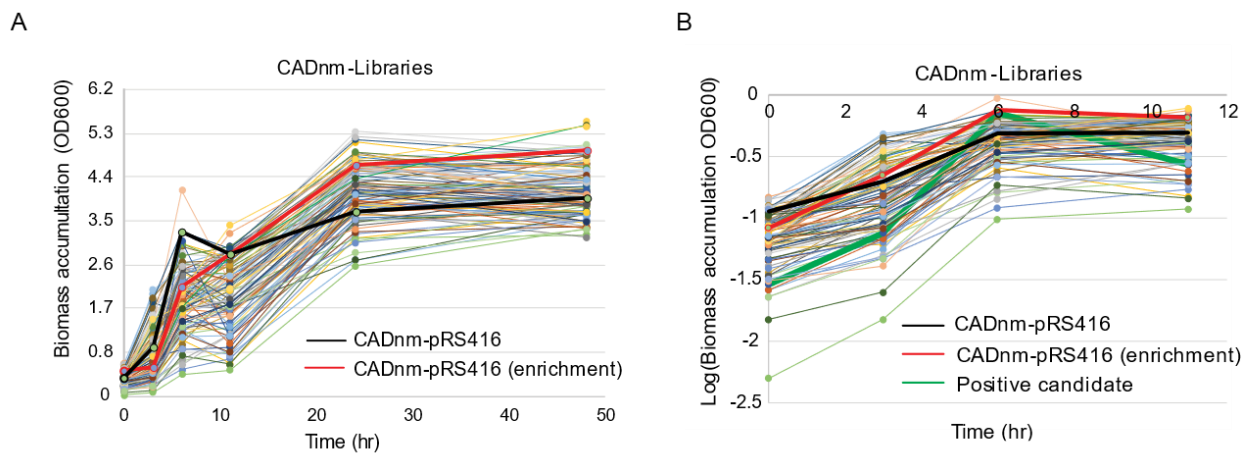


**Figure 5.15.** Growth profile evaluation of CADnm RAGE 2.0 libraries versus control CADnm-pRS416 in SC-Ura liquid medium supplemented with 20 g/L glucose and 3.5% LA at pH 3, A) biomass accumulation versus time B) growth rate versus time.

**Table 5.3.** Gene targets of top candidates from growth profile evaluation in selecting medium

| Gene         | Regulation | Repeatability | Comments   |
|--------------|------------|---------------|--|
| <i>tup1</i>  | Down       | 21/35         | Chromatin-silencing transcriptional regulator  |
| <i>tma10</i> | Down       | 2/35          | Protein abundance increases in response to DNA replication stress  |
| <i>stf1</i>  | Down       | 1/35          | ATPase-binding protein   |
| <i>phd1p</i> | Down       | 1/35          | Transcriptional activator that enhances pseudohyphal growth; physically interacts with the Tup1-Cyc8 complex and recruits Tup1p to its targets |
| <i>bmh1</i>  | Up         | 5/35          | Regulation protein   |
| <i>tup1</i>  | Up         | 5/35          | Chromatin-silencing transcriptional regulator  |

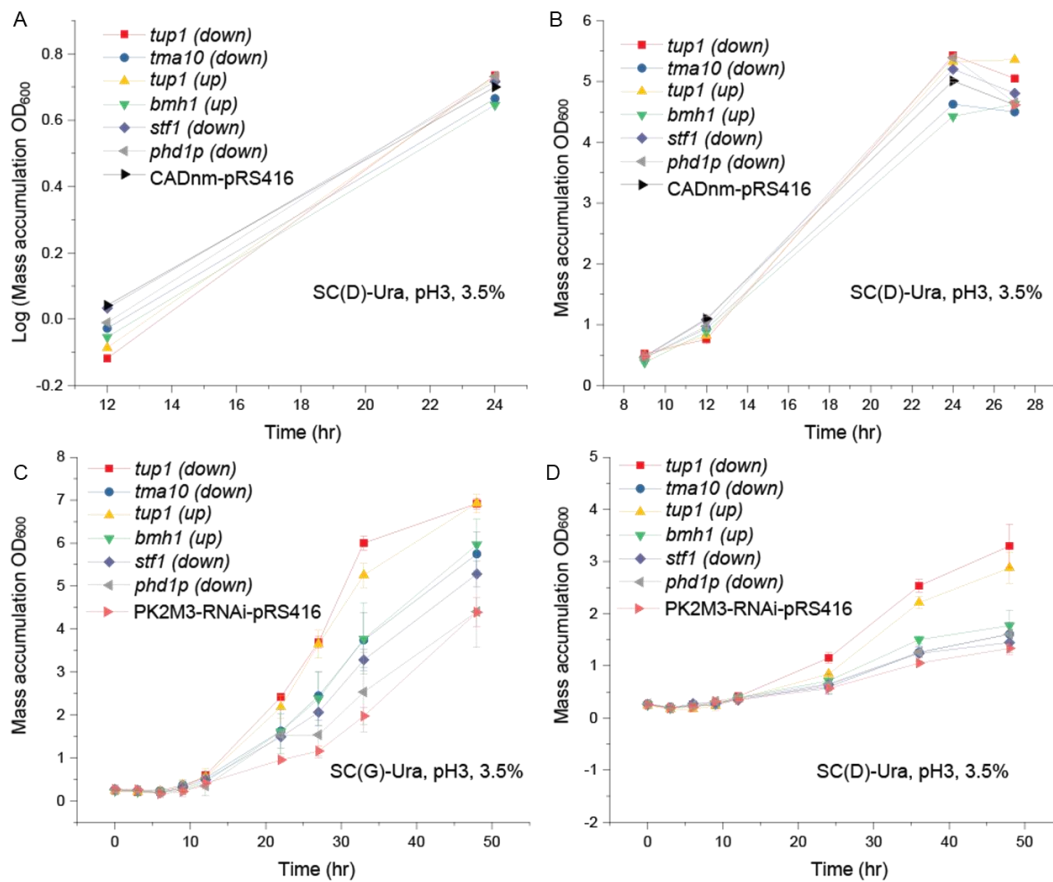


**Figure 5.16.** Growth profile evaluation of mutants versus control strain. A) log phase growth rate and B) mass accumulation of CADnm-mutants and control CADnm-pRS416 in SC-Ura with 20 g/L glucose and 3.5% LA at pH 3. C) mass accumulation of PK2M3-RNAi-mutants and control PK2M3-RNAi-pRS416 in SC-Ura with 20 g/L galactose and 3.5% LA at pH 3. D) mass accumulation of PK2M3-RNAi-mutants and control PK2M3-RNAi-pRS416 in SC-Ura with 20 g/L glucose and 3.5% LA at pH 3. The error bars represent the standard deviation of biologically triplicate experiments.

### 5.2.5. PK2M3nm-RNAi RAGE 2.0 Library

The PK2M3-RNAi-RAGE 2.0-overexpression and knockdown libraries were created by transforming the plasmid library pRS416-RAGE2.0-overexpression and pRS416-RAGE2.0-knockdown into the parent strain PK2M3-RNAi.  $10^6$  colonies were obtained for each library to ensure adequate coverage of all genes. The libraries were screened and analyzed by the method discussed in Section 5.2.3. Although the library mutants did not show as strong acid tolerance as the wildtype CADnm-pRS416, a lot of good candidates were identified with greatly improved acid tolerance compared with the parent strain PK2M3-RNAi-pRS416 (Figure 5.17). BG assay also indicated a few candidates with improved LA production in small-scale fermentation test.

21 candidates with either strongest acid tolerance or highest LA production were verified by re-transforming the corresponding plasmids into the fresh background PK2M3-RNAi. All selected mutants had higher final OD<sub>600</sub> than the parent strain PK2M3-RNAi-pRS416 (Figure 5.18). The mutants with stronger acid tolerance may not result in higher LA production (Figure 5.19). Permanent mutants of top three candidates, FA3, RG4, and RD5, with highest LA production and good acid tolerance were constructed by integrating the genetic regulation part into the chromosome of PK2M3-RNAi using YIp pRS404. Among them, except PK2M3-RNAi-FA3 in which an uncharacterized gene being overexpressed, both PK2M3-RNAi-RG4 and PK2M3-RNAi-RD5 have different genes being down-regulated. They are *fbal* and *htb1* encoding fructose-biphosphate aldolase and core histone protein required for chromatin assembly and chromosome function respectively.

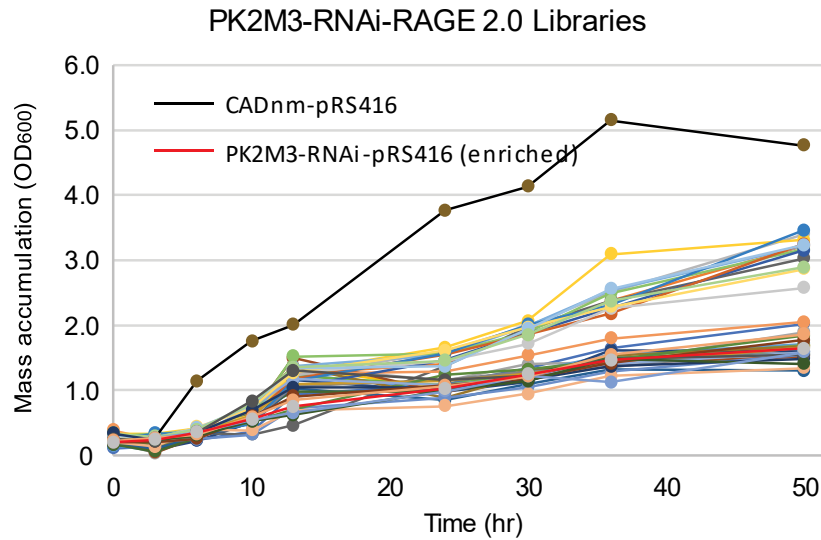


**Figure 5.17.** Growth profile of PK2M3-RNAi-RAGE 2.0 libraries versus wild type CADnm-pRS416 and parent strain PK2M3-RNAi-pRS416 in selection medium SC-Ura supplemented with 20 g/L glucose and 3.5% LA at pH 3.

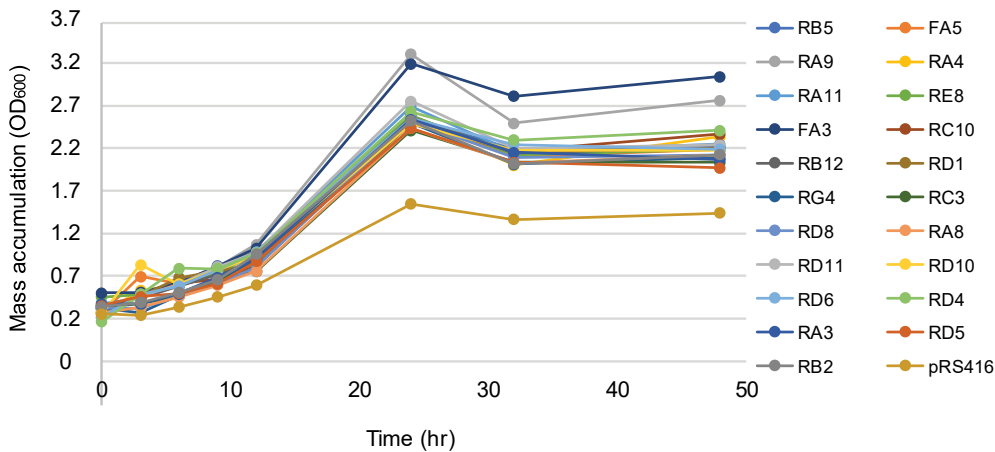


**Figure 5.18.** Growth profile verification of top 21 mutants from the first-round screening versus the parent strain PK2M3-RNAi-pRS416 in selecting medium SC-Ura supplemented with 20 g/L glucose and 3.5% LA at pH 3.

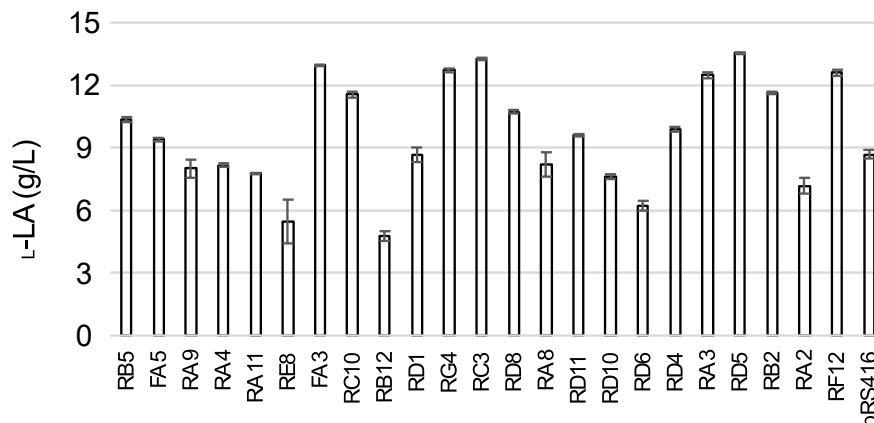


**Figure 5.19.** L-LA production in 2-mL falcon tube fermentation (SC-Ura supplemented with 50 g/L glucose) measured by HPLC. The error bars represent the standard deviation of biologically triplicate experiments.

Among, PK2M3-RNAi-FA3, PK2M3-RNAi-RD5 and PK2M3-RNAi-RG4, only PK2M3-RNAi-FA3 shew stronger acid tolerance compared with the parent strain (Figure 5.20 A). Compared with PK2M3-RNAi-pRS416-RD5 and RG4, the permanent mutants PK2M3-RNAi-RD5 and PK2M3-RNAi-RG4 only have single copy of gene regulation module, which may result in weaker acid tolerance. In the shake-flask fermentation with minimum medium SC supplemented with 50 g/L glucose, the glucose consumption rate of FA3 was faster than that of other three strains (Figure 5.20 B). Three mutants had higher L-LA production rate and production than the parent strain. PK2M3-RNAi-FA3 produced 1.5 times more L-LA than the parent strain and had highest final OD<sub>600</sub> at the end of fermentation (Figure 5.20 C&D). Thus PK2M3-RNAi-FA3 was chosen as the best candidates to do semi-batch fermentation.

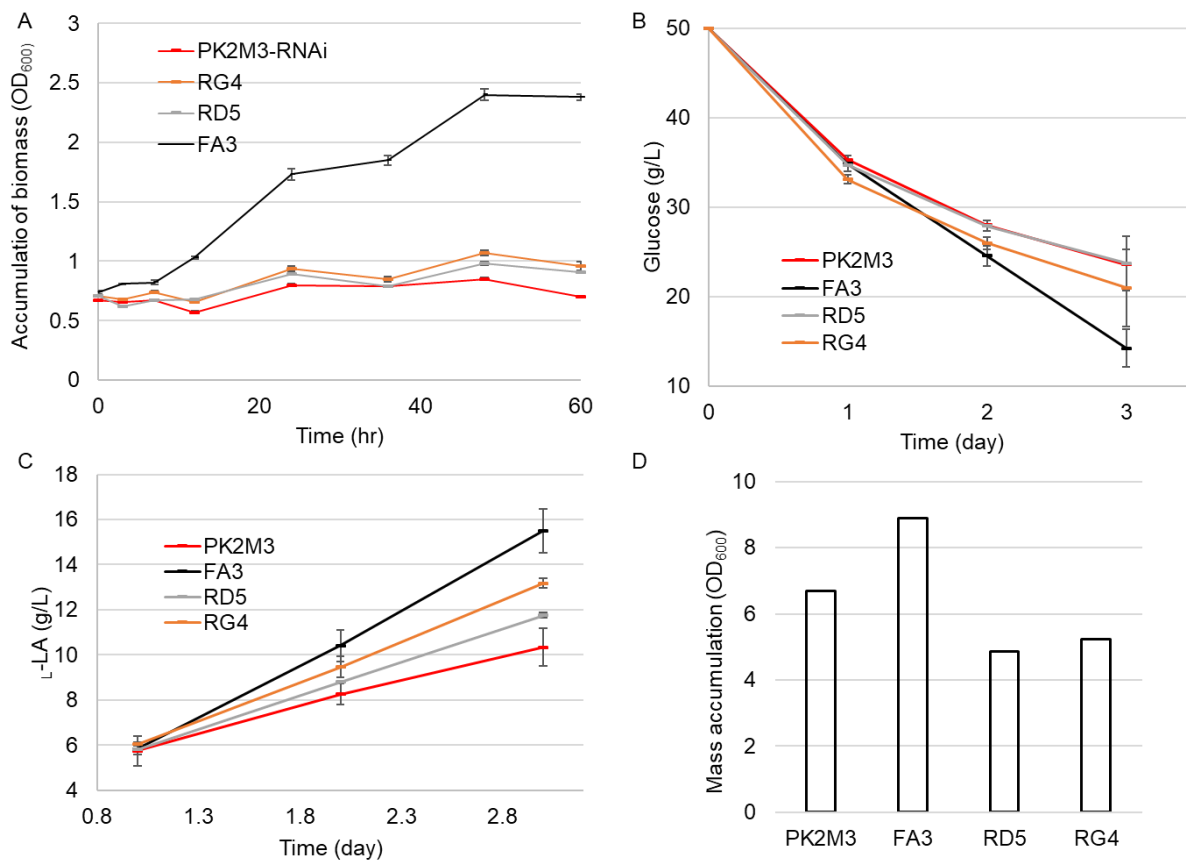


**Figure 5.20.** Acidic tolerance and L-LA productivity of PK2M3-RNAi-FA3, RG4, RD5 versus the parent strain PK2M3-RNAi-pRS416. A) growth profile evaluation in the selecting medium SC-Ura supplemented with 20 g/L glucose and 3.5% LA at pH 3. B) glucose consumption in flask fermentation with SC supplemented with 50 g/L glucose. C) L-LA production in the flask fermentation. D) Final OD<sub>600</sub> in the flask fermentation. The error bars represent the standard deviation of biologically triplicate experiments.

### 5.2.6. PK2M3nm-PAID6 CRISPR-AID Library

PK2M3-PAID6-Activation, PK2M3-PAID6-Inactivation and PK2M3-PAID6-Deletion libraries were created by transforming plasmid libraries pRS426-CRISPR-Activation, pRS426-CRISPR-Inactivation and pRS426-CRISPR-Deletion into the parent strain PK2M3-PAID6.  $3 \times 10^6$ ,  $2 \times 10^6$  and  $1 \times 10^6$  colonies were obtained for each library respectively to ensure the adequate coverage. The libraries were screened and analyzed by the method discussed in section 5.2.3. Top 28

candidates from the first-round acid tolerance and BG assay screening were picked for further verification. Among them, 14 candidates were from activation library; 11 candidates were from inactivation library and only 3 candidates were from the deletion library. The plasmids from the top candidates were extracted and sequenced to elucidate the target gene. The mutants with overexpression of an uncharacterized gene 4833, knockdown of *tef1*, or *spt4* are especially interesting since there are more than two screened mutants targeting at those genes respectively.

28 candidates were verified by re-transforming the corresponding plasmids into the fresh background PK2M3-PAID6 strain. Only four mutants A-A5, I-E5, I-H7 and I-H8 had higher final OD<sub>600</sub> than the parent strain PK2M3-PAID6-pRS426 (Figure 5.21). They are mutants with 4833 being overexpressed, *tef1*, *spt4* and *som1* being down regulated respectively. *Tef1* and *spt4* encode translational elongation factor and transcriptional elongation factor respectively. SOM1 is the subunit of the mitochondrial inner membrane peptidase. None of them has been reported to improve yeast acid tolerance in the literature.

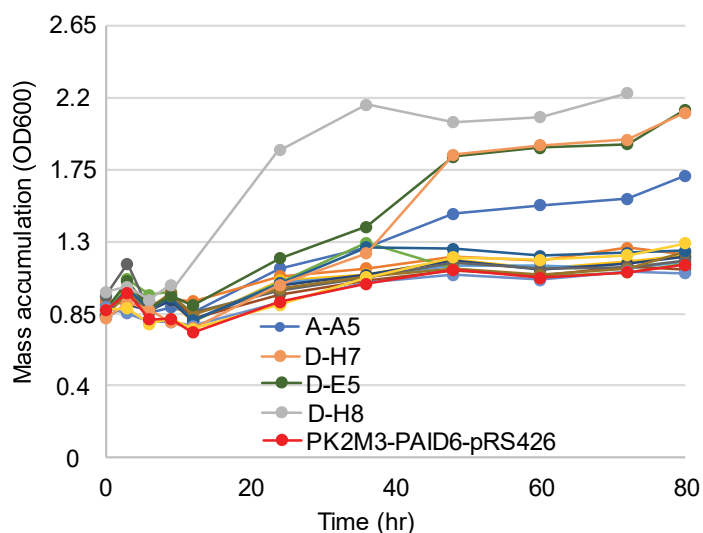


**Figure 5.21.** Growth profile verification of top 28 mutants from the first-round screening versus the parent strain PK2M3-PAID6-pRS426 in selecting medium SC-Ura supplemented with 20 g/L glucose and 3.5% LA at pH 3.

To make the stable mutant, gene-targeting module including the gRNA were integrated into the pre-tested spots in the genomic DNA of the parent strain by using CRISPR-based gene-editing strategy. The insertion of extracellular DNA at those spots does not affect the strain's overall phenotype. The resulted mutants PK2M3-PAID6-H7, E5 and A5 still had stronger acidic tolerance than the parent strain PK2M3-PAID6-pRS426 (Figure 5.22A). In the shake-flask fermentation with minimum medium SC supplemented with 50 g/L glucose, PK2M3-PAID6-A5 and E5 grew faster, consumed glucose faster and produced more LA than the other three strains. Interestingly, although PK2M3-PAID6-H7 had strongest acid tolerance among all mutants, it produced least LA within 4-day fermentation, which means stronger acid tolerance may not lead to higher LA production. From the first round CRISPR-AID library screening, two mutants were identified with improved acid tolerance and LA production compared with the parent strain. They are PK2M3-RNAi-A5 in which an uncharacterized gene 4388 being overexpressed, and PK2M3-RNAi-E5 in which *tef1* being transcriptional down regulated.



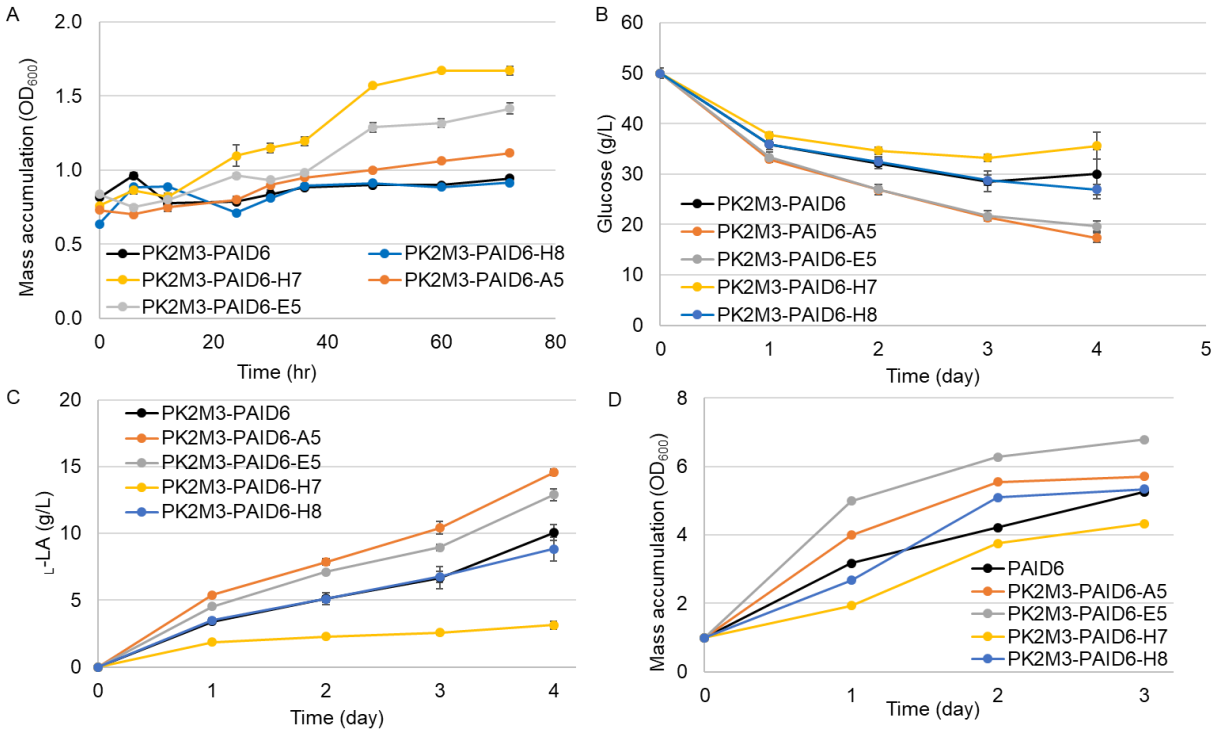


**Figure 5.22.** Acidic tolerance and L-LA production of PK2M3-PAID6-A5, E5, H7 and H8 versus the parent strain PK2M3-PAID6. A) growth profile evaluation in the selecting medium SC-Ura (3.5% LA, pH 3). B) glucose consumption in flask fermentation with SC supplemented with 50 g/L glucose. C) L-LA production in flask fermentation. D) mass accumulation in flask fermentation. The error bars represent the standard deviation of biologically triplicate experiments.

### 5.2.7. Fermentation

We also evaluated L-LA production of PK2M3-RNAi-FA3 in fed-batch bioreaction at pH 3.0 using a 1L bench-top bioreactor. In 500 mL fed-batch fermentation, by consuming 68 g glucose, up to 52 g/L of L-LA was produced with a yield of 0.77 g/g.

## 5.3 Conclusion

In this study, we constructed a LA producing mutant PK2M3 that can produce 40 g/L L-LA in fed-batch fermentation with YPD medium. We constructed RNAi and CRISPR-AID machinery in PK2M3 and using PK2M3 as the parent strain to apply genome-wide engineering to improve the

acid tolerance and LA overproduction. The first-round engineering resulted in one permeant mutant from PK2M3-RAGE 2.0 library and two mutants from PK2M3-CRISPR-AID libraries with up to 2.5-times acid tolerance and 1.5-times LA production compared with the parent strain. The best mutant PK2M3-RNAi-FA3 with an unknown gene overexpressed can produce up to 52 g/L L-LA in fed-batch fermentation with SC medium. To adapt the selection process into ACE platform for high throughput screening, we also developed a growth-based LA biosensor and an automated quantification assay based on industry-standard BioProfile Analyzer. The best candidates from the first-round engineering would be used as the new parent strain for multiple rounds engineering.

## 5.4 Future Work

Pk2M3-RNAi-FA3 will be used to perform second or third round genome-wide engineering to further improve the acid tolerance and LA production. We will also develop the whole engineering and selection process on iBioFAB and using automotive cellular platform to realize iterative engineering in high throughput manner.

LA is exported out of the cell after being synthesized. At low pH, lactic acid is present in its protonated form and can therefore enter the cell by diffusion. General bulk fermentation followed by Fluorescence Activated Cell Sorting (FACS) cannot be used to identify the mutants producing more LA than others. We are establishing a microfluidics droplet system. Droplet-based microfluidics system can be used to generate water in oil droplet with similar size to compartmentalize single cells, which enable the analysis of metabolites released from or secreted by the cells.<sup>13</sup> Stephanopoulos and co-workers used microfluidic system and build-in fluorescence-based sorting facility to successfully enriched L-lactate -producing *E. coli* clones 5,800X from a population containing one L-lactate producer per 10<sup>4</sup> D-lactate producers.<sup>14</sup> Alper and co-workers

recently using double emulsion (W/O/W) to sort out riboflavin overproduced *Yarrowia lipolytica*.<sup>15</sup> We plan to combine L-lactate biosensor with both single water in oil (W/O) droplet system followed by breaking the droplet for FACS and double emulsion (W/O/W) that would be directly applied on FACS to screen out high LA producing mutants.

## 5.5 Experimental Procedures

### 5.5.1. Strains and Media and Culture Conditions

All yeast mutants used in this study are described in Table 5.4. *S.cerevisiae* CEN.PK2-1C strain (*MATa ura3-52 trp1-289 leu2-3,112 his3Δ1 MAL2-8C SUC2*) was used as a parental strain in this study. The deletion of ADH and PDC gene inhibited the mutant's growth in glucose media. All mutants were cultivated in YP medium (20 g/L peptone and 10 g/L yeast extract), synthetic complete (SC) or synthetic drop-out medium (SC drop-out) (1.67 g/L Difco Yeast Nitrogen Base without amino acids, 5 g/L ammonium sulfate, 0.83 g/L synthetic complete drop out mix) supplemented with 20 g/L galactose.

For rich medium fermentation, all yeast cells were cultivated in YP medium supplemented with 20, 50 or 100 g/L glucose. For selective medium fermentation, yeast cells were cultivated in synthetic complete (SC) or synthetic drop-out medium (SC drop-out) supplemented with 20, 50 or 100 g/L glucose. Pre-cultured cells ( $OD_{600}=1$ ) were inoculated in 5 mL of media containing 50 g/L glucose in a 50 mL screw cap conical tube, and then cultured at 30 °C with shaking at 250 rpm. For shake flask fermentation, precultured cells ( $OD_{600}=1$ ) were cultivated in 20 mL of media medium containing 50 g/L glucose in a 125 mL conical flask.

Acidic selecting agar plates were made of normal SC or SC-Ura plate supplemented with 3.5% LA at pH 3.0. Acidic selecting medium were made of normal SC or SC-Ura plate supplemented with 3.5% LA at pH 3.0.

Fed-batch fermentation was performed in 500 mL SC medium containing 50 g/L glucose using a 1L bench-top bioreactor at 30°C with agitation speed of 450 rpm and air flow rate of 1.0 vvm. The pH of the culture medium was maintained at 3.5 by using 4 N NaOH. Strain PK2M3-RNAi-FA3 was pre-cultured in SC medium containing 20 g/L glucose and inoculated into the fermenter with initial OD<sub>600</sub> of 10. The feeding solution (600 g/L glucose and half the vol of 2XSC) was intermittently added to the culture medium when the glucose concentration was lower than 5 g/L.

**Table 5.4.** The strain information of this study.

| Strains          | Genotype and description   | Reference  |
|------------------|--|------------|
| CEN.PK2-1C       | <i>MATa ura3-52 trp1-289 leu2-3,112 his3Δ1 MAL2-8C SUC2</i>  | EUROSCARF  |
| PK2M1            | CEN.PK2.1C<br><i>adh1Δ::loxP::adh4Δ::loxP::gpd1Δ::loxP::gpd2Δ::loxP</i>  | This Study |
| PK2M2            | PK2M1 <i>adh1Δ::P<sub>TEF1</sub>-Lp.ldh-T<sub>TEF1</sub></i>   | This Study |
| PK2M3            | PK2M1 <i>adh1Δ::P<sub>TEF1</sub>-Lpm.ldh-T<sub>TEF1</sub></i>  | This Study |
| PK2M4            | PK2M1 <i>adh1Δ::P<sub>TEF1</sub>-Lb.ldh-T<sub>TEF1</sub></i>   | This Study |
| PK2M5            | PK2M1 <i>adh1Δ::P<sub>TEF1</sub>-Ro.ldh-T<sub>TEF1</sub></i>   | This Study |
| PK2M3-RNAi       | PK2M3 d:: <i>TEF1p-Ago-TPI1-Dcr</i>  | This Study |
| PK2M3-PAID6      | PK2M3 KanMX- <i>TDH3p-dLbCpf1-VP64-p65-ADH1t-ENO2p-Csy4-PGK1tTPI1p-dSpCas9-RD11-RD5-RD2-TPI1t-TEF1p-SaCas9-TEF1t</i>   | This Study |
| CADnm            | CEN.PK2-1C d:: <i>TEF1p-Ago-TPI1-Dcr</i>   | 7          |
| PK2M3-RNAi-FA3   | PK2M3-RNAi pRS404- <i>TEF1p-fa3-PGK1t</i>  | This Study |
| PK2M3-RNAi-RD5   | PK2M3-RNAi pRS404- <i>PGK1t-htb1-TEF1p</i>   | This Study |
| PK2M3-RNAi-RG4   | PK2M3-RNAi pRS404- <i>PGK1t-fba1-TEF1p</i>   | This Study |
| PK2M3-PAID6-A5   | PK2M3-PAID6 <i>SAR52p-LbCpf1 scaffold-4833 gRNA-SUP4t</i>  | This Study |
| Table 5.4. cont. |  |            |
| PK2M3-PAID6-H7   | PK2M3-PAID6 <i>SAR52p-SpSgRNA structure-spt4 gRNA-SUP4t</i>  | This Study |
| PK2M3-PAID6-E5   | PK2M3-PAID6 <i>SAR52p-SpSgRNA structure-tef1 gRNA-SUP4t</i>  | This Study |
| PK2M3-PAID6-H8   | PK2M3-PAID6 <i>SAR52p-SpSgRNA structure-som1 gRNA-SUP4t</i>  | This Study |
| JHY5610          | CEN.PK2-1C <i>adh1Δ::loxP adh2Δ::loxP adh3Δ::loxP adh4Δ::loxP::adh5Δ::loxP gpd1Δ::loxP gpd2Δ::loxP::dld1Δ::P<sub>TDH3</sub>-Lm.ldhA-T<sub>CYC1</sub>-loxP-kanMX-loxP</i> | 9          |
| JHY5617*         | JHY 5610: <i>erf2Δ, SUR<sup>245S</sup>-kanMX</i>   | 9          |

## 5.5.2. Plasmid Construction

All major primer and plasmids used in this study are described in Table 5.5 and Table 5.6 respectively.

**Table 5.5.** All major primers used in this study

| Name                              | Sequence   | Description  |
|-----------------------------------|--|--|
| <b>loxP-ADH5-rev</b>              | cgataggccagctaagtggatcgagattgatcaaacctctggc<br>cataggccactagtgat   |  |
| <b>TEF1t-loxP-for</b>             | gatattgctgtaacaaatactttgatcgggcgtat cagctgaagcttcgtacg             | <i>Overlap extension PCR to construct TEF1p-LDH-TEF1p-Loxp-KanMx-Loxp cassette</i> |
| <b>TEF1t-rev</b>                  | atagcgccgatcaaagta   |  |
| <b>ADH5-TEF1p-for</b>             | atgccttcgcaagtcattcctgaaaaacaaaaggctattgtcttt gcggatagcttcaaaatg   |  |
| <b>ADH5-for</b>                   | atgccttcgcaagtcatt   |  |
| <b>ADH5-rev</b>                   | cgataggccagctaagtg   |  |
| <b>GFP-for</b>                    | tagcaatctaatactaaagtttaattacaaa atgcgtaaaggagaagaa                 | <i>Construct pRS414-GFP</i>  |
| <b>GFP-rev</b>                    | tgatcatgaattaataaaaagtgttcgcaaattattgtatagttcatc                   |  |
| <b>GFPrc-for</b>                  | atctaagtttaattacaaaactattgtatagttcatc                              | <i>Construct pRS416-GFPrc</i>  |
| <b>GFPrc-rev</b>                  | cgatttcaattcaattcaatatgagtaaaggagaagaa                             |  |
| <b>pRS404-Insert_fwd</b>          | cgataagcttgatcgaattcagcaacaggcgcttgga                              | <i>Construct pRS404-TEF1p-FA3, RD5, RG4-PGK1t</i>                                  |
| <b>pRS404-Insert_rev</b>          | cgctctagaactagtgatccaggaagaatacactatactggatctaaagagtac             |  |
| <b>X-3-INT-SNR52F</b>             | atcaggcacgaaggcacactcgtatgcatgtgttgaaacttgaaaagataatgatg           | <i>Together with pSg335 to make mutant PK2M3-PAID6-H7</i>                          |
| <b>X-3-INT-M13R</b>               | ttccatggggtcgcaactttcccgggtgacctctacatgtaggaaacagctatgacctg        |  |
| <b>XI-1-INT-SNR52F</b>            | gcgccggtttctcttccacggaataccaagccatctttgaaaagataatgatg              | <i>Together with pSg337 to make mutant PK2M3-PAID6-H8</i>                          |
| <b>XI-1-INT-M13R</b>              | ctgtacgcagcatttagcagagatttgccaatgccaagaaaggaaacagctatgacctg        |  |
| <b>XII-2-INT-SNR52F</b>           | tgcgtctaacgctttgcccacttgatttctattataggactttgaaaagataatgatg         | <i>Together with pSg341 to make mutant PK2M3-PAID6-E5</i>                          |
| <b>XII-2-INT-M13R</b>             | aagaaattcttctgtgcttcatcaaaacgcgaaaattcgaggaaacagctatgacctg         |  |
| <b>XI-3-INT-SNR52F</b>            | ccaatcaaagaagcatcggttcagatcgagcaaaactgtagctttgaaaagataatgatg       | <i>Together with pSg339 to make mutant PK2M3-PAID6-A5</i>                          |
| <b>XI-3-INT-M13R</b>              | tgacatcaaaactacaaaaccgagattggacatatagcacaggaaacagctatgacctg        |  |
| <b>LA001</b>                      | gtaccgggccccctcgagaagcttctgtctttcttg                               | <i>Construct pRS405-LAb1/LAb2</i>  |
| <b>LA002</b>                      | agttcttctcttactcattattgtaatatgtgtgtttgttg                          |  |
| Table 5.5. cont.                  |  |  |
| <b>LA003</b>                      | aatctaagtttaattacaaaatgattgtttaccagacgc                            | <i>Construct pRS416-LIdR</i>   |
| <b>LA004</b>                      | cgatttcaattcaattcaattcaaaactttcttttttttggtggtgcgcttttctcccctcgaatg |  |
| <b>pRS426-HindIII-TEF1p-for</b>   | aatacgactcactatagg   | <i>Construct pRS426-TEF1p-PGK1t</i>  |
| <b>pRS426-BamHI-PGK1t-rev</b>     | taaaggaacaaaagctg  |  |
| <b>LIdR-cm-GA-for</b>             | aatctaagtttaattacaaa atgattgtttgccaaga                             | <i>Construct pRS416-LIdRcm</i>   |
| <b>LIdR-cm-GA-rev</b>             | cgatttcaattcaattcaatttaaacctttctttttttttg                          |  |
| <b>pRS426-HindIII-TEF1p-for-3</b> | gtcgacggatcgataagctt agcaacaggcgcttgga                             | <i>Construct pRS426-TEF1p-LIdR-PGK1t</i>   |
| <b>pRS426-BamHI-PGK1t-rev-3</b>   | gatccccggggtgcaggaatt caggaagaatacactatactggat                     |  |

**Table 5.6.** The major plasmids used in this study

| <b>Plasmid</b>                        | <b>Genotype</b>  | <b>Source or Reference</b>    |
|---------------------------------------|--|-------------------------------|
| <b>pH5-<i>Lpldh</i></b>               | pRS425-TEF1p- <i>Lpldh</i> -TEF1t                      | This study                    |
| <b>pH5-<i>Lpml dh</i></b>             | pRS425-TEF1p- <i>Lpml dh</i> -TEF1t                    | This study                    |
| <b>pH5-<i>Lbldh</i></b>               | pRS425-TEF1p- <i>Lbldh</i> -TEF1t                      | This study                    |
| <b>pH5-<i>Roldh</i></b>               | pRS425-TEF1p- <i>Roldh</i> -TEF1t                      | This study                    |
| <b>pRS414-GFP</b>                     | pRS414-TEF1p-GFP-HX7Tt                                 | This study                    |
| <b>pRS416-GFPrc</b>                   | pRS414-TEF1p-GFPrc-HXPGK1t                             | This study                    |
| <b>pRS-Ago</b>                        | pRS-delta-KanMX-LoxP-TEF1p-AGO1-PGK1t-TPI1p-DCR1-GPD1t | <sup>10</sup>                 |
| <b>pRS404-FA3</b>                     | pRS404- <i>TEF1p-fa3-PGK1t</i>                         | This study                    |
| <b>pRS404-RD5</b>                     | pRS404- <i>PGK1t-htb1-TEF1p</i>                        | This study                    |
| <b>pRS404-RG4</b>                     | pRS404- <i>PGK1t-fba1-TEF1p</i>                        | This study                    |
| <b>pSg335</b>                         | pRS426-X-3-gRNA  | Lian et. al.<br>(unpublished) |
| <b>pSg337</b>                         | pRS426-XI-1-gRNA                                       | Lian et. al.<br>(unpublished) |
| <b>pSg341</b>                         | pRS426-XII-2-gRNA                                      | Lian et. al.<br>(unpublished) |
| <b>pSg339</b>                         | pRS426-XI-3-gRNA                                       | Lian et. al.<br>(unpublished) |
| <b>pRS405-LAb1</b>                    | pRS405- <i>LAB3-GFP-PGK1t</i>                          | This study                    |
| <b>pRS405-LAb2</b>                    | pRS405- <i>LAB3-GFP-PGK1t</i>                          | This study                    |
| <b>pRS405-LAb3</b>                    | pRS405- <i>LAB3-GFP-PGK1t</i>                          | This study                    |
| <b>pRS416-LldR</b>                    | pRS416- <i>TEF1p-LldR-PGK1t</i>                        | This study                    |
| <b>pRS416-LldRcm</b>                  | pRS416- <i>TEF1p-LldRcm-PGK1t</i>                      | This study                    |
| <b>pRS425-LldRcm</b>                  | pRS426- <i>TEF1p-LldRcm-PGK1t</i>                      | This study                    |
| <b>pRS416-RAGE 2.0-Overexpression</b> | pRS416- <i>TEF1p-cDNA-PGK1t</i>                        | <sup>7</sup>                  |
| <b>pRS416-RAGE 2.0-Knockdown</b>      | pRS416- <i>TEF1p-cDNArc-PGK1t</i>                      | <sup>7</sup>                  |
| <b>pRS426-CRISPR-A</b>                | pRS426-SAR52p- <i>LbCpf1</i> scaffold-gRNA-SUP4t       | Lian et. al.<br>(unpublished) |
| Table 5.6. cont.                      |  |                               |
| <b>pRS426-CRISPR-I</b>                | pRS426-SAR52p- <i>SpSgRNA</i> structure-gRNA-SUP4t     | Lian et. al.<br>(unpublished) |
| <b>pRS426-CRISPR-D</b>                | pRS426-SAR52p- <i>SaRNA</i> structure-gRNA-SUP4t       | Lian et. al.<br>(unpublished) |

### 5.5.3. Construction of Genetically Manipulated Strains

PK2M1 was created by deleting *adh1*, *adh4*, *gpd1* and *gpd2* in CEN.PK2-1C consecutively using Cre-mediated gene knockouts methods.<sup>16</sup> PK2M2, PK2M3, PK2M4 and PK2M5 were created by

replacing *ADH5* with *Lp-ldh*, *Lpm-ldh*, *Lp-ldh* and *Ro-ldh* respectively using Cre-mediated gene knock-in methods.<sup>16</sup>

#### 5.5.4. Analytical Methods

To determine the concentration of acetate, ethanol, glucose and lactate, all samples collected from culture supernatants were centrifuged 10 minutes at 13000 rpm and the supernatant were quantified by high performance liquid chromatography (HPLC). HPLC analysis was performed in UltiMate 3000 HPLC system (Thermo Fishers Scientific) equipped with a Bio-Rad Aminex HPX-87H column at 60 °C with 5 mM H<sub>2</sub>SO<sub>4</sub> at a flow rate of 0.6 mL/min and refractive index (RI) as a detector keeping at 35 °C. Cell growth was monitored by determining optical density at 600 nm.

#### 5.5.5. Bromocresol Green Assay

Lactic acid and bromocresol green were purchased from Sigma-Aldrich (St. Louis, MO). Bromocresol green reaction solution (BG) was prepared by dissolving 60 mg bromocresol green powder into 1 L distillation water. The pH of the solution was adjusted to 5.5 while the solution just turned into deep blue by using sodium hydroxide. All fermentation samples (around 20 g/L) were diluted 5 times. While doing the measurements, 200 uL BG solution was added in a Corning UV-Transparent Microplates with clear flat bottom (ThermoFisher Scientific, Rockford, IL). 2 uL diluted fermentation sample was mixed well with reaction solution and the A<sub>616 nm</sub> absorbance was recorded with Cary 300 UV-Vis spectrophotometer (Agilent Technologies, Santa Clara, CA)

#### 5.5.6. LOD Assay

L-Lactic acid, lactate oxidase from *Aerococcus viridans* (L9795) and Fluorometric Hydrogen Peroxide Assay kit (FHP) were purchased from Sigma-Aldrich (St. Louis, MO). Lactate oxidase master mix (LOD-MM) was prepared by suspended LOD with assay buffer from FHP assay kit

resulting in 0.01 U/uL solution. FHP master mix (MM) was prepared right before the measurements by following the FHP assay kit protocol. All fermentation samples (around 20 g/L concentration) were diluted 200 times with assay buffer. While doing the measurements, 50 uL LOD-MM mixed with 50 uL MM and was added in a Corning 96-well, clear bottom fluorescence plate (ThermoFisher Scientific, Rockford, IL). 2 uL diluted fermentation sample was mixed well with reaction solution. The plate was incubated at room temperature for 30 minutes. The fluorescent signal was detected using a Tecan Infinite M1000 PRO microplate reader (Morrisville, NC). The excitation and emission wavelength of FHP kit were set at 540 nm and 590 nm respectively. All experiments were performed in triplicate.

### 5.5.7. Sensor Activity Assays

For the characterization of L-LA sensor/regulating gene circuit in *S. cerevisiae* CEN.PK2.1C, PK2M1 strain was transformed with each circuit-containing plasmid and plated on SC-His-Ura plates supplemented with 20 g/L glucose. Single colonies were inoculated into 2 mL SC-Ura-His liquid medium supplemented with 20 g/L glucose. Overnight culture was sub-cultured one time to synchronize the growth. The subculture was inoculated in 2 mL of SC-Ura liquid medium supplemented with 20 g/L glucose and different amount of L-LA with an initial OD<sub>600</sub> of 1.0. Strains were cultured at 30 °C and 250 rpm. Samples were taken at 24 hr for flow cytometry analysis.

For the characterization of L-LA sensor/regulating gene circuit in L-LA producing *S. cerevisiae*. PK2M3, PK2M4 and PK2M5 was transformed with each circuit-containing plasmid and plated on SC-His-Ura plates supplemented with 20 g/L glucose. Single colonies were inoculated into 2mL SC-Ura-His liquid medium supplemented with 20 g/L glucose. Overnight culture was sub-cultured one time to synchronize the growth. The subculture was inoculated in 2



mL of SC-Ura liquid medium supplemented with 20 g/L glucose, or 100 mM citrate-phosphate with an initial OD<sub>600</sub> of 1.0 or YPD liquid medium with an initial OD<sub>600</sub> of 0.4. Strains were cultured at 30 °C and 250 rpm. Samples were taken at 24 hr for flow cytometry analysis.

### 5.5.8. Library Construction and Screening

In the CAD, PK2M3-RNAi or PK2M3-PAID6 strains, the standard LiAc/ssDNA/PEG protocol was used to transform 10 ug to 20 ug RAGE or CRISPR-AID library plasmids based on the transformation efficiency of about 0.5 ~ 3×10<sup>5</sup> cfu/ug. The library DNA (20 ug) was able to achieve a library size of more than 1×10<sup>6</sup> to ensure a nearly complete coverage of the yeast genome.<sup>10</sup> Following the transformation, the RAGE library yeast cells were plated onto 150 mm diameter Petri-dish plates of solid SC(G)-U medium supplemented with 3.5% LA at pH 3.0. The CRISPR-AID library yeast cells were recovered in SC(G)-URA medium to saturation and plated onto 150 mm diameter Petri-dish plates of solid SC(G)-U medium supplemented with 3.5% LA at pH 3.0. The number of cells were adjusted so that each plate would form about 10<sup>4</sup> on SC-URA plate while about 10<sup>3</sup> on an SC-URA (pH3, 3% LA) plate. The library and control plates were incubated at 30 °C for 3-4 days. Thirty three colonies whose sizes were bigger than the largest colonies on the control plates or first appeared on the selection plate were picked from the library plates. The growth performances of the selected colonies and the control strain were compared in SC(D)-Ura liquid medium with 3.5% LA at pH3. The LA production levels of the mutants and control were compared in SC-Ura medium supplemented with 50g/L glucose and evaluated by BG assay. The plasmids from the top strains whose growth behaviors or LA production were considerably better than the control strain were isolated and amplified by *E. Coli*. The plasmids were sequenced to identify the gene targets. The selected plasmids were then individually retransformed in a fresh background parent strain. Growth behaviors and LA production were

evaluated again to confirm the improved quality compared with the parent strain. To confirm a given gene-target, a designed mutant was constructed by integrating the corresponding RNAi cassette or CRISPR AID modular part into the chromosome of a fresh background strain.

## 5.6 References

- 1 Castro-Aguirre, E., Iñiguez-Franco, F., Samsudin, H., Fang, X. & Auras, R. Poly(lactic acid)—Mass production, processing, industrial applications, and end of life. *Advanced Drug Delivery Reviews* **107**, 333-366, (2016).
- 2 Upadhyaya, B. P., DeVeaux, L. C. & Christopher, L. P. Metabolic engineering as a tool for enhanced lactic acid production. *Trends Biotechnol* **32**, 637-644, (2014).
- 3 Abdel-Rahman, M. A. & Sonomoto, K. Opportunities to overcome the current limitations and challenges for efficient microbial production of optically pure lactic acid. *J. Biotechnol.* **236**, 176-192, (2016).
- 4 Song, J. Y. *et al.* Introduction of a bacterial acetyl-CoA synthesis pathway improves lactic acid production in *Saccharomyces cerevisiae*. *Metab Eng* **35**, 38-45, (2016).
- 5 Baek, S. H. *et al.* Improvement of d-Lactic Acid Production in *Saccharomyces cerevisiae* Under Acidic Conditions by Evolutionary and Rational Metabolic Engineering. *Biotechnol J* **12**, (2017).
- 6 Lian, J., Hamedirad, M., Hu, S. & Zhao, H. Combinatorial metabolic engineering using an orthogonal tri-functional CRISPR system. *Nature Communications* **8**, 1688, (2017).
- 7 Si, T. *et al.* Automated multiplex genome-scale engineering in yeast. *Nature Communications* **8**, 15187, (2017).
- 8 Xiao, H. & Zhao, H. Genome-wide RNAi screen reveals the E3 SUMO-protein ligase gene SIZ1 as a novel determinant of furfural tolerance in *Saccharomyces cerevisiae*. *Biotechnology for Biofuels* **7**, 78, (2014).
- 9 Baek, S.-H. *et al.* Improvement of d-Lactic Acid Production in *Saccharomyces cerevisiae* Under Acidic Conditions by Evolutionary and Rational Metabolic Engineering. *Biotechnology Journal* **12**, 1700015, (2017).
- 10 Si, T., Luo, Y., Bao, Z. & Zhao, H. RNAi-assisted genome evolution in *Saccharomyces cerevisiae* for complex phenotype engineering. *ACS synthetic biology* **4**, 283-291, (2015).
- 11 Goers, L. *et al.* Whole-cell *Escherichia coli* lactate biosensor for monitoring mammalian cell cultures during biopharmaceutical production.
- 12 Aguilera, L. *et al.* Dual role of LldR in regulation of the lldPRD operon, involved in L-lactate metabolism in *Escherichia coli*. *J. Bacteriol.* **190**, 2997-3005, (2008).
- 13 Mazutis, L. *et al.* Single-cell analysis and sorting using droplet-based microfluidics. *Nat. Protoc.* **8**, 870-891, (2013).
- 14 Wang, B. L. *et al.* Microfluidic high-throughput culturing of single cells for selection based on extracellular metabolite production or consumption. *Nat. Biotechnol.* **32**, 473-478, (2014).
- 15 Wagner, J. M. *et al.* A comparative analysis of single cell and droplet-based FACS for improving production phenotypes: Riboflavin overproduction in *Yarrowia lipolytica*. *Metab Eng* **47**, 346-356, (2018).

- 16 Gueldener, U., Heinisch, J., Koehler, G. J., Voss, D. & Hegemann, J. H. A second set of loxP marker cassettes for Cre-mediated multiple gene knockouts in budding yeast. *Nucleic Acids Res.* **30**, e23-e23, (2002).